Functional Genomic Approaches to Study Human Adenoviruses and Frontier Research on miRNAs

---

Dissertation

zur

Erlangung der naturwissenschaftlichen Doktorwürde
(Dr. sc. nat.)

vorgelegt der

Mathematisch-naturwissenschaftlichen Fakultät

der

Universität Zürich

von

HUNG VIET TRINH

aus Vietnam

Promotionkomitee

PD. Dr. Silvio Hemmi
Prof. Dr. Urs F. Greber
Prof. Dr. Michael O. Hengartner
Prof. Dr. Gunter Meister
Prof. Dr. Markus Stoffel

ZÜRICH 2011

TABLE OF CONTENTS

SUMMARY

Viruses are self-organized, symmetrical and rather simple structures, which can cause devastating diseases in humans and animals. They are able to readily react to cellular cues by changing gene expressions and conformations, which in turn enables dynamic interactions with their hosts. A large body of research has shown that the full complexity of viruses is unfolded as soon as they interact with host cells. Although studies of virus-host interactions have emerged as a key driving force in the research of infectious diseases, our understanding of the systems properties of viral infections has remained incomplete. Human adenoviruses (HAdVs) are most commonly associated with respiratory and gastrointestinal tract infections. In addition, HAdVs are the most common viral vectors in clinical gene transfer trials. Although HAdVs have been well characterized, there are many unresolved aspects, such as receptor usage by species B viruses (HAdV-B), dynamic expression profiles of viral and cellular proteins in the infected cells, and how this can be influenced by signal transduction, or virally encoded miRNAs.

To address some of these issues, we employed comprehensive functional genomics and biochemistry approaches to obtain a global picture of the infection dynamics of HAdVs in cultured cells, from entry to gene regulations. In the stage of HAdV entry, we studied the interaction of HAdV-B3/HAdV-B7 fiber knob (FK) to cellular receptor CD46 by using Biacore and quantitative microscopy. In the progress of dynamic interactions and regulations, we targeted three molecular levels including miRNA, mRNA and proteins by using quantitative transcriptomics and proteomics of both viruses and host infected human epithelial cells. The transcriptomics analysis was carried out by using the Agilent microarray and deep sequencing while proteomics was performed by using iTRAQ-8plex labeling of peptides or label-free method, followed by LC-MS/MS analyses at different time points of infection with different HAdV types. Subsequently, the networks were analyzed by using Metacore. For identifying novel miRNAs, we applied both *in silico* predictions and multi-detection methods including RT-PCR, miRNA microarray, deep sequencing and Northern blot analysis.

Our results show that direct binding of HAdV-B3/HAdV-B7-FK to CD46 occurs by an avidity mechanism and resolves the controversy about CD46 being a receptor for

HAdV-B. Based on quantitative transcriptomics, proteomics and miRNAs, we defined some common networks of HAdV serotypes of 3, 5, 11p and 35, such as cytoskeleton and cell cycle. We found new components such as galectin-1 (gal-1) and galectin-3 (gal-3), which were triggered to be secreted into the cell culture supernate. Preliminary data suggested that gal-1 and gal-3 interacted with CD46 as well as viral capsids including hexon and penton. Concerning the miRNAs, we found four small viral miRNAs (vmiRNAs) derived from VA-RNAI and one small vmiRNA derived from a non-coding viral sequence. Based on *in silico* analyses of potential targets for these vmiRNAs and transcriptomics analysis we found that there are many potential cellular and viral gene targets. In summary, this study addressed several systems aspects of HAdV infections, including post-translational modifications, potential anti-viral factors of innate immunity, small vmiRNAs, and it clarified the role of CD46 for HAdV-B infections.

ZUSAMMENFASSUNG

Viren sind autark organisiert, besitzen symmetrische und eher einfache Strukturen, können aber bei Mensch und Tier verheerende Krankheiten auslösen. Mittels Änderungen ihrer Genexpression und Strukturen passen sie sich problemlos an spezifische Eigenschaften der Zellen an, was ihnen eine dynamische Interaktion mit ihren Wirtszellen ermöglicht. Umfangreiche Untersuchungen zeigten, dass sich die volle Komplexität der Viren bereits beim ersten Kontakt mit der Wirtszelle manifestiert. Obwohl sich Untersuchungen der Virus-Wirtszellinteraktionen als Schlüssel zur Erforschung von Infektionskrankheiten erwiesen haben, bleibt unser Verständnis der Systemeigenschaften von Virusinfektionen immer noch lückenhaft. Humane Adenoviren (HAdVs) sind häufig mit Erkrankungen der Atemwege und des Verdautrakts assoziiert. Darüber hinaus sind HAdVs die am häufigsten verwendeten Vektoren für klinische Gentransfer-Versuche. Obwohl HAdVs gut erforscht sind, gibt es immer noch ungelöste Aspekte, wie zum Beispiel die Rezeptorverwendung der Vertreter der Spezies-B HAdV-Untergruppe (HAdV-B), Dynamik der Genexpressions- und Zellproteinprofile infizierter Zellen, und wie diese durch Signalübermittlungen und miRNAs beeinflusst werden.

Um einige dieser Fragen anzugehen haben wir umfangreiche „functional gemomics“ und biochemische Methoden verwendet, mit dem Ziel, einen Überblick über die Infektionsdynamik von HAdVs zu erhalten. Bezüglich des Zell-Eintritts der Spezies-B-Viren haben wir mittels Biacore-Messungen und quantitativer Mikroskopie die Interaktion von HAdV-B3/HAdV-B7 fiber knob (FK)-Proteinen mit zellulärem CD46-Rezeptor untersucht. Zur Erforschung der dynamischen Interaktionen und deren Regulierungen haben wir Untersuchungen auf drei molekularen Stufen ausgeführt. Diese beinhalteten quantitative Transkriptom- und Proteomanaylse von miRNAs, mRNAs und Proteinen sowohl von Viren als auch von infizierten Epithelzellen. Die Transkriptomanalyse wurde mittels Verwendung der Agilent microarray- und deep sequencing-Methode ausgeführt, während für die Proteomanalyse die iTRAQ-8plex Peptid-Markierungsmethode oder die Markier-freie Analysemethode in Kombination mit LC-MS/MS angewandt wurden, beides mit unterschiedlichen Adenovirus Serotypen

und Zellmaterial von unterschiedlichen Zeitpunkten. Mit Hilfe von Metacore wurden anschliessend Netzwerkinteraktionen analysiert. Zur Identifizierung neuer miRNAs verwendeten wir einerseits *in silico* Vorhersagen, und andererseits mehrere Detektierungsmethoden, wie RT-PCR, miRNA microarray, deep sequencing and Northern blot-Analyse.

Unsere Resultate zeigten, dass mittels eines Aviditätsmechanismus direkte Bindung von HAdV-B3/HAdV-B7-FK an CD46 erfolgt, was die Kontroverse um CD46 als Rezeptor für HAdV-B klärt. Basierend auf quantitativen Transkriptom-, Proteom-, und miRNA-Analysen haben wir gemeinsame Netzwerkinteraktionen für die HAdV 3, 5, 11p and 35 Serotypen definiert, die zum Beispiel Zytoskelett, und Zellzyklus beinhalteten. Wir entdeckten neue Komponenten wie Galectin-1 (Gal-1) und Galectin-3 (Gal-3), welche zur Sekretion in den Zellkulturüberstand angeregt wurden. Vorläufige Daten lassen darauf schliessen, dass Gal-1 und Gal-3 mit CD46 und mit viralen Capsiden inklusive Hexon und Penton interagieren. Bezüglich miRNAs haben wir vier kleine miRNAs (vmirRNAs) gefunden, die von VA-RNAI hergeleitet sind, und eine kleine vmiRNA, die von nicht-kodierender Virus-Sequenz hergeleitet ist. Basierend auf *in silico*-Analysen von möglichen Targets dieser vmiRNAs, wie auch auf Transkriptomanalysen, haben wir zahlreiche zelluläre und virale Targets gefunden. Zusammengefasst, die hier beschriebenen Untersuchungen hatten mehrere Aspekte von HAdV-Infektionen im Fokus, inklusive postranslationelle Modifizierungen, potenzielle antivirale Faktoren des angeborenen Immunsystems, sowie kleine vmiRNAs, und sie klärte den Rolle von CD46 bei HAdV-B Infektionen.

PROJECT OUTLINE

PROJECT 1: **Avidity effect of interaction between CD46 in human adenovirus species B fiber knobs**

Objectives: to determine the affinities between HAdV-B3/HAdV-B7-FK to CD46.

Methods: competition assays (flow cytometry), microscopic kinetics (Fluorescence Recovery After Photobleaching (FRAP), kinetics/affinity (Biacore).

Results: all experimental data including competition assay, microscopic kinetics and Biacore strongly supports direct binding of HAdV-B3/HAdV-B7-FK to CD46. High density of CD46 on cell surface is required for binding to HAdV-B3/B7-FK.

References: Hung V. Trinh*, Guillaume Lesage*, Venus Chennamparampil, Christoph Burckhardt, Stefan Schauer, Menzo Havenga, Urs F. Greber, and Silvio Hemmi. Avidity-based mechanism allows human adenovirus 3 and 7 to use CD46 as receptor (submitted to J. Virol).

Notice (*): equal contribution

PROJECT 2: Functional genomics approaches to study molecular system dynamics of human adenovirus infection

Objectives: to gain insights into the molecular dynamics governed by HAdV-B3, HAdV-C5, HAdV-B11 and HAdV-B35 infections.

Methods: quantitative analysis for cellular miRNAs, transcriptomics for gene expression and quantitative proteomics for protein expression using iTRAQ-label and label free methods and network interaction by Metacore.

Results: complete web-lab and statistical analysis for the quantitative transcriptomics gene expression and miRNA expression and quantitative proteomics for 3, 12, 24 and 48 h time courses of HAdV-B3, HAdV-C5, HAdV-B11 and HAdV-B35 infections

References:

Hung V. Trinh, Jonas Grossmann, Peter Gehrig, Bernd Roschitzki, Urs Greber, Silvio Hemmi. Comparison of iTRAQ-8plex and label-free quantitation in human adenoviruses (manuscript is included in this thesis).

Hung V. Trinh, Peter Gehrig, Hansruedi Baetschmann, Hubert Rehrauer, Andrea Patrignani, Jonas Grossmann, Michael O Hengartner, Urs Greber, Silvio Hemmi. Functional genomics approaches to study molecular system dynamics of human adenovirus type 3 infection (manuscript in preparation).

Hung V. Trinh, Peter Gehrig, Hansruedi Baetschmann, Hubert Rehrauer, Andrea Patrignani, Jonas Grossmann, Ralph Schlapbach, Urs Greber, Silvio Hemmi. Comparison of system cellular networks regulated by human adenoviruses type 3, 5, 11 and 35 infections (manuscript in preparation).

Hung V. Trinh, Peter Gehrig, Bernd Roschitzki, Walter Nickel, Urs Greber, Silvio Hemmi. Infection of human adenovirus type 3 induces secretion of galectin-1 (manuscript in preparation).

PROJECT 3: Computational and experimental analysis of potential miRNAs encoded by human adenoviruses

Objectives: to identify novel miRNAs encoded by HAdV-B3 (HAdV-B3-miRNAs).

Methods: *in silico* miRNA predictions, experimental validations (RT-PCR, Northern blot analysis, miRNA microarray, Ago2 immunoprecipitation), mass parallel sequencing, target prediction in comparison with quantitative transcriptomcis and proteomics.

Results: 25 vmiRNAs were detected by stem-loop RT-PCR out of 75 predicted miRNAs. Mass parallel sequencing of small RNAs derived from HAdV-B3-infected cells revealed 32 sequences reads with more than 10 reads. We observed a potential cluster of vmiRNAs located in an intronic region, encoding 3-5 vmiRNAs. In addition, the 5' and 3' ends of both VA-RNAI and VA-RNAII regions gave rise to high small RNA expression levels when analyzed by miRNA microarray and deep sequencing. Five vmiRNAs were further confirmed by both Northern blot analysis using total RNA and by stem-loop RT-PCR following immunoprecipitation by Ago2 antibody. To determine the potential targets of these vmiRNAs, we compared obtained transriptomics data to *in silico* target predictions.

References: Hung V. Trinh, Silvia Gutnik, Remy Bruggmann, Malik Yousef, Weihong Qi, Sirisha Aluri, Gunter Meister, Markus Stoffel, Urs Greber, Silvio Hemmi. Computational and experimental analysis of potential miRNAs encoded by human adenoviruses type 3 (manuscript is included in this thesis)

INTRODUCTION

Chapter 1: General introduction in virology

What are viruses, and how do they evolve?

Viruses are the smallest biological entities carrying genomes and proteins. They have coevolved tightly with their hosts, and hence they should be considered to be classified in the tree of live [1-4]. They do not have organelles and cannot replicate themselves. They need functioning cells for their replications. They only come to life when they have invaded a host cell. They infect most of organisms including animals, plants, eubacteria or archaea [5]. Since the first discovery of the tobacco mosaic virus by Martinus Beijerinck in 1898 [6], many different types of viruses have been described [7].

Virus particles (known as virions) consist of the genetic material made from either double strand (ds) DNA or single strand (ss) DNA, dsRNA, ssRNA(+), ssRNA(-), ssRNA reverse or dsDNA reverse transcribed, based on the Baltimore classification (http://expasy.org/viralzone/). Capsid proteins protect genetic material and they shape the virions. The shapes of viruses range from simple helical and icosahedral forms to more complex structures. In most cases, genetic materials are released from capsids inside the host cells and enter into nuclei using host machineries followed by transcription and replication of the viral genes.

Viruses are found wherever there is life in almost all living organisms [8]; however our understanding of how they evolved remains unsolved. There are several hypotheses how viruses could have emerged. The “escape hypothesis” suggests that viruses evolved by escape from the host as DNA like plasmids or transposons containing mobile genetic elements (see experimentation in maize by McClintock [9]). The “coevolution hypothesis” by Mahy and Van Regenmortel [10] suggests that viruses evolved from complex molecules of protein and nucleic acid at the same time as cells first appeared on earth and hence evolved dependently from cellular machinery for billions of year. Both of these hypotheses cannot explain the complexities of virus formation, capsid structures and replication mechanisms. Recently, viruses have been recognized as ancient with origins that pre-date the divergence of life into the three domains [10].

Replication cycles

In order to enter a cell, viruses typically interact with a receptor on the plasma membrane of the host cell. Different viruses use different receptors for entry. For instance, World haemorrhagic fever arenaviruses uses transferrin receptor 1 as primary receptor [11], human immunodeficiency virus (HIV) uses CD4 as attachment receptor [12] and human cytomegalovirus enters to the cells through epidermal growth factor receptor (EGFR) [13]. Following the attachment step, viruses enter into the host cells by receptor-mediated endocytosis or membrane fusion or pore-mediated penetration or possibly by a piggy-back process on cellular cargo (Fig. 1). Viruses undergo major conformational changes leading to internalization and subsequent penetration of an endosomal membrane or the plasma membrane [14,15]. Virus internalization into the host cell via receptor-mediated endocytosis can occur via clathrin-mediated endocytosis, caveolin-mediated endocytosis or clathrin- and caveolin-independent endocytosis [16,17]. In case of some non-enveloped picornaviruses [18], they can release their genome into the host cytoplasm through creation of a pore in the host membrane. In plant and bacteria containing a thick cell wall, viruses evolved a genome injection mechanism and left the capsids outside. The membrane fusion or capsid penetration can be triggered by low pH or particular ionic cues in endosomes. The viral genomes often reach the nuclei and import their genome into the nucleoplasm. The virus then replicates independently from the host replications in case of episomal genomes or together with the host DNA if the viral DNA is integrated into the host chromosomes, e.g., in case of retroviruses. Upon transcription and translation of viral proteins, the viral components assemble into new virions, which are then released from the host cells by lysis or non-lytic secretion processes, and start a new replication cycle.

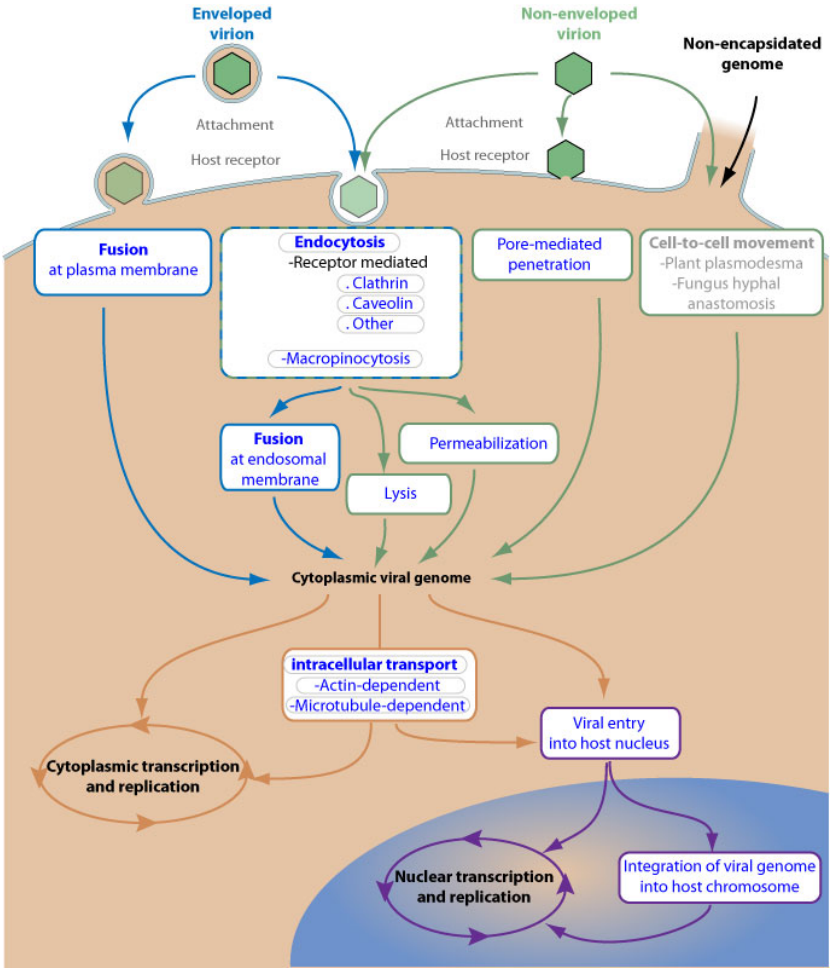

Fig. 1. Virus entry. Adapted from ViralZone (http://expasy.org/viralzone/).

Viruses in human diseases and prevention

Viruses cause many serious human diseases such as hemorrhagic fevers, AIDS, or respiratory disease. Some viruses like hepatitis B and C viruses can cause life-long or chronic infections and continuously replicate in the body despite the host defense [19]. The influenza H1N1 virus spread all over the world in 1918 and killed nearly 100 million people [20]. HIV originated from Africa and infected over 38 million people. It is estimated that 2.7 million new cases infections occurred and 2 million people died in 2007 [21] (http://data.unaids.org/).

Once viruses infect the host cells, it is difficult to eliminate them. Therefore, the prevention of virus infections is the most effective way. Thus, vaccines are used to prevent viral infections by creating a robust, specific and long lasting immune

response. The use of vaccines has resulted in a dramatic decline in morbidity and mortality associated with various life-threatening viruses such as polio, measles, mumps and rubella and eradicated smallpox infections [22]. Vaccines are combined to prevent over thirteen viral human infections of humans [23].

Chapter 2: Molecular analyses of viruses

MicroRNAs: an emerging class of post-transcriptional regulators of gene expression

MicroRNAs (miRNAs) are small non-coding RNAs of 18–24 nucleotides in length. miRNA lin-4 and its target mRNA, lin-14 were discovered by Ambros, Ruvkun and colleagues in *Caenorhabiditis elegans* [24,25]. Subsequently, an increasing number of miRNAs were identified in the major metazoan species including plants [26], human [27,28], and viruses [29]. Up to now, 1,048 experimentally characterized human miRNAs are registered in the miRNA database miRbase 16 (http://microrna.sanger.ac.uk/).

More recently, it has become evident that miRNAs are involved in many biological processes such as developmental timing, differentiation and cell death [30], cancer [31,32], diabetes [33], cardiovascular diseases [34,35], and virus infections [36,37]. An exciting development in the miRNA field has been the rapidly accumulating evidence that dysregulation of miRNAs may contribute to many additional diseases. A promising result in miRNA related therapeutics against chronic hepatitis C virus infection was recently provided by miR-122 in primates [38].

Given the important function of miRNAs in biological systems, this raises the question of how miRNAs work? miRNAs bind to the 3' untranslated regions (3' UTRs) of the target mRNAs, which results in their sequence-specific cleavage, translational repression or deadenylation, resulting in post-transcriptional gene silencing [39]. miRNAs are transcribed by RNA Polymerase II or III in the nucleus to form large pri-miRNA transcripts (Fig. 2). Next, they are processed by the microprocessor Drosha-DGCR8 (Pasha) into pre-miRNAs of 70-110 nucleotides, which are translocated into the cytoplasm by Exportin 5. Subsequently, the pre-miRNAs are recruited by Dicer to generate single-strand mature miRNAs of 18-24 nucleotides, which are incorporated into the miRNA-associated multiprotein RNA-induced silencing complex (miRISC). The mature miRNA then binds to complementary sites in the mRNA target and affects gene expression. The degree of complementarity can determine whether silencing occurs at the level of protein translation (imperfect) or by target-mRNA cleavage (perfect) [39-41].

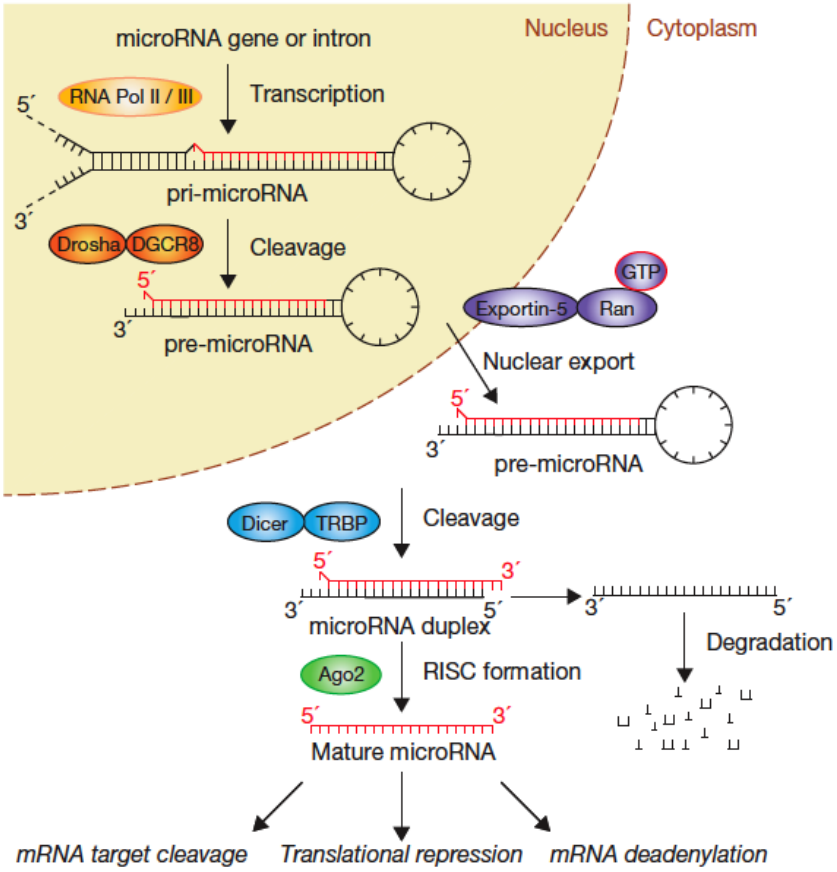

Fig. 2. The biogenesis of miRNAs [41]. miRNAs are first transcribed from coding or non-coding sequences. In most cases, they are derived from non-coding sequences and give rise to pri-miRNAs. The pri-miRNAs are further processed by Drosha and DGCR8 into pre-miRNAs (70-110 nucleotides). The pre-miRNAs are then exported to the cytoplasm where they are finally processed to mature miRNAs (18-25 nucleotides). The mature miRNAs are guided by the RISC complex to target 3'UTRs or 5'UTRs of target mRNAs causing their degradation or translational repression [39].

miRNAs encoded by viruses and their functions

It is not surprising that miRNAs play roles in viral infections, given their omnipresence in multicellular organisms. Currently, there are 235 vmiRNAs deposited in miRBase version 16 (http://www.mirbase.org/cgi-bin/browse.pl).

In 2004, Pfeffer *et al.* identified the first virus-encoded miRNAs expressed in B cells latently infected with EBV [29]. Since then, twenty-five EBV pre-miRNAs have been

reported in B cells and nasopharyngeal carcinomas [42-44]. In influenza A, each 5'-end of the eight viral RNA genomic segments was found to encode a vmiRNA [45]. Synthesis of vRNA requires the RNA-dependent RNA polymerase RdRp, nucleoprotein and the nuclear export protein NS2. Moreover, vmiRNAs are detectable during replication of various influenza A virus subtypes across multiple host species and associate physically with the RdRp. The depletion of these vmiRNAs resulted in a dramatic loss of vmiRNA in a segment-specific manner [45], suggesting that vmiRNAs regulate the switch from transcription to replication.

Efficient productive replication of viruses relies on the ability to exploit the biosynthetic machinery of the infected cells. Processes regulated by vmiRNAs include, in addition to autoregulation of viral genes, inactivation of apoptosis as well as innate host cell defense mechanisms, such as the IFN pathway, establishment and/or maintenance of latent infection, stimulation of cellular growth, oncogenesis and pathogenesis [46]. Current evidence indicates that viruses use their own vmiRNAs to manipulate both cellular and viral gene expression [47]. Viral genes controlled by endogenous miRNA include, i.e. the early SV40 T antigen, which is down-regulated by the miRNA miR-S1 expressed late in infection. This is advantageous for the virus since it limits the susceptibility of infected cells to cytotoxic T cells [48]. Another example for vmiRNAs targeting viral gene expression is EBV miR-BART2. It targets viral DNA polymerase (BALF5). During productive EBV replication, the BALF5 mRNA is cleaved [49]. The miR-BART2 is expressed during latent infection; however, DNA polymerase catalytic subunit (BALF5) is a lytic gene. Induction of lytic replication is controlled by miR-BART2 expression, suggesting miR-BART2 may regulate the latent-lytic switch by preventing premature BALF5 expression. In EBV, latent membrane protein 1 (LMP-1), inducing cell proliferation during latency, is targeted by three EBV miRNAs, miR-BART1-5p, miRBART16, and miR-BART17-5p [50]. Overexpression of these vmiRNAs causes inhibition of growth and stimulation of apoptosis [50].

Besides viral genes, vmiRNAs also target cellular genes involved in cell proliferation, survival and antiviral defense pathways [47]. HCMV expresses another immunoevasion miRNA that targets the mRNA encoding major histocompatibility complex class I polypeptide-related sequence B (MICB) [51]. MICB is a ligand for a cell-surface receptor

of natural killer (NK) cells, which are innate immune cells that provide one of the early lines of defense against viral infection. The MICB–receptor interaction is a key regulator of NK-cell activity and hence of NK-cell killing of virus-infected cells. BCLAF1, a protein involved in apoptosis, was identified as a target of KSHV miR-K5 in both B cells and endothelial cells [52]. Small interfering RNA inhibition of BCLAF1 resulted in an increase in lytic KSHV replication, suggesting that modulation of BCLAF1 by KSHV miRNAs might promote the reversion of latent infection [52].

In contrast, cellular miRNAs also target viral genes in different actions. In HIV-1, a cluster of cellular miRNAs including miR-28, miR-125b, miR-150, miR-223 and miR-382 target the 3' end of mRNAs, promoting HIV-1 latency in resting primary CD4+ T lymphocytes [53]. In another aspect, vmiRNAs disrupt the global cellular miRNA expression by overexpression of vmiRNAs during infection, resulting in a global down-regulation of cellular miRNAs [54]. In turn, down-regulation of cellular miRNAs may be involved in virus infection. For instance, down-regulation of cellular miR-27 enhances MCMV infection [55]. The question then arises whether cellular miRNAs can be used as therapeutic targets to inhibit or enhance virus infectivity or immunity.

More recently, vmiRNAs or noncoding RNAs were shown to be involved in regulation of cellular miRNAs. The human cytomegalovirus miRNA miR-UL112 acts synergistically with a cellular miR-376a to promote the escape from immune elimination [56]. The 3'UTR binding site in MHCB overlaps with both viral and cellular miRNAs, which suggests that human viruses may have coevolved with their natural human host to develop unique mechanisms to escape recognition and elimination by cells of the immune system. In another recent finding in Herpesvirus saimiri, viral U-rich noncoding RNAs of unknown function called HSUR1 and HSUR2 constitute the binding sites for cellular miR-27 [57]. Transient knockdown and ectopic expression of HSUR 1 demonstrated that it directs degradation of mature miR-27 in a sequence-specific and binding-dependent manner. This result suggests that viral noncoding RNAs can modulate host-cell gene expression via the miRNA pathway [57].

Virus infections modulate cellular miRNA expression

Virus infections have been shown to regulate cellular gene expression in multiple ways including via signaling cascades. Commonly, Toll-like receptors (TLR) are a major anti-viral signaling pathway activated upon virus infection. For instance, dendritic cell (DC) activation requires phagocytosis of infected material, followed by signaling through the dsRNA receptor TLR3 [58]. Following activation of TLR signaling, the transcriptional modulators such as NF kappa B are triggered which eventually regulates the expression of oncogenic miRNAs [59].

To determine the different expression levels of cellular miRNAs after virus infections, many recent studies have performed miRNA expression profiling with different viruses. This included HIV-1 [60], EBV [61] and HAdV-B3 [62]. The infection of HIV-1 causes down-regulation of most of the cellular miRNAs including anti-vmiRNAs and up-regulation of few cellular miRNAs including the miR-17-92 cluster [60]. It has been known that HIV-1 actively suppresses the expression of this polycistronic miRNA cluster miR-17/92, which is required for efficient viral replication [63]. Later, Houzet *et al.* performed miRNA profiling in the peripheral blood mononuclear cells of HIV-infected patients and revealed 59 down-regulated and 3 up-regulated cellular miRNAs indicating significant regulation of cellular miRNAs by virus infection [64]. In case of EBV, an oncogenic human Herpes virus, 9 cellular miRNAs were up-regulated while 7 cellular miRNAs were down-regulated by more than a 2-fold change [61]. The proto-oncogene protein (c-MYB) is targeted by miR-155, and a tumor suppressor gene SIAH1 is targeted by miR-424. Both miR-115 and miR-424 are upregulated, which suggests that EBV virus modulates tumorigenesis [61]. In Influenza, a group of miRNAs including miR-200a and miR-223 are differentially expressed in mouse cells where their predicted cellular targets are inversely correlated with the expression of these miRNAs [65]. More recently, Qi *et al.* applied deep sequencing to quantify the relative expression changes of cellular miRNAs in HAdV-B3-infected laryngeal epithelial cells [62], which resulted in 44 up-regulated and 36 down-regulated miRNAs of 492 quantified cellular precursor miRNAs.

Approaches to identify the factors involved in virus-host interaction

Identification of host factors involved in virus-host interactions has been established for some human viruses including HIV [66], West Nile virus (WNV) [67], dengue virus [68], Hepatitis C virus (HCV) [69] and influenza virus [70] by using interfering siRNA screens and computational network databases. Brass and Konig *et al.* identified a number of factors including cellular and viral encoded factors that regulate multiple processes of HIV infection, and life-threatening opportunistic infections [66,67,71]. 305 host factors affecting WNV infection were identified by a similar genome-wide RNAi screen approach [67]. Among these, ubiquitin ligase CBLL1 was found and it is required for WNV infection and endoplasmic reticulum lead to reduction of viral infection. 42 conserved factors were found to be required for Dengue virus infection of both fly and human cells [68]. Phosphatidylinositol 4-kinase (PI4KA) and α-subunit of the coat protein I (COPI) were identified as factors involved in HCV infection [69]. Inhibitors of COPI and PI4KA blocked HCV replication [69]. Furthermore, Li *et al.* addressed comprehensive factors which act in the signaling network interaction in HCV [72]. Cellular factors regulating viral replication, kinase signaling, ubiquitination and so on were revealed in influenza [70,73].

Although interference siRNA is a powerful method to identify cellular factors involved in the regulation network, the interaction of virus-host occurs in multiple dimensions in a highly dynamic manner. Thus, a proper quantitative approach for multi molecular levels such as mRNA, proteins and small regulator miRNAs together with computing network can be helpful to define significantly regulated components in complex biological systems. On one hand, Damm *et al.* discussed such approaches by using single-particle tracking (SPT) combined with computational analysis and modeling, and genome-wide RNA interference to reveal the host components required for virus entry [74]. This approach can potentially reveal the virus dynamics in real-time. On the other hand, global quantitative analysis of multi molecular levels in these systems is proposed. For example, the global mRNA and miRNA expressions have been analyzed [75,76]. Lim *et al.* showed that inversely correlated predicted target genes for miR-1 and miR-124 regulate gene expression [77]. Similarly, certain levels of inversed correlation between miRNA expression and their target predictions were shown in several biological models in human liver development [76] and melanoma [78]. In addition,

Baek *et al.* compared the miRNA and protein expression in parallel by introducing miR-223 in mouse neutrophils. Hundreds of genes, which are the targets of miR-223, were repressed [75]. The repression of some targets was revealed at the protein level and not at mRNA level, which indicated that the impact of miRNA on protein output can be readily determined.

The complex quantitative approaches (mRNAs, proteins and miRNAs) and network-based methods have not been used so far to identify the factors involved in virus-host interactions. Therefore, we aimed to utilize such a comprehensive approach for human HAdV-B3, HAdV-C5, HAdV-B11 and HAdV-B35 infections of human lung adenocarcinoma epithelial cells.

Chapter 3: Human adenoviruses and their use in gene therapy

General background of human adenoviruses

Human adenoviruses (HAdVs) were initially isolated in 1953 from cultured human adenoid tissue samples [79]. Since then, HAdVs have on one side served as model systems to study various aspects of molecular and cellular biology, including DNA replication, gene and cell cycle regulation, RNA splicing, and viral entry and transformation [80]. On the other side HAdVs have become the most widely used and most extensively studied viruses for gene delivery/therapy purposes such as targeting genetic diseases, for cancer treatment and vaccination [81,82]. A total of 55 different human HAdV serotypes have been identified, which are classified into species A-G [83,84]. The HAdV species B is further divided into subgroup B1 (HAdV-B3, HAdV-B7, HAdV-B16, HAdV-B21 and HAdV-B50) and B2 (HAdV-B11, HAdV-B14, HAdV-B34 and HAdV-B35).

HAdV as a vector tool to deliver target genes for gene therapy

Gene therapy is still a highly experimental and immature field of biomedicine that, after about two decades of clinical applications, has finally begun to demonstrate incontrovertible clinical therapeutic efficacy in several serious diseases, including cancer and childhood immunodeficiency. The most widely used HAdV vectors in the clinics are derived from serotypes HAdV-C2 and HAdV-C5. However, limited expression of the receptor for HAdV-C2/HAdV-C5 has been reported for cell types and tissues, for instance, polarized airway epithelial cells [85-88] and brain tissue [89]. In order to overcome low transduction efficiency of species C-based vectors for cellular targets with low virus receptor, alternative HAdV species B such as HAdV-B3 or HAdV-B35 have been evaluated. Species B vectors revealed an extended tropism compared to species C vectors and were able to efficiently infect, e.g., hematopoietic cells and DCs, but also numerous cancer cells [90-94]. Therefore, an emerging issue that remains to be solved for improvement of gene therapy includes detailed characterization of HAdV species B-host interactions.

Anti-viral drugs for HAdVs

In general, HAdVs cause mild infection of the upper respiratory tract, gastrointestinal tract, and the eye [95,96], but can lead to more serious complications in immunocompromised patients and very young children [97]. Infections with HAdV-B3 are a major cause of acute febrile and severe respiratory illness, and most symptomatic HAdV infections affect children or military recruits [98]. Infections of HAdVs induced the innate immune responses involving regulation of cytokines and activation of effector leukocytes [99]. Therefore, the treatment for HAdV infections would be an important task in case of highly immunocompromised patients. However, at the moment, a cure for HAdV infections is not available, and no specific drug has been approved by the Food and Drug Administration for treating HAdV infections.

Two broad spectrum anti-viral drugs, cidofovir and ribavirin are currently used to treat HAdV-infected patients [100]. Cidofovir is a cyclic nucleoside phosphonate, which interferes with DNA replication [101]. It acts as deoxynucleotide triphosphate (dNTP) analogue, which binds to viral DNA polymerase and inhibits the viral replication process [102]. Ribavirin also acts as a nucleoside analogue, but was found to be efficient in species C HAdV only [103]. Other potential anti-viral drugs such as dehydroepiandrosterone, epiandrosterone analogue [104] and stavudine [105] are being tested. More recently, small miRNA approaches have been applied in tests of HAdV-C5 replication in mouse by introducing the miRNAs binding sites to decrease expression of viral genes [106]. Introducing three liver-specific miRNA binding sites into E1A, Ylosmaki *et al.* have recently evaluated attenuation of HAdV replication in liver Huh7 cells [107]. Further studies in mice with injection of a variant with four miRNA binding sites showed 50- and 80-fold decrease at 6 and 96 h post infection (p.i.), respectively, accompanied by a strong abrogation of liver toxicity [106].

Chapter 4: The HAdV particle, genome organization and gene expression

HAdV structure

HAdVs are non-enveloped icosahedral (20 facets and 12 vertices) particles with a diameter of 70 to 100 nm [108,109]. The particles are composed of an outer protein capsid and an inner, linear dsDNA-associated core (Fig. 3A). The genome consists of about 36 kbp encoding 40 to 50 early and late genes. The capsid is composed mainly of geometrically arranged hexon proteins further stabilized by the "cementing" proteins IX, VIII and IIIa and 12 penton bases at each vertex [110]. The major coat proteins include hexon (polypeptide II), penton base (polypeptide III) and fiber (polypeptide IV). The penton complex at the vertex is formed from penton base, a pentamer of polypeptide III and fiber forming a trimer. Thus, an intriguing symmetry mismatch occurs within the penton complex. The complexes of the capsid were recently resolved by atomic structure at 3.6 Å resolution by electron microscopy (cryo-EM) [111] and at 3.5 Å resolution by x-ray crystallography [112]. These findings provided substantial advance in understanding of how major and minor capsid proteins interact within the virion (Fig. 3B) [113].

Other minor coat proteins including polypeptides IIIa, VI, VIII and IX act as capsid cement (Fig. 3B). Protein IIIa exposes the outer surface of the virion where it contacts four different hexons [114]. Its role appears to be that of a rivet whose function is to hold the capsid facets together. Protein VI (27.2 kDa full length, ~22 kDa cleaved) has been assigned to a position on the inner capsid surface. It anchors the rings of peripentonal hexons and connects the highly ordered capsid to the less ordered core region and connects the bases of two adjacent peripentonal hexons [114]. Protein VIII is very small (~25 kDa full length, ~14 kDa cleaved) which is located on the inner surface underneath the inner boundaries of penton base and hexons [111]. Polypeptide IX (14-15 kDa) is the best characterized of the minor proteins. Protein IX stabilizes the virion, but is not required for assembly. Mutants lacking protein IX are more thermolablile than wild type [115,116]. The protein IX is inlaid into the outer surface of the capsid-not on the outer surface itself but halfway down the hexon [111]. These detailed understandings will provide new opportunities to improve rationale design of new virions for gene therapy.

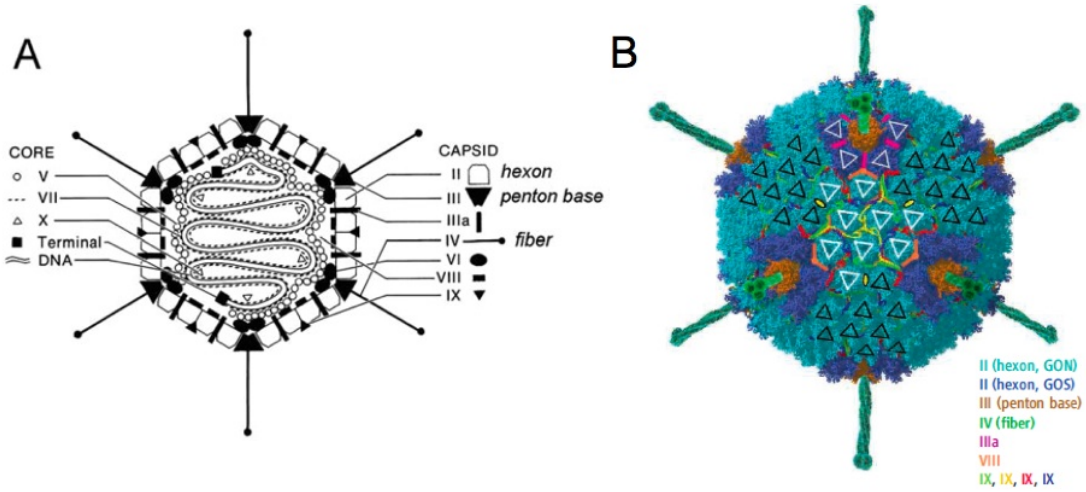

Fig. 3. HAdV virion. (A) Section of HAdV structure, revealing viral protein components and viral DNA [108]. The HAdV virion contains seven capsid proteins with major coat proteins (hexon, penton and fiber), double-strand DNA, and four DNA-associated proteins or core proteins. (B) Superposed on a medium-resolution image of the virion surface are triangles [111,113]. One network structure is mediated by protein IIIa at the vertices, within group-of-six (GOS) tiles, a penton base and its five surrounding hexons. Another is mediated by ropes (protein IX) that lash hexons together to form group-of-nine (GON) tiles and bind GONs to GONs. A third is mediated by IIIa and VIII, and binds each GOS to five surrounding GONs. The triangles represent four GONs in the center, in white, and three GONs surrounding it, in black [111,113].

The HAdV genome organization and its gene expression

The HAdV genome is organized into six transcription units. Transcription of E1, E3, VA-RNA and late proteins occurs from the plus-strand and thus from left to right. Transcription of E2 and E4 occurs from the minus-strand and thus from right to left. The immediate early E1A transcription unit is the first to be expressed. E1A yields multiple polypeptides due to alternate mRNA splicing. In HAdV-B3, it yields a 13S 28 kDa, 12S 25 kDa and 9S 7 kDa mRNA and polypeptide, respectively (Fig. 4). The 13S and 12S mRNAs encode nuclear targeting sequence at the carboxy terminus, while 9S mRNA does not. One of the multiple functions of E1A is to act as

transcriptional co-activator of the other early genes including E1B, E2, E3, E4 and the major late promoter (MLP) and to stimulate DNA synthesis (Fig. 4) [117].

Similar to E1A, E1B also produces multiple alternatively spliced mRNAs including 21 kDa and 55 kDa polypeptides in HAdV-B3. A primary function of both the 21 kDa and 55 kDa E1B polypeptides is to protect infected cells from apoptosis induced by E1A proteins and other processes associated with infection, thus keeping them alive long enough to manufacture large quantities of progeny virus [118].

The E2 region consists of two alternatively splicing regions, termed E2A and E2B, which encode three proteins necessary for synthesis of viral DNA. Of major importance is the terminal binding protein (TP), which is essential to prime viral DNA synthesis. The pTP also mediates attachment of the HAdV genome to specific sites on the nuclear matrix [119]. Covalent attachment of pTP/TP has been suggested to protect viral DNA from exonucleases and facilitate unwinding of DNA duplex at the origin of replication. The pTP exists as a stable heterodimer with E2B DNA polymerase (Pol) and participates in initiation of DNA replication [120]. The Pol catalyzes both the initiation and elongation steps of HAdV DNA replication [121]. Similar to other DNA polymerases, Pol also exhibits an intrinsic 3´→5´ proofreading exonuclease activity [122]. E2A DNA binding protein (DBP) is synthesized in both early and late phase in the infectious cycle and is involved in DNA replication, as well as early and late gene expression [123]. DBP binds to single-stranded DNA with cooperativity and high affinity, thus protecting single-stranded DNA from nuclease attack [124,125].

The increased concentration of viral DNA templates appears to be sufficient to induce transcription of the intermediate pIX and IVa2 genes encoded within the E2 transcription unit. The IVa2 protein is the second adenoviral transcriptional activator: Its specific binding to two adjacent sequences within the first intron of the MLP transcription unit activates the late phase of viral DNA replication [126].

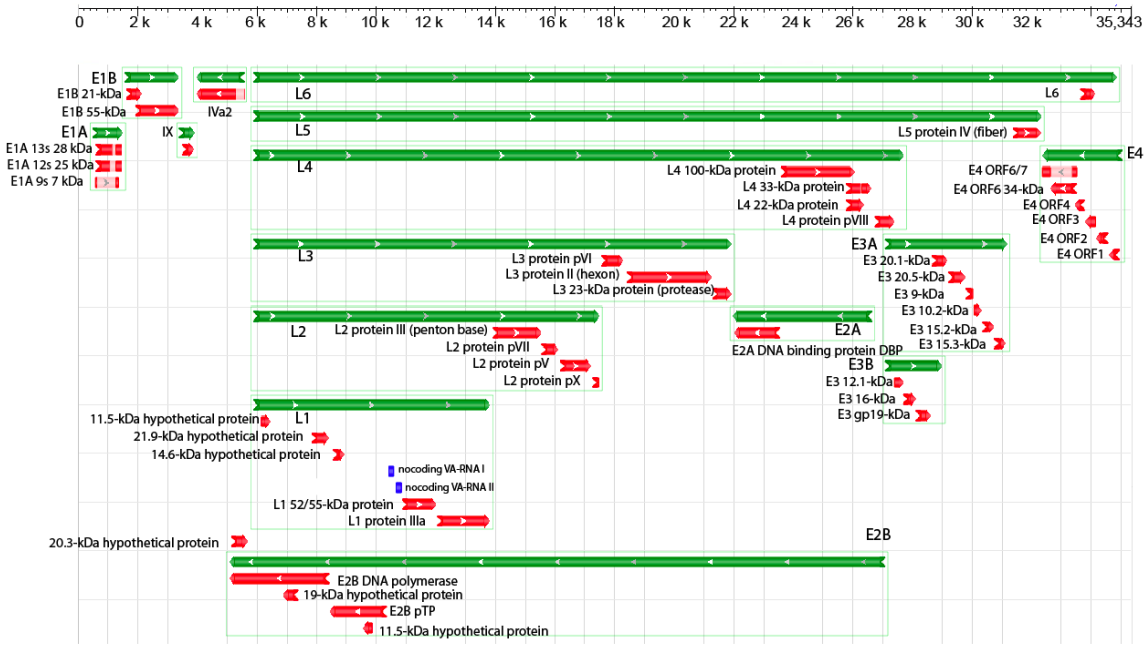

Fig. 4. Genome organization and transcription units of HAdV-B3. The green bars represent transcription units, whereas the red bars represent encoding proteins or ORFs. The length of the bar indicates the relative length of transcription unit or encoding sequences. The genome annotation is adapted from NCBI.

The early region 3 (E3) encodes several mRNAs through alternative splicing. E3 consists of E3A and E3B regions with multisplicing products (Fig. 4). Among the E3 products is the gp19K glycoprotein. It is present largely in the endoplasmic reticulum, where it binds to certain class I histocompatibility antigens, preventing transport to the cell surface. Such inhibition allows infected cells to suppress lysis by class I-restricted, HAdV specific cytotoxic T lymphocytes, an obvious advantage to production and spread of viral progeny [127]. E3 RID-beta, an HAdV-encoded receptor internalization and degradation (RID) protein (previously named E3-10.4K/14.5K), is composed of RIDalpha and RIDbeta subunits and is implicated in tumor necrosis factor (TNF) receptor family and epidermal growth factor receptor (EGFR) down-regulation [128]. In addition, it was suggested to have lipid homeostasis functions [129].

The E4 transcription unit is located at the extreme right end of the HAdV genome and encodes six ORFs in HAdV-B3. E4 products possess a wide range of activities crucial to successful viral replication [130]. E4 products contribute a major source of inflammation

in recipients of gene therapy vectors with E1A deletion. E4orf4 is a death factor, and works in part by inducing a Src-mediated cytoplasmic apoptotic signal leading to caspase-independent membrane blebbing and cell death.

Chapter 5: Virus receptors and entry of HAdVs

The entry of HAdVs first occurs at the plasma membrane of epithelial cells, which are protected by the extracellular matrix containing multiple glycosylated proteins. The different HAdV species bind to different receptors. For species C HAdV-C2 and HAdV-C5, the initial interactions occur through binding of the fiber knob domain to the Coxsackie B virus-Adenovirus attachment receptor (CAR) (Fig. 5) [131], a widely distributed immunoglobulin gene family member. CAR is involved in cell-cell contacts at tight and adherence junctions [132] and knockout of CAR in the mouse results in severe defects in embryonic heart development and death at embryonic day 12 [133]. After binding to CAR, the species C HAdVs engage a secondary receptor, αv containing heterodimeric integrins for internalization [134,135], which facilitate viral endocytosis into clathrin-coated pits and signaling into target cells. Cytosolic virus particles are transported along microtubules by directional motion [136,137] towards the nucleus and the genome is imported into the nucleus upon docking to the CAN/Nup214 receptor [138].

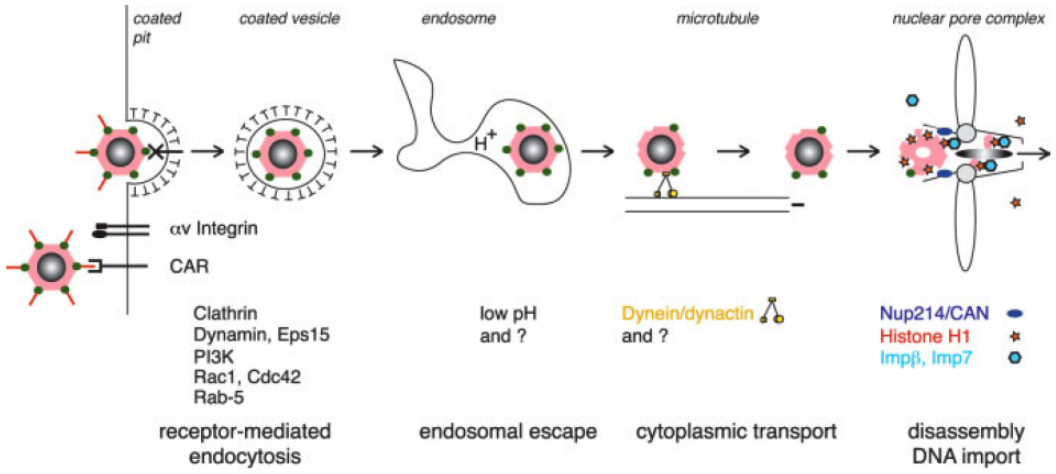

Fig. 5. Entry pathway of HAdV-C2/HAdV-C5 in epithelial cells [139]. Fiber knob of HAdV-C2/HAdV-C5 binds to the primary CAR receptor followed by binding of penton base to αv integrins. The binding triggers clathrin-mediated viral endocytosis. The large GTPase dynamin, PI3K, the small GTPases Rac1, and Cdc42 are required for the endocytosis. Coated vesicles are delivered into endosomes where pH is lower than cytosol environment. Ad particles escape from endosomes and travel by microtubule-dependent and dynein/dynactin-dependent viral

transport to reach the nuclear pore complex where it recognizes nuclear receptor CAN/Nup214 and it disassembles upon recruiting the nuclear histone H1 and the H1 import factors importin β and importin 7.

In case of species B HAdVs, CD46 has been shown as a primary receptor for HAdV-B3 [140,141], HAdV-B7 [141], HAdV-B11 [141,142] and HAdV-B35 [141,143]. Receptor utilization of CD46 is not restricted to species B viruses. Additional HAdVs that bind to CD46 include species D HAdV-D37 and HAdV-D49 [144,145]. The widely expressed CD46 belongs to a family of regulators, which prevent complement activation on autologous tissue [146]. CD46 also links innate and adaptive immunity in macrophages and lymphocytes [147]. The extracellular domain of CD46 consists of four amino-terminal copies of an approximately 60-amino-acid structural motif, termed short consensus repeat (SCR), followed by one to three Ser-Thr-Pro (STP) rich domain(s), a short region of unknown function proximal to the cell membrane, a transmembrane spanning domain, and a carboxy-terminal cytoplasmic tail. Antibody blocking assays, together with infectivity and mutagenesis studies revealed that binding of human HAdV-B35 to CD46 occurs through the N-terminal two SCR I-II domains [148-150].

As already mentioned, data by Sirena *et al.* and Fleischli *et al.* where they used rodent cells ectopically expressing CD46 indicated that HAdV-B3/HAdV-B7 utilizes CD46 as a primary receptor [140,141]. In contrast, other groups suggested alternative receptors rather than CD46. For instance, the Curiel group suggested that HAdV-B3 and other members of HAdV species B utilize CD80 and CD86 as attachment receptors [151,152]. The group of Arnberg suggested that all species B Ads except Ad3 and Ad7 would utilize CD46, and all serotypes including HAdV-B3 and HAdV-B7 would bind to a second, so far elusive common receptor (sBAR) [142,153]. However, the Lieber group suggested an additional unknown receptor X, neither CD46 nor CD80/86, for HAdV-B3/HAdV-B7 [154], which they recently showed to be desmoglein 2 (DSG2). In Hela cells, DSG2 also served as a receptor for HAdV-B11 and HAdV-B14 [155]. These results do not resolve the issue of how a junction protein such as DSG2 is accessed by a virus from the apical side, nor do they show whether DSG2 or CD46 or both together are used as

attachment receptors. Wang *et al.* also suggested that upon HAdV-B3 binding, DSG2 triggers events reminiscent of epithelial-to-mesenchymal transition, leading to transient opening of intercellular junctions [155]. The underlying mechanisms remain however unknown.

Here we aimed to characterize how HAdV-B3/HAdV-B7 binds to CD46 in cells and *in vitro*. We discovered that these species B2 HAdV use the CD46 receptor by an avidity mechanism.

Chapter 6: Molecular analyses of HAdV infections

Transcriptomics in HAdVs

Transcriptomics has been applied with various HAdV serotypes using infection time courses to define up- and down-regulated genes. Following HAdV-A12 infection of Hela cells, Dort *et al.* documented the up-regulation of cellular immune response genes including G1P2, IFIT1, and IFIT2 within 12 h p.i.. [156]. At 48 h p.i., expression of most cellular genes turned down [156]. HAdV-C2 infection resulted in 382 significantly up- or down-regulated genes with more than 1.5-fold change during 10 to 20 h p.i., compared to 79 genes in HAdV-A12 [157]. Among these, 55% of the regulated genes were commonly detected in both HAdV-A12 and HAdV-C2, suggesting some shared network in both these infections [157]. Microarray analysis of early infections of HAdV-C2 in primary lung fibroblast cells revealed significant changes in a number of genes encoding transcription factors including ATF3, ATF4, KLF4, KLF6 and ELK3, and immune response factors (NR4A1 and CEBPB) [158]. Zhao *et al.* further analyzed extensively the transcriptomics in HAdV-C2, which resulted in 988 genes with more than 2-fold expression changes [159]. In HAdV-C5, 2,000 significant genes, which account for 10% of analyzed transcripts, were changed more than 2-fold [160].

In addition to wild-type HAdVs, the gene expression profiles for HAdV vectors with E1/E3 deletions were investigated. Infection of HAdV-C5-E1/E3 deletion in HB2 cells resulted in 24 and 95 significantly regulated genes at 24 h and 72 h p.i. [161]. Again, a large number of genes involved in innate and inflammatory immune responses were observed. Similar to this study, Rao *et al.* showed 345 genes with expression changes over 2-fold compared to wild-type HAdV-C5 [162], suggesting that E1B is one of the major factors altering gene expression changes during HAdV-C5 infections. HAdV-C2 with E1/E3 or E1/E2b/E3 deletions revealed significant dysregulation of 15% measured transcripts with the majority of genes involved in innate responses and proinflammatory responses [163] [164]. Particularly, the signaling adapter protein MyD88 acted as a significant HAdV immunity amplifier and regulator in vivo [163].

Although many studies have addressed the transcriptomics of HAdV-C2/C5 infected cells, no study has conducted transcriptomics with HAdV species B. Vectors derived

from HAdV species B represent promising tools for future gene therapy approaches. Therefore, finding common and unique regulation patterns among the different types of species B will contribute to a better understanding of tropism and infectivity of these vectors.

Viral miRNAs encoded by HAdVs and their actions

HAdVs express extremely abundant VA-RNAI and VA-RNAI, which are composed of 160-176 nt and form dsRNAs with hairpin structures. The major structural features of these RNAs including terminal stem, apical stem-loop and central domain are conserved in all HAdVs, except the location of the loop [165]. Recently, these VA-RNAs were found to be transported by Exportin 5 to the cytoplasm, where they accumulate in the late phase of virus infection [166]. Both VA-RNAs seem to inhibit RNA interference by possibly saturating Exportin 5, Dicer and RISC due to high expression during the late phase of HAdV replication [167]. VA-RNAI was found to be processed into about 22 nt RNAs, but seems to be a poor Dicer substrate, as only about 1% of VA-RNAI molecules was processed [168]. Removal of both VA-RNAI and VA-RNAII was reported to result in a dramatic decrease in viral replication capacity [169], but could be compensated by two small-structured RNAs (EBER 1 and EBER 2) encoded by EBV [170]. A recent study revealed that late in HAdV-infected cells, 80% of the RISC complexes were loaded with VA-RNAII, although VA-RNAI is the more abundantly expressed RNA [171]. As the authors were able to isolate processed VA-RNA species from polyribosomes, they speculated that these represent true miRNAs. Nevertheless, these studies pointed to the possibility that VA-RNAI may serve two functions during HAdV propagation. It appears to antagonize the cellular defense pathways against both long and short dsRNA by binding the two key enzymes in the respective pathways, dsRNA-activated protein synthesis inhibitor (PKR) of the IFN pathway and Dicer of the RNA silencing pathway. PKR is a kinase, which is activated by viral replication. The activated PKR phosphorylates eukaryotic initiation factor 2 (eIF-2), which prevents initiation of translation [172]. VA-RNA binds PKR, inhibiting its activation and permitting protein synthesis [173]. HAdV mutants without VA-RNAs revealed a defect

in the viral replication process due to PKR-mediated translational arrest in IFN-treated cells [174]. Similarly, EBRR1 RNA can bind to PKR [175] and partially reduce the inhibition of protein synthesis by PKR in reticulocyte lysates [176]. However, the EBERs do not counteract IFN effects on vesicular stomatitis virus replication or B-lymphocyte transformation by EBV [177].

More recently, targets of miRNA (mivaRNAI-138) derived from 3'end of HAdV-C5 VA-RNAI were found to include the splicing and translation regulator TIA-1, which was down-regulated in infected cells or in transfected cells expressing mivaRNAI-138 [178]. In addition, transfection of a plasmid expressing both VA-RNAs caused down-regulation of another 33 genes, while transfection of VA-RNAI alone resulted in down-regulation of 30 genes, and transfection of mivaRNAI-138 in down-regulation of 26 genes. These findings strongly suggest that endogenous miRNAs play important roles in the infectious life cycle in HAdV.

To summarize, miRNAs are small and highly flexible to target multiple mRNAs without triggering dsRNA response pathways. They represent attractive candidates for the regulation of both viral and host cell gene expression.

References

1. Raoult, D.*, et al.* The 1.2-megabase genome sequence of Mimivirus. *Science* **306**, 1344-1350 (2004).
2. Moreira, D. & Lopez-Garcia, P. Comment on "The 1.2-megabase genome sequence of Mimivirus". *Science* **308**, 1114; author reply 1114 (2005).
3. Moreira, D. & Lopez-Garcia, P. Ten reasons to exclude viruses from the tree of life. *Nat Rev Microbiol* **7**, 306-311 (2009).
4. Ludmir, E.B. & Enquist, L.W. Viral genomes are part of the phylogenetic tree of life. *Nat Rev Microbiol* **7**, 615; author reply 615 (2009).
5. Koonin, E.V., Senkevich, T.G. & Dolja, V.V. The ancient Virus World and evolution of cells. *Biol Direct* **1**, 29 (2006).
6. Flint, S.J., Enquist, L.W., Krug, R.M., Racaniello, V.R. & Skalka, A.M. Principles of Virology: Molecular Biology, Pathogenesis, and Control. (ASM Press, 2000).
7. Breitbart, M. & Rohwer, F. Here a virus, there a virus, everywhere the same virus? *Trends Microbiol* **13**, 278-284 (2005).
8. Iyer, L.M., Balaji, S., Koonin, E.V. & Aravind, L. Evolutionary genomics of nucleo-cytoplasmic large DNA viruses. *Virus Res* **117**, 156-184 (2006).
9. Mc, C.B. The origin and behavior of mutable loci in maize. *Proc Natl Acad Sci U S A* **36**, 344-355 (1950).
10. Mahy, W.J. & Van Regenmortel, M.H.V. (eds.). *Desk Encyclopedia of General Virology*, 24-28 (Oxford: Academic Press, 2009).
11. Radoshitzky, S.R.*, et al.* Transferrin receptor 1 is a cellular receptor for New World haemorrhagic fever arenaviruses. *Nature* **446**, 92-96 (2007).
12. Deng, H.*, et al.* Identification of a major co-receptor for primary isolates of HIV-1. *Nature* **381**, 661-666 (1996).
13. Wang, X., Huong, S.M., Chiu, M.L., Raab-Traub, N. & Huang, E.S. Epidermal growth factor receptor is a cellular receptor for human cytomegalovirus. *Nature* **424**, 456-461 (2003).
14. Lee, K.K. Architecture of a nascent viral fusion pore. *EMBO J* **29**, 1299-1311 (2010).
15. Donald, J.E.*, et al.* From the Cover: Transmembrane orientation and possible role of the fusogenic peptide from parainfluenza virus 5 (PIV5) in promoting fusion. *Proc Natl Acad Sci U S A* **108**, 3958-3963 (2011).
16. Marsh, M. & Helenius, A. Virus entry: open sesame. *Cell* **124**, 729-740 (2006).
17. Mercer, J., Schelhaas, M. & Helenius, A. Virus entry by endocytosis. *Annu Rev Biochem* **79**, 803-833 (2010).
18. Brabec, M.*, et al.* Opening of size-selective pores in endosomes during human rhinovirus serotype 2 in vivo uncoating monitored by single-organelle flow analysis. *J Virol* **79**, 1008-1016 (2005).
19. Bertoletti, A. & Gehring, A. Immune response and tolerance during chronic hepatitis B virus infection. *Hepatol Res* **37 Suppl 3**, S331-338 (2007).
20. Johnson, N.P. & Mueller, J. Updating the accounts: global mortality of the 1918-1920 "Spanish" influenza pandemic. *Bull Hist Med* **76**, 105-115 (2002).
21. Gao, F.*, et al.* Origin of HIV-1 in the chimpanzee Pan troglodytes troglodytes. *Nature* **397**, 436-441 (1999).
22. Lane, J.M. Mass vaccination and surveillance/containment in the eradication of smallpox. *Curr Top Microbiol Immunol* **304**, 17-29 (2006).
23. Arvin, A.M. & Greenberg, H.B. New viral vaccines. *Virology* **344**, 240-249 (2006).
24. Lee, R.C., Feinbaum, R.L. & Ambros, V. The C. elegans heterochronic gene lin-4 encodes small RNAs with antisense complementarity to lin-14. *Cell* **75**, 843-854 (1993).
25. Wightman, B., Ha, I. & Ruvkun, G. Posttranscriptional regulation of the heterochronic gene lin-14 by lin-4 mediates temporal pattern formation in C. elegans. *Cell* **75**, 855-862 (1993).
26. Reinhart, B.J., Weinstein, E.G., Rhoades, M.W., Bartel, B. & Bartel, D.P. MicroRNAs in plants. *Genes Dev* **16**, 1616-1626 (2002).
27. Bentwich, I.*, et al.* Identification of hundreds of conserved and nonconserved human microRNAs. *Nat Genet* **37**, 766-770 (2005).

28. Calin, G.A., *et al.* Frequent deletions and down-regulation of micro- RNA genes miR15 and miR16 at 13q14 in chronic lymphocytic leukemia. *Proc Natl Acad Sci U S A* **99**, 15524-15529 (2002).
29. Pfeffer, S., *et al.* Identification of virus-encoded microRNAs. *Science* **304**, 734-736 (2004).
30. Reinhart, B.J., *et al.* The 21-nucleotide let-7 RNA regulates developmental timing in Caenorhabditis elegans. *Nature* **403**, 901-906 (2000).
31. Lu, J., *et al.* MicroRNA expression profiles classify human cancers. *Nature* **435**, 834-838 (2005).
32. O'Donnell, K.A., Wentzel, E.A., Zeller, K.I., Dang, C.V. & Mendell, J.T. c-Myc-regulated microRNAs modulate E2F1 expression. *Nature* **435**, 839-843 (2005).
33. Poy, M.N., *et al.* A pancreatic islet-specific microRNA regulates insulin secretion. *Nature* **432**, 226-230 (2004).
34. Chen, J.F., *et al.* Targeted deletion of Dicer in the heart leads to dilated cardiomyopathy and heart failure. *Proc Natl Acad Sci U S A* **105**, 2111-2116 (2008).
35. Zhao, Y., *et al.* Dysregulation of cardiogenesis, cardiac conduction, and cell cycle in mice lacking miRNA-1-2. *Cell* **129**, 303-317 (2007).
36. Jopling, C.L., Yi, M., Lancaster, A.M., Lemon, S.M. & Sarnow, P. Modulation of hepatitis C virus RNA abundance by a liver-specific MicroRNA. *Science* **309**, 1577-1581 (2005).
37. Lecellier, C.H., *et al.* A cellular microRNA mediates antiviral defense in human cells. *Science* **308**, 557-560 (2005).
38. Lanford, R.E., *et al.* Therapeutic silencing of microRNA-122 in primates with chronic hepatitis C virus infection. *Science* **327**, 198-201 (2010).
39. Filipowicz, W., Bhattacharyya, S.N. & Sonenberg, N. Mechanisms of post-transcriptional regulation by microRNAs: are the answers in sight? *Nat Rev Genet* **9**, 102-114 (2008).
40. Kim, Y.K. & Kim, V.N. Processing of intronic microRNAs. *EMBO J* **26**, 775-783 (2007).
41. Winter, J., Jung, S., Keller, S., Gregory, R.I. & Diederichs, S. Many roads to maturity: microRNA biogenesis pathways and their regulation. *Nat Cell Biol* **11**, 228-234 (2009).
42. Cai, X., *et al.* Epstein-Barr virus microRNAs are evolutionarily conserved and differentially expressed. *PLoS Pathog* **2**, e23 (2006).
43. Grundhoff, A., Sullivan, C.S. & Ganem, D. A combined computational and microarray-based approach identifies novel microRNAs encoded by human gamma-herpesviruses. *RNA* **12**, 733-750 (2006).
44. Zhu, J.Y., *et al.* Identification of novel Epstein-Barr virus microRNA genes from nasopharyngeal carcinomas. *J Virol* **83**, 3333-3341 (2009).
45. Perez, J.T., *et al.* Influenza A virus-generated small RNAs regulate the switch from transcription to replication. *Proc Natl Acad Sci U S A* **107**, 11525-11530 (2010).
46. Sarnow, P., Jopling, C.L., Norman, K.L., Schutz, S. & Wehner, K.A. MicroRNAs: expression, avoidance and subversion by vertebrate viruses. *Nat Rev Microbiol* **4**, 651-659 (2006).
47. Skalsky, R.L. & Cullen, B.R. Viruses, microRNAs, and host interactions. *Annu Rev Microbiol* **64**, 123-141 (2010).
48. Sullivan, C.S., Grundhoff, A.T., Tevethia, S., Pipas, J.M. & Ganem, D. SV40-encoded microRNAs regulate viral gene expression and reduce susceptibility to cytotoxic T cells. *Nature* **435**, 682-686 (2005).
49. Barth, S., *et al.* Epstein-Barr virus-encoded microRNA miR-BART2 down-regulates the viral DNA polymerase BALF5. *Nucleic Acids Res* **36**, 666-675 (2008).
50. Lo, A.K., *et al.* Modulation of LMP1 protein expression by EBV-encoded microRNAs. *Proc Natl Acad Sci U S A* **104**, 16164-16169 (2007).
51. Stern-Ginossar, N., *et al.* Host immune system gene targeting by a viral miRNA. *Science* **317**, 376-381 (2007).
52. Ziegelbauer, J.M., Sullivan, C.S. & Ganem, D. Tandem array-based expression screens identify host mRNA targets of virus-encoded microRNAs. *Nat Genet* **41**, 130-134 (2009).
53. Huang, J., *et al.* Cellular microRNAs contribute to HIV-1 latency in resting primary CD4+ T lymphocytes. *Nat Med* **13**, 1241-1247 (2007).

54. Dolken, L., *et al.* Mouse cytomegalovirus microRNAs dominate the cellular small RNA profile during lytic infection and show features of posttranscriptional regulation. *J Virol* **81**, 13771-13782 (2007).
55. Buck, A.H., *et al.* Post-transcriptional regulation of miR-27 in murine cytomegalovirus infection. *RNA* **16**, 307-315 (2010).
56. Nachmani, D., Lankry, D., Wolf, D.G. & Mandelboim, O. The human cytomegalovirus microRNA miR-UL112 acts synergistically with a cellular microRNA to escape immune elimination. *Nat Immunol* **11**, 806-813 (2010).
57. Cazalla, D., Yario, T. & Steitz, J.A. Down-regulation of a host microRNA by a Herpesvirus saimiri noncoding RNA. *Science* **328**, 1563-1566 (2010).
58. Schulz, O., *et al.* Toll-like receptor 3 promotes cross-priming to virus-infected cells. *Nature* **433**, 887-892 (2005).
59. Taganov, K.D., Boldin, M.P., Chang, K.J. & Baltimore, D. NF-kappaB-dependent induction of microRNA miR-146, an inhibitor targeted to signaling proteins of innate immune responses. *Proc Natl Acad Sci U S A* **103**, 12481-12486 (2006).
60. Yeung, M.L., *et al.* Changes in microRNA expression profiles in HIV-1-transfected human cells. *Retrovirology* **2**, 81 (2005).
61. Imig, J., *et al.* microRNA profiling in Epstein-Barr virus-associated B-cell lymphoma. *Nucleic Acids Res* (2010).
62. Qi, Y., *et al.* High-throughput sequencing of microRNAs in adenovirus type 3 infected human laryngeal epithelial cells. *J Biomed Biotechnol* **2010**, 915980 (2010).
63. Triboulet, R., *et al.* Suppression of microRNA-silencing pathway by HIV-1 during virus replication. *Science* **315**, 1579-1582 (2007).
64. Houzet, L., *et al.* MicroRNA profile changes in human immunodeficiency virus type 1 (HIV-1) seropositive individuals. *Retrovirology* **5**, 118 (2008).
65. Li, Y., *et al.* MicroRNA expression and virulence in pandemic influenza virus-infected mice. *J Virol* **84**, 3023-3032 (2010).
66. Konig, R., *et al.* Global analysis of host-pathogen interactions that regulate early-stage HIV-1 replication. *Cell* **135**, 49-60 (2008).
67. Krishnan, M.N., *et al.* RNA interference screen for human genes associated with West Nile virus infection. *Nature* **455**, 242-245 (2008).
68. Sessions, O.M., *et al.* Discovery of insect and human dengue virus host factors. *Nature* **458**, 1047-1050 (2009).
69. Tai, A.W., *et al.* A functional genomic screen identifies cellular cofactors of hepatitis C virus replication. *Cell Host Microbe* **5**, 298-307 (2009).
70. Konig, R., *et al.* Human host factors required for influenza virus replication. *Nature* **463**, 813-817 (2010).
71. Brass, A.L., *et al.* Identification of host proteins required for HIV infection through a functional genomic screen. *Science* **319**, 921-926 (2008).
72. Li, Q., *et al.* A genome-wide genetic screen for host factors required for hepatitis C virus propagation. *Proc Natl Acad Sci U S A* **106**, 16410-16415 (2009).
73. Shapira, S.D., *et al.* A physical and regulatory map of host-influenza interactions reveals pathways in H1N1 infection. *Cell* **139**, 1255-1267 (2009).
74. Damm, E.M. & Pelkmans, L. Systems biology of virus entry in mammalian cells. *Cell Microbiol* **8**, 1219-1227 (2006).
75. Baek, D., *et al.* The impact of microRNAs on protein output. *Nature* **455**, 64-71 (2008).
76. Tzur, G., *et al.* Comprehensive gene and microRNA expression profiling reveals a role for microRNAs in human liver development. *PLoS One* **4**, e7511 (2009).
77. Lim, L.P., *et al.* Microarray analysis shows that some microRNAs downregulate large numbers of target mRNAs. *Nature* **433**, 769-773 (2005).
78. Gutierrez, N.C., *et al.* Deregulation of microRNA expression in the different genetic subtypes of multiple myeloma and correlation with gene expression profiling. *Leukemia* **24**, 629-637 (2010).
79. Hilleman, M.R. & Werner, J.H. Recovery of new agent from patients with acute respiratory illness. *Proc Soc Exp Biol Med* **85**, 183-188 (1954).
80. Philipson, L. Adenovirus--an eternal archetype. *Curr Top Microbiol Immunol* **199 (Pt 1)**, 1-24 (1995).
81. McConnell, M.J. & Imperiale, M.J. Biology of adenovirus and its use as a vector for gene therapy. *Hum Gene Ther* **15**, 1022-1033 (2004).

82. Tatsis, N. & Ertl, H.C. Adenoviruses as vaccine vectors. *Mol Ther* **10**, 616-629 (2004).
83. Benkö, M., Harrach, B. & Russell, W.C. Family Adenoviridae. in *Virus Taxonomy: classification and nomenclature of viruses. Seventh report of the International Committee on Taxonomy of Viruses* (eds. Van Regenmortel, M.H.V.*, et al.*) 227-238 (Academic Press, San Diego, 2000).
84. Walsh, M.P.*, et al.* Computational Analysis Identifies Human Adenovirus Type 55 as a Re-emergent Acute Respiratory Disease Pathogen. *J Clin Microbiol* (2009).
85. Grubb, B.R.*, et al.* Inefficient gene transfer by adenovirus vector to cystic fibrosis airway epithelia of mice and humans. *Nature* **371**, 802-806 (1994).
86. Pickles, R.J.*, et al.* Limited entry of adenovirus vectors into well-differentiated airway epithelium is responsible for inefficient gene transfer. *J Virol* **72**, 6014-6023 (1998).
87. Walters, R.W.*, et al.* Basolateral localization of fiber receptors limits adenovirus infection from the apical surface of airway epithelia. *J Biol Chem* **274**, 10219-10226 (1999).
88. Zabner, J., Freimuth, P., Puga, A., Fabrega, A. & Welsh, M.J. Lack of high affinity fiber receptor activity explains the resistance of ciliated airway epithelia to adenovirus infection. *J Clin Invest* **100**, 1144-1149 (1997).
89. Chillon, M.*, et al.* Group D adenoviruses infect primary central nervous system cells more efficiently than those from group C. *J Virol* **73**, 2537-2540 (1999).
90. Havenga, M.J.*, et al.* Improved adenovirus vectors for infection of cardiovascular tissues. *J Virol* **75**, 3335-3342. (2001).
91. Havenga, M.J.*, et al.* Exploiting the natural diversity in adenovirus tropism for therapy and prevention of disease. *J Virol* **76**, 4612-4620. (2002).
92. Knaan-Shanzer, S.*, et al.* Highly efficient targeted transduction of undifferentiated human hematopoietic cells by adenoviral vectors displaying fiber knobs of subgroup B. *Hum. Gene Ther.* **12**, 1989-2005 (2001).
93. Rea, D.*, et al.* Highly efficient transduction of human monocyte-derived dendritic cells with subgroup B fiber-modified adenovirus vectors enhances transgene-encoded antigen presentation to cytotoxic T cells. *J. Immunol.* **166**, 5236-5244 (2001).
94. Shayakhmetov, D.M., Papayannopoulou, T., Stamatoyannopoulos, G. & Lieber, A. Efficient gene transfer into human CD34(+) cells by a retargeted adenovirus vector. *J Virol* **74**, 2567-2583 (2000).
95. Wadell, G. Adenoviruses. in *Encyclopedia of virology*, Vol. 1 (eds. Webster, R.G. & Granoff, A.) 1-7 (Academic Press Inc., New York, 1994).
96. Horwitz, M. The Adenoviridae and their replication. in *Virology*, Vol. 2 (ed. Fields, B.N.a.K., D. M.) 1679-1721 (Raven Press, New York, 1990).
97. Leen, A.M. & Rooney, C.M. Adenovirus as an emerging pathogen in immunocompromised patients. *Br J Haematol* **128**, 135-144 (2005).
98. Ryan, M.A.*, et al.* Large epidemic of respiratory illness due to adenovirus types 7 and 3 in healthy young adults. *Clin. Infect. Dis.* **34**, 577-582 (2002).
99. Muruve, D.A. The innate immune response to adenovirus vectors. *Hum Gene Ther* **15**, 1157-1166 (2004).
100. Waye, M.M.Y. & Sing, C.W. Anti-Viral Drugs for Human Adenoviruses. *Pharmaceuticals* **3**, 3343-3354 (2010).
101. Hoffman, J.A., Shah, A.J., Ross, L.A. & Kapoor, N. Adenoviral infections and a prospective trial of cidofovir in pediatric hematopoietic stem cell transplantation. *Biol Blood Marrow Transplant* **7**, 388-394 (2001).
102. Kinchington, P.R., Araullo-Cruz, T., Vergnes, J.P., Yates, K. & Gordon, Y.J. Sequence changes in the human adenovirus type 5 DNA polymerase associated with resistance to the broad spectrum antiviral cidofovir. *Antiviral Res* **56**, 73-84 (2002).
103. Morfin, F.*, et al.* In vitro susceptibility of adenovirus to antiviral drugs is species-dependent. *Antivir Ther* **10**, 225-229 (2005).
104. Romanutti, C., Bruttomesso, A.C., Castilla, V., Galagovsky, L.R. & Wachsman, M.B. Anti-adenovirus activity of epiandrosterone and dehydroepiandrosterone derivatives. *Chemotherapy* **56**, 158-165 (2010).
105. D'Cruz, O.J. & Uckun, F.M. Stampidine: a selective oculo-genital microbicide. *J Antimicrob Chemother* **56**, 10-19 (2005).
106. Cawood, R.*, et al.* Use of tissue-specific microRNA to control pathology of wild-type adenovirus without attenuation of its ability to kill cancer cells. *PLoS Pathog* **5**, e1000440 (2009).

107. Ylosmaki, E., *et al.* Generation of a conditionally replicating adenovirus based on targeted destruction of E1A mRNA by a cell type-specific MicroRNA. *J Virol* **82**, 11009-11015 (2008).
108. Shenk, T. Adenoviridae: the viruses and their replication. in *Virology* (eds. Fields, B.N., Howley, P.M., Griffin, D.E. & al., e.) 2265-2300 (Lippincott-Raven Publisher, Philadelphia, 2001).
109. Russell, W.C. Adenoviruses: update on structure and function. *J Gen Virol* **90**, 1-20 (2009).
110. Rux, J.J. & Burnett, R.M. Adenovirus structure. *Hum Gene Ther* **15**, 1167-1176 (2004).
111. Liu, H., *et al.* Atomic structure of human adenovirus by cryo-EM reveals interactions among protein networks. *Science* **329**, 1038-1043 (2010).
112. Reddy, V.S., Natchiar, S.K., Stewart, P.L. & Nemerow, G.R. Crystal structure of human adenovirus at 3.5 A resolution. *Science* **329**, 1071-1075 (2010).
113. Harrison, S.C. Virology. Looking inside adenovirus. *Science* **329**, 1026-1027 (2010).
114. Stewart, P.L., Fuller, S.D. & Burnett, R.M. Difference imaging of adenovirus: bridging the resolution gap between X-ray crystallography and electron microscopy. *EMBO J* **12**, 2589-2599 (1993).
115. Colby, W.W. & Shenk, T. Adenovirus type 5 virions can be assembled in vivo in the absence of detectable polypeptide IX. *J Virol* **39**, 977-980 (1981).
116. Ghosh-Choudhury, G., Haj-Ahmad, Y. & Graham, F.L. Protein IX, a minor component of the human adenovirus capsid, is essential for the packaging of full length genomes. *EMBO J* **6**, 1733-1739 (1987).
117. Shenk, T. & Flint, J. Transcriptional and transforming activities of the adenovirus E1A proteins. *Adv Cancer Res* **57**, 47-85 (1991).
118. White, E., Cipriani, R., Sabbatini, P. & Denton, A. Adenovirus E1B 19-kilodalton protein overcomes the cytotoxicity of E1A proteins. *J Virol* **65**, 2968-2978 (1991).
119. Schaack, J., Ho, W.Y., Freimuth, P. & Shenk, T. Adenovirus terminal protein mediates both nuclear matrix association and efficient transcription of adenovirus DNA. *Genes Dev* **4**, 1197-1208 (1990).
120. Pronk, R. & van der Vliet, P.C. The adenovirus terminal protein influences binding of replication proteins and changes the origin structure. *Nucleic Acids Res* **21**, 2293-2300 (1993).
121. Ramachandra, M. & Padmanabhan, R. Expression, nuclear transport, and phosphorylation of adenovirus DNA replication proteins. *Curr Top Microbiol Immunol* **199 (Pt 2)**, 50-88 (1995).
122. King, A.J., Teertstra, W.R., Blanco, L., Salas, M. & van der Vliet, P.C. Processive proofreading by the adenovirus DNA polymerase. Association with the priming protein reduces exonucleolytic degradation. *Nucleic Acids Res* **25**, 1745-1752 (1997).
123. Klessig, D.F. & Grodzicker, T. Mutations that allow human Ad2 and Ad5 to express late genes in monkey cells map in the viral gene encoding the 72K DNA binding protein. *Cell* **17**, 957-966 (1979).
124. Monaghan, A., Webster, A. & Hay, R.T. Adenovirus DNA binding protein: helix destabilising properties. *Nucleic Acids Res* **22**, 742-748 (1994).
125. Zijderveld, D.C. & van der Vliet, P.C. Helix-destabilizing properties of the adenovirus DNA-binding protein. *J Virol* **68**, 1158-1164 (1994).
126. Lutz, P. & Kedinger, C. Properties of the adenovirus IVa2 gene product, an effector of late-phase-dependent activation of the major late promoter. *J Virol* **70**, 1396-1405 (1996).
127. Ginsberg, H.S., *et al.* Role of early region 3 (E3) in pathogenesis of adenovirus disease. *Proc Natl Acad Sci U S A* **86**, 3823-3827 (1989).
128. Lichtenstein, D.L., Krajcsi, P., Esteban, D.J., Tollefson, A.E. & Wold, W.S. Adenovirus RIDbeta subunit contains a tyrosine residue that is critical for RID-mediated receptor internalization and inhibition of Fas- and TRAIL-induced apoptosis. *J Virol* **76**, 11329-11342 (2002).
129. Cianciola, N.L. & Carlin, C.R. Adenovirus RIDalpha protein reveals novel autophagic mechanism that regulates cholesterol homeostasis. *Autophagy* **6**, 296-298 (2010).
130. Bridge, E., Medghalchi, S., Ubol, S., Leesong, M. & Ketner, G. Adenovirus early region 4 and viral DNA synthesis. *Virology* **193**, 794-801 (1993).

131. Bergelson, J.M.*, et al.* Isolation of a common receptor for Coxsackie B viruses and adenoviruses 2 and 5. *Science* **275**, 1320-1323 (1997).
132. Walters, R.W.*, et al.* Adenovirus fiber disrupts CAR-mediated intercellular adhesion allowing virus escape. *Cell* **110**, 789-799 (2002).
133. Dorner, A.A.*, et al.* Coxsackievirus-adenovirus receptor (CAR) is essential for early embryonic cardiac development. *J Cell Sci* **118**, 3509-3521 (2005).
134. Wickham, T.J., Mathias, P., Cheresh, D.A. & Nemerow, G.R. Integrins alpha v beta 3 and alpha v beta 5 promote adenovirus internalization but not virus attachment. *Cell* **73**, 309-319 (1993).
135. Zhang, Y. & Bergelson, J.M. Adenovirus receptors. *J Virol* **79**, 12125-12131 (2005).
136. Burckhardt, C.J. & Greber, U.F. Virus movements on the plasma membrane support infection and transmission between cells. *PLoS Pathog* **5**, e1000621 (2009).
137. Gazzola, M.*, et al.* A stochastic model for microtubule motors describes the in vivo cytoplasmic transport of human adenovirus. *PLoS Comp Biol* **in revision**(2009).
138. Greber, U.F. & Way, M. A superhighway to virus infection. *Cell* **124**, 741-754 (2006).
139. Meier, O. & Greber, U.F. Adenovirus endocytosis. *J Gene Med* **6 Suppl 1**, S152-163 (2004).
140. Sirena, D.*, et al.* The Human Membrane Cofactor CD46 Is a Receptor for Species B Adenovirus Serotype 3. *J Virol* **78**, 4454-4462 (2004).
141. Fleischli, C.*, et al.* Species B adenovirus serotypes 3, 7, 11 and 35 share similar binding sites on the membrane cofactor protein CD46 receptor. *J Gen Virol* **88**, 2925-2934 (2007).
142. Segerman, A.*, et al.* Adenovirus type 11 uses CD46 as a cellular receptor. *J Virol* **77**, 9183-9191 (2003).
143. Gaggar, A., Shayakhmetov, D.M. & Lieber, A. CD46 is a cellular receptor for group B adenoviruses. *Nat Med* **9**, 1408-1412 (2003).
144. Lemckert, A.A.*, et al.* Generation of a novel replication-incompetent adenoviral vector derived from human adenovirus type 49: manufacture on PER.C6 cells, tropism and immunogenicity. *J Gen Virol* **87**, 2891-2899 (2006).
145. Wu, E. & Nemerow, G.R. Virus yoga: the role of flexibility in virus host cell recognition. *Trends Microbiol* **12**, 162-169 (2004).
146. Liszewski, M.K., Kemper, C., Price, J.D. & Atkinson, J.P. Emerging roles and new functions of CD46. *Springer Semin Immunopathol* **27**, 345-358 (2005).
147. Russell, S. CD46: a complement regulator and pathogen receptor that mediates links between innate and acquired immune function. *Tissue Antigens* **64**, 111-118 (2004).
148. Fleischli, C.*, et al.* The distal short consensus repeats 1 and 2 of the membrane cofactor protein CD46 and their distance from the cell membrane determine productive entry of species B adenovirus serotype 35. *J Virol* **79**, 10013-10022 (2005).
149. Gaggar, A., Shayakhmetov, D.M., Liszewski, M.K., Atkinson, J.P. & Lieber, A. Localization of regions in CD46 that interact with adenovirus. *J Virol* **79**, 7503-7513 (2005).
150. Sakurai, F.*, et al.* The short consensus repeats 1 and 2, not the cytoplasmic domain, of human CD46 are crucial for infection of subgroup B adenovirus serotype 35. *J Control Release* **113**, 271-278 (2006).
151. Short, J.J.*, et al.* Adenovirus serotype 3 utilizes CD80 (B7.1) and CD86 (B7.2) as cellular attachment receptors. *Virology* **322**, 349-359 (2004).
152. Short, J.J., Vasu, C., Holterman, M.J., Curiel, D.T. & Pereboev, A. Members of adenovirus species B utilize CD80 and CD86 as cellular attachment receptors. *Virus Res* (2006).
153. Marttila, M.*, et al.* CD46 is a cellular receptor for all species B adenoviruses except types 3 and 7. *J Virol* **79**, 14429-14436 (2005).
154. Wang, H.*, et al.* Identification of CD46 binding sites within the adenovirus serotype 35 fiber knob. *J Virol* **81**, 12785-12792 (2007).
155. Wang, H.*, et al.* Desmoglein 2 is a receptor for adenovirus serotypes 3, 7, 11 and 14. *Nat Med* **17**, 96-104 (2011).
156. Dorn, A.*, et al.* Identification of specific cellular genes up-regulated late in adenovirus type 12 infection. *J Virol* **79**, 2404-2412 (2005).

157. Granberg, F., Svensson, C., Pettersson, U. & Zhao, H. Modulation of host cell gene expression during onset of the late phase of an adenovirus infection is focused on growth inhibition and cell architecture. *Virology* **343**, 236-245 (2005).
158. Granberg, F., Svensson, C., Pettersson, U. & Zhao, H. Adenovirus-induced alterations in host cell gene expression prior to the onset of viral gene expression. *Virology* **353**, 1-5 (2006).
159. Zhao, H., Granberg, F. & Pettersson, U. How adenovirus strives to control cellular gene expression. *Virology* **363**, 357-375 (2007).
160. Miller, D.L., Myers, C.L., Rickards, B., Coller, H.A. & Flint, S.J. Adenovirus type 5 exerts genome-wide control over cellular programs governing proliferation, quiescence, and survival. *Genome biology* **8**, R58 (2007).
161. Scibetta, A.G., Copier, J., Barrett, A., Chaplin, T. & Taylor-Papadimitriou, J. Gene expression changes induced by a recombinant E1-/E3- adenovirus type 5 vector in human mammary epithelial cells. *Intervirology* **48**, 350-361 (2005).
162. Rao, X.M.*, et al.* Gene expression profiles of normal human lung cells affected by adenoviral E1B. *Virology* **350**, 418-428 (2006).
163. Hartman, Z.C.*, et al.* Adenovirus infection triggers a rapid, MyD88-regulated transcriptome response critical to acute-phase and adaptive immune responses in vivo. *J Virol* **81**, 1796-1812 (2007).
164. Hartman, Z.C., Black, E.P. & Amalfitano, A. Adenoviral infection induces a multi-faceted innate cellular immune response that is mediated by the toll-like receptor pathway in A549 cells. *Virology* **358**, 357-372 (2007).
165. Ma, Y. & Mathews, M.B. Structure, function, and evolution of adenovirus-associated RNA: a phylogenetic approach. *J Virol* **70**, 5083-5099 (1996).
166. Lu, S. & Cullen, B.R. Adenovirus VA1 noncoding RNA can inhibit small interfering RNA and MicroRNA biogenesis. *J Virol* **78**, 12868-12876 (2004).
167. Thimmappaya, B., Weinberger, C., Schneider, R.J. & Shenk, T. Adenovirus VAI RNA is required for efficient translation of viral mRNAs at late times after infection. *Cell* **31**, 543-551 (1982).
168. Sano, M., Kato, Y. & Taira, K. Sequence-specific interference by small RNAs derived from adenovirus VAI RNA. *FEBS Lett* **580**, 1553-1564 (2006).
169. Bhat, R.A. & Thimmappaya, B. Adenovirus mutants with DNA sequence perturbations in the intragenic promoter of VAI RNA gene allow the enhanced transcription of VAII RNA gene in HeLa cells. *Nucleic Acids Res* **12**, 7377-7388 (1984).
170. Bhat, R.A. & Thimmappaya, B. Two small RNAs encoded by Epstein-Barr virus can functionally substitute for the virus-associated RNAs in the lytic growth of adenovirus 5. *Proc Natl Acad Sci U S A* **80**, 4789-4793 (1983).
171. Xu, N., Segerman, B., Zhou, X. & Akusjarvi, G. Adenovirus virus-associated RNAII-derived small RNAs are efficiently incorporated into the rna-induced silencing complex and associate with polyribosomes. *J Virol* **81**, 10540-10549 (2007).
172. Siekierka, J., Mariano, T.M., Reichel, P.A. & Mathews, M.B. Translational control by adenovirus: lack of virus-associated RNAI during adenovirus infection results in phosphorylation of initiation factor eIF-2 and inhibition of protein synthesis. *Proc Natl Acad Sci U S A* **82**, 1959-1963 (1985).
173. Kitajewski, J.*, et al.* Adenovirus VAI RNA antagonizes the antiviral action of interferon by preventing activation of the interferon-induced eIF-2 alpha kinase. *Cell* **45**, 195-200 (1986).
174. O'Malley, R.P., Mariano, T.M., Siekierka, J. & Mathews, M.B. A mechanism for the control of protein synthesis by adenovirus VA RNAI. *Cell* **44**, 391-400 (1986).
175. Clarke, P.A., Schwemmle, M., Schickinger, J., Hilse, K. & Clemens, M.J. Binding of Epstein-Barr virus small RNA EBER-1 to the double-stranded RNA-activated protein kinase DAI. *Nucleic Acids Res* **19**, 243-248 (1991).
176. Clarke, P.A., Sharp, N.A. & Clemens, M.J. Translational control by the Epstein-Barr virus small RNA EBER-1. Reversal of the double-stranded RNA-induced inhibition of protein synthesis in reticulocyte lysates. *Eur J Biochem* **193**, 635-641 (1990).
177. Swaminathan, S., Huneycutt, B.S., Reiss, C.S. & Kieff, E. Epstein-Barr virus-encoded small RNAs (EBERs) do not modulate interferon effects in infected lymphocytes. *J Virol* **66**, 5133-5136 (1992).

178. Aparicio, O.*, et al.* Adenovirus VA RNA-derived miRNAs target cellular genes involved in cell growth, gene expression and DNA repair. *Nucleic Acids Res* **38**, 750-763 (2010).

PUBLICATION AND MANUSCRIPTS

Avidity binding of human adenovirus serotypes 3 and 7 to the membrane cofactor CD46 triggers infection

Hung V. Trinh[1,2†], Guillaume Lesage[1,2†], Venus Chennamparampil[1], Christoph J. Burckhardt[1‡], Stefan Schauer[3], Menzo Havenga[4§], Urs F. Greber[1] and Silvio Hemmi[1*]

[1]*Institute of Molecular Life Sciences, University of Zurich, Winterthurerstrasse 190, CH-8057 Zurich, Switzerland*

[2]*Life Science Zurich Graduate School, Molecular Life Science Program*

[3]*Functional Genomics Center Zurich, University of Zurich, Winterthurerstrasse 190, Zurich 8057, Switzerland*

[4]*Crucell Holland BV, Archimedesweg 4, 2333 CN Leiden, The Netherlands*

[†]Equal contribution

__Corresponding author__:* Dr. Silvio Hemmi, *Institute of Molecular Life Sciences Zurich, Winterthurerstrasse 190, CH-8057 Zurich, Switzerland; Phone: +41 44 635 3120; Fax: +41 44 635 6811; E-mail: silvio.hemmi@imls.uzh.ch*

[‡]*Present address: Department of Cell Biology, Harvard Medical School, Boston, Massachusetts 02115, USA*

[§]*Present address: Batavia Bioservices BV, Zernikedreef 9, 2333 CK Leiden, The Netherlands*

Abbreviations: Ad, adenovirus; CAR, Coxsackie virus B and Ad receptor; FK, fiber knob; MFI, mean fluorescence intensity; MOI, multiplicity of infection; MV, measles virus; p.i. post infection; ROI region of interest; RU, resonance units; SPR, surface plasma resonance; vp, virus particle

Running title: Species B adenovirus receptor

Abstract: 249 words
Total text: 8,874 words

Abstract

The species B human adenoviruses (short Ad) debatably infect epithelial and hematopoietic cells upon attaching to the CD46 or desmoglein 2 receptor by one or several of their twelve fiber knob trimers (FK). The B1 viruses Ad3/7/16/21/50 acutely infect eyes and respiratory organs, and the B2 viruses Ad11/14/34/35 kidney and urinary tracts. Receptors commonly capture multivalent ligands by avidity, as measured for example by increased ligand binding with increased receptor density. To test if avidity explains the controversy of CD46 receptor function in species B1 infections, we measured the dissociation constants (K_D) of Ad3/7-FK on immobilized CD46 using biosensors. At high CD46 densities, Ad3/7-FK had K_D values 15-fold higher than Ad11/35-FK, and poorly bound to low density CD46, unlike Ad11/35-FK. The cell surface levels of ectopically expressed CD46 in CHO or human M010119 melanoma cells lacking desmoglein 2 positively correlated with Ad3/7 infections, while Ad11/35 infections of CD46-positive cells were independent of CD46 levels. Soluble CD46 crosslinked with anti-CD46 antibodies strongly blocked Ad3/7/11/35 infections, while soluble CD46 alone blocked Ad11/35 only. Soluble Ad3/7-FKs poorly inhibited Ad3/7 infection of CHO-CD46 cells, unlike Ad11/35-FKs, which efficiently blocked Ad3/7/11/35 illustrating that Ad3/7-FKs bind with lower affinity to CD46 than Ad11/35-FKs. Ad3/7-FKs, nonetheless, reduced the time of fluorescence recovery after photo-bleaching of eGFP-CD46, and inhibited Ad3/7 infection of A549 cells expressing high levels of CD46. Together, these data show that avidity binding of Ad3/7 to CD46 leads to infection of CD46-positive cells, and provides a paradigm for receptor recruitment by a multivalent ligand.

Introduction

Human *Adenoviridae* are comprised of 55 types, classified into seven species, A to G (http://www.vmri.hu/~harrach/AdVtaxlong.htm), based on genome sequence comparison, hemagglutination and additional features. The B1 viruses Ad3, Ad7, Ad16, Ad21, Ad50 (short Ad3/7/16/21/50) predominantly infect the upper respiratory tract, whereas the B2 viruses Ad11/14/34/35 are associated with kidney and urinary tract infections with fatal outcome in immunocompromised patients (27, 50, 60). Recent epidemiological reports described the reemergence of several of these virus types associated with outbreaks of respiratory disease (5, 29, 35, 68). The tropism of species B viruses is broader than that of the C species, and includes cancer cells, dendritic cells and hematopoietic stem cells. This feature makes the B species interesting vectors for gene therapy and vaccination approaches (48).

Ads attach to their host cells by binding of the trimeric fiber protein to a cellular surface receptor. The fiber protein consists of a tail for anchorage to the penton base, a shaft of variable length, and a globular fiber knob (FK). The latter is responsible for the binding of the virus particle to a primary attachment receptor (38). Species B Ads bind a different cell surface receptor than most of the other species members (67). CD46 has been identified as a cellular attachment receptor for species B serotypes, including Ad11 (53), Ad35 (14) and Ad3 (55), and species D Ad37 and Ad49 (28, 65). The widely expressed CD46 belongs to a family of regulators, which prevent complement activation on autologous tissue (30). CD46 also links innate and adaptive immunity in macrophages and lymphocytes (47). The extracellular domain of CD46 consists of four amino-terminal copies of an approximately 60-amino-acid structural motif, termed short consensus repeat (SCR), followed by one to three Ser-Thr-Pro (STP) rich domain(s), a short region of unknown function proximal to the cell membrane, a transmembrane spanning domain, and a carboxy-terminal cytoplasmic tail. Antibody blocking assays, together with infectivity and mutagenesis studies revealed that binding of human Ad35 to CD46 occurs through the N-terminal two SCR I-II domains (12, 15, 49).

Whether CD46 functions as an attachment receptor for all species B types has been controversial. Virus competition, CD46 antibody blocking, and siRNA knock down of CD46 suggested that more than one receptor exists for species B Ads (14, 18, 34, 52, 53, 55, 59). It was suggested that all species B Ads except Ad3 and Ad7 would utilize CD46, and all serotypes including Ad3 and Ad7 would bind to a second, so far elusive common receptor (sBAR) (34, 52). Another group proposed an alternative classification, where group I members (Ad16/21/35/50) would almost exclusively use CD46, while group II members (Ad3/7/14) would not use CD46 but receptor X, more recently suggested to be desmoglein 2, and the only member of group III (Ad11p) would be able to use both receptors (59, 61). Both classifications contrast, however, with findings by others, who reported functional utilization of CD46 by Ad3 and Ad7 in rodent cells ectopically expressing CD46 (11, 12, 19, 55, 56).

Affinity analysis of monovalent interactions of different species B FKs to CD46 SCR I-II revealed a broad range of affinities, with similar dissociation constants (K_D) for Ad11 and Ad35-FK (Ad11/35-FK) in the range of 5 to 19 nM, but strongly increased K_D values of 284 nM for Ad21-FK and 437 nM for Ad16-FK, and an about 2,000-fold reduced affinity for both, Ad7-FK and Ad14-FK to CD46 SCR I-II, compared to Ad11-FK (8, 42, 43). The crystal structures of FKs for Ad3 (9), Ad35 (41, 62), Ad16 (42), and Ad7 and Ad14 (43) have revealed a generally conserved overall fold and trimeric organization. Interestingly, the different FKs have low sequence identity, especially at the surface loops, which mediate binding to CD46, as indicated by co-crystal structures of CD46 SCR I-II with Ad11-FK (44), or Ad21-FK (8). These crystal structures also suggested interactions of the trimeric fiber molecule with three CD46 molecules, albeit involving substantial differences in the number and types of contacts. The binding surface on CD46 SCR I-II for Ad11-FK comprises a large continuous area of 1,681 $Å^2$, with three main contact points composed of fiber knob DG, HI and the IJ loop residues. A more recent co-crystal structure of Ad11-FK complexed to an extended CD46 SCR I-IV confirmed the involvement of the DG and HI loops, but not of the IJ loop (45). Together, this wealth of structural evidence indicates that there are no central binding motifs among species B Ads, which would explain the macroscopic observations that there is a wide range of affinities for CD46 between the different FKs (8, 42, 62).

Here we tested the hypothesis that avidity effects determine if the low affinity CD46-binders Ad3/7-FK attach to CD46, and thereby allow these viruses to use CD46 as an entry receptor. We used biosensor measurements to demonstrate that affinities of Ad3/7-FKs to immobilized CD46 are enhanced at increased receptor densities, and Ad3/7 infection of CD46-negative CHO or human melanoma cells increased with increasing levels of ectopic CD46. We further show that multimerized soluble CD46 blocked Ad3/7 infection, and that Ad3/7-FK reduced fluorescence recovery after photo-bleaching of eGFP-CD46 and reduced Ad3/7 infection in A549 cells expressing high levels of CD46. These data argue that CD46 is a receptor for all species B adenoviruses on cells provided that it is present at sufficient levels. Ad3/7/14 can hence use CD46 or possibly desmoglein 2 as functional receptors.

Materials and Methods

Viruses and cells.

Ad3CMV-eGFP, Ad7CMV-eGFP Ad11CMV-eGFP and Ad35CMV-eGPF containing the CMV-eGFP expression cassette in the deleted E1 region were prepared at concentrations of $7.1x10^{11}$, $1.6x10^{11}$, $6.6x10^{11}$ $1.3x10^{12}$ virus particles (vp)/ml and have been described previously (11, 12). Ad3 (prototype strain GB), Ad7 (prototype strain Gomen), Ad11p and Ad35 (Holden strain) were radio labeled as described earlier (12). Specific activities were in the range of 2.6×10^{-5} to 4.9×10^{-5} cpm/vp.

Chinese hamster cell lines CHO-K1 and CHO-15B6 (containing a mutation in the N-acetylglucosamininyl-transferase 1), the human 293T and 911 embryonic kidney cells, and the A549 lung carcinoma cells were grown in Dulbecco's modified Eagle's medium (DMEM) plus 8% fetal bovine serum (FBS). The primary human melanoma cell cultures M010119 were grown in RPMI 1640 plus 8% FBS as described earlier (51). CHO-CD46 cell lines stably expressing the BC1 splice isoform were generated as described for the BHK-CD46 cells (55). For stable transfection of CHO-15B6 and M010119 cells with the N-terminal eGFP-tagged CD46-encoding cDNA (eGFP-CD46), a PCR-amplified CD46 sequence was cloned into pcDNA3.1-CARSP-eGFP-CAR (Burckhardt et al, in preparation), replacing the mature CAR cDNA. In the resulting construct, the 19 amino acid residues of the human CAR signal peptide sequence were followed by two spacer residues, 239 residues of eGFP, ten additional spacer residues, and 344 residues of the mature CD46 BC1 isoform. To avoid eGFP-induced dimerization of the tagged CD46, an A206K mutant of eGFP was utilized (66). Following selection in DMEM plus 8% FBS and 0.8 mg/ml G418, individual clones were picked and screened giving rise to the limiting dilution clone CHO-eGFP-CD46#33.5. To generate human melanoma M010119 and lung carcinoma A549 cells expressing eGFP-CD46, a lentiviral expression system was used. For this, the eGFP-CD46 cDNA was subcloned into the lentiviral pBlasti vector (25), and lentiviral vectors were generated by transient transfection in 293T cells. M010119 and A549 cells transduced with lentiviral vector pBlasti-eGFP-CD46 were selected in blasticidin-containing

medium at 4 µg / ml. Resulting bulk cultures M010119-eGFP-CD46#8 and A549-eGFP-CD46#2 revealed homogenous CD46 expression.

Immunoreagents.

Cytofluorometric analysis, CD46-specific antibodies and secondary fluorochrome conjugates have been described previously (12, 55). The hybridoma cell line secreting the MCI20.6 anti-CD46 antibody was a generous gift from Denis Gerlier (37). Monoclonal 8E5-anti desmoglein 2 was purchased from Santa Cruz Inc., and goat anti-human IgG-Fc from BETHYL Lab. Inc..

Virus binding and transduction assays.

Binding experiments including radio-labeled Ads were performed as described previously (12). For eGFP expression analysis, triplicates of 10^5 cells were seeded in 12-well plates. After incubation for 3 h at 37°C, 5% CO_2, the cells were infected with recombinant eGFP-expressing Ads at virus concentrations of 10, 100, or 1,000 vp/cell. Medium was replaced 5 h p.i., and cells were analyzed two days p.i. by flow cytometric analysis (Cytomics FC 500; Beckman Coulter).

For FK competition experiments, cells were seeded in triplicate 12-well plates and were allowed to adhere as above. After 3 h, the medium was removed and the cells were washed with cold PBS. For blocking with FK proteins, serial 5-fold dilutions of the different FKs were prepared in PBS, resulting in concentrations of 5,000, 1,000, 200, 40, and 8 ng/ml. 500 µl of FK dilutions were added to the cells and incubated for 1 h on ice under constant shaking. Subsequently, eGFP-encoding Ad vectors were added and incubated for 1 h. The amount of virus added was optimized in preceding experiments and was adjusted such that for all five eGFP-expressing vectors, similar reporter expression levels in the range of 100 to 500 were obtained by FACS measurement. Thus, for A549 cell transduction, Ad3-, 5-, 7-, 11-, and 35-eGFP vectors were used at 14,800, 2,825, 8,200, 1,314 and 2,540 vp/cell, respectively. For

CHO-CD46#2, the virus input was adjusted to 29,600, 2,825, 8,200, 657 and 1,088 vp/cell, respectively. The cells were washed twice with cold PBS and were returned to standard cell culture conditions. Analysis of cells was performed two days p.i., as described above. For competition experiments including recombinant CD46ex-huFc, FK proteins were replaced with the indicated concentrations of CD46ex-huFc or CARex-huFc. In case of including cross-linking of CD46ex-huFc and CARex-huFc, the adapter proteins were pre-incubated on ice with goat anti-human IgG antibody for 30 min before adding to the cells. Statistical evaluation was performed using Student's *t* test.

Generation of recombinant soluble Ad receptor and fiber knob proteins. Production of the soluble CD46ex-huFc and CARex-huFc has been described earlier (10, 55). CD46ex-huFc comprises 295 amino acids of the mature extracellular domain including all SCR I-IV domains, the STP of BC1, plus the short region of unknown function, fused to the 232 amino acids of the human IgG1-Fc domain including hinge, CH2 and CH3 regions. Production of CD46-SCR I-II consisting of 145 amino acids, including a N-terminal his-tag and spacer, has been described in (12). CARex-huFc protein comprises the extracellular domain of the Coxsackie virus B and Ad receptor fused to the human IgG1-Fc domain. The five recombinant FKs derived from Ad3, 5, 7, 11, and 35 were produced using the Bac-to-Bac baculovirus expression system (pFastBac, Stratagene). All FKs contained a N-terminal 6xhis-tag used for single step Ni-NTA-agarose affinity chromatography, followed by the recognition site for TEV protease. FK comprised the fiber sequence residues 114 to 319 for Ad3 (NCBI gene bank ID (GI) 78059423), 384 to 581 for Ad5 (GI: 56160559), 126 to 325 for Ad7 (GI: 51173336), 126 to 325 for Ad11 (GI: 56160807), and 126 to 323 for Ad35 (GI: 56160945). Calculated weights of the FK monomer/trimers were 26.28/78.85, 24.98/74.95, 25.63/76.89, 25.90/77.71, and 25.50/76.50 kDa for FK of Ad3, 5, 7, 11, and 35, respectively.

Fluorescence recovery after photo-bleaching (FRAP).

For FRAP experiments, CHO-eGFP-CD46#33.5 or A549-eGFP-CD46#8 cells were seeded in 6 channel µ-slide IV ibiTreat (ibidi®) at 10,000 cells/well one day prior to analysis. Soluble FKs were then added to the wells at various concentrations ranging from 0.1 to 64 ng/µl and incubated at 37°C for 15 min before recording with confocal microscopy. We noticed that at the concentration of 64 ng/µl, Ad11/35-FKs had a slight toxic effect on the cells, illustrated by blebbing of the membrane rendering experimentation at higher concentration non-physiological. FRAP was performed on a Leica SP5 confocal laser scanning microscope (Leica Microsystems) with the following setup. eGFP was excited using the 476 and 488 nm lines of an Ar laser and emission was recorded in the range of 496 to 560 nm at a pinhole size of one airy disc and a pixel size of 0.13 µm. Bleaching was performed with the built in "FRAP wizard" at a laser power of 80%, while imaging was performed at 6-8%. The imaging procedure was as follows: first 10 images at a speed of 1.314 s/frame to determine the initial fluorescence level, then a square region of interest (ROI) of 3x3 micrometer was bleached twice with a speed of 1.314 s/frame. The initial recovery phase was then monitored by 10 images at the same fast speed followed by a set of 20 images recorded with a 5 s interval to monitor the slow recovery. Finally the series were concluded by 10 images recorded at the speed of 1.314 s/frame to establish the plateau value reached at the end of the recovery. Exposing the ROI twice to 80-100% intensity of the laser was sufficient to generate photo-bleaching of the fluorescent signal in the ROI. The background signal was first measured in an unbleached region outside the cell and subtracted, and second, the signal was normalized with an unbleached control area on the same cell. The intensity values were displayed relative to pre-bleach values obtained from the first 10 frames. The fluorescence recovery curves were fitted using a least squares method applying a hyperbole function: $\text{Signal}_{\text{normalized}}(t) = a+b*t/(t_{½}+t)$, where a is the offset of the curve after bleaching and b is the amplitude of recovery at the end of the experiment and $t_{1/2}$ is the half maximum recovery time. Mean and standard error of the mean were obtained from fits to single recovery curves.

Surface plasmon resonance (SPR) analysis for kinetics/affinity between CD46 and Ad-FKs

SPR experiments were performed on a Biacore T100 system (GE Healthcare) at 25°C equipped with a CM5 sensor chip. All reagents including amine-coupling kit, HBS-P+ and CM5 chips were purchased from Biacore (GE Healthcare). Buffer HBS-P+ pH 7.4 (10 mM HEPES, pH 7.4, 150 mM NaCl, 0.05% (v/v) Surfactant P20) was used as running buffer for the entire measurement. Each CM5 chip contained four flow cells, designated Fc1-Fc4. The Fc2/Fc4 were used to immobilize the CD46ex-huFc ligand, while Fc1/Fc3 were used to immobilize the CARex-huFc ligand. The immobilization procedure included three steps; surface activation by using a 1:1 mix of 0.4 M 1-ethyl-3-(3-dimethylaminopropyl)-carbodiimide in water (EDC) and 0.1 M N-hydroxysuccinimide in water (NHS) for 420 s with a flow rate of 5 µl/min, immobilization of 0.12 µM ligands in 10 mM sodium acetate pH 4.0 buffer, and deactivation of excess reactive groups by using 1 M ethanolamine-HCl pH 8.0 for 420 s with a flow rate of 5 µl/min. Following completion of immobilization, the sensor chip was conditioned three times with 50 mM NaOH to stabilize the surface. For initial binding assays, Ad3-, 11- and 35-FK analytes were injected at 18.75 and 150 nM, and Ad7-FK at 11.07 and 88.59 nM in HBS-P+ buffer at either 30 or 50 µl/min using a contact time of 240 or 280 s. For kinetic studies, Ad3, 7, 11 and 35 FK analytes were injected at 0.27, 0.82, 2.47, 7.41, 22.22 and 66.67 nM in HBS-P+ buffer at either 30 or 50 µl/min using a contact time of 300 or 360 s and a dissociation time of 3,600 s. After each binding cycle, the CM5 surface chip was regenerated by injection of 3 M $MgCl_2$ for 30 to 45 s, followed NaOH in a range of 4–50 mM for 20 s. All analyte concentrations were repeated twice and the obtained sensograms were corrected by subtracting the data from the reference flow cell and from blank buffer injections (double referencing).

Kinetic/affinity analysis of FK binding to immobilized CD46 was performed using three models in combination with the Biacore T100 evaluation software version 2.0.3. A first included a 1:1 fitting model provided by the Biacore T100 evaluation software itself, which failed to describe the obtained binding data satisfyingly. Second, two trivalent models were tested and included the equations described by Lortat-Jacob *et al*. (31) and a variation of the equations described by Fournel *et al*. (13) (Johan Hoebeke,

personal communication). Both trivalent models resulted in reasonable good fitting for Ad11- and 35-FK to immobilized CD46 judged by χ^2 values, but they showed relatively large errors for Ad3- and Ad7-FK binding kinetics. Third, a two-stage reaction model was applied to globally fit the binding data, which provided the lowest χ^2 values for all four FK binding reactions. In this model, analyte (A) binds to ligand (B) to form the complex AB, then complex AB changes to ABx, which cannot dissociate directly to A+B. The net reactions are described by equations 1–6, where σ_{kd1}, σ_{kd2}, σ_{ka1}, and σ_{ka2} are standard deviation for individual k_{d1}, k_{d2}, k_{a1}, and k_{a2}, respectively. σKD is the standard deviation for overall K_D.

$$A + B \underset{kd_1}{\overset{ka_1}{\Leftrightarrow}} AB \underset{kd_2}{\overset{ka_2}{\Leftrightarrow}} ABx \text{ (Eq.1)}$$

$$A = conc$$

$$B[0] = R\max, \frac{dB}{dt} = -(ka_1 * A * B - kd_1 * AB) \text{ (Eq.2)}$$

$$AB[0] = 0, \frac{dAB}{dt} = (ka_1 * A * B - kd_1 * AB) - (ka_2 * AB - kd_2 * ABx) \text{ (Eq.3)}$$

$$ABx[0] = 0, \frac{dABx}{dt} = (ka_2 * AB - kd_2 * ABx) \text{ (Eq.4)}$$

$$\text{Total response}: AB + ABx + RI$$

$$KD = \frac{kd_1}{ka_1}\frac{kd_2}{kd_2 + ka_2} \text{ (Eq.5)}$$

$$\sigma KD = \sqrt{(\frac{kd_2}{ka_1(kd_2 + ka_2)}\partial_{kd_1})^2 + (\frac{kd_1(kd_2 + ka_2) - kd_1kd_2}{ka_1(kd_2 + ka_2)^2}\sigma_{kd_2})^2}$$

$$+(\frac{kd_1kd_2}{ka_1^{\,2}(kd_2 + ka_2)}\sigma_{ka_1})^2 + (\frac{kd_1kd_2}{ka_1(kd_2 + ka_2)}\sigma_{ka_2})^2 \text{ (Eq.6)}$$

Results

Binding and affinity determinations of CD46 to Ad3/7/11/35-FK by surface plasmon resonance.

To characterize species B Ad interactions with CD46 we applied biosensor technology using soluble CD46 and the FKs of Ad3/7/11/35, which were predominantly present in trimeric form as concluded from SDS-PAGE analyses (SFig. 1A, B). Initial Biacore experiments using sensor chips had previously been described for immobilized FKs and monovalent CD46-SCR I-II as soluble analyte thereby avoiding avidity effects of CD46 (8, 42, 43, 62, 63). The SCR I-II domain comprised the binding sites for the FKs (12, 44, 49, 62). Under these conditions, we determined the affinities of Ad11/35-FK to CD46-SCR I-II, and found that they were consistent with a 1:1 (monophasic) binding model, where one surface FK monomer interacted with one soluble CD46-SCR I-II (data not shown). Ad3/7-FK, however, did not bind to immobilized CD46-SCR I-II, most likely due to low affinity of their monomers to CD46-SCRI-II, in agreement with earlier data for Ad7-FK (43).

In a reversed set-up of the SPR measurements we immobilized the extracellular domain of CD46 fused to human Fc (CD46ex-huFc, see 55) to the flexible dextran matrix of the sensor chip and used FKs as analytes. CD46ex-huFc is a disulfide-linked dimer, as suggested by native gel electrophoresis (SFig. 1C), in comparison with SDS-PAGE analyses of the reduced protein of 85 kDa apparent molecular weight (not shown). We first tested if different concentrations of immobilized CD46ex-huFc would give different binding responses for the FKs.

Hereto, flow cell 2 (Fc2) of the CM5 sensor chip was coated with high density of CD46ex-huFc (2,630 resonance units, RU), and the control Fc1 with high density of CARex-huFc (3,431 RU). In a parallel set up, Fc4 was coated with low surface density of CD46ex-huFc (345 RU), and Fc3 with low density of CARex-huFc (278 RU). We then determined the sensograms for Ad3/7/11/35-FK binding to CD46ex-huFc using differential analyses of Fc2-1 and Fc4-3 pairs, respectively. We noticed that higher

concentrations of soluble Ad3/7-FK (150 and 89 nM, respectively) were required than Ad11/35-FK (18.75 nM) to reach equilibrium binding at high CD46ex-huFc density levels (Fig. 1A-D). At equilibrium binding, both Ad3/7-FK and Ad11/35-FK slowly dissociated, indicative for stable complexes. At low CD46ex-huFc density, the Ad11/35-FKs and to a very low extent also Ad7-FK but not Ad3-FK showed detectable binding. The absolute binding values R_{max} varied by factors of 2-3 between Ad3 and Ad7-FK, and Ad11 and Ad35-FK, as well as different technical replicas of the experiments, possibly reflecting different degrees of FK purities and chip conditions.

Combined binding kinetics and affinity measurements were carried out for each of the four FKs. For this, we used three independent measurements in the range of 0.27, 0.82, 2.47, 7.41, 22.22 and 66.67 nM, and two different high-density CD46 biosensor chips of 2,630 RU and 1,121 RU. Both biosensor chips gave similar results (Fig. 1E-H, STable 1). In addition, Ad3-FK binding was found to be independent of the flow rate at the standard flow rate of 30 µl/min and an increased flow rate of 55 µl/min (STable 1), excluding the possibility that the binding reactions were influenced by mass transfer effects (36). The values for the kinetic rate constants were highly reproducible for the individual FKs, with low standard errors for the association and dissociation constants (see Fig. 1E-H, STable 1). The kinetics and binding data could be best fitted to a two-stage reaction model rather than monophasic, or trivalent binding models (see equations in *Materials and Methods*). Modeling of the measured association and dissociation rate constants and R values was carried out based on global fittings for k_{a1}, k_{a2}, k_{d1} and k_{d2}, and local calculations of R_{max}, and % χ^2/R_{max}. All % χ^2/R_{max} values were below 5%. The average apparent K_D values (Table 1) were not significantly different for Ad3-FK (2.48 $x10^{-10}$ M) and Ad7-FK (3.70 $x10^{-10}$ M), whereas the apparent K_D for Ad11-FK and Ad35-FK were 10-15-fold lower (*P*=0.002/0.0669 for Ad3/7 compared to Ad11, and *P*=0.0014/0.063 for Ad3/7 *versus* Ad35) and amounted to 2.46 $x10^{-11}$ and 1.78 $x10^{-11}$ M, respectively. Thus, the 10-15-fold difference between the apparent K_D values for Ad3/7 and Ad11/35 at high CD46 densities deviated considerably from the 2,000-fold differences of K_D reported for the monovalent CD46 binding to Ad7-FK and Ad11-FK (43). Since the measurements were performed using similar set ups, this suggests that at high surface densities of CD46, trimeric FK

interacts with two or even three CD46 binding sites and the resulting avidity effects overcome low affinity restrictions of single FK–CD46 interactions.

Increasing ectopic expression of CD46 leads to enhanced transduction of adenovirus species B Ad3, 7, 11, and 35 in rodent and human cells.

To test if avidity effects are manifested on cells, we analyzed the influence of CD46 expression levels on species B serotype binding and infectivity. We and others had shown earlier that rodent cells such as hamster BHK and CHO cells, or mouse Ltk^- and B16 cells stably expressing CD46 become sensitive to infection with various human species B Ads, including Ad3, 7, 11, and 35 (11, 12, 19, 55, 56). Yet, binding of Ad3/7 to such cells has not been found by others (14, 18, 34, 52, 53, 59), suggesting that threshold levels of CD46 expression could be important for binding of these serotypes to CD46.

To address this question, we generated clonal CHO cells stably expressing variable levels of the CD46 BC1 isoform and compared their species B serotype binding and transduction properties. The highest levels of CD46 were measured in CHO-CD46#2 cells with an arbitrary mean fluorescence intensity (MFI) of 161, followed by CHO-CD46#1 (MFI of 45), and CHO-CD46#6 (MFI of 33) (Fig. 2A). All three CHO clones were derived from CHO-15B6 cells. Additional CHO-CD46#RC cells, which were derived from CHO-K1 cells (3) and expressed similar CD46 levels as CHO-CD46#1 were included as controls in the transduction study. These cells gave similar data to CHO-CD46#1 and are not shown here. We noticed, however, that the CD46 stably transfected cells had broader expression ranges than for example human lung carcinoma A549 cells, which had an MFI of 74. We therefore used the stably CD46 expressing CHO cells exclusively at low passage numbers to ensure comparable expression levels.

For initial comparative binding assays, cells were incubated with 1,000 vp of [^{3}H]-thymidine-labeled wild type Ad3/7/11/35 followed by determination of cell-associated viruses by liquid scintillation counting (Fig. 2B). CHO-CD46#2 cells expressing the

highest levels of CD46 revealed highest virus binding for all four viruses, followed by CHO-CD46#1 and CHO-CD46#6 cells, which bound 2-4-fold more virus compared to parental CHO cells. Binding of Ad3/7/11 to A549 cells was intermediate when compared to CHO-CD46#2 and CHO-CD46#1 cells, whereas binding of Ad35 was higher to A549 than CHO-CD46#2 cells.

Since binding experiments have a relatively low dynamic range, we performed transduction experiments using eGFP-expressing vectors as a read out for infectivity. We first compared the virus-blocking activity of the anti-CD46 antibody MEM-258 for Ad3 infection in A549 and CHO-CD46#2 cells. Pre-incubation with this antibody resulted in 49% reduction in A549 cells and 86% reduction in CHO-CD46#2 cells at the highest concentration of 20 µg/ml tested (Fig. 2C). This is in good agreement with our earlier results reporting more than 90% blocking of Ad3 binding to rodent BHK-CD46 cells, and 40% blocking to human K562 cells (55). The data are also compatible with other studies reporting variable inhibition of Ad3 binding to human cells, with an upper 48% inhibition in human Huh7 hepatoblastoma cells (59).

When eGFP transgene expression was analyzed following inoculation with increasing amounts of recombinant Ad3/7/11/35 expressing eGFP, a robust increase of transgene expression was found in all four CHO-CD46 cells (including CHO-CD46#RC cells), when compared to the parental cells (Fig. 2D and Table 2). At a virus concentration of 1,000 vp/cell, e.g., Ad3-mediated eGFP expression increased 18-fold in CHO-CD46#6 cells, 55-fold in CHO-CD46#1 cells, and 192-fold in CHO-CD46#2 cells, when compared to parental CHO cells. When standardized to A549 cells, Ad3-eGFP-mediated transgene expression levels amounted to 0.24% in parental CHO cells, 19% in CHO-CD46#6 cells (with 2.2-fold lower CD46 than A549), 60% in CHO-CD46#1 cells (with about 1.5-fold lower CD46 than A549), and 211% in CHO-CD46#2 cells (2.2-fold higher CD46 than A549). For better comparison of transduction efficiency, vp/cell concentrations necessary to reach the arbitrary MFI value of 100 were calculated (Table 2). These values followed the same pattern, as highest input of 8,207 Ad3 vp/cell was needed for CHO-CD46#6 cells, 2,597 vp/cell for CHO-CD46#1 cells, and 717 vp/cell for CHO-CD46#2 cells to reach comparable transduction levels. Transduction with Ad7 was about 2-fold more efficient than Ad3 when comparing vp/ml

values necessary to reach MFI of 100. Ad11/35 consistently transduced all tested cells more efficiently than Ad3/7, including control A549 cells and parental CHO cells. When standardized to Ad35, Ad3 infection of CHO-CD46#6, #1, #2 and A549 needed 27-, 16-, 4.2- and 2.7-fold higher vp input to obtain the MFI value of 100, respectively. For Ad7, these numbers amounted to 9.5-, 7.3-, 1.57 and 1.1-fold. In contrast, Ad11 had in this assay a similar transduction efficacy as Ad35. Of note, when using Ad5-eGF in these cells, resulting eGFP reporter levels do not change more than a factor of 2 within the different CD46-expressing clones compared to parental CHO cells.

We also tested whether human melanoma M010119 cells with low CD46 expression (MFI of 17.8) were increasingly transduced with Ad-eGFP vectors by increasing CD46 levels. Stable transfection of these cells (M010119-eGFP-CD46#8) resulted in about nine-fold higher CD46 expression levels (MFI of 155, Fig. 2E left panel), compared to the parental cells. In this case, an N-terminal eGFP-tagged CD46 BC1 isoform was used, in which the endogenous signal peptide was replaced by the CAR signal peptide, followed by the eGFP sequence and the sequence of the mature CD46 BC1 isoform. Of note, the receptor function of the eGFP-tagged CD46 form was retained for all four species B serotypes tested in M010119-eGFP-CD46#8 cells (Fig. 2F), as well as in the additionally established CHO-eGFP-CD46#33.5 and A549-eGFP-CD46#2 cells (SFig. 2B, D). The eGFP-CD46 fusion protein retained the binding capacity of those monoclonal antibodies that interfere with virus binding, that is, M177, 13/42, GB24, MEM258 (SFig. 2E, 11), whereas an almost complete loss of binding was observed for CD46 antibodies weakly or not interfering with virus binding (Tra-2, E4.3, MCI20.6). In A549-eGFP-CD46#2 cells, this allowed discriminating between endogenous CD46 level and the sum of endogenous and additionally expressed eGFP-tagged CD46, which amounted to a two-fold difference (SFig. 2C).

When using 1,000 vp/cell, M010119-eGFP-CD46#8 cells with the nine-fold higher CD46 level revealed 86-, 26-, 2.1- and 2.3-fold enhancement of reporter eGFP for Ad3/7/11/35 mediated transduction, respectively, when compared to parental M010119 cells (Fig. 2F, Table 3). Determination of vp/cell ratios necessary to reach MFI value of 100, revealed 127-, 52-, 3.1-, and 2-fold enhancement of Ad3/7/11/35-mediated transduction, respectively. Of note, both, the parental M010119 low-CD46 cells as well

as the M010119-eGFP-CD46#8 high-CD46 cells expressed no desmoglein 2, when analyzed by cytofluorometric means (Fig. 2E, middle and right panel), in contrast to A549 cells which expressed high levels of desmoglein 2. Transduction analysis was also performed for CHO-eGFP-CD46#33.5 cells (SFig. 2A, B), which expressed 2.3-fold higher levels of CD46 when compared to A549 cells (and thus similar levels as the CHO-CD46#2 cells). MFI 100 virus concentrations determined for these cells (Table 4), were in the same range as those determined for CHO-CD46#2 cells (Table 2). Further, the A549-eGFP-CD46#2 cells with about 2-fold higher CD46 expression than parental cells (SFig. 2C), revealed a tendency of maximal 2-fold increase of sensitivity to the species B vectors (Table 4).

In summary, ectopic expression of CD46 in rodent cells, or enhanced expression of CD46 in human CD46 low cells negative for desmoglein 2 resulted in increased infection of Ad3/7/11/35 species B serotypes. Infection efficacy of Ad3/7 correlated with CD46 density levels in these cells, whereas Ad11 reached a plateau with the medium CHO-CD46#1 cells and Ad35 already with the lowest CHO-CD46#6 cells. This is compatible with the notion that Ad3/7 exert a lower affinity for CD46 than Ad11/35, but suggests that avidity effects help to overcome the low affinity.

Cross-linking of soluble CD46 leads to enhanced blocking of Ad3 and Ad7 infection in CHO-CD46 and A549 cells.

We earlier documented that soluble CD46ex-huFc was at least 100-fold more potent at blocking Ad11/35 binding to rodent cells expressing CD46, when compared to Ad3 and 7 (11). To further test the hypothesis that avidity allows Ad3/7 to use CD46 as a functional receptor, we repeated the virus blocking assays with CD46ex-huFc, but included this time complexed or cross-linked adapter protein. We reasoned that antibody-mediated complexes of CD46ex-huFc could provide locally more binding sites per molecule, mimicking more closely the situation on the cell membrane where CD46 can diffuse freely and forms clusters following multivalent binding (7).

When using 50, 500, and 5,000 ng/ml of CD46ex-huFc protein alone, only Ad11-eGFP and Ad35-eGFP mediated transgene expressions were significantly reduced in CHO-CD46#2 and A549 cells (Fig. 3A-D). At the intermediate concentration of 500 ng/ml CD46ex-huFc, transgene expression levels were reduced by 85 to 92% for both cell types. In contrast, even at the highest concentration of 5,000 ng/ml, CD46ex-huFc did not result in any significant reduction of Ad3/7 mediated transgene expression, when compared to negative controls including the CARex-huFc protein (Fig.3B, D). However, when combining CD46ex-huFc protein at a concentration of 500 ng/ml with two-fold increasing amounts of cross-linking goat-anti human Fc antibody, significant blocking was also achieved for both Ad3 and Ad7-mediated transgene expression. Inhibition followed a precipitin-type curve reaching a plateau in the range of 500, 1,000 or 2,000 ng/ml of goat anti-human Fc. Highest blocking for Ad3-eGFP amounted to 65% in CHO-CD46#2 cells and 83% in A549 cells, and for Ad7-eGFP, highest blocking achieved was 77% in both cell types. Thus, by multimerizing CD46ex-huFc, the complexed protein became a potent blocker of Ad3/7. A similarly multimerized complex consisting of CARex-huFc had no significant effects on Ad3/7 infection.

Fiber knob-mediated species B Ad cross competition assays in CHO-CD46 A549 and cells.

To further characterize affinity differences and receptor usage by species B Ads, we performed blocking studies with species B Ads and soluble FKs in CHO-CD46#2 and A549 cells. CHO-CD46#2 cells were included since they do not express desmoglein 2 (61), whereas in human A549 cells, both types of receptors are present (18, 19, 34, 52, 53).

Virus inhibition assays were performed using five different eGFP-expressing vectors as readout for binding and infectivity. For CHO-CD46#2 cells, Ad3/7/11/35-eGFP inputs of 29,600, 8,200, 657, and 1,088 vp/cell, respectively, were used. For A549 cells, the virus inputs amounted to 14,800, 8,200, 1,314 and 2,540 vp/cell, and in addition, for Ad5-eGFP an input of 2,825 was applied. The virus input concentrations were determined in preceding experiments and were chosen such that the unblocked

transgene expression values amounted to fluorescence intensity values in the range of about 200, thereby allowing an optimal dynamic range (not shown). All five Ad FK proteins were tested in a dose-dependent manner with the highest concentration of 5,000 ng/ml diluted in a 5-fold dilution series to the lowest concentration of 8 ng/ml (Fig 4A, B and Table 5). Specificity of this assay was confirmed by the finding that the species C Ad5-FK only gave rise to inhibition of its corresponding virus, but not for any of the species B serotypes. The same was found for the individual species B FKs, which only inhibited species B serotypes, but not the species C Ad5-eGFP.

The cross-competition assays revealed differences in the capacity of the individual FKs to compete with species B viruses. The Ad3/7-FKs on one side, and Ad11/35-FKs on the other side showed similar behavior, which, however, was different in the two cell types tested. In CHO-CD46#2 cells, Ad3/7-FKs elicited at best weak competition for corresponding and non-corresponding Ad3 and Ad7, and no effect at all on non-corresponding Ad11 and Ad35. This is illustrated by the 40% inhibition of Ad3-eGFP transduction at the highest applied Ad3-FK concentration of 5,000 ng/ml, and a non-significant 7% inhibition for Ad7-eGFP transduction. Ad3-FK concentrations necessary for 50% inhibition (FK-50%) were larger than the highest concentration used and could thus not be calculated. Ad7-FK was more efficient than Ad3-FK, and using 5,000 ng/ml, 86 and 81% of Ad3/7 mediated eGFP expression was inhibited, respectively. FK-50% inhibition values for Ad7-FK were determined to be 169 and 2,690 ng/ml for Ad3/7-mediated transgene expression, respectively.

In contrast, Ad11/35-FKs led to efficient blocking of corresponding as well as all non-corresponding viruses in these cells. Thus, applying 5,000 ng/ml of Ad11-FK, inhibitions between 97 to 99% were obtained for of Ad3-, Ad7-, Ad11-, and Ad35-mediated transgene expression, respectively, and the corresponding FK-50% inhibition values amounted to 14, 79, 22, and 37 ng/ml, respectively. Likewise, Ad35-FK blocking efficiency was in the range of 85 to 97% at 5,000 ng/ml, and the corresponding FK-50% values were 5, 63, 14, and 26 ng/ml.

The binding inhibition pattern found for A549 cells was different than for CHO-CD46#2 cells. In A549 cells, Ad3/7-FKs very efficiently competed for corresponding and non-corresponding Ad3 and 7 in A549 cells (Fig. 4B, Table 5). This resulted for Ad3-FK at highest concentration of 5,000 ng/ml in 93 and 78% blocking efficiency of Ad3- and 7-mediated eGFP expression, respectively, with FK-50% Ad3/7 inhibition values of 25 and 23 ng/ml, respectively. With highest concentrations of Ad7-FK, blocking efficiency of 95 and 87% was achieved for Ad3/7-mediated eGFP expression, respectively, with FK-50% values of 17 and 31 ng/ml, respectively. However, as for CHO-CD46#2 cells, Ad3/7-FKs revealed no effect on non-corresponding Ad11 and Ad35 in A549 cells. Ad11-FK efficiently blocked all four species B serotypes, with FK-50% inhibition values of 31, 87, 13, 13 ng/ml, whereas Ad35-FK was less efficient at inhibiting Ad3 and 7, with FK-50% values of 470, and 4'459 ng/ml, respectively, but very efficient at inhibiting Ad11 and 35, with FK-50% values of 33 and 5 ng/ml, respectively.

In summary, blocking studies with Ad3/7-FKs revealed different effects for corresponding viruses in CHO-CD46 cells or human A549 cells. In CHO-CD46 cells, the observed low blocking efficiency confirms the low affinity of the Ad3/7 soluble FK molecules to CD46. In contrast, the efficient blocking activity of Ad3/7-FK in A549 suggests lower dependency of Ad3/7 on avidity effects in A549 than CHO-CD46 cells.

eGFP-CD46 photo-bleaching recovery analysis in presence of Ad3-, 7-, 11-, and 35-FK in CHO-eGFP-CD46 and A549-eGFP-CD46 cells.

In order to further address the observed difference in blocking potency of the serotype B1 FKs in CHO-CD46#2 cells compared to human A549 cells, we performed FRAP studies in CHO-eGFP-CD46#33.5 and A549-eGFP-CD46#2 cells. These cells express defined levels of eGFP-tagged CD46 (SFig. 2A, C), with CHO-eGFP-CD46#33.5 expressing tagged CD46 only, and A549-eGFP-CD46#2 expressing an about equal mix of eGFP-tagged and untagged CD46. To test whether the individual species B FKs had any effects on the fluorescence recovery following photo-bleaching, recovery of the fluorescent signal of the eGFP-tagged CD46 was monitored in absence or presence of the different trimeric FKs (Fig. 5A-F, SFig. 4A-F).

We first compared the effect of the individual FKs in CHO-eGFP-CD46#33.5 cells by applying a single concentration of 2.5 ng / µl (Fig. 5A). At this concentration, neither Ad3 nor Ad7-FK induced any significant change in recovery of the fluorescence signal, as Ad3/7-$t_{1/2}$ amounted to 2.3 ±0.5 s and 1.2 ±0.3 s, respectively, compared to the control and Ad5-FK $t_{1/2}$ values of 1.6 ±0.3 s and 2.7 ±0.5 s. In contrast, the cells incubated with the Ad35/11-FKs revealed a delayed rate of recovery of similar magnitude, with Ad11-FK and Ad35FK-$t_{1/2}$ of 7.8 ±1.5 s and 5.9 ±1.0 s, respectively. The mobile fraction (M_f) was replenished for all samples to the control level after less than two minutes (SFig 4A). To further refine these observations, we performed FRAP experiments with increasing concentrations of the individual FKs in the same cells. When using four-fold increasing Ad3-FK concentrations ranging from 4 ng/µl to 64 ng/µl, again no effect on fluorescence recovery was noticed (Fig. 5B, SFig. 4B). Titration of the Ad7-FK led to similar results (data not shown). When using 0.1, 1, and 4 ng/µl of either Ad11-FK (Fig. 5C, SFig. 4C) or Ad35-FK (Fig. 5D, SFig. 4D), already the lowest concentration of 0.1 ng/µl had a significant effect on the fluorescence recovery. The corresponding Ad11- and Ad35-FK-$t_{1/2}$ values amounted to 9.3 ±1.7 s, and 8.1 ±1.4 s, respectively. Applying the highest concentration of 4 ng/µl of these FKs resulted in an about four-fold increase of $t_{1/2}$ values characteristic for the eGFP-CD46 fluorescence recovery. To confirm the specificity of the system used here, Ad5-FK was included in the FRAP study, but revealed no effect on CD46 recovery (Fig. 5E, SFig. 4E).

Finally, we tested the same set-up in A549-eGFP-CD46#8 cells (Fig. 5F, SFig. 4F). Applying 4 ng/µl of Ad11/35-FKs elicited a strong reduction of the CD46 dynamic, resulting in Ad11- and Ad35-FK-$t_{1/2}$ values of 21.0 ±2.2 s and 13.7 ±3.3 s compared to Ad5-FK $t_{1/2}$ value of 6.7 ±0.9 s at 64 ng/µl. The highest Ad3/7-FK concentrations of 64 ng/µl revealed a slower recovery (Ad3FK-$t_{1/2}$=10.5 +/-1.2s and Ad7-$t_{1/2}$=9.3+/-1.4s). In summary, the FRAP assays with an inherently low sensitivity dynamic scale are in agreement with a complete dependency on avidity for Ad3/7 infection of CHO-CD46 cells, and a lesser dependency on avidity for A549 cells.

Discussion

To initiate infection of susceptible cells, enveloped and non-enveloped viruses use multiple binding strategies, characterized by a broad range of affinity interactions when analyzed for single binding interaction sites (21, 64). Viruses with low affinities include, e.g., influenza virus with an affinity in the millimolar range for sialic acid, and other viruses with affinities in the micromolar range for their protein receptors as determined by biacore, such as rhinovirus for intercellular adhesion molecule-1, echovirus for decay-accelerating factor, and reovirus for junction adhesion molecule (2, 4, 26, 57).

Avidity captures low affinity interactions

Biologically meaningful binding of viruses to low affinity receptors occurs, when virus particles expose multiple binding sites. This allows for avidity effects and increases overall affinity. Avidity is characterized by a synergistic (and not additive) combination of individual bond affinities, which depends sensitively on the structure and geometry of the involved molecules (33). For example, in the case of an IgG with a valency of two, avidity can lead to a strong increase of overall affinity, when compared to corresponding monovalent Fab fragments (see e.g., an early study from 16). Particularly strong avidity effects were also reported for low affinity ErbB2-specific single chain variable fragment antibodies, where the antibody fragment with the lowest affinity showed highest avidity increase upon dimerization (39). Interestingly, avidity mechanisms have been suggested to allow the species B Ad16 to use CD46 for productive infection by increasing the affinity to CD46 by 70-fold compared to Ad11 (42). In addition, viruses containing trimeric attachment receptors, such as the reovirus sigma 1 protein or the long and short fibers of bacteriophage T4, have been suggested to employ avidity mechanisms for infection (31).

The Ad3/7 and also Ad14 were claimed to be CD46 non-binders due to their low affinity interactions with CD46 (14, 18, 34, 52, 53, 59). Several lines of evidence from our study here support avidity-based mechanisms for Ad3/7 infection of CD46 positive cells. First, the binding of species B Ad3/7-FK to immobilized CD46 on a biosensor

chip was more dependent on the receptor density than binding of Ad11/35-FK, and the Ad3/7-FK binding had only 10-15 fold lower apparent affinity than Ad11/35-FK. This result deviates significantly from a previous report of 2,000-fold difference for monovalent affinities for Ad7/11-FK (43). Second, Ad3/7 infection correlated with the levels of ectopically expressed CD46, while Ad11/35 infection was saturated at low CD46 expression levels. Third, crosslinking of soluble CD46 increased its blocking effect on Ad3/7 infection in human A549 cells and CHO-CD46 cells. Fourth, soluble Ad3/7-FKs inefficiently blocked Ad3/7 infection of CHO-CD46 cells, unlike Ad11/35-FKs, which efficiently blocked all four tested B serotypes, confirming that Ad3/7 FKs bind with lower affinity to CD46 than Ad11/35 FKs. These data support and extend our earlier binding site mapping studies, which showed that Ad3/7 engage CD46 through similar surfaces as species B2 Ad11/35 (11). In support of this, the recent SPR studies by Persson *et al.* revealed a broad variation of CD46 binding affinities, and the authors concluded that Ad7/11/14/35 are capable to bind to the same epitopes on CD46 (43). All these data are in accordance with the observations that both the low affinity CD46 binder Ad3 and the high affinity binder Ad35 use virtually identical pathways to infect human cells that are CD46-positive (1, 23).

Similar to the species B serotypes, also the CAR-tropic species C Ad serotypes have a broad spectrum of CAR affinities over nearly 3 orders of magnitude, ranging from the low affinity binder Ad9 to the high affinity binder Ad5 (24). In addition, avidity effects could be measured by an increase of FK affinity from about 25 nM for monomeric immobilized Ad2 FK to 1 nM for multivalent immobilized CAR in SPR assays employing minimal-sized proteins produced in *E.coli* (31). The avidity-driven multivalent binding reaction to immobilized high density CAR (200 RU equivalent to our CD46 high density chips) could be fitted to a trivalent binding model. We thus consider it likely that many different Ads use avidity effects. Avidity effects for Ad–receptor interactions can occur at two levels. The trivalent FK protein can increase the overall affinity compared to a monovalent protein, and the virus particle with 12 fiber trimers can possibly simultaneously form multiple contact points with the cell surface. Both of these mechanisms can contribute to increase the overall affinities of the virus particle to its receptor.

Apparent K_D values for species B Ads differ from monovalent K_D values of previous studies

The apparent K_D values determined here for Ad3/7 are about 5 logs lower, and 3 logs lower for Ad11/35 compared to the K_D values for the monovalent CD46 interactions (8, 42, 43, 62, 63). There are several reasons for these differences. For example, the CD46-SCR I-II protein used in other studies was produced in mutant CHO cells and contained homogenous, high mannose N-linked carbohydrates (43). In addition, and perhaps more importantly, our CD46 protein was produced in normal CHO cells, and consisted of an antibody-like dimer comprising the complete extracellular domain, and presumably also O- and N-linked glycosylations (55). The extended CD46 SCR I-IV domain has recently found to reveal a somewhat different binding to Ad11-FK, as the contact site did not include the IJ loop previously described for CD46 SCR I-II interaction (45). The dimeric nature of our CD46ex-huFc could explain why our kinetic data for the binding of the four species B Ads fit better to two-stage reaction models than to trivalent binding models, described earlier for Ad2-FK interaction with CAR (31). Importantly, we could internally compare the different affinities, since we performed all species B FK affinity measurements with the same set-up of bound CD46 ligand. We suggest, thus, that the observed K_D differences between the monovalent and trivalent affinities of the Ad3/7/11/35-FKs truly reflect avidity effects. Of note, 4 log avidity effects have been observed in binding of dimeric ephrin-A5 ligand to dimerized EphA3 receptor (40).

Virus–receptor affinity *versus* receptor density

A recent systematic study with retargeted MV vectors has shown that viruses displaying HER2/neu-specific single-chain variable fragment antibodies had high avidity and cell killing ability due to dozens of single chain molecules in the viral envelope, even if their single affinities were in the micromolar range (20). This study also noticed a receptor threshold level for productive infection, together with an inverse

correlation of attachment receptor affinity and receptor density requirements for infection. In particular, suprathreshold affinities did not further enhance the efficiency of MV infection, which corresponds well with our results for high affinity CD46 binders Ad11/35. It also fits well with another observation showing that Ad35 FK mutants with either 4-fold or 60-fold higher affinity at the monovalent interaction level did not translate into corresponding higher transduction efficiencies, regardless of the CD46 receptor density present on cells (63).

With the FK neutralization experiments in CHO-CD46#2 expressing cells, we noticed that Ad3/7-FKs did not efficiently compete against the binding of corresponding virus particles, in contrast to Ad11/35-FKs, which efficiently blocked all four viruses. This is due to low affinity of Ad3/7-FK for CD46, since binding of the different species B Ads is restricted to CD46 in these cells (11, 55). This conclusion was corroborated by the findings that soluble CD46ex-huFc inefficiently inhibited binding of Ad3/7 to the cells, in agreement with weak blocking efficiency of Ad3/7 by soluble CD46 (11, 59), and also by soluble monovalent CD46 for MV infection (54). Ad3/7 inhibition was, however, strongly enhanced by crosslinking the CD46ex-huFc protein (Fig. 3), suggesting that crosslinked CD46ex-huFc mimics the multiple interaction situation when the virus contacts the cell surface. Similarly, CD46 crosslinking by genetically fusing the CD46 ectodomain to the octamer oligomerization domain of C4b binding protein resulted in a 2 log enhanced MV neutralizing activity *in vitro* and *in vivo* due to enhanced virus binding (6).

These data suggest that the receptor density is of key importance not only for interaction of CD46 with trimeric FK, but also the multivalent virus particle. Together or alone, this gives rise to avidity effects, which allow Ad3/7 to infect cells expressing sufficient levels of CD46 (11, 19, 55). The lack of Ad3/7 infection in CHO-CD46 cells reported by other groups is most likely due to low CD46 expression levels, and also assay systems of low sensitivity or limited dynamic range (14, 17, 34, 53, 59).

Desmoglein 2 versus CD46 as receptor for Ad3/7

Down regulation of CD46 by RNA interference in human cells did not reduce Ad3/7 infection unlike Ad35 infection (19, 59), and blocking studies with CD46 antibodies showed only partial inhibition of Ad3/7 infection up to 50% depending on the cell type (55, 59). This lead to the suggestion that human cells express an alternative receptor X for Ad3/7/14, which recently was identified to be desmoglein 2 (61). Based on biochemical experiments, it was suggested that receptor X is a trypsin and cation-dependent factor (53, 59), features that were both confirmed for desmoglein 2.

Our data here show that in human M010119 melanoma cells that lack desmoglein 2, Ad3/7 uses CD46 as functional receptor. We have unpublished data indicating that in a total of sixteen primary human melanoma cultures, half were negative for desmogelin 2, but were all positive for CD46 (not shown). To further evaluate the role of the two receptors for Ad3/7 infection, it remains to be determined how widespread desmoglein 2 expression levels are among human cells and tissues, and to what extent the individual receptors contribute to virus infection in cells co-expressing both receptors. The observation that none of the receptor antibodies alone achieved more than 50 to 60% virus blocking in human cells (55, 59, 61) suggests that both receptors simultaneously serve as attachment receptors. Depending on the affinities of Ad3/7 for the individual receptors, one receptor might be predominantly used if the other receptor falls below a critical threshold level.

Alternatively, desmoglein 2 or yet another factor Y could associate with CD46 and modulate the oligomeric state of CD46. This could explain our observation that Ad3/7-FKs reduced the time of fluorescence recovery after photo-bleaching of eGFP-CD46 in A549 cells, but not in CHO-CD46#2 cells (Fig. 5). It is also possible that desmoglein 2 or factor Y is a tethering factor for CD46, which prolongs the half-life of CD46, and thereby enhances the CD46 levels at the plasma membrane. In support of this scenario, the CD46 surface levels are known to be regulated by endocytosis. In the absence of ligand, CD46 undergoes constitutive clathrin-mediated internalization and recycling back to the plasma membrane in human and rodent cells (7). When crosslinked by an antibody, CD46 is taken up by macropinocytosis and degraded. If the CD46 ligand is Ad3 or Ad35, macropinosomes are lysed and virus particles escape from endosomal degradation by entering to the cytosol (1, 23). Any conditions that

lead to clustering or enhanced cell surface levels of CD46 could enhance the avidity effects for the low affinity binding B serotypes. Such conditions could include recruitment of CD46 into lipid domains (58) or association with integrins or tetraspanins (32). In this sense, receptor Y would be a modulator for CD46 function, and would not be required for Ad3 infection if the CD46 levels were sufficiently high.

In summary, our study shows that species B1 adenoviruses use low affinity interactions and avidity to bind to the CD46 receptor. This has important consequences for tropism and possibly evolution of the species B1 viruses, where viral receptor-binding proteins are under selective pressure and undergo constant variation to evade neutralization by antibodies (22, 42). High affinity binding could, for example, represent a dead-end in evolutionary terms, as such viruses are constrained to a single receptor. Weak affinity to a receptor could be the first step in gaining access to a new attachment receptor. Conspicuously, several Ad serotypes have been reported to utilize more than one attachment receptor (67). For example, the species D Ad9 with a very short fiber was found to allow fiber-independent binding of the penton base directly to integrins, if integrins were present in sufficient amounts (46). In integrin-low cells, the virus instead used CAR for productive infection. Avidity effects of the Ad3/7 serotypes for CD46 could hence provide a large affinity window for attachment, and expand the repertoire of the viruses for other receptors.

Acknowledgements

We thank Leta Fuchs for technical assistance, Richard Sutton, Baylor College of Medicine, Houston Texas for providing the pBlasti lentiviral vector system, Denis Gerlier, Université Lyon, Lyon, France, for providing the MCI20.6 anti-CD46 hybridoma, and the FACS Core Facility Irchel from the University of Zurich for cell sorting service. We also thank for Dr. Johan Hoebeke, Kessel-Lo, Belgium for providing the equations and algorithms to evaluate the SPR data with trivalent binding model. This work was supported by the Kanton Zürich (SH, UFG) and by the grant 31003A-116856 of the Swiss National Science Foundation (SH).

References

1. **Amstutz, B., M. Gastaldelli, S. Kalin, N. Imelli, K. Boucke, E. Wandeler, J. Mercer, S. Hemmi, and U. F. Greber.** 2008. Subversion of CtBP1-controlled macropinocytosis by human adenovirus serotype 3. EMBO J **27:**956-69.
2. **Barton, E. S., J. C. Forrest, J. L. Connolly, J. D. Chappell, Y. Liu, F. J. Schnell, A. Nusrat, C. A. Parkos, and T. S. Dermody.** 2001. Junction adhesion molecule is a receptor for reovirus. Cell **104:**441-51.
3. **Buchholz, C. J., U. Schneider, P. Devaux, D. Gerlier, and R. Cattaneo.** 1996. Cell entry by measles virus: long hybrid receptors uncouple binding from membrane fusion. J Virol **70:**3716-23.
4. **Casasnovas, J. M., and T. A. Springer.** 1995. Kinetics and thermodynamics of virus binding to receptor. Studies with rhinovirus, intercellular adhesion molecule-1 (ICAM-1), and surface plasmon resonance. J Biol Chem **270:**13216-24.
5. **Chmielewicz, B., J. Benzler, G. Pauli, G. Krause, F. Bergmann, and B. Schweiger.** 2005. Respiratory disease caused by a species B2 adenovirus in a military camp in Turkey. J Med Virol **77:**232-7.
6. **Christiansen, D., P. Devaux, B. Reveil, A. Evlashev, B. Horvat, J. Lamy, C. Rabourdin-Combe, J. H. Cohen, and D. Gerlier.** 2000. Octamerization enables soluble CD46 receptor to neutralize measles virus in vitro and in vivo. J Virol **74:**4672-8.
7. **Crimeen-Irwin, B., S. Ellis, D. Christiansen, M. J. Ludford-Menting, J. Milland, M. Lanteri, B. E. Loveland, D. Gerlier, and S. M. Russell.** 2003. Ligand binding determines whether CD46 is internalized by clathrin-coated pits or macropinocytosis. J. Biol. Chem. **278:**46927-46937.
8. **Cupelli, K., S. Muller, B. D. Persson, M. Jost, N. Arnberg, and T. Stehle.** 2010. Structure of adenovirus type 21 knob in complex with CD46 reveals key differences in receptor contacts among species B adenoviruses. J Virol **84:**3189-200.
9. **Durmort, C., C. Stehlin, G. Schoehn, A. Mitraki, E. Drouet, S. Cusack, and W. P. Burmeister.** 2001. Structure of the fiber head of Ad3, a non-CAR-binding serotype of adenovirus. Virology **285:**302-12.
10. **Ebbinghaus, C., A. Al-Jaibaji, E. Operschall, A. Schoffel, I. Peter, U. F. Greber, and S. Hemmi.** 2001. Functional and selective targeting of adenovirus to high-affinity Fcgamma receptor I-positive cells by using a bispecific hybrid adapter. J Virol **75:**480-9.
11. **Fleischli, C., D. Sirena, G. Lesage, M. J. Havenga, R. Cattaneo, U. F. Greber, and S. Hemmi.** 2007. Species B adenovirus serotypes 3, 7, 11 and 35 share similar binding sites on the membrane cofactor protein CD46 receptor. J Gen Virol **88:**2925-34.
12. **Fleischli, C., S. Verhaagh, M. Havenga, D. Sirena, W. Schaffner, R. Cattaneo, U. F. Greber, and S. Hemmi.** 2005. The distal short consensus repeats 1 and 2 of the membrane cofactor protein CD46 and their distance from the cell membrane determine productive entry of species B adenovirus serotype 35. J Virol **79:**10013-10022.
13. **Fournel, S., S. Wieckowski, W. Sun, N. Trouche, H. Dumortier, A. Bianco, O. Chaloin, M. Habib, J. C. Peter, P. Schneider, B. Vray, R. E. Toes, R. Offringa, C. J. Melief, J. Hoebeke, and G. Guichard.** 2005. C3-symmetric peptide scaffolds are functional mimetics of trimeric CD40L. Nat Chem Biol **1:**377-82.
14. **Gaggar, A., D. M. Shayakhmetov, and A. Lieber.** 2003. CD46 is a cellular receptor for group B adenoviruses. Nat Med **9:**1408-12.
15. **Gaggar, A., D. M. Shayakhmetov, M. K. Liszewski, J. P. Atkinson, and A. Lieber.** 2005. Localization of regions in CD46 that interact with adenovirus. J Virol **79:**7503-13.
16. **Greenbury, C. L., D. H. Moore, and L. A. Nunn.** 1965. The Reaction with Red Cells of 7s Rabbit Antibody, Its Sub-Units and Their Recombinants. Immunology **8:**420-31.
17. **Gustafsson, B., W. Huang, G. Bogdanovic, F. Gauffin, A. Nordgren, G. Talekar, D. A. Ornelles, and L. R. Gooding.** 2007. Adenovirus DNA is detected at increased frequency in Guthrie cards from children who develop acute lymphoblastic leukaemia. Br J Cancer **97:**992-4.
18. **Gustafsson, D. J., A. Segerman, K. Lindman, Y. F. Mei, and G. Wadell.** 2006. The Arg279Gln [corrected] substitution in the adenovirus type 11p (Ad11p) fiber knob abolishes EDTA-resistant binding to A549 and CHO-CD46 cells, converting the phenotype to that of Ad7p. J Virol **80:**1897-905.

19. **Hall, K., M. E. Blair Zajdel, and G. E. Blair.** 2009. Defining the role of CD46, CD80 and CD86 in mediating adenovirus type 3 fiber interactions with host cells. Virology **392:**222-9.
20. **Hasegawa, K., C. Hu, T. Nakamura, J. D. Marks, S. J. Russell, and K. W. Peng.** 2007. Affinity thresholds for membrane fusion triggering by viral glycoproteins. J Virol **81:**13149-57.
21. **Helenius, A.** 2007. Virus entry and uncoating, p. 99-118. *In* D. M. Knipe and P. M. Howley (ed.), Fields Virology, vol. 1. Walters Kluwer, Lippincott Williams & Wilkins, Philadelphia, Baltimore, New York, London, Buenos Aires, Hong Kong, Sydney, Tokyo.
22. **Howitt, J., C. W. Anderson, and P. Freimuth.** 2003. Adenovirus interaction with its cellular receptor CAR. Curr Top Microbiol Immunol **272:**331-64.
23. **Kalin, S., B. Amstutz, M. Gastaldelli, N. Wolfrum, K. Boucke, M. Havenga, F. DiGennaro, N. Liska, S. Hemmi, and U. F. Greber.** 2010. Macropinocytotic uptake and infection of human epithelial cells with species B2 adenovirus type 35. J Virol **84:**5336-50.
24. **Kirby, I., R. Lord, E. Davison, T. J. Wickham, P. W. Roelvink, I. Kovesdi, B. J. Sutton, and G. Santis.** 2001. Adenovirus type 9 fiber knob binds to the coxsackie B virus-adenovirus receptor (CAR) with lower affinity than fiber knobs of other CAR-binding adenovirus serotypes. J Virol **75:**7210-4.
25. **Kumar, M., B. Keller, N. Makalou, and R. E. Sutton.** 2001. Systematic determination of the packaging limit of lentiviral vectors. Hum Gene Ther **12:**1893-905.
26. **Lea, S. M., R. M. Powell, T. McKee, D. J. Evans, D. Brown, D. I. Stuart, and P. A. van der Merwe.** 1998. Determination of the affinity and kinetic constants for the interaction between the human virus echovirus 11 and its cellular receptor, CD55. J Biol Chem **273:**30443-7.
27. **Leen, A. M., and C. M. Rooney.** 2005. Adenovirus as an emerging pathogen in immunocompromised patients. Br J Haematol **128:**135-44.
28. **Lemckert, A. A., J. Grimbergen, S. Smits, E. Hartkoorn, L. Holterman, B. Berkhout, D. H. Barouch, R. Vogels, P. Quax, J. Goudsmit, and M. J. Havenga.** 2006. Generation of a novel replication-incompetent adenoviral vector derived from human adenovirus type 49: manufacture on PER.C6 cells, tropism and immunogenicity. J Gen Virol **87:**2891-9.
29. **Lewis, P. F., M. A. Schmidt, X. Lu, D. D. Erdman, M. Campbell, A. Thomas, P. R. Cieslak, L. D. Grenz, L. Tsaknardis, C. Gleaves, B. Kendall, and D. Gilbert.** 2009. A community-based outbreak of severe respiratory illness caused by human adenovirus serotype 14. J Infect Dis **199:**1427-34.
30. **Liszewski, M. K., C. Kemper, J. D. Price, and J. P. Atkinson.** 2005. Emerging roles and new functions of CD46. Springer Semin Immunopathol **27:**345-58.
31. **Lortat-Jacob, H., E. Chouin, S. Cusack, and M. J. van Raaij.** 2001. Kinetic analysis of adenovirus fiber binding to its receptor reveals an avidity mechanism for trimeric receptor-ligand interactions. J Biol Chem **276:**9009-15.
32. **Lozahic, S., D. Christiansen, S. Manie, D. Gerlier, M. Billard, C. Boucheix, and E. Rubinstein.** 2000. CD46 (membrane cofactor protein) associates with multiple beta1 integrins and tetraspans. Eur. J. Immunol. **30:**900-907.
33. **Mammen, M., S. Choi, and G. M. Whitesides.** 1998. Polyvalent Interactions in Biological Systems: Implications for Design and Use of Multivalent Ligands and Inhibitiors. Angewandte Chemie International Edition **37:**2754-94.
34. **Marttila, M., D. Persson, D. Gustafsson, M. K. Liszewski, J. P. Atkinson, G. Wadell, and N. Arnberg.** 2005. CD46 is a cellular receptor for all species B adenoviruses except types 3 and 7. J Virol **79:**14429-36.
35. **Metzgar, D., M. Osuna, A. E. Kajon, A. W. Hawksworth, M. Irvine, and K. L. Russell.** 2007. Abrupt emergence of diverse species B adenoviruses at US military recruit training centers. J Infect Dis **196:**1465-73.
36. **Myszka, D. G.** 1999. Improving biosensor analysis. J Mol Recognit **12:**279-84.
37. **Naniche, D., G. Varior-Krishnan, F. Cervoni, T. F. Wild, B. Rossi, C. Rabourdin-Combe, and D. Gerlier.** 1993. Human membrane cofactor protein (CD46) acts as a cellular receptor for measles virus. J Virol **67:**6025-32.
38. **Nemerow, G. R., L. Pache, V. Reddy, and P. L. Stewart.** 2009. Insights into adenovirus host cell interactions from structural studies. Virology **384:**380-8.

39. **Nielsen, U. B., G. P. Adams, L. M. Weiner, and J. D. Marks.** 2000. Targeting of bivalent anti-ErbB2 diabody antibody fragments to tumor cells is independent of the intrinsic antibody affinity. Cancer Res **60:**6434-40.
40. **Pabbisetty, K. B., X. Yue, C. Li, J. P. Himanen, R. Zhou, D. B. Nikolov, and L. Hu.** 2007. Kinetic analysis of the binding of monomeric and dimeric ephrins to Eph receptors: correlation to function in a growth cone collapse assay. Protein Sci **16:**355-61.
41. **Pache, L., S. Venkataraman, G. R. Nemerow, and V. S. Reddy.** 2008. Conservation of fiber structure and CD46 usage by subgroup B2 adenoviruses. Virology **375:**573-9.
42. **Pache, L., S. Venkataraman, V. S. Reddy, and G. R. Nemerow.** 2008. Structural variations in species B adenovirus fibers impact CD46 association. J Virol **82:**7923-31.
43. **Persson, B. D., S. Muller, D. M. Reiter, B. B. Schmitt, M. Marttila, C. V. Sumowski, S. Schweizer, U. Scheu, C. Ochsenfeld, N. Arnberg, and T. Stehle.** 2009. An arginine switch in the species B adenovirus knob determines high-affinity engagement of cellular receptor CD46. J Virol **83:**673-86.
44. **Persson, B. D., D. M. Reiter, M. Marttila, Y. F. Mei, J. M. Casasnovas, N. Arnberg, and T. Stehle.** 2007. Adenovirus type 11 binding alters the conformation of its receptor CD46. Nat Struct Mol Biol **14:**164-6.
45. **Persson, B. D., N. B. Schmitz, C. Santiago, G. Zocher, M. Larvie, U. Scheu, J. M. Casasnovas, and T. Stehle.** 2010. Structure of the extracellular portion of CD46 provides insights into its interactions with complement proteins and pathogens. PLoS Pathog **6**.
46. **Roelvink, P. W., I. Kovesdi, and T. J. Wickham.** 1996. Comparative analysis of adenovirus fiber-cell interaction: adenovirus type 2 (Ad2) and Ad9 utilize the same cellular fiber receptor but use different binding strategies for attachment. J Virol **70:**7614-21.
47. **Russell, S.** 2004. CD46: a complement regulator and pathogen receptor that mediates links between innate and acquired immune function. Tissue Antigens **64:**111-8.
48. **Sakurai, F., K. Kawabata, and H. Mizuguchi.** 2007. Adenovirus vectors composed of subgroup B adenoviruses. Curr Gene Ther **7:**229-38.
49. **Sakurai, F., S. Murakami, K. Kawabata, N. Okada, A. Yamamoto, T. Seya, T. Hayakawa, and H. Mizuguchi.** 2006. The short consensus repeats 1 and 2, not the cytoplasmic domain, of human CD46 are crucial for infection of subgroup B adenovirus serotype 35. J Control Release **113:**271-8.
50. **Schmitz, H., R. Wigand, and W. Heinrich.** 1983. Worldwide epidemiology of human adenovirus infections. Am J Epidemiol **117:**455-66.
51. **Schmitz, M., C. Graf, T. Gut, D. Sirena, I. Peter, R. Dummer, U. F. Greber, and S. Hemmi.** 2006. Melanoma cultures show different susceptibility towards E1A-, E1B-19 kDa- and fiber-modified replication-competent adenoviruses. Gene Ther **13:**893-905.
52. **Segerman, A., N. Arnberg, A. Erikson, K. Lindman, and G. Wadell.** 2003. There are two different species B adenovirus receptors: sBAR, common to species B1 and B2 adenoviruses, and sB2AR, exclusively used by species B2 adenoviruses. J. Virol. **77:**1157-1162.
53. **Segerman, A., J. P. Atkinson, M. Marttila, V. Dennerquist, G. Wadell, and N. Arnberg.** 2003. Adenovirus type 11 uses CD46 as a cellular receptor. J Virol **77:**9183-91.
54. **Seya, T., M. Kurita, T. Hara, K. Iwata, T. Semba, M. Hatanaka, M. Matsumoto, Y. Yanagi, S. Ueda, and S. Nagasawa.** 1995. Blocking measles virus infection with a recombinant soluble form of, or monoclonal antibodies against, membrane cofactor protein of complement (CD46). Immunology **84:**619-25.
55. **Sirena, D., B. Lilienfeld, M. Eisenhut, S. Kalin, K. Boucke, R. R. Beerli, L. Vogt, C. Ruedl, M. F. Bachmann, U. F. Greber, and S. Hemmi.** 2004. The Human Membrane Cofactor CD46 Is a Receptor for Species B Adenovirus Serotype 3. J Virol **78:**4454-4462.
56. **Sirena, D., Z. Ruzsics, W. Schaffner, U. F. Greber, and S. Hemmi.** 2005. The nucleotide sequence and a first generation gene transfer vector of species B human adenovirus serotype 3. Virology **343:**283-98.
57. **Skehel, J. J., and D. C. Wiley.** 2000. Receptor binding and membrane fusion in virus entry: the influenza hemagglutinin. Annu Rev Biochem **69:**531-69.

58. **Tang, H., A. Kawabata, M. Takemoto, K. Yamanishi, and Y. Mori.** 2008. Human herpesvirus-6 infection induces the reorganization of membrane microdomains in target cells, which are required for virus entry. Virology **378:**265-71.
59. **Tuve, S., H. Wang, C. Ware, Y. Liu, A. Gaggar, K. Bernt, D. Shayakhmetov, Z. Li, R. Strauss, D. Stone, and A. Lieber.** 2006. A new group B adenovirus receptor is expressed at high levels on human stem and tumor cells. J Virol **80:**12109-20.
60. **Wadell, G.** 2000. Adenoviruses, p. 307-327. *In* A. J. Zuckerman, J. E. Banatvala, and J. R. Pattison (ed.), Principles and Practice of Clinical Virology, Fourth Edition ed. John Wiley & Sons, Ltd.
61. **Wang, H., Z. Y. Li, Y. Liu, J. Persson, I. Beyer, T. Moller, D. Koyuncu, M. R. Drescher, R. Strauss, X. B. Zhang, J. K. Wahl, 3rd, N. Urban, C. Drescher, A. Hemminki, P. Fender, and A. Lieber.** 2011. Desmoglein 2 is a receptor for adenovirus serotypes 3, 7, 11 and 14. Nat Med **17:**96-104.
62. **Wang, H., Y. C. Liaw, D. Stone, O. Kalyuzhniy, I. Amiraslanov, S. Tuve, C. L. Verlinde, D. Shayakhmetov, T. Stehle, S. Roffler, and A. Lieber.** 2007. Identification of CD46 binding sites within the adenovirus serotype 35 fiber knob. J Virol **81:**12785-92.
63. **Wang, H., Y. Liu, Z. Li, S. Tuve, D. Stone, O. Kalyushniy, D. Shayakhmetov, C. L. Verlinde, T. Stehle, J. McVey, A. Baker, K. W. Peng, S. Roffler, and A. Lieber.** 2008. In vitro and in vivo properties of adenovirus vectors with increased affinity to CD46. J Virol **82:**10567-79.
64. **Wang, J.** 2002. Protein recognition by cell surface receptors: physiological receptors versus virus interactions. Trends Biochem Sci **27:**122-6.
65. **Wu, E., S. A. Trauger, L. Pache, T. M. Mullen, D. J. von Seggern, G. Siuzdak, and G. R. Nemerow.** 2004. Membrane cofactor protein is a receptor for adenoviruses associated with epidemic keratoconjunctivitis. J Virol **78:**3897-905.
66. **Zacharias, D. A., J. D. Violin, A. C. Newton, and R. Y. Tsien.** 2002. Partitioning of lipid-modified monomeric GFPs into membrane microdomains of live cells. Science **296:**913-6.
67. **Zhang, Y., and J. M. Bergelson.** 2005. Adenovirus receptors. J Virol **79:**12125-31.
68. **Zhu, Z., Y. Zhang, S. Xu, P. Yu, X. Tian, L. Wang, Z. Liu, L. Tang, N. Mao, Y. Ji, C. Li, Z. Yang, S. Wang, J. Wang, D. Li, and W. Xu.** 2009. Outbreak of acute respiratory disease in China caused by B2 species of adenovirus type 11. J Clin Microbiol **47:**697-703.

Legends to figures

Fig. 1. Subtracted SPR sensograms for Ad3-, Ad7-, Ad11- and Ad35-FK interacting with CD46. Soluble receptor CD46ex-huFc was immobilized on a CM5 chip at high density in Fc2 (2,630 RU, 1, 3) and low density in Fc4 (345 RU, 2, 4). Control CARex-huFc was immobilized at high density in Fc1 (3,431 RU, 1, 3) and low density in Fc3 (278 RU, 2, 4). (A) to (D), FK analytes were injected over the sensor surface at 18.75 and 150 nM concentrations for Ad3-FK (A), Ad11-FK (C) and Ad35-FK (D), and at 11.07 and 88.59 nM for Ad7-FK (B), respectively. Association times were either 240 or 280 s. (E) to (H), overlay of analyte responses for Ad3-, Ad7-, Ad11- and Ad35-FK at different concentrations. Measurements were performed using the CD46 high-density 2,630 RU CM5 chip. Serial concentrations of 0.27, 0.82, 2.47, 7.41, 22.22 and 66.67 nM of Ad3-FK (E), Ad7-FK (F), Ad11-FK (G), and Ad35-FK (H) were injected in HBS-P+ buffer at 30 μl/min under contact time of 300 s and dissociation time of 3,600 s (for better visibility only four of the six binding curves are shown). Data evaluation was fitted globally by two-stage reaction model with Biacore T100 evaluation software, and resulting kinetics/affinity results are listed in STable 1 and summarized in Table 1.

Fig. 2. Binding and transduction of adenovirus species B viruses to cells with increasing CD46 levels. (A) Flow cytometry profiles of CD46 expression in A549 human lung cells, parental rodent CHO and four different stable and clonal CHO-CD46 transfectants. Numbers after slash indicate mean fluorescence intensity values (MFI) resulting from utilizing the MCI20.6 anti-CD46 antibody, controls using isotype control were in the range from 0.8 to 1 (not shown). (B) For Ad binding assays, 5×10^5 of human A549 cells, and the different rodent CHO-CD46 cells were incubated on ice with 1,000 vp of the indicated [^{3}H]-labeled species B serotypes. After incubation for 2 h, the cells were washed and cell-associated radioactivity was determined. Mean values and standard deviations of triplicates from one representative experiment are shown. Asterisks indicate here and in the experiments below the level of significance (*P<0.05; **P<0.005; ***P<0.0005 for comparisons of corresponding Ad binding (infection) in parental CHO versus CD46-transfected cells). (C) CD46 antibody-mediated inhibition of Ad3-eGFP transduction. A549 and CHO-CD46#2 cells were pre-incubated in absence or presence of MEM258 anti-CD46 or control E1-1 anti-CAR antibody for 1 h,

followed by addition of Ad3-eGFP for another 1 h, and eGFP analysis 48 h p.i.. GFP expression levels were normalized to values obtained with the E1-1 antibody, and p-values were calculated for corresponding values. (D) Transduction assays of human A549, parental CHO and CHO-CD46 expressing cells. 10^5 cells were incubated with eGFP expressing Ad3, Ad7, Ad11, and Ad35 vectors at increasing virus concentrations of 10, 100, and 1,000 vp/cell. eGFP expression was analyzed two days p.i. by flow cytometry and are expressed as MFI. (E) Flow cytometry profiles of CD46 (left panel) and desmoglein 2 (middle and right panel). Parental M010119 and stable transfected M010119-eGFP-CD46#8 cells were stained with GB24 anti-CD46 (stains both, endogenous and eGFP-tagged CD46) or with 8E5 anti-desmoglein 2 antibody. Staining of A549 was included for comparison. (F) Transduction assays of human parental and stable CD46-transfected M010119 melanoma cells. Cells were transduced and tested as described above. Background fluorescence intensity for uninfected M010191-eGFP-CD46 cells was higher due to the eGFP-tagged CD46 in these cells.

Fig. 3. Cross-linking of CD46ex-huFc strongly increases blocking of Ad3/7 infection in CHO-CD46#2 and A549 cells. (A) CHO-CD46#2 cells or (C) A549 cells were pre-incubated for 1 h in the cold using the indicated concentrations of adapter CD46ex-huFc alone or in combination with a 2-fold increase series of goat-anti human Fc antibody. Following addition of the different eGFP-expressing vectors for another 1 h, cells were washed and analyzed 48 h p.i. Controls included replacement of CD46ex-huFc with CARex-huFc for CHO-CD46#2 cells (B) and A549 cells (D). Asterisks indicate the level of significance (*P<0.05; **P<0.005; ***P<0.0005 for comparisons of corresponding Ad infection using CD46ex-huFc versus CARex-huFc).

Fig. 4. Inhibition of Ad3-, Ad7-, Ad11-, and Ad35-eGFP transduction in CHO-CD46#2 and A549 cells by recombinant Ad fiber knobs. Cells were pre-incubated for 1 h in the cold using a 5-fold dilution series of the individual FK proteins, followed by addition of the different eGFP-expressing vectors for another 1 h. (A) For CHO-CD46#2 cells, the viral inputs amounted to 29,600, 8,200, 657, and 1,088 vp / cell for Ad3-, Ad7-, Ad11-, and Ad35-eGFP, respectively. The virus input concentrations had been determined in preceding experiments and were chosen such that the unblocked transgene

expression values amounted to fluorescence intensity values of about 200. eGFP analysis was performed 48 h p.i.. FKs are color-coded as follows: Ad5-FK in green, Ad3-FK in red, Ad7-FK in purple, Ad11-FK in cyan and Ad35-FK in dark blue. (B) For A549 cells virus inputs amounted to 14,800, 8,200, 1,314, 2,540 and 2,825 vp/cell for Ad3-, Ad7-, Ad11-, Ad35-, and Ad5-eGFP, respectively. Otherwise, the procedure was the same as above.

Fig. 5. Analysis of FK binding interaction to fluorescence-tagged CD46 by confocal FRAP. 10^4 CHO-eGFP-CD46#33.5 cells (A-E), or A549-eGFP-CD46#2 cells (F) were seeded in each of the six µ-slide channels one day prior imaging. (A) Fluorescence recovery kinetics of FRAP experiments performed in presence of 2.5 ng/µl of Ad5-, 3-, 7-, 11- and 35-FK. The data are depicted as $_{1/2}$ values, the time required to reach 50% of complete recovery. (B) to (E) Titration of the effect of Ad3-FK (B), Ad11-FK (C), Ad35-FK (D), and Ad5-FK (E), using the indicated range of FKs. (F) Comparison of the effect of 64 ng/µl of Ad5-, 3-, 7-FK, and 4 ng/µl of Ad11- and 35-FK in A549-GPF-CD46#2 cells. The control sample (no FK) is depicted in black and the FKs are color-coded as in Fig. 4. Error bars represent standard errors of the means. Statistical significance was assessed by t-tests with a threshold p-value set at 0.01.

Table 1. Summary kinetics/affinity analyses of Ad-FKs binding to immobilized CD46ex-huFc

	k_{a1} ($M^{-1}s^{-1}$)	k_{d1} (s^{-1})	k_{a2} (s^{-1})	k_{d2} (s^{-1})	K_D ± SEM (M)
Ad3-FK	2.30×10^{5}	6.88×10^{-4}	2.01×10^{-3}	1.76×10^{-4}	$2.48 \pm 0.27 \times 10^{-10}$
Ad7-FK	1.44×10^{5}	4.19×10^{-4}	1.94×10^{-3}	1.99×10^{-4}	$3.70 \pm 1.38 \times 10^{-10}$
Ad11-FK	9.27×10^{5}	3.27×10^{-4}	5.41×10^{-3}	1.60×10^{-4}	$2.46 \pm 1.50 \times 10^{-11}$
Ad35-FK	3.08×10^{6}	4.66×10^{-4}	1.25×10^{-3}	1.29×10^{-4}	$1.78 \pm 1.04 \times 10^{-11}$

Values are averages of three individual measurements

Table 2. Species B serotype-mediated eGFP transgene expression in different CHO-CD46-expressing cells compared to parental CHO and human A549 cells

	eGFP expression levels: Fold change compared to CHO[a]		
	CHO-CD46#6	CHO-CD46#1	CHO-CD46#2
Ad3-eGFP	18	55	192
Ad7-eGFP	37	85	354
Ad11-eGFP	40	88	79
Ad35-eGFP	60	106	96

	eGFP expression levels: % of A549 expression[b]			
	CHO	CHO-CD46#6	CHO-CD46#1	CHO-CD46#2
Ad3-eGFP	0.24	19	60	211
Ad7-eGFP	0.23	21	50	202
Ad11-eGFP	1.03	49	105	95
Ad35-eGFP	2.66	177	305	284

	eGFP expression levels: vp/cell needed to reach MFI 100[c]			
	CHO-CD46#6	CHO-CD46#1	CHO-CD46#2	A549
Ad3-eGFP	8,207 (27)	2,597 (16)	717 (4.2)	1,513 (2.7)
Ad7-eGFP	2,919 (9.5)	1,210 (7.3)	267 (1.57)	602 (1.1)
Ad11-eGFP	634 (2.1)	291 (1.8)	314 (1.8)	329 (0.6)
Ad35-eGFP	307	165	170	562

[a] Ratio of eGFP mean fluorescence intensity levels from CD46-expressing cell line to parental CHO were determined for 1,000 vp/cell input.

[b] Percentage of eGFP mean fluorescence intensity levels of CD46-expressing cells relative to A549 cells were determined for 1,000 vp/cell input.

[c] Regression lines were calculated for the eGFP expression levels; numbers in parentheses correspond to fold-higher virus concentration input compared to Ad35-eGFP.

Table 3. eGFP transgene expression analysis in M010119 and M010119-eGFP-CD46#8 cells

	eGFP expression levels: Fold change compared to M010119[a]	eGFP expression levels: vp/cell needed to reach MFI 100[b]	
		M010119	M010119-eGFP-CD46#8
Ad3-eGFP	86	34,513	271 (127)
Ad7-eGFP	26	4,695	91 (52)
Ad11-eGFP	2.1	344	110 (3.1)
Ad35-eGFP	2.3	258	130 (2.0)

[a] Ratio of eGFP mean fluorescence intensity levels from M010119-eGFP-CD46#8 cells to parental M010119 cells were determined for 1,000 vp/cell input.

[b] Regression lines were calculated for the eGFP expression levels. Numbers in parenthesis correspond to fold-enhancement of transduction efficiency in M010119-eGFP-CD46#8 cells compared to M010119 cells, based on MFI 100 values.

Table 4. eGFP transgene expression analysis in CHO-eGFP-CD46#33.5 and A549-eGFP-CD46#2 cells

	eGFP expression levels: vp/cell needed to reach MFI 100[a]		
	CHO-eGFP-CD46#33.5	A549-eGFP-CD46#2[b]	A549
Ad3-eGFP	823	497 (1.1)	559
Ad7-eGFP	270	258 (1.6)	412
Ad11-eGFP	397	247 (1.4)	354
Ad35-eGFP	110	171 (2.1)	358

[a] Regression lines were calculated for the eGFP expression levels.

[b] Numbers in parenthesis correspond to fold-enhancement of transduction efficiency in A549-eGFP-CD46#2 cells compared to parental A549 cells, based on MFI 100 values.

Table 5. Inhibition of Ad3/7/11/35-eGFP and Ad5-eGFP-mediated reporter expression by fiber knob cross competition.

Competitor	Cells	% Inhibition of eGFP expression [a]				
		Ad3-eGFP	Ad7-eGFP	Ad11-eGFP	Ad35-eGFP	Ad5-eGFP
Ad3-FK	CHO-CD46	40	7	18	-3	nd
	A549	93	78	28	18	17/-9
Ad7-FK	CHO-CD46	86	81	21	-10	nd
	A549	95	87	4	-18	2/12
Ad11-FK	CHO-CD46	99	98	99	97	nd
	A549	93	95	99	100	-10/-6
Ad35-FK	CHO-CD46	98	85	97	96	nd
	A549	74	56	99	99	-1/-7
Ad5-FK	CHO-CD46	1	-35	16	0	nd
	A549	24	9	-21	29	26/97
		FK concentration for 50% inhibition (ng/ml) [b]				
		Ad3-eGFP	Ad7-eGFP	Ad11-eGFP	Ad35-eGFP	Ad5-eGFP
Ad3-FK	CHO-CD46	nd	nd	nd	nd	nd
	A549	25	23	nd	nd	nd
Ad7-FK	CHO-CD46	169	2'690	nd	nd	nd
	A549	17	31	nd	nd	nd
Ad11-FK	CHO-CD46	14	21	22	37	nd
	A549	31	87	13	14	nd
Ad35-FK	CHO-CD46	5	63	14	26	nd
	A549	470	4,459	33	5	105

[a]Data correspond to inhibitions obtained using 5,000 ng/ml FK concentration in Fig. 2C, D.

[b]Data were calculated by applying regression lines to values in Fig. 2C, D. nd: not determined.

STable 1. Overview kinetics/affinity analysis of Ad-FKs binding to immobilized CD46ex-huFc

Annalyte / RU chip / binding experiment	Flow rate (ul / min)	k_{a1} ($M^{-1}s^{-1}$) [a]	k_{d1} (s^{-1})	k_{a2} (s^{-1})	k_{d2} (s^{-1})	% χ^2/R_{max}	K_D (M)
Ad3-FK / 1121 / 1	55	2.04×10^5 (0.0014)	7.11×10^{-4} (0.019)	1.97×10^{-3} (0.0037)	1.64×10^{-4} (0.0022)	0.64 - 1.31	2.68×10^{-10} (0.0093)
Ad3-FK / 1121 / 2	30	1.92×10^5 (0.0013)	7.18×10^{-4} (0.020)	2.03×10^{-3} (0.0037)	1.65×10^{-4} (0.0022)	0.66 - 1.28	2.81×10^{-10} (0.0101)
Ad3-FK / 2630 / 3	30	2.93×10^5 (0.0035)	6.36×10^{-4} (0.019)	2.02×10^{-3} (0.0046)	1.98×10^{-4} (0.0029)	1.36 - 2.78	1.94×10^{-10} (0.0079)
Ad7-FK / 1121 / 4	30	4.20×10^4 (0.012)	3.39×10^{-4} (0.059)	3.77×10^{-3} (0.036)	5.08×10^{-5} (0.061)	0.03 - 0.50	1.07×10^{-10} (0.0249)
Ad7-FK / 2630 / 5	30	2.44×10^5 (0.0047)	5.88×10^{-4} (0.015)	1.18×10^{-3} (0.0035)	2.58×10^{-4} (0.0064)	0.44 - 0.93	4.32×10^{-10} (0.0195)
Ad7-FK / 2630 / 6	30	1.44×10^5 (0.0046)	3.30×10^{-4} (0.011)	8.67×10^{-4} (0.048)	2.90×10^{-4} (0.015)	0.25 - 0.71	5.72×10^{-10} (0.0419)
Ad11-FK / 1121 / 7	30	9.04×10^5 (0.021)	9.86×10^{-5} (0.091)	6.96×10^{-4} (0.11)	7.57×10^{-5} (0.39)	2.86 - 5.05	1.07×10^{-11} (0.0531)
Ad11-FK / 2630 / 8	30	7.96×10^5 (0.012)	3.93×10^{-4} (0.018)	1.03×10^{-3} (0.0054)	1.28×10^{-4} (0.01)	0.27 - 3.72	5.47×10^{-11} (0.0527)
Ad11-FK / 2630 / 9	30	1.08×10^6 (0.00086)	4.90×10^{-4} (0.032)	1.45×10^{-2} (0.023)	2.77×10^{-4} (0.046)	3.52 - 4.19	8.48×10^{-12} (0.199)
Ad35-FK / 1121 / 10	30	3.54×10^6 (0.0088)	2.16×10^{-4} (0.015)	1.12×10^{-3} (0.0081)	1.06×10^{-4} (0.0037)	0.12 - 3.03	5.23×10^{-12} (0.0751)
Ad35-FK / 2630 / 11	30	2.12×10^6 (0.0034)	7.96×10^{-4} (0.030)	1.33×10^{-3} (0.0042)	1.51×10^{-4} (0.0049)	0.27 - 3.08	3.85×10^{-11} (0.0222)
Ad35-FK / 2630 / 12	30	3.60×10^6 (0.0057)	3.85×10^{-4} (0.019)	1.30×10^{-3} (0.0061)	1.31×10^{-4} (0.0076)	0.16 - 4.76	9.76×10^{-12} (0.0833)

[a] values in parentheses are errors of the fitting procedure

Legends to supplemental figures

SFig. 1. Analysis of recombinant Ad-FK and CD46ex-huFc proteins. (A, B) Individual FK proteins were produced using the Baculovirus expression system. Purified FK proteins from Ad3, Ad5, Ad7, Ad11, and Ad35 were analyzed by either 12.5% reducing PAGE and sypro ruby red staining (A), or by 10% native PAGE and Coomassie Blue staining (B). (C) Analysis of recombinant CD46ex-huFc. Three µg of purified CD46ex-huFc were analyzed by 10% native PAGE and Coomassie Blue staining.

SFig. 2. Characterization of eGFP-tagged CD46 in CHO-eGFP-CD46#33.5 and A549-eGFP-CD46#2 cells. (A) Flow cytometry profile of eGFP-tagged CD46 expression in CHO-eGFP-CD46#33.5 cells. Cells were stained with GB24 anti-CD46 antibody. Staining of A549 was included for comparison. (B) Test for functionality of eGFP-tagged CD46 in CHO-eGFP-CD46#33.5 cells. 10^5 CHO-eGFP/CD46#33.5 cells were transduced with increasing concentrations of 10, 100, and 1,000 vp/cell of eGFP expressing Ad3, Ad7, Ad11, and Ad35 vectors. eGFP expression levels were analyzed two days p.i. by flow cytometry and are expressed as MFI. Asterisks indicate the level of significance (*P<0.05; **P<0.005; ***P<0.0005 for comparisons of corresponding Ad infection in parental CHO versus CHO-eGFP-CD46#33.5 cells). (C) Flow cytometry profile of CD46 expression in A549-eGFP-CD46#2 (left panel) and parental A549 cells (right panel). Cells were stained with MCI20.6 anti-CD46 antibody (stains endogenous form of CD46 only), and M177 anti-CD46 antibody (stains total pool of CD46). (D) Test for functionality of eGFP-tagged CD46 in A549-eGFP-CD46#2 cells. Transduction was performed as described above for CHO-eGFP-CD46#33.5 cells and included A549-eGFP-CD46#2 cells (left panel) and parental A549 cells (right panel). (E) Binding of CD46-specific antibodies to eGFP-tagged CD46. Flow cytometry analysis of A549 cells expressing normal CD46 and CHO-eGFP/CD46#33 cells expressing eGFP-tagged CD46 was performed using the CD46 antibodies known to block species B Ads (M177, 13/42, GB24, and MEM258), and antibodies with weak blocking activity (Tra-2, E4.3, MCI20.6).

SFig. 3. FRAP and mobility fraction (Mf) analysis of the eGFP-CD46 in presence of human Ad-FK 5, 3, 7, 11 and 35. The mobility of the fluorescence-tagged CD46 receptor was monitored by confocal microscopy over time after photo-bleaching. Each plot comprises the average fluorescence recovery curves for the indicated FKs and the corresponding histogram illustrating the Mf at the end of the recovery. The $\tau 1/2$ values illustrated in Fig. 5 were obtained from the same set of data. (A) Fluorescence recovery curve of FRAP experiments performed in presence of 2.5 ng/µl of Ad5-, 3-, 7-, 11- and 35-FK. (B) to (E) Titration of the effect of Ad3-FK (B), Ad11-FK (C), Ad35-FK (D), and Ad5-FK (E), using the indicated range of FKs. (F) Comparison of the effect of 64 ng/µl of Ad5-, 3-, 7-FK, and 4 ng/µl of Ad11- and 35-FK in A549-GPF-CD46#2 cells. The control sample (no FK) is depicted in black and each FK is color-coded as follows: Ad5-FK in green, Ad3-FK in red, Ad7-FK in pink, Ad11-FK in cyan and Ad35-FK in dark blue. Error bars represent standard error of the means.

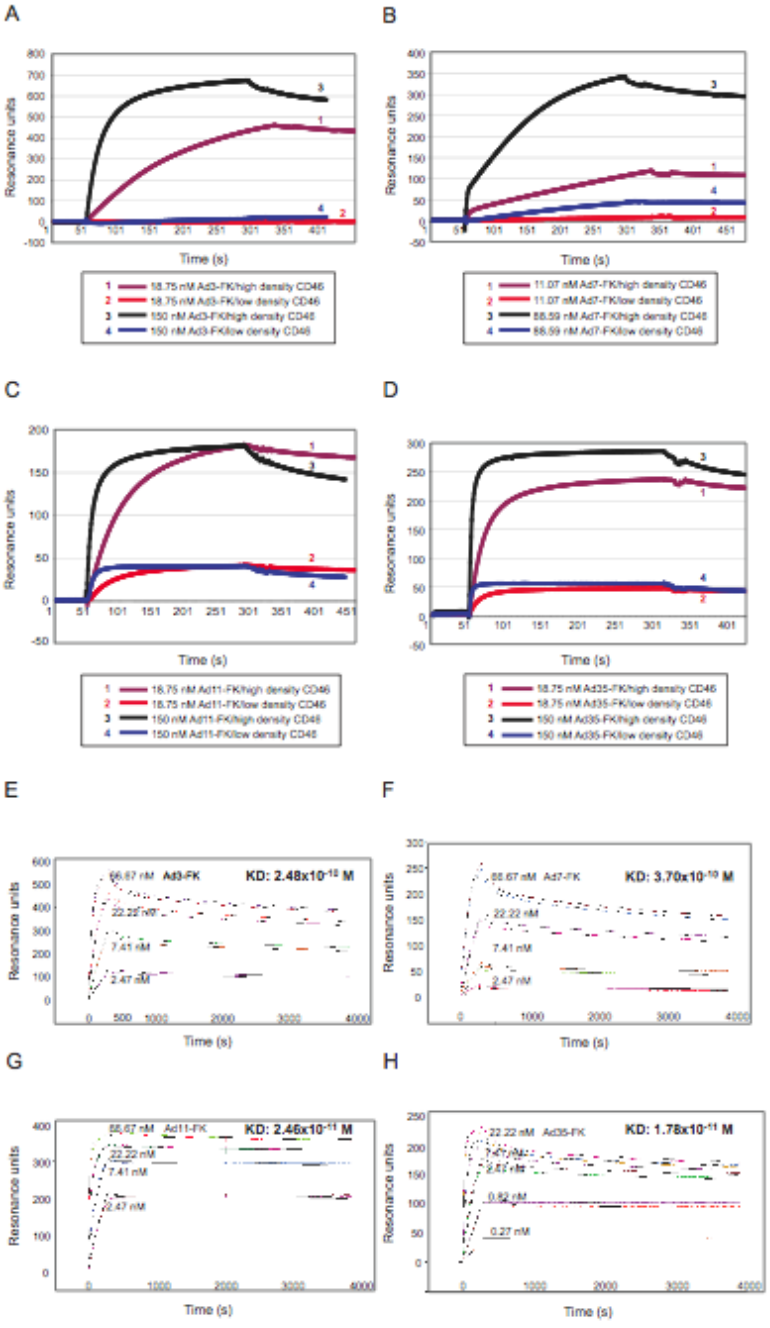
A
Resonance units
Time (s)
1 18.75 nM Ad3-FK/high density CD46
2 18.75 nM Ad3-FK/low density CD46
3 150 nM Ad3-FK/high density CD46
4 150 nM Ad3-FK/low density CD46
B
Resonance units
Time (s)
1 11.07 nM Ad7-FK/high density CD46
2 11.07 nM Ad7-FK/low density CD46
3 88.59 nM Ad7-FK/high density CD46
4 88.59 nM Ad7-FK/low density CD46
C
Resonance units
Time (s)
1 18.75 nM Ad11-FK/high density CD46
2 18.75 nM Ad11-FK/low density CD46
3 150 nM Ad11-FK/high density CD46
4 150 nM Ad11-FK/low density CD46
D
Resonance units
Time (s)
1 18.75 nM Ad35-FK/high density CD46
2 18.75 nM Ad35-FK/low density CD46
3 150 nM Ad35-FK/high density CD46
4 150 nM Ad35-FK/low density CD46
E
66.67 nM Ad3-FK
KD: 2.48x10-12 M
22.22 nM
7.41 nM
2.47 nM
Resonance units
Time (s)
F
66.67 nM Ad7-FK
KD: 3.70x10-10 M
22.22 nM
7.41 nM
2.47 nM
Resonance units
Time (s)
G
66.67 nM Ad11-FK
KD: 2.46x10-11 M
22.22 nM
7.41 nM
2.47 nM
Resonance units
Time (s)
H
22.22 nM Ad35-FK
KD: 1.78x10-11 M
0.82 nM
0.27 nM
Resonance units
Time (s)

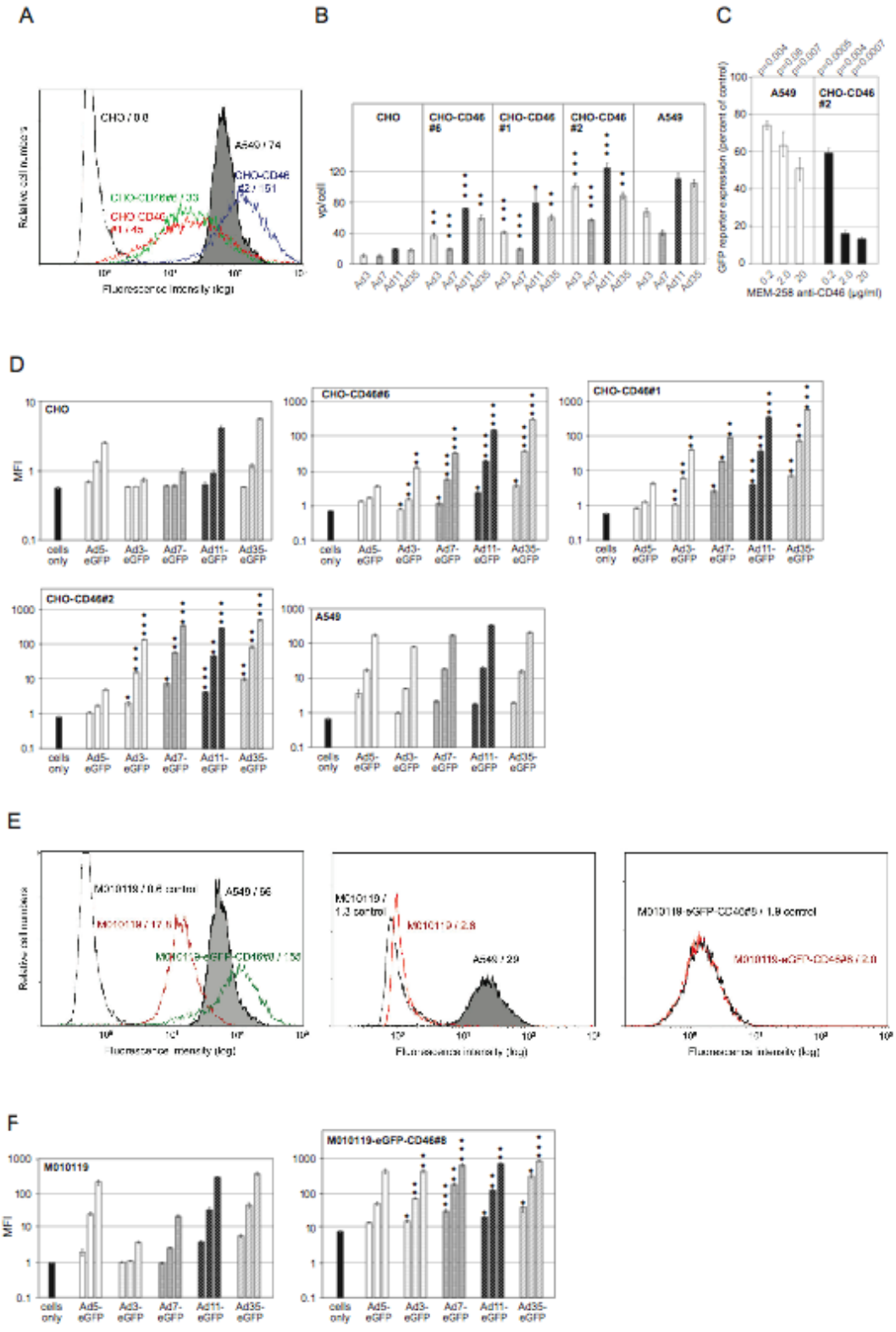
A
B
C
D
E
F
CHO / 0.6
A549 / 74
CHO-CD46#2 / 51
CHO-CD46#6 / 33
CHO-CD46#1 / 45
Relative cell numbers
Fluorescence intensity (log)
CHO
CHO-CD46 #6
CHO-CD46 #1
CHO-CD46 #2
A549
vp/cell
Ad3
Ad7
Ad11
Ad35
p=0.004
p=0.08
p=0.007
p=0.0005
p=0.004
p=0.0007
GFP reporter expression (percent of control)
MEM-258 anti-CD46 (µg/ml)
0.2
2.0
20
MFI
cells only
Ad5-eGFP
Ad3-eGFP
Ad7-eGFP
Ad11-eGFP
Ad35-eGFP
CHO-CD46#6
CHO-CD46#1
CHO-CD46#2
M010119 / 0.6 control
A549 / 56
M010119 / 17.6
M010119-eGFP-CD46#6 / 155
M010119 / 1.2 control
M010119 / 2.8
A549 / 29
M010119-eGFP-CD46#6 / 1.8 control
M010119-eGFP-CD46#6 / 2.0
M010119
M010119-eGFP-CD46#6

A

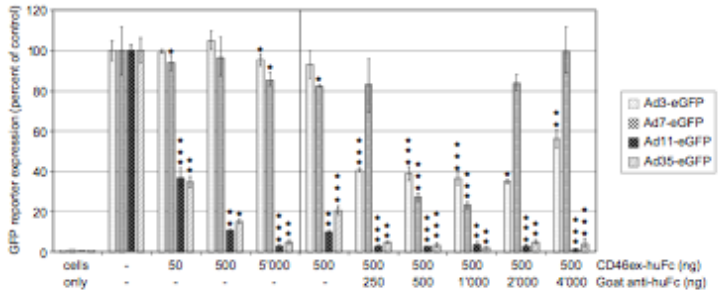
GFP reporter expression (percent of control)
120
100
80
60
40
20
0
Ad3-eGFP
Ad7-eGFP
Ad11-eGFP
Ad35-eGFP
cells - 50 500 5'000 500 500 500 500 500 500 CD46ex-huFc (ng)
only - - - - - 250 500 1'000 2'000 4'000 Goat anti-huFc (ng)

B

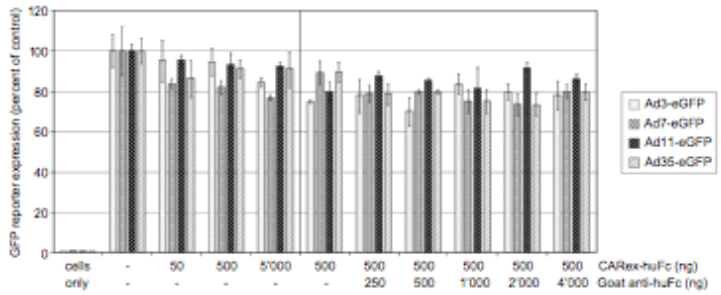
GFP reporter expression (percent of control)
120
100
80
60
40
20
0
Ad3-eGFP
Ad7-eGFP
Ad11-eGFP
Ad35-eGFP
cells - 50 500 5'000 500 500 500 500 500 500 CARex-huFc (ng)
only - - - - - 250 500 1'000 2'000 4'000 Goat anti-huFc (ng)

C

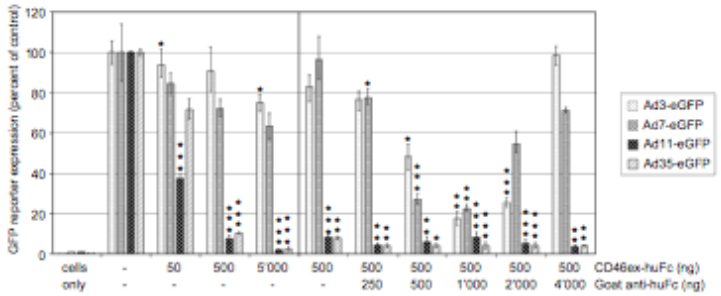
GFP reporter expression (percent of control)
120
100
80
60
40
20
0
Ad3-eGFP
Ad7-eGFP
Ad11-eGFP
Ad35-eGFP
cells - 50 500 5'000 500 500 500 500 500 500 CD46ex-huFc (ng)
only - - - - - 250 500 1'000 2'000 4'000 Goat anti-huFc (ng)

D

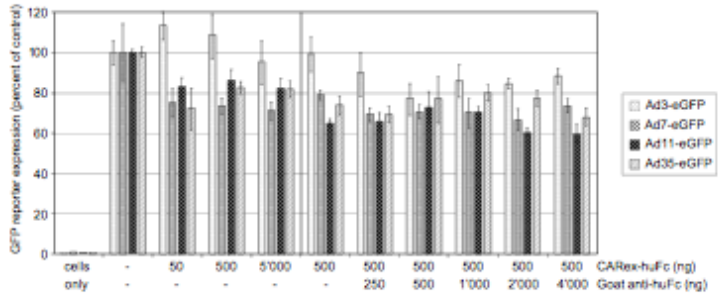
GFP reporter expression (percent of control)
120
100
80
60
40
20
0
Ad3-eGFP
Ad7-eGFP
Ad11-eGFP
Ad35-eGFP
cells - 50 500 5'000 500 500 500 500 500 500 CARex-huFc (ng)
only - - - - - 250 500 1'000 2'000 4'000 Goat anti-huFc (ng)

A

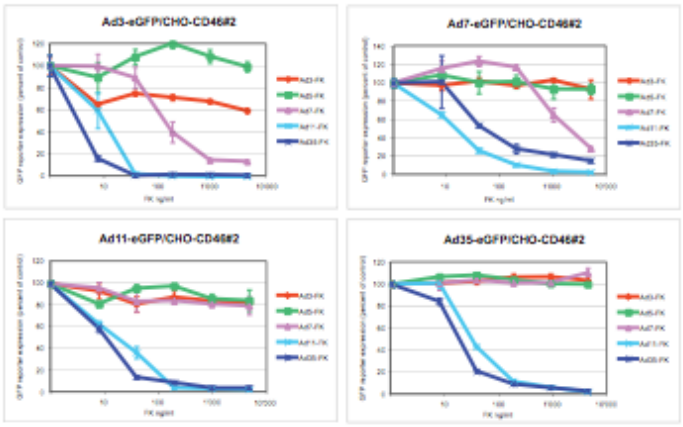
Ad3-eGFP/CHO-CD46#2
Ad7-eGFP/CHO-CD46#2
Ad11-eGFP/CHO-CD46#2
Ad35-eGFP/CHO-CD46#2

B

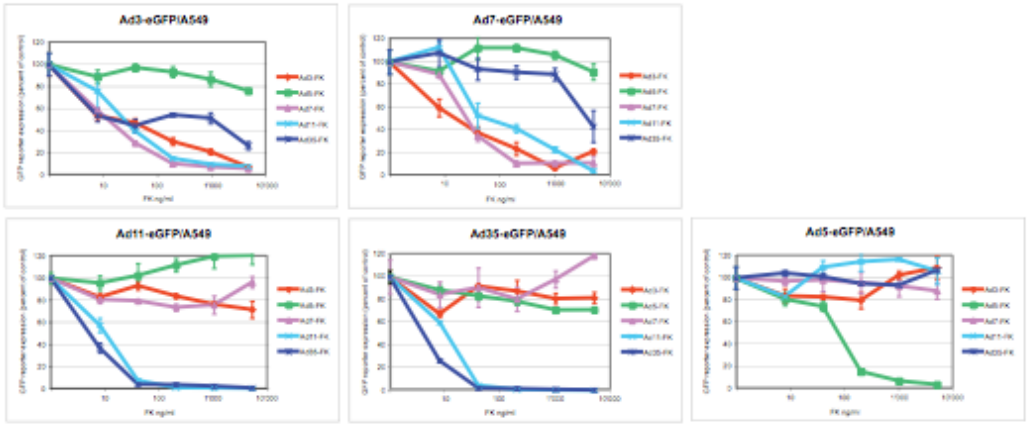
Ad3-eGFP/A549
Ad7-eGFP/A549
Ad11-eGFP/A549
Ad35-eGFP/A549
Ad5-eGFP/A549

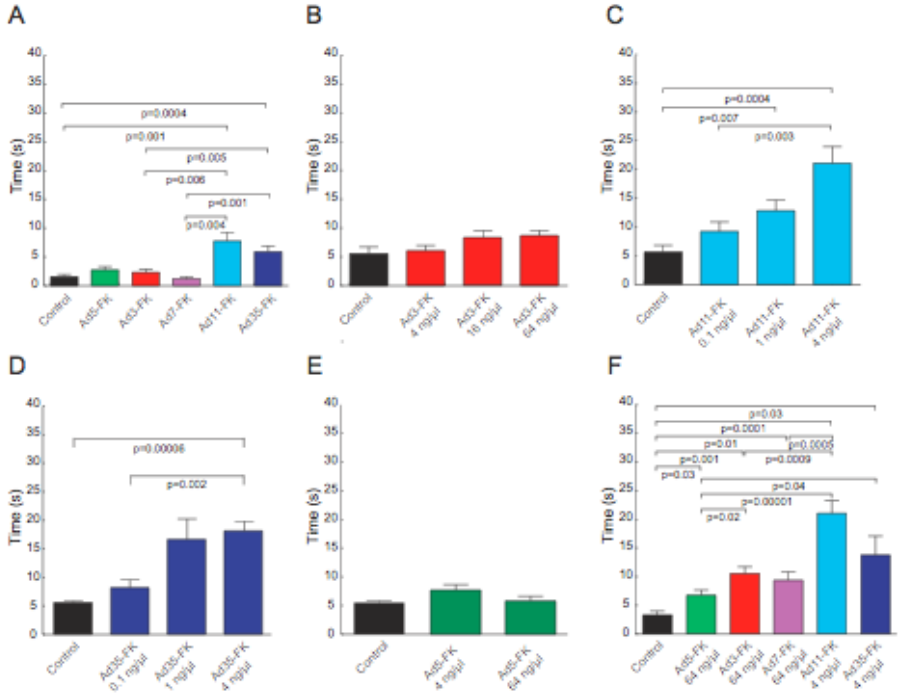
A
B
C
D
E
F
Time (s)
p=0.0004
p=0.001
p=0.005
p=0.006
p=0.001
p=0.004
Control
Ad5-FK
Ad3-FK
Ad7-FK
Ad11-FK
Ad35-FK
Ad3-FK 4 ng/µl
Ad3-FK 16 ng/µl
Ad3-FK 64 ng/µl
p=0.0004
p=0.007
p=0.003
Ad11-FK 0.1 ng/µl
Ad11-FK 1 ng/µl
Ad11-FK 4 ng/µl
p=0.00006
p=0.002
Ad35-FK 0.1 ng/µl
Ad35-FK 1 ng/µl
Ad35-FK 4 ng/µl
Ad5-FK 4 ng/µl
Ad5-FK 64 ng/µl
p=0.03
p=0.0001
p=0.01
p=0.0005
p=0.001
p=0.0009
p=0.03
p=0.04
p=0.00001
p=0.02
Ad5-FK 64 ng/µl
Ad3-FK 64 ng/µl
Ad7-FK 64 ng/µl
Ad11-FK 4 ng/µl
Ad35-FK 4 ng/µl

Trinh sFig. 1

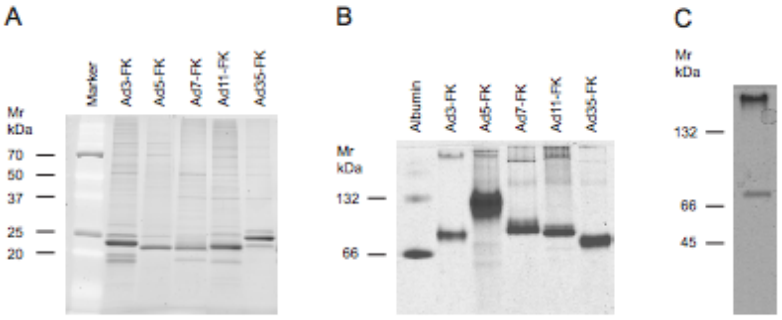
A
Marker
Ad3-FK
Ad5-FK
Ad7-FK
Ad11-FK
Ad35-FK
Mr
kDa
70
50
37
25
20
B
Albumin
Ad3-FK
Ad5-FK
Ad7-FK
Ad11-FK
Ad35-FK
Mr
kDa
132
66
C
Mr
kDa
132
66
45

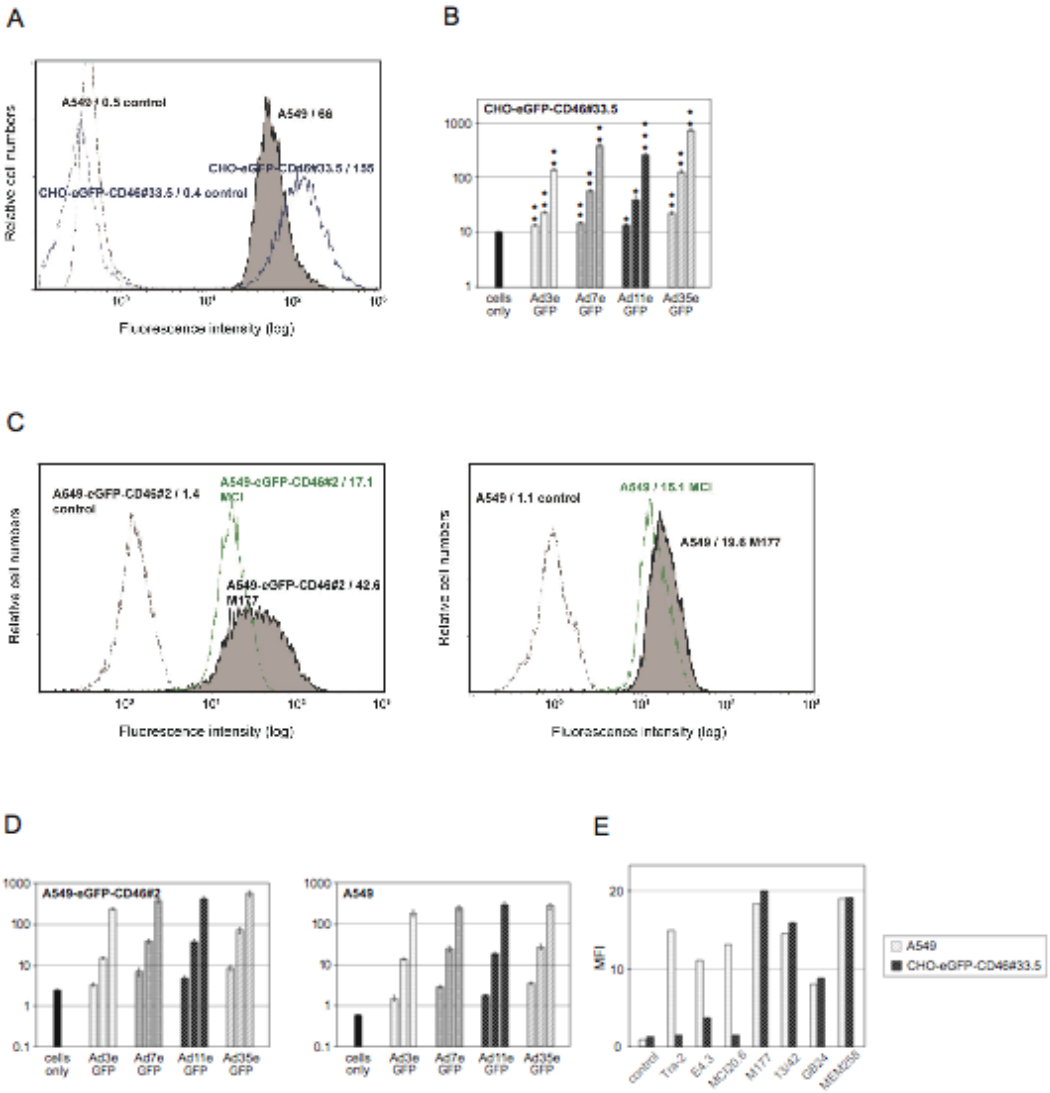
A
B
C
D
E
A549 / 0.5 control
A549 / 68
CHO-eGFP-CD46#33.5 / 155
CHO-eGFP-CD46#33.5 / 0.4 control
Relative cell numbers
Fluorescence intensity (log)
CHO-eGFP-CD46#33.5
cells only
Ad3e GFP
Ad7e GFP
Ad11e GFP
Ad35e GFP
A549-eGFP-CD46#2 / 1.4 control
A549-eGFP-CD46#2 / 17.1 MCI
A549-eGFP-CD46#2 / 42.6 M177
A549 / 1.1 control
A549 / 15.1 MCI
A549 / 19.8 M177
A549-eGFP-CD46#2
A549
MFI
control
Tra-2
E4.3
MCI26.6
M177
13/42
GB24
MEM258
A549
CHO-eGFP-CD46#33.5

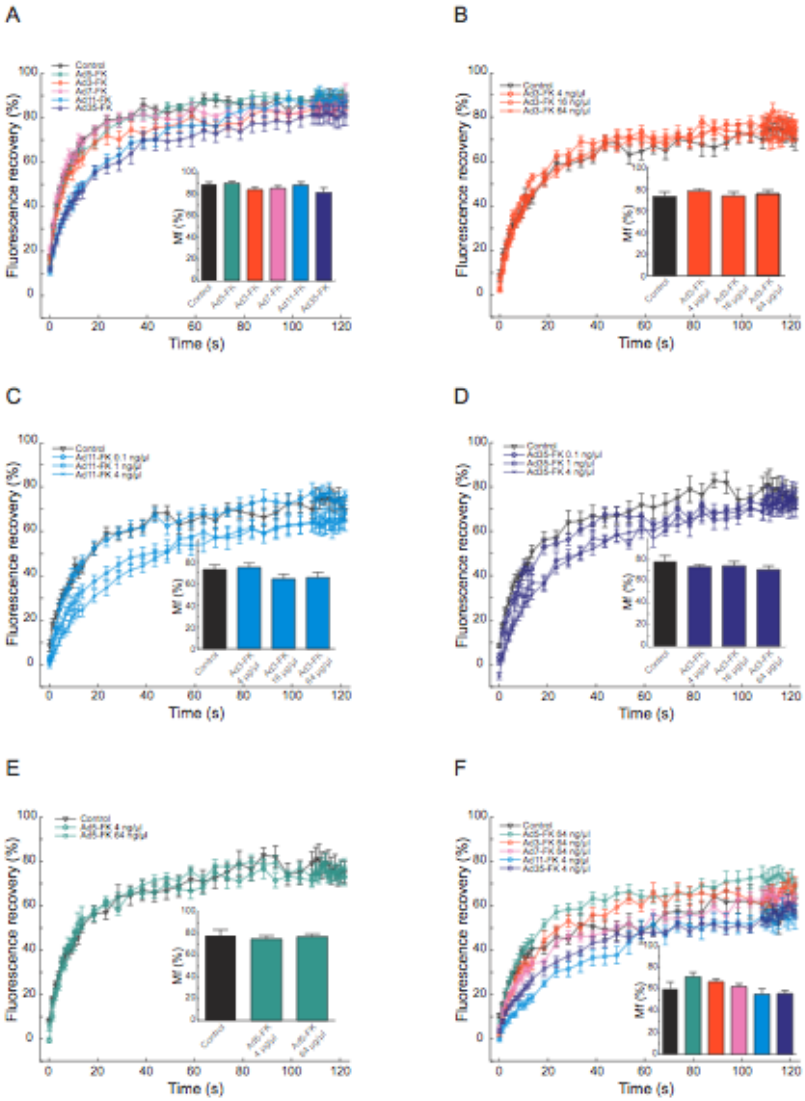
A
B
C
D
E
F
Fluorescence recovery (%)
Time (s)
MF (%)
Control
Ad5-FK
Ad3-FK
Ad7-FK
Ad11-FK
Ad35-FK
Ad3-FK 4 ng/µl
Ad3-FK 16 ng/µl
Ad3-FK 64 ng/µl
Ad11-FK 0.1 ng/µl
Ad11-FK 1 ng/µl
Ad11-FK 4 ng/µl
Ad35-FK 0.1 ng/µl
Ad35-FK 1 ng/µl
Ad35-FK 4 ng/µl
Ad5-FK 4 ng/µl
Ad5-FK 64 ng/µl
Ad7-FK 64 ng/µl

Comparative analyses of quantitative iTRAQ-8plex-based and label-free proteomics for human adenovirus infections

Hung V. Trinh[1,2], Jonas Grossmann[3], Peter Gehrig[3], Bernd Roschitzki[3], Ralph Schlapbach[3], Urs Greber[1], Silvio Hemmi[1*]

[1]*Institute of Molecular Life Sciences, University of Zurich, Winterthurerstrasse 190, CH-8057 Zurich, Switzerland*

[2]*Life Science Zurich Graduate School, Molecular Life Science Program*

[3]*Functional Genomics Center Zurich, University of Zurich, Winterthurerstrasse 190, Zurich 8057, Switzerland*

***Corresponding author:** Dr. Silvio Hemmi, *Institute of Molecular Life Sciences Zurich, Winterthurerstrasse 190, CH-8057 Zurich, Switzerland; Phone: +41 44 635 3120; Fax: +41 44 635 6811; E-mail: silvio.hemmi@imls.uzh.ch*

Abbreviations: human adenovirus (HAdV), ProteinPilot (PP), ScaffoldQ+ (Sc*), Progenesis LC-MS (PL); ProgenesisF-T2PQ (PF2); ProgenesisF-T3PQ (PF3), isobaric tag for relative and absolute quantitation (iTRAQ).

Abstract: 175 words

Total text: 9,442 words

Abstract

Both iTRAQ-label and label-free methods are widely used in quantitative proteome analysis. Here, we aimed to compare iTRAQ-label and label-free quantitation using human A549 cells infected with adenovirus type 3 (HAdV-B3) and type 5 (HAdV-C5). iTRAQ-labeled protein samples were quantified using ProteinPilot (PP) or ScaffoldQ+ (Sc+) software while non-labeled samples were performed using Progenesis LC-MS (PL) or ProgenesisF-T2PQ (PF2) software. As a result, R^2 correlation coefficients were archived between 0.48 and 0.78 for iTRAQ-label while 0.5 and 0.86 for label-free experiments. Overall, the label-free method resulted in higher dynamic range than the iTRAQ-label method and its ratio seemed to be more accurate than iTRAQ-labeling, as suggested by Western-blotting of two downregulated proteins of galectin-1 and transferrin receptor in HAdV-B3-infected cells to non-infected cells. Our results strongly support the notion that iTRAQ-label tends to underestimate the actual ratios and label-free can be used as an alternative method to overcome this problem. Beyond solving the technical issue, we also uncovered protein regulation patterns upon HAdV-B3 or HAdV-C5 infection, which contribute to a better understanding of pathogen-host interactions.

.

Introduction

Quantitative proteomics based on mass spectrometry (MS) has recently become an important component of biological and clinical research, allowing, e.g., the identification of new functional modules and pathways, or the detection of disease biomarkers [1, 2]. Relative quantitation of two or more samples for studies of differential protein expression is of particular importance. Such quantitative results can be gained by use of stable isotope labels or by label-free approaches [3-5].

Several labeling methods have been developed relying on the mass differences between light and heavy isotopes such as ^{2}H, ^{13}C, ^{15}N, and ^{18}O to allow relative protein quantitation using MS. *In vivo* metabolic labeling methods were introduced, with cell-culture enrichment using stable isotope labeled amino acids (SILAC), particularly, arginine [6], lysine [7], tyrosine [8] and leucine [9]. The SILAC labels are of advantage for use in cell culture, but cannot be applied for direct labeling of purified protein or peptide samples. For direct labeling, two most popular chemical labeling strategies are being used. The first, isotope coded affinity tags (ICAT) allows labeling of cysteine-containing peptides followed by enrichment and MS analysis [10]. However, peptides devoid of cysteine residues can not be measured. The isobaric tag for relative and absolute quantitation (iTRAQ) system by Applied Biosystems was developed for relative quantitation and also for absolute quantification with internal peptide standards [11]. Since the iTRAQ reagents react with primary amines of N-termini or lysine residues, most peptides can be efficiently labeled. iTRAQ reporter ions are subsequently released during collision-induced dissociation (CID) fragmentation, and their relative intensities are used for protein quantitation. In contrast to ICAT and SILAC, where two or three samples are compared at a time, iTRAQ allows simultaneous labeling and quantification of four samples [11], or eight samples [12]. By combining multiple samples in one run, the instrument running time for analyses and variations between the different runs are considerably reduced. Other advantages of iTRAQ include their compatibility with different MS platforms, including MALDI-TOF/TOF, Q-TOF, Orbitrap-XL and Orbitrap-Velos instruments. High-throughput quantitative proteomics combined with iTRAQ-label produces large datasets. To quantify the iTRAQ ratios, for example, an array of bioinformatic tools was introduced, including ProQuant (Applied Biosystems), TandTRAQ [13], Multi-Q [14], Mascot 2.2

(Matrix Science, London, UK), Sc+ (http://www.proteomesoftware.com/) and PP [15]. PP utilizes Paragon as a search algorithm. Unlike ProteinPilot (PP), Scaffold does not contain a search engine, but it uses Bayesian statistics to estimate peptide and protein identification probabilities based on Mascot or other search outputs. The (more) recently up-dated ScaffoldQ+ (Sc+) version contains all features for iTRAQ quantitation. Although iTRAQ-labeling has been widely applied, there is an ongoing dispute concerning the accuracy of the deduced protein quantitations when using this method, particularly when dealing with sample mixtures of high complexity [16]. Whereas microarrays can measure differences in expression levels spanning over 3 orders of magnitude, iTRAQ-labels typically reveal fold changes of less than 2 orders of magnitude [17]. From a technical point of view, this may be perceived as a limitation of the iTRAQ-labeling method for quantitative proteomics.

There are two general approaches for label-free quantitation, measurement of spectral peak intensities [18] and spectral counting [19]. The label-free approach can be applied for both shotgun and targeted proteomics [20]. Moreover, it is not only a cost-effective method but also more reproducible [21]. However, correct interpretation of quantitation levels obtained by label-free methods necessitates extended processing of raw LC/MS data, facing high demands with respects to the bioinformatic tools. Thus, multiple software analyses make the data interpretation more reliable. Due to a variety of factors, including peptide compositions, their physicochemical properties and local chemical environment and counting of spectrum-peptide matches are often not an accurate measures of protein abundance [22, 23]. To overcome the bias of MS/MS spectral counting, Lu *et al.* developed the Absolute Proteomics Expression counting method including correction factors that predict detection rates of peptides to obtain a better protein quantitation result [24]. More recently, Grossmann *et al.* adapted a method for the label-free quantitation by selecting the top N most intense precursor ions per protein, depending on the quality of acquired data (TNPQ) [25]. The N can be varied from the top two most intense features (T2PQ) to the top three most intense features (T3PQ) or more [25]. Unlike other label-free quantitation softwares, Progenesis LC-MS (PL, Nonlinear Dynamics) uses vectors to match all experiments to one reference sample in order to achieve a good reference map for comparison. Next, a global scaling factor for each LC-MS run is estimated to normalize all runs. The peptide abundance is the sum of the peak areas within the isotope boundaries while the protein abundance is the sum of the

abundances of all peptide ions, which have been identified as coming from the same protein. Finally, the peak lists are exported in the mgf format and can be used for the Mascot search engine, which later on imports Mascot results back into PL. Due to high-throughput and high speed of MS instruments and based on improved reproducibility of pre-fractionating complex peptide mixtures by LC, label-free quantitative proteomic methods are increasingly considered as reliable and they are used to complement labeling methods [26].

The controversy which quantitative proteomics method is more reliable is still ongoing. Several comparative studies have been performed including analysis of different isotope labels, and use of isotope label versus (vs) label-free approaches [27, 28]. In general, isotope labels offer higher reproducibility in quantitation, while label-free methods require highly reproducible LC-MS/MS platforms [3]. The comparison study for different isotope labels including DIGE, ICAT and iTRAQ indicated that iTRAQ is more sensitive than ICAT [27]. In another study, Patel et al. compared iTRAQ-label and label-free methods, which resulted in 79 common proteins quantified by both methods [28]. However, the issue which quantitation method is more reliable for complex samples remains unsolved.

In this study, we further evaluated whether the iTRAQ-labeling tends to underestimate differences in the actual expression level of proteins compared to label-free method. We performed a large-scale proteome analysis of complex protein samples derived from human lung adenocarcinoma cells infected with human adenovirus type 3 (HAdV-B3) or type 5 (HAdV-C5). Adenoviruses are significant pathogens causing respiratory disease, gastroenteritis, acute hemorrhagic cystitis, meningoencephalitis or conjunctivitis [29-32]. We compared the correlations of up- or down-regulated proteins of HAdV-B3/HAdV-C5-infected cells to non-infected cells when using iTRAQ-label vs label-free approaches. Since HAdVs are widely used and the most extensively studied viruses for gene delivery/therapy purposes [33, 34], the accurate analyses of global protein expression changes in infected cells will hence contribute to enhance the understanding of virus–host interactions.

Experimental Section

Cells, virus and sample preparation for quantitative proteome analysis.

Human A549 lung adenocarcinoma epithelial cells were cultured in Dulbecco's modified Eagle's medium (Sigma) supplemented with 8% fetal bovine serum. A549 cells were infected with HAdV-B3 or HAdV-C5 using a multiplicity of infection (MOI) of 200 infectious virus particles/cell. Control non-infected and HAdV-B3/C5 infected-cells were harvested at 24 hours (h) post infection (p.i.). The cells were washed twice by centrifugation in phosphate-buffered saline. The cell pellets were then resuspended by sonication in lysis buffer containing 10 mM Hepes pH 7.4, 150 mM NaCl, 1% NP-40, 0.5% sodium deoxycholate, 0.1% sodium dodecyl sulfate (SDS), and protease inhibitor cocktail (Roche). Non-solubilized material was removed by centrifugation at 16,000 × g for 20 minutes (min). The proteins contained in the supernatant were precipitated by addition of trichloroacetic acid (TCA) to 20% and twice washed with 100% acetone. Finally, the proteins were solubilized in 0.5 M triethylammonium bicarbonate pH 8.5 plus 0.2% SDS, 1 M urea and 15% methanol. Protein concentrations were measured by the Qubit method (Invitrogen). For downstream analysis by LC-MS/MS, 30 μg of individual protein samples were used.

For the iTRAQ-8plex labeling experiments, 30 μg proteins were reduced in 2 mM of Tris[2-carboxyethyl] phosphine (TCEP) at 37°C for 1 h and the cysteine residues were blocked in 10 mM methyl methanethiosulfonate (MMTS) at room temperature for 15 min followed by trypsin digestion (modified trypsin, Promega) at a protease:protein ratio of 1:12.5 (w/w) at 37°C for 8-10 h. iTRAQ-8plex reagents (Applied Biosystems) were added to the peptide samples, which were incubated at room temperature for 140 min. The reaction was stopped by addition of 10 mM KH_2PO_4, 25% acetonitrile (ACN), pH 2.6 (solvent A), followed by centrifugation at 16,000 x g for 10 min to remove the aggregated proteins.

Chromatography and mass spectrometric analyses.

The digested protein samples were separated by using multidimensional liquid chromatography. In the first dimension, the peptide mixtures were fractionated using a strong

cation exchange chromatography (SCX) column (Polysulphoethyl A, 2.1 mm inner diameter, 200 mm length, 300 Å pore size, 5 µm particle size, PolyLC Inc.) A linear binary gradient from solvent A (10 mM KH_2PO_4, 25% ACN, pH 2.6) to solvent B (10 mM KH_2PO_4, 0.35 M KCl, 25% ACN, pH 2.6) was applied: 0% to 5% solvent B in 15 min, 5% to 35% B in 35 min, and 35% to 100% B in 10 min. The entire run lasted 90 min, and 27 SCX fractions were collected. These fractions were vacuum-dried and redissolved in 0.1% trifluoroacetic acid (TFA), 5% ACN. Based on the SCX chromatograms, the 27 SCX fractions were combined into 8 pools. All pools were further desalted by Sep-Pak C_{18} columns (Waters), which were equilibrated by 100% methanol, 80% ACN, and washed by 0.5% ACN plus 0.1% TFA. Peptides were loaded on the pre-treated columns, which then were washed twice with 0.1% TFA, 5% ACN. Finally, peptides were eluted with 0.1% TFA, 80% ACN, vacuum-dried and redissolved in 0.1% TFA, 5% ACN.

The pooled SCX fractions were then separated in a second dimension by reversed-phase liquid chromatography on an Ultimate chromatography instrument (Dionex) coupled with MALDi-MS/MS. LC-MALDI-MS/MS is the off-line separation of peptides on a capillary liquid chromatography (LC) system. The cleaned peptide samples were automatically injected by a Famos autosampler and separated by an UltiMate capillary LC system (Dionex/LC Packings) and load onto a C_{18} PepMap main column (75 µm ID, 150 mm length, 100 Å pore size, 3 µm particle size; Dionex) using a linear binary gradient (solvent A: 0.1% TFA; solvent B: 0.1% TFA, 80% ACN). HPLC linear gradients were increased by solvent B from 0% (10 min) to 50% (100 min) and from 50% to 100% (112 min). The peptides eluting from the LC column were then mixed with 3-4 mg/ml of matrix α-Cyano-4-hydroxycinnamic acid (Bruker Daltonics) in 0.1% TFA, 70% ACN containing internal neurotensin peptide (Sigma), and were automatically deposited onto an Opti-TOF® LC MALDI plate (Applied Biosystems) by using a Probot spotting device. Four SCX pools gave rise to 1,664 spots on each LC MALDI plate. MS/MS analysis was conducted with a 4800 MALDI-TOF/TOF instrument (Applied Biosystems).

Mass spectrometric analysis was performed on a 4800 MALDI-TOF/TOF instrument equipped with a 355 nm Nd:YAG laser. Mass spectra were acquired in positive reflectron mode in the mass range from m/z 850 to 4000, with a focus mass of m/z 2100. They were

generated by accumulating data from 600 laser pulses, and they were internally recalibrated based on the molecular mass of the neurotensin peptide. The ten most intensive peptide ion signals showing a S/N ratio > 100 were subjected to MS/MS acquisition. Peptide collision-induced dissociation was conducted at a collision energy of 1 kV and at a gas pressure of approximately 2.5 x 10^{-6} Torr. During MS/MS acquisition, a method with a stop condition was used. In this method, a minimum of 1000 and a maximum of 2000 laser pulses were allowed for each spectrum.

For the label-free approach, 30 μg proteins were reduced in 5 mM of TCEP at 37°C for 1 h and blocked in 10 mM iodoacetamide at room temperature for 30 min followed by trypsin digestion at 37°C for 8-10 h. The trypsin digestion was stopped by adding 5% TFA and the pH value was adjusted by 10 mM KH_2PO_4, 25% ACN, pH 2.6. The aggregated proteins were removed by centrifugation at 16,000 x g for 10 min. The protein digests were purified by using Sep-Pak C_{18} columns (Waters). The desalted peptides were vacuum-dried and dissolved in 0.2% formic acid and 3% ACN. The samples were injected into an Eksigent-nano-HPLC system (Eksigent Technologies, Dublin CA, USA) by an autosampler and separated on a self-made reverse-phase tip column (75 µm × 80 mm) packed with C_{18} material (3 µm, 200 Å, AQ, Bischoff GmbH, Leonberg, Germany). The column was equilibrated with 97% solvent A (A: 1% ACN; 0.2% formic acid in water) and 3% solvent B (B: 80% ACN, 0.2% formic acid in water). Peptides were eluted using the following gradient: 0-50 min, 3-30% B; 50-58 min, 30-50% B, and 58-60 min, 50-97% B at a flow rate of 0.2 µL/min. High accuracy mass spectra were acquired on an LTQ-ICR-FT-Ultra mass spectrometer (Thermo Scientific, Bremen, Germany) in the mass range of 300-2,000 m/z and at a target value of $1x10^6$ ions and a resolution of 100,000 at m/z 400. Up to five data dependent MS/MS were recorded in parallel in the linear ion trap from the most intense ions with charge states 2+ or 3+ using collision induced dissociation. Target ions already selected for MS/MS acquisition were dynamically excluded for 120 seconds.

Database searches and quantitative proteome analysis.

Both PP and Mascot search engines were used for protein identification from iTRAQ data acquired on a MALDI-TOF/TOF instrument. Only Mascot was utilized to identify proteins from data acquired on the LTQ-FT-ICR instrument for label-free quantitation. For the analysis with PP v3.0 (Applied Biosystems), the acquired data was directly fetched from the Oracle database and searched with the Paragon algorithm. For the analyses with Mascot, peak lists (mgf files) were generated using Mascot Distiller software v2.3 (Matrix Science Ltd., London, UK). The same database, which contains a non-redundant protein database for both human and HAdVs proteins (www.uniprot.org) and a few of HAdV entries derived from NCBI, was applied for both PP and Mascot searches. The combined database contains 41,135 entries in total including the concatenated reversed decoy entries, which were added in order to estimate the protein false discovery rate (FDR) [35].

In Mascot searches, tolerances of 25 ppm for peptide masses and 0.25 Da for fragment ions were considered for data obtained by using the MALDI-TOF/TOF instrument. In case of data obtained by LTQ-FT-ICR analyses, tolerances of 5 ppm for peptides and of 0.6 Da for fragment ions were used. In all searches, carbamidomethylation or MMTS modification of cysteine residues was selected as fixed modifications and oxidation was considered as variable modification. To obtain a protein FDR below 5%, identified proteins were filtered on peptide levels of an ion score ≥ 30.

Next, PP and Sc+ (Proteome Software) were used for protein quantitation of iTRAQ-labeled samples. For PP, background correction was applied and biological modifications were allowed. To obtain a protein FDR under 5%, protein identifications were filtered with PP score ≥ 1.3 (equivalent to 95% confidence). PP Analysis resulted in both protein identification and quantification. In contrast, we only used the protein identification feature from Mascot searches and applied the quantification feature from Sc+. To improve reliability and confidence of protein quantitation, all precursors ion signals showing an intensity ≤ 50 were discarded before the data were imported into Sc+. The quantitative analyses for the label-free approaches were performed by using the commercial PL software (Nonlinear Dynamics) as recommended by the vendor on the one hand or the Progenesis feature data export was combined with the emerging “high flyer” strategy to quantify proteins based on LC-MS signals. The idea of this strategy termed ProgenesisF-T2PQ (top 2 protein quantitation, PF2)

or ProgenesisF-T3PQ (top 3 protein quantitation, PF3) [25], is that irrespective of how many peptides are found for one particular protein, only the most intense (n) precursor signals are used to produce a quantitative protein value. We adapted this method referred to as PF2 or PF3, respectively, based on the aligned Progenesis feature map by averaging the top N normalized volumes of features from the same protein.

Western blot analysis.

40 µg/lane of A549 cell lysate proteins were separated on 10 or 15% SDS-PAGE, respectively. The rabbit-anti human galectin-1 (LGALS1) antibody was a generous gift from Walter Nickel (University of Heidelberg, Germany). The monoclonal mouse anti-human transferrin receptor 1 (CD71) antibody (clone 3B8 2A1) was purchased from Hycult Biotech, and the monoclonal mouse anti-α-tubulin antibody (DM1A) was purchased from Sigma. Secondary horseradish peroxidase- conjugated anti-mouse antibodies (cat: NA931V), were purchased from GE Healthcare. Signal detection was performed in the chemiluminescent scanning mode of Image reader LAS 3000 (FUJIFILM Science Lab), and signal quantitation was performed using ImageGauge version 3 (FUJIFILM Science Lab).

Results

Workflow for quantitative proteome analysis using iTRAQ-label and label-free methods.

Two independent workflows for iTRAQ-based and label-free approaches using lysates of non-infected A549 or HAdV-B3/HAdV-C5-infected A549 cells were applied (Fig. 1A). Cell lysates were harvested after 24 h p.i. and proteins were precipitated by TCA, followed by trypsin digestion. For the iTRAQ-label approach, the tryptic peptides were labeled with iTRAQ-8plex reagents, separated by SCX chromatography following reverse-phase chromatography and spotted onto MALDI plates. The mass spectrometric analyses were performed on the MALDI-TOF/TOF instrument. Protein quantitation based on iTRAQ data was performed with PP and Sc+ softwares. For the label-free approach, protein digests were analyzed with LC-MS/MS without pre-fractionation. Next, PL, PF2 and PF3 were used for protein quantitation of the label-free samples.

An overview of the subsequently performed data comparisons is shown in Fig. 1B. We first compared the biological replicates within either iTRAQ-label or label-free quantitations. Next, we compared the iTRAQ-label data set with the two different quantitation softwares PP vs Sc+. Likewise, we compared the label-free data set with the two different softwares PL vs PF2. Finally, we addressed the correlation between iTRAQ-label and label-free methods by comparing four sets of PP vs PL, PP vs PF2, Sc+ vs PL, and Sc+ vs PF2.

Reproducibility of iTRAQ-based protein quantitation analyzed by ProteinPilot or ScaffoldQ+ quantitation software.

First we used the two commonly applied commercial softwares PP and Sc+ for analysis of the data acquired by the iTRAQ-labeling procedure. As a result, 1,538 proteins were quantified for HAdV-B3-infected and non-infected control cells, and 1,548 proteins for HAdV-C5-infected and non-infected cells, among 1,802 identified proteins with confidence over 95% (PP score 1.3) and protein FDR of 1.89% (Fig. 2). We then checked the reproducibility of two biological replicates for each condition. The squared Pearson correlation analysis

revealed a R^2 of 0.55 for HAdV-B3-infected cells, and a R^2 of 0.76 for HAdV-C5-infected cells (Fig. 3A and STable 1).

Similarly, we also observed reproducibility between two biological replicates with Sc+ with a Pearson correlation R^2 of 0.49 for HAdV-B3-infected cells and R^2 of 0.69 for HAdV-C5-infected cells with 1,340 and 1,343 quantified proteins in HAdV-B3- and HAdV-C5-infected cells, respectively, with 0% protein FDR (Fig. 3B and STable 1).

Comparison of ProteinPilot and ScaffoldQ+ quantitations for iTRAQ-label analyses.

Comparison of squared Pearson correlations between PP and Sc+ revealed reasonable good correlation, with a R^2 of 0.7 for proteins of HAdV-B3-infected cells, and a R^2 of 0.71 for proteins of HAdV-C5-infected cells (Fig. 3E and STable 1). This indicated that the quantitation of iTRAQ-labeling data was reliable, independent of the algorithm or search engine was used for quantitation. The deduced slope values of 0.8 and 0.84 for proteins of HAdV-B3- and HAdV-C5-infected cells, respectively, indicated that the expression changes quantified by Sc+ were slightly more significant than those quantified by PP. In addition, most of the proteins quantified by Sc+ were also found by using PP. For proteins of HAdV-B3-infected cells, 1,263 proteins overlapped between PP and Sc+, whereas for proteins of HAdV-C5-infected cells, 1,267 proteins overlapped between PP and Sc+. The ratios for most of the quantified proteins were similar between PP and Sc+ (STable 1). In 827 (65.5%) out of 1,263 proteins of HAdV-B3-infectecd cells, the ratios were found in the range of ±20% variations based on log 2 ratio between PP and Sc+, while for HAdV-C5-infected cells, 819 (64.6%) out of 1,267 proteins were found in this range.

Of note, the viral proteins were only detected in virus-infected samples, but not in non-infected cells. The up-regulated proteins thus consisted of viral and cellular proteins in both, PP and Sc+ analyses. When using PP, 37 proteins were found to be up-regulated with threshold of 0.6 (log2 ratio) in HAdV-B3-infected cells, and 51 proteins were down-regulated in these cells (STable 2). Likewise, for HAdV-C5-infected cells, 33 proteins were up-regulated and 20 proteins were down-regulated. Within Sc+, 31 proteins were found up-regulated and 50 proteins were down-regulated in HAdV-B3-infected cells, while 23 proteins

were up-regulated and 25 proteins were down-regulated in HAdV-C5-infected cells. All together, for proteins of HAdV-B3-infected cells, 74 proteins were found up- or down-regulated with both, the PP and the Sc+ program, whereas for proteins from HAdV-C5-infected cells, 40 proteins were determined to be significantly changed by both analysis programs.

12 and five viral proteins were detected in HAdV-B3-infected cells by use of PP and Sc+, respectively. For HAdV-C5-infected cells, 18 and nine viral proteins were detected by use of PP and Sc+, respectively. This is likely due to result from a different scoring algorithm in the PP software.

For one protein of the 1,263 quantified proteins of HAdV-B3-infected cells, and two proteins of the 1,267 quantified proteins of HAdV-C5-infected cells, the quantitation using PP and Sc+ gave rise to ambiguous results (STable 2). These included eukaryotic translation initiation factor 3 subunit F (EIF3F, O00303) in HAdV-B3-infected cells, which revealed a change of -1.12 log2 ratio with PP and a change of -0.6 log2 ratio with Sc+. The different quantitation values for this protein were due to the filtering parameters of PP and Sc+. In the Sc+, both ion precursors and their MS/MS fragmentations were used for protein quantitation while in the PP only one ion precursor and its MS/MS fragmentation was applied. These two ion precursors had different quantitative values; thus results were different depending whether one or two ions were used for quantitation. In case of sterol-4-alpha-carboxylate 3-dehydrogenase, decarboxylating (NSDHL, Q15738), it was quantified by 1.1 of log2 ratio change in PP, and no significant change in Sc+ in HAdV-C5-infected cells. The different quantitation results also derived from a different number of ion precursors were applied for quantitation. Two different precursors were used for PP quantitation whereas one precursor ion was taken into account for Sc+ quantitation. In this case, one precursor ion showed differently in expression level while the other one had no different expression. The one without significant difference was used for Sc+ quantitation. For the case of DNA polymerase epsilon subunit 4, it was up-regulated by 0.85 of log2 ratio with PP while it was down-regulated by -0.90 of log2 ratio with Sc+ in HAdV-C5-infected cells (STable 2). Unlike the other two previous cases described above, both two precursor ions were applied for both PP

and Sc+ quantitation but two precursor ions had low intensity of reporter ions which created a bias in the PP quantitation. This bias caused the different results.

Reproducibility of label-free quantitation analyzed by Progenesis LC-MS, ProgenesisF-T2PQ or ProgenesisF-T3PQ quantitation software.

Three analysis platforms were used to quantify the data acquired by the label-free procedure. With PL quantification based on Mascot search, we were able to quantify 661 proteins in HAdV-B3-infected cells and 660 proteins in HAdV-C5-infected cells, with a squared Pearson correlation R^2 of 0.50 for proteins of HAdV-B3-infected cells, and R^2 value of 0.80 for proteins of HAdV-C5-infected cells (Fig. 3C and STable 1). 48 proteins were found up-regulated in HAdV-B3-infected cells, including sixteen viral proteins, whereas 39 proteins were down-regulated in these cells (STable 2). For HAdV-C5-infected cells, 59 proteins were found to be up-regulated, including seventeen viral proteins, and five proteins were down-regulated.

In parallel to the analysis by PL, the label-free data were also quantified by using our own high flyer strategy PF2 and PF3. As a result, 439 proteins for both HAdV-B3- and HAdV-C5-infected cells were quantified based on the PF2 feature (Table 1). Correlations amounted to R^2 of 0.62 for proteins of HAdV-B3-infected cells, and R^2 of 0.86 for HAdV-C5-infected cells (Fig. 3D and STable 1). Details of proteins with significant changes exceeding the threshold of +/- 0.6 (log2 ratio) are shown in STable 2. Using PF2, 42 proteins were found to be up-regulated in HAdV-B3-infected cells, including sixteen viral proteins, and 37 proteins were down-regulated. In HAdV-C5-infected cells, 54 proteins were determined to be up-regulated, including seventeen viral proteins, and seven proteins were found to be down-regulated. Among the significantly de-regulated cellular proteins, 17 proteins were commonly found in both, HAdV-B3- and HAdV-C5-infected cells. Most of the commonly regulated proteins had the same trend of either up- or down-regulation.

Using PF3, we quantified 347 proteins in both, HAdV-B3- and HAdV-C5-infected cells (STable 1). Comparison of the data obtained with PF2 vs PF3 revealed a squared Pearson correlation R^2 of 0.97 for proteins from HAdV-B3-infected cells and R^2 of 0.99 for proteins of HAdV-C5-infected cells (SFig. 1 and STable 1). Since the obtained correlation was high and

since PF2 had higher sensitivity than PF3, all subsequent comparisons within label-free and iTRAQ-8plex approaches were performed using PF2.

Comparison of Progenesis LC-MS and ProgenesisF-T2PQ quantitations for label-free analyses methods.

When we compared the squared Pearson correlation between PL and PF2 data, the resulting correlation R^2 amounted to 0.93 for proteins of HAdV-B3-infected cells, and 0.96 for proteins of HAdV-C5-infected cells for 439 common quantified proteins (Fig. 3F and STable 1). 78 proteins, including sixteen viral proteins, were significantly up- or down-regulated in HAdV-B3-infected cells. All of those proteins revealed parallel trends. 57 proteins were significantly up- or down-regulated in HAdV-C5-infected cells, including 16 viral proteins. These results indicated a high reproducibility of biological replicates when analyzing label-free quantitation with the two PL and PF2 software. In summary, the differential expression patterns of cellular proteins found in HAdV-B3/HAdV-C5-infected cells compared to non-infected cells were well correlated between the two software. This suggests that the observed difference in expression pattern correlated to the different serotypes used, and did not result from using different analysis software or algorithms.

Comparison of quantitative proteomics with iTRAQ-label and label-free quantitation.

Next we performed a systematic comparison of the data obtained by iTRAQ-labeling and by label-free quantitation. Since both, iTRAQ-labeling as well as label-free quantitation, were previously analyzed by two different softwares, this resulted in four pair to pair comparisons.

The comparison of PP (iTRAQ-label) and PL (label-free) revealed a correlation R^2 of 0.48 for proteins of HAdV-B3-infected cells, and R^2 of 0.73 for proteins of HAdV-C5-infected cells within 564 and 569 common quantified proteins in HAdV-B3- and HAdV-C5-infected cells, respectively (Fig. 4A). Among the proteins quantified by HAdV-B3-infected cells, 23 proteins, including twelve viral proteins were significantly up- or down-regulated in both, iTRAQ-8plex (by PP) and label-free (by PL) (STable 2). For the proteins of HAdV-C5-infected cells, this

comparison resulted in eighteen significantly up- or down-regulated proteins with both methods. All of them had the same trend of regulation, but the fold-change in the label-free approach was in general higher compared to the iTRAQ-labeling approach, illustrated by slope values of 1.06 for proteins of HAdV-B3-infected cells and 1.20 for proteins of HAdV-C5-infected cells. This is seen for instance for the viral proteins of HAdV-B3 and HAdV-C5 (STable 2).

Most of the cellular proteins with significant expression changes revealed the same trend for both analysis programs, except two proteins, including P62633 (cellular nucleic acid-binding protein, CNBP), which was down-regulated with iTRAQ-label (by -0.74 of log2 ratio) but up-regulated with label-free (by 1.01 of log2 ratio) in HAdV-B3-infected cells. In contrast, P68036 (ubiquitin-conjugating enzyme E2 L3, UBE2L3) was up-regulated with iTRAQ-label (by 0.88 of log2 ratio), while down-regulated with label-free (by -1.34 of log2 ratio) in HAdV-B3 infected cells. In these cases, precursor ion resulted in low intensities and only one precursor ion was taken into quantitation. Thus, it is difficult to judge which quantitation method was more reliable in these cases.

The squared Pearson correlation of the comparison of PP (iTRAQ-label) and PF2 (label-free) gave rise to higher R^2 values compared to the pair of PP and PL. Thus we obtained a R^2 of 0.69 for HAdV-B3 including 406 proteins, and a R^2 of 0.78 for HAdV-C5 including 410 proteins (Fig. 4B and STable 1). For proteins of HAdV-B3-infected cells, 22 proteins were significantly changed in both iTRAQ-8plex (PP) and label-free (PF2) (STable 2). For proteins of HAdV-C5-infected cells, 18 proteins showed significant changes. However, not all proteins could be directly compared, since certain proteins with significant expression changes were only quantified with the iTRAQ-label, but not with the label-free-method. The number of proteins quantified by using the iTRAQ-8plex method is higher than in the label-free method. This is due to the pre-fractionation of complex peptide mixtures prior to LC-MS/MS in the iTRAQ-label workflow, while no pre-fractionation was applied in the label-free approach. Similarly to what was found in the PP vs PL comparison, fold-changes of protein expression levels were more pronounced for the data derived by PF2 compared to PP, illustrated by slope values of 1.22 and 1.35 for proteins of HAdV-B3- and HAdV-C5-infected cells, respectively.

For the comparison of Sc+ vs PL, the squared Pearson correlation R^2 was 0.37 for 532 proteins identified in HAdV-B3-infected cells, and 0.60 for 535 proteins identified in HAdV-C5-infected cells (Fig. 4C, STable 1). For proteins of HAdV-B3-infected cells, 20 proteins were significantly changed in both iTRAQ-8plex (Sc+) and label-free (PL) (STable 2). For proteins of HAdV-C5-infected cells, nine proteins showed a significant change. The slope values of PL vs Sc+ were 1.11 for proteins of HAdV-B3-infected cells and 1.28 in case of proteins from HAdV-C5-infected cells, indicating again that dynamic changes were more pronounced in the label-free approach compared to the iTRAQ-labeling method.

Similar to the squared Pearson correlation of Sc+ vs PL comparison, the R^2 Pearson correlation of Sc+ vs PF2 was 0.54 for 394 identified proteins in HAdV-B3-infected cells, and 0.71 for 396 proteins identified in HAdV-C5-infected cells (Fig. 4D, STable 1). For proteins of HAdV-B3-infected cells, thirteen proteins were significantly changed in both iTRAQ-8plex (Sc+) and label-free (PF2) (STable 2). For proteins of HAdV-C5-infected cells, nine proteins were found to be significantly regulated. For most of the commonly quantified proteins by Sc+ and PF2, significant changes were only seen in the label-free approach analyzed with PF2 (STable 2). The slope values of PF2 vs Sc+ amounted to 1.30 for proteins of HAdV-B3-infected cells, and 1.59 for proteins of HAdV-C5-infected cells. All these results showed that quantification of proteins with label-free methods were more sensitive to changes in protein abundance than the iTRAQ-labeling method.

Western blot quantitation for galectin-1 and transferrin receptor in HAdV-B3-infected cells.

We followed up on two proteins which were found to be down-regulated by both iTRAQ-label and label-free approaches and performed Western quantitation of galectin-1 (LGALS1, P0938) and transferrin receptor (TFRC, P02786). For both proteins, down-regulation was more pronounced for HAdV-B3-infected cells than for HAdV-C5-infected cells, and was characterized by higher fold-changes with the label-free approach than with the iTRAQ-labeling approach (STable 2). LGALS1 revealed log2 ratios of -2.81 to -2.73 for PL and Progenesis-T3PQ analysis, respectively, and -1.57 to -1.50 for PP and Sc+ analysis,

respectively. TFRC revealed log2 ratios of -1.28 to -1.27 for PL and PF2 analysis, respectively, and -0.65 to -0.61 for Sc+ and PP analysis, respectively. For the Western blot analysis, we prepared biological replicates of HAdV-B3-infected A549 cell lysates collected 24 h p.i. and compared protein expression levels to those of non-infected cell lysates. Signals of LGALS1 and TFRC were compared with α-tubulin as a reference (Fig. 5A). Quantitation of the Western signals revealed a log2 -3.93 down-regulation for LGALS1 (Fig. 5B) and a log2 -4.66 down-regulation for TFRC (Fig. 5C). Thus, the obtained fold changes in expression levels were closer to the values obtained with the label-free approach than with the iTRAQ-labeling approach. This is in agreement with the notion of underestimating signals in the iTRAQ-label quantitation method.

Discussion and conclusions

Technical issues of quantitative proteome analysis.

The biological replicates for HAdV-B3- and HAdV-C5-infected cells showed fairly good correlations, in both iTRAQ-label, and label-free quantitation, irrespective of the particular quantitation software or strategy was used. With the same dataset obtained from iTRAQ-label, PP searches resulted in 1,538 quantified proteins in HAdV-B3-infected cells and 1,548 proteins in HAdV-C5-infected cells with ≥ 95% protein confidence (1.89% FDR) while Sc+ using the Mascot search engine showed 1,340 and 1,343 quantified proteins in HAdV-B3- and HAdV-C5-infected cells, respectively, on peptide level of an ion score ≥ 30 (resulting in 0% FDR). Among these, 1,263 proteins in HAdV-B3-infected cells and 1,267 proteins in HAdV-C5-infected cells were commonly quantified by both the Sc+ and PP and the intersection could therefore be used to correlate the quantitative answers. In the label-free method, PL quantified 661 proteins in HAdV-B3-infected cells and 660 proteins in HAdV-C5-infected cells while PF2 quantified 439 proteins in both HAdV-B3 and HAdV-C5-infected cells. The reduction to 439 proteins is explained by the fact that the PF2 method by definition requires at least two peptides per protein. All proteins, which were quantified by PF2, were also quantified by PL. In this study, the peptide complexity in the iTRAQ-label approach was reduced with a pre-fractionation step by using SCX-HPLC prior to LC-MS/MS, while pre-fractionation of peptides in the label-free method was not considered prior LC-MS/MS. Therefore, the number of proteins quantified by the label-free method was much smaller than in the fractionated iTRAQ-label samples. Here, we wanted to compare and to correlate the different ratios of common proteins being quantified by both iTRAQ-based and label-free approaches.

An important issue is whether the ratio in iTRAQ-label is comparable to that of label-free quantitation. As already noticed in the result section with sets of iTRAQ-label and label-free comparisons for HAdV-B3- and HAdV-C5-infected cells vs non-infected cells, the change of differentially expressed proteins generally resulted in the same direction with either up or down-regulation for both iTRAQ-label and the label-free quantitation. This indicates that ratiometric analyses by both iTRAQ-label and label-free quantitation are reliable. However,

the fold changes of both viral and cellular proteins tend to be larger dynamic range in the label-free method compared to the iTRAQ-label. Western blotting of the two significantly changed proteins LGALS1 and TFRC further suggested that the ratios quantified by the label-free method was closer to the Western blot analyses than the iTRAQ-label data. These results further support the previous notion by others that iTRAQ-label tends to underestimate the actual ratio in large-scale analysis of complex proteome samples [16, 17].

Advantages and drawbacks of quantitative proteomics using iTRAQ and label-free methods.

The findings that the label-free method provided a high dynamic order and was closer to the data from Western blotting than the iTRAQ-label approach is important for studies that aim to provide high accuracies of protein ratios for different samples. The finding of underestimation of iTRAQ-label is in agreement with previous observations [16, 17]. There are a number of reasons, how iTRAQ-labeling could cause underestimation of the actual fold change; (i), technical reasons include that some additional precursors with similar masses but of completely different peptides are also selected for CID (for these additional peptides one can assume that the ratio of the reporters are close to one, since for most of the proteins the ratio should not undergo dramatic changes). This will shift the ratio towards one, which results in an underestimation of the quantitation of the peptide of interest that is identified in the CID spectrum. The label-free method does not have this drawback if the LCMS signals are properly aligned, they should correspond to only single peptides; (ii), identification and quantification are based on MS/MS data while other methods rely on both full MS and subsequent fragmentation of precursor ions; (iii), iTRAQ reagents can pose problems for many types of mass spectrometers due to the mass cut-off and due to contamination with impurities. Despite recent improvements of iTRAQ reporter intensity in iTRAQ-8plex compared to iTRAQ-4plex and algorithms in PP software to correct for background signals, the issue of underestimated ratios remains problematic. This is illustrated by the fact that this study used the iTRAQ-label combined with background correction mode in PP version 3.

Both the iTRAQ-8plex as well as label-free quantitation offers benefits and disadvantages (pros and cons). An advantage of the iTRAQ-8plex over the lable-free method is the ability to run to 8 samples within a single LC-MS/MS experiment, while label-free quantitation requires individual LC-MS/MS experiments, which consumes more machine time. On the other hand, which samples are compared with what other samples have to be determined upfront. This limits multiplexing in labeling approaches as for label-free approaches (if a successful aligning can be achieved) this can even be done at later stages.

The former difficulty in handling of pre-fractionation steps of complex peptides prior to LC-MS/MS in data analysis nowadays can be overcome by recent software development such as a new release of PL software package. Taking advantage of pre-fractionation prior to LC-MS/MS or target proteomics represents a breakthrough for label-free quantitation because it adapts reliable quantitation, sensitivity and costs as well as time effectiveness. One crucial technical issue with label-free quantitation that remains to be considered is reproducibility. This includes maintaining the same retention times for multi-runs on the same LC column and running the same MS instrument. Thus, for deeply fractionated samples in multiple dimensions, the labeling approach probably is still preferred.

Biological impact of the quantitative proteomics experiments.

Both the iTRAQ-label and label-free methods allowed us to identify a number of significantly regulated proteins in HAdV-B3- or HAdV-C5-infected cells. For instance, ferritin light chain (FTL, P02792) was up-regulated 1.6 to 1.65 of log2-fold in HAdV-B3 and 2.13 to 2.45 of log2-fold in HAdV-C5, when using PP and Sc+, respectively (STable 2). FTL plays an important role for iron homeostasis and delivery of iron to cells. Another example is ITGB5 or β_5 integrin(P18084), which was down-regulated by -0.6 to -0.75 of log2-fold in both HAdV-B3 and HAdV-C5 infected cells. ITGB5 belongs to the heterodimeric integrin protein family, and $\alpha_v\beta_5$ integrin functions as a receptor for fibronectin [36] and vitronectin [37]. Both, $\alpha_v\beta_3$ and $\alpha_v\beta_5$ integrins have been shown to function as internalization receptors during HAdV-C5 infection and HAdV-B3 infections [38-43]. αvβ3 has recently been shown to be recruited from the basolateral to the apical side of polarized cells upon cytokine stimulation to facilitate apical

invasion by HAdV-C5 or C2 [44]. In addition, high expression of ITGB5 was required for efficient HAdV-medicated gene transfer in the human airway cells [45].

Another example, LGALS1 was significantly down-regulated in HAdV-B3-infected cells (-2.81 of log2 ratio) although less significantly changed in HAdV-C5-infected cells. The down-regulation was shown by both the iTRAQ-label and label-free quantitation (STable 2). The LGALS1 belongs to the lectin protein family, which functions in both extracellular and intracellular signaling [46]. LGALS1 interacts with the extracellular parts of cell surface and matrix glycoproteins, as well as with cytoplasmic and nuclear proteins to trigger multiple signaling pathways. Consequently, LGALS1 contributes to modulation of the immune and inflammatory responses [47]. In addition, LGALS1 has been shown to be involved in infection of several viruses such as Nipah virus [48] and human immunodeficiency virus (HIV) [49]. In the case of Nipah virus, LGALS1 inhibits virus attachment and host cell fusion by binding N-linked oligosaccharides from the virion envelope or capsid glycoproteins, promoting their crosslinking and oligomerization. In contrast, LGALS1 was found to act as a host factor to promote HIV infection by stabilization of virus attachment anchors to host cells. The role for LGALS1 in HAdV infections remains unknown. Thus, our finding of LGALS1 down-regulation during HAdV infection may hint at an interesting role of LGALS1 during HAdV infections.

Another protein, immune modifier peptide thymosin alpha 1 (P06454, STable2) [50], was found to be down-regulated in HAdV-B3-infected cells by both the iTRAQ-label and label-free approaches. Thymosin alpha 1 has been clinically tested in combination with other drugs to confer resistance to certain infectious agents such as hepatitis B virus [51]. The regulation of thymosin alpha 1 upon HAdV infections may represent an interesting topic for improvement of gene therapy efforts.

Interestingly, we observed a number of proteins that showed different regulation patterns between HAdV-B3- and HAdV-C5-infected cells. They could relate to differences in the infectious pathways or more complex features of the infections. For instance, heterogeneous nuclear ribonucleoprotein H3 (HNRNPH3, P31942), which is involved in splicing and participates in early heat shock-induced splicing arrest [52], was down-regulated in HAdV-B3- (-0.85 of log2 ratio) and up-regulated in HAdV-C5-infected cells (0.62 of log2 ratio). Another example, thioredoxin domain-containing protein 17 (TXNDC17, Q9BRA2), which modulates

TNF-alpha signaling and NF-kappa-B activation [53], was down-regulated in HAdV-B3- (-1.25 of log2 ratio) and up-regulated in HAdV-C5-infected cells (0.7 of log2 ratio). It has been shown previously that HAdV-2C E3-19 K protein activated transcription factor NF-kappa-B [54]. Thus, the deregulation of TXNDC17 may be involved in a HAdV serotype-specific antiviral response.

Overall, our findings provide new insights into advantages and disadvantages of iTRAQ-label and label-free quantitation and support the earlier notions of underestimating the actual fold changes by the iTRAQ-label approach. The obtained quantitative data of up- and down-regulated cellular proteins can now be followed up to further increase our understanding of HAdV-host cell interactions.

Acknowledgements

We thank Claudia Fortes, Functional Genomics Center Zurich, for assistance in peptide separation using HPLC. This work was funded by University of Zurich Forschungs-Kredit (credit number: 57113401) and University of Zurich University Research Priority Program (URPP) Systems Biology/Functional Genomics as well as Swiss SystemsX.ch initiative, grant LipidX-2008/011 to Greber, U.F.

References

1. Anderson, N. L.; Anderson, N. G.; Pearson, T. W.; Borchers, C. H.; Paulovich, A. G.; Patterson, S. D.; Gillette, M.; Aebersold, R.; Carr, S. A., A human proteome detection and quantitation project. *Mol Cell Proteomics* **2009,** 8, (5), 883-6.

2. Whiteaker, J. R., The increasing role of mass spectrometry in quantitative clinical proteomics. *Clin Chem* 56, (9), 1373-4.

3. Bantscheff, M.; Schirle, M.; Sweetman, G.; Rick, J.; Kuster, B., Quantitative mass spectrometry in proteomics: a critical review. *Anal Bioanal Chem* **2007,** 389, (4), 1017-31.

4. Sechi, S.; Oda, Y., Quantitative proteomics using mass spectrometry. *Curr Opin Chem Biol* **2003,** 7, (1), 70-7.

5. Schulze, W. X.; Usadel, B., Quantitation in mass-spectrometry-based proteomics. *Annu Rev Plant Biol* **2010,** 61, 491-516.

6. Ong, S. E.; Kratchmarova, I.; Mann, M., Properties of 13C-substituted arginine in stable isotope labeling by amino acids in cell culture (SILAC). *J Proteome Res* **2003,** 2, (2), 173-81.

7. Martinovic, S.; Veenstra, T. D.; Anderson, G. A.; Pasa-Tolic, L.; Smith, R. D., Selective incorporation of isotopically labeled amino acids for identification of intact proteins on a proteome-wide level. *J Mass Spectrom* **2002,** 37, (1), 99-107.

8. Ibarrola, N.; Molina, H.; Iwahori, A.; Pandey, A., A novel proteomic approach for specific identification of tyrosine kinase substrates using [13C]tyrosine. *J Biol Chem* **2004,** 279, (16), 15805-13.

9. Ong, S. E.; Blagoev, B.; Kratchmarova, I.; Kristensen, D. B.; Steen, H.; Pandey, A.; Mann, M., Stable isotope labeling by amino acids in cell culture, SILAC, as a simple and accurate approach to expression proteomics. *Mol Cell Proteomics* **2002,** 1, (5), 376-86.

10. Gygi, S. P.; Rist, B.; Gerber, S. A.; Turecek, F.; Gelb, M. H.; Aebersold, R., Quantitative analysis of complex protein mixtures using isotope-coded affinity tags. *Nat Biotechnol* **1999,** 17, (10), 994-9.

11. Ross, P. L.; Huang, Y. N.; Marchese, J. N.; Williamson, B.; Parker, K.; Hattan, S.; Khainovski, N.; Pillai, S.; Dey, S.; Daniels, S.; Purkayastha, S.; Juhasz, P.; Martin, S.; Bartlet-Jones, M.; He, F.; Jacobson, A.; Pappin, D. J., Multiplexed protein quantitation in Saccharomyces cerevisiae using amine-reactive isobaric tagging reagents. *Mol Cell Proteomics* **2004,** 3, (12), 1154-69.

12. Choe, L.; D'Ascenzo, M.; Relkin, N. R.; Pappin, D.; Ross, P.; Williamson, B.; Guertin, S.; Pribil, P.; Lee, K. H., 8-plex quantitation of changes in cerebrospinal fluid protein expression in subjects undergoing intravenous immunoglobulin treatment for Alzheimer's disease. *Proteomics* **2007,** 7, (20), 3651-60.

13. Laderas, T.; Bystrom, C.; McMillen, D.; Fan, G.; McWeeney, S., TandTRAQ: an open-source tool for integrated protein identification and quantitation. *Bioinformatics* **2007,** 23, (24), 3394-6.

14. Lin, W. T.; Hung, W. N.; Yian, Y. H.; Wu, K. P.; Han, C. L.; Chen, Y. R.; Chen, Y. J.; Sung, T. Y.; Hsu, W. L., Multi-Q: a fully automated tool for multiplexed protein quantitation. *J Proteome Res* **2006,** 5, (9), 2328-38.

15. Shilov, I. V.; Seymour, S. L.; Patel, A. A.; Loboda, A.; Tang, W. H.; Keating, S. P.; Hunter, C. L.; Nuwaysir, L. M.; Schaeffer, D. A., The Paragon Algorithm, a next generation search engine that uses sequence temperature values and feature probabilities to identify peptides from tandem mass spectra. *Mol Cell Proteomics* **2007,** 6, (9), 1638-55.

16. Chong, P. K.; Gan, C. S.; Pham, T. K.; Wright, P. C., Isobaric tags for relative and absolute quantitation (iTRAQ) reproducibility: Implication of multiple injections. *J Proteome Res* **2006,** 5, (5), 1232-40.

17. Ow, S. Y.; Salim, M.; Noirel, J.; Evans, C.; Rehman, I.; Wright, P. C., iTRAQ underestimation in simple and complex mixtures: "the good, the bad and the ugly". *J Proteome Res* **2009,** 8, (11), 5347-55.

18. Chelius, D.; Bondarenko, P. V., Quantitative profiling of proteins in complex mixtures using liquid chromatography and mass spectrometry. *J Proteome Res* **2002,** 1, (4), 317-23.

19. Zhang, B.; VerBerkmoes, N. C.; Langston, M. A.; Uberbacher, E.; Hettich, R. L.; Samatova, N. F., Detecting differential and correlated protein expression in label-free shotgun proteomics. *J Proteome Res* **2006,** 5, (11), 2909-18.

20. Ahrens, C. H.; Brunner, E.; Qeli, E.; Basler, K.; Aebersold, R., Generating and navigating proteome maps using mass spectrometry. *Nat Rev Mol Cell Biol* **2010,** 11, (11), 789-801.

21. Neilson, K. A.; Ali, N. A.; Muralidharan, S.; Mirzaei, M.; Mariani, M.; Assadourian, G.; Lee, A.; van Sluyter, S. C.; Haynes, P. A., Less label, more free: Approaches in label-free quantitative mass spectrometry. *Proteomics* **2011,** 11, (4), 535-53.

22. Kuster, B.; Schirle, M.; Mallick, P.; Aebersold, R., Scoring proteomes with proteotypic peptide probes. *Nat Rev Mol Cell Biol* **2005,** 6, (7), 577-83.

23. Mallick, P.; Schirle, M.; Chen, S. S.; Flory, M. R.; Lee, H.; Martin, D.; Ranish, J.; Raught, B.; Schmitt, R.; Werner, T.; Kuster, B.; Aebersold, R., Computational prediction of proteotypic peptides for quantitative proteomics. *Nat Biotechnol* **2007,** 25, (1), 125-31.

24. Lu, P.; Vogel, C.; Wang, R.; Yao, X.; Marcotte, E. M., Absolute protein expression profiling estimates the relative contributions of transcriptional and translational regulation. *Nat Biotechnol* **2007,** 25, (1), 117-24.

25. Grossmann, J.; Roschitzki, B.; Panse, C.; Fortes, C.; Barkow-Oesterreicher, S.; Rutishauser, D.; Schlapbach, R., Implementation and evaluation of relative and absolute quantification in shotgun proteomics with label-free methods. *J Proteomics* 73, (9), 1740-6.

26. Zhu, W.; Smith, J. W.; Huang, C. M., Mass spectrometry-based label-free quantitative proteomics. *J Biomed Biotechnol* 2010, 840518.

27. Wu, W. W.; Wang, G.; Baek, S. J.; Shen, R. F., Comparative study of three proteomic quantitative methods, DIGE, cICAT, and iTRAQ, using 2D gel- or LC-MALDI TOF/TOF. *J Proteome Res* **2006,** 5, (3), 651-8.

28. Patel, V. J.; Thalassinos, K.; Slade, S. E.; Connolly, J. B.; Crombie, A.; Murrell, J. C.; Scrivens, J. H., A comparison of labeling and label-free mass spectrometry-based proteomics approaches. *J Proteome Res* **2009,** 8, (7), 3752-9.

29. Hayashi, S.; Hogg, J. C., Adenovirus infections and lung disease. *Curr Opin Pharmacol* **2007,** 7, (3), 237-43.

30. Hierholzer, J. C., Adenoviruses in the immunocompromised host. *Clin Microbiol Rev* **1992,** 5, (3), 262-74.

31. Greber, U. F.; Way, M., A superhighway to virus infection. *Cell* **2006,** 124, (4), 741-54.

32. Burckhardt, C. J.; Greber, U. F., Virus movements on the plasma membrane support infection and transmission between cells. *PLoS Pathogens* **2009,** in press.

33. McConnell, M. J.; Imperiale, M. J., Biology of adenovirus and its use as a vector for gene therapy. *Hum Gene Ther* **2004,** 15, (11), 1022-33.

34. Tatsis, N.; Ertl, H. C., Adenoviruses as vaccine vectors. *Mol Ther* **2004,** 10, (4), 616-29.

35. Kall, L.; Storey, J. D.; MacCoss, M. J.; Noble, W. S., Assigning significance to peptides identified by tandem mass spectrometry using decoy databases. *J Proteome Res* **2008,** 7, (1), 29-34.

36. Busk, M.; Pytela, R.; Sheppard, D., Characterization of the integrin alpha v beta 6 as a fibronectin-binding protein. *J Biol Chem* **1992,** 267, (9), 5790-6.

37. Memmo, L. M.; McKeown-Longo, P., The alphavbeta5 integrin functions as an endocytic receptor for vitronectin. *J Cell Sci* **1998,** 111 (Pt 4), 425-33.

38. Bergelson, J. M., Receptors mediating adenovirus attachment and internalization. *Biochem Pharmacol* **1999,** 57, (9), 975-9.

39. Takayama, K.; Ueno, H.; Pei, X. H.; Nakanishi, Y.; Yatsunami, J.; Hara, N., The levels of integrin alpha v beta 5 may predict the susceptibility to adenovirus-mediated gene transfer in human lung cancer cells. *Gene Ther* **1998,** 5, (3), 361-8.

40. Wickham, T. J.; Filardo, E. J.; Cheresh, D. A.; Nemerow, G. R., Integrin alpha v beta 5 selectively promotes adenovirus mediated cell membrane permeabilization. *J Cell Biol* **1994,** 127, (1), 257-64.

41. Amstutz, B.; Gastaldelli, M.; Kalin, S.; Imelli, N.; Boucke, K.; Wandeler, E.; Mercer, J.; Hemmi, S.; Greber, U. F., Subversion of CtBP1-controlled macropinocytosis by human adenovirus serotype 3. *EMBO J* **2008,** 27, (7), 956-69.

42. Shayakhmetov, D. M.; Eberly, A. M.; Li, Z. Y.; Lieber, A., Deletion of penton RGD motifs affects the efficiency of both the internalization and the endosome escape of viral particles containing adenovirus serotype 5 or 35 fiber knobs. *J Virol* **2005,** 79, (2), 1053-61.

43. Meier, O.; Boucke, K.; Hammer, S. V.; Keller, S.; Stidwill, R. P.; Hemmi, S.; Greber, U. F., Adenovirus triggers macropinocytosis and endosomal leakage together with its clathrin-mediated uptake. *J. Cell. Biol.* **2002,** 158, (6), 1119-1131.

44. Lutschg, V.; Boucke, K.; Hemmi, S.; Greber, U. F., Chemotactic anti-viral cytokines promote infectious apical entry of human adenovirus into polarized epithelial cells. *Nat. Comm* **2011,** (in revision).

45. Goldman, M. J.; Wilson, J. M., Expression of alpha v beta 5 integrin is necessary for efficient adenovirus-mediated gene transfer in the human airway. *J Virol* **1995,** 69, (10), 5951-8.

46. Liu, F. T.; Rabinovich, G. A., Galectins as modulators of tumour progression. *Nat Rev Cancer* **2005,** 5, (1), 29-41.

47. Rabinovich, G. A.; Ilarregui, J. M., Conveying glycan information into T-cell homeostatic programs: a challenging role for galectin-1 in inflammatory and tumor microenvironments. *Immunol Rev* **2009,** 230, (1), 144-59.

48. Garner, O. B.; Aguilar, H. C.; Fulcher, J. A.; Levroney, E. L.; Harrison, R.; Wright, L.; Robinson, L. R.; Aspericueta, V.; Panico, M.; Haslam, S. M.; Morris, H. R.; Dell, A.; Lee, B.; Baum, L. G., Endothelial galectin-1 binds to specific glycans on nipah virus fusion protein and inhibits maturation, mobility, and function to block syncytia formation. *PLoS Pathog* **2010,** 6, (7), e1000993.

49. Ouellet, M.; Mercier, S.; Pelletier, I.; Bounou, S.; Roy, J.; Hirabayashi, J.; Sato, S.; Tremblay, M. J., Galectin-1 acts as a soluble host factor that promotes HIV-1 infectivity through stabilization of virus attachment to host cells. *J Immunol* **2005,** 174, (7), 4120-6.

50. Garaci, E.; Pica, F.; Sinibaldi-Vallebona, P.; Pierimarchi, P.; Mastino, A.; Matteucci, C.; Rasi, G., Thymosin alpha(1) in combination with cytokines and chemotherapy for the treatment of cancer. *Int Immunopharmacol* **2003,** 3, (8), 1145-50.

51. Lau, G. K.; Nanji, A.; Hou, J.; Fong, D. Y.; Au, W. S.; Yuen, S. T.; Lin, M.; Kung, H. F.; Lam, S. K., Thymosin-alpha1 and famciclovir combination therapy activates T-cell response in patients with chronic hepatitis B virus infection in immune-tolerant phase. *J Viral Hepat* **2002,** 9, (4), 280-7.

52. Mahe, D.; Mahl, P.; Gattoni, R.; Fischer, N.; Mattei, M. G.; Stevenin, J.; Fuchs, J. P., Cloning of human 2H9 heterogeneous nuclear ribonucleoproteins. Relation with splicing and early heat shock-induced splicing arrest. *J Biol Chem* **1997,** 272, (3), 1827-36.

53. Jeong, W.; Chang, T. S.; Boja, E. S.; Fales, H. M.; Rhee, S. G., Roles of TRP14, a thioredoxin-related protein in tumor necrosis factor-alpha signaling pathways. *J Biol Chem* **2004,** 279, (5), 3151-9.

54. Pahl, H. L.; Sester, M.; Burgert, H. G.; Baeuerle, P. A., Activation of transcription factor NF-kappaB by the adenovirus E3/19K protein requires its ER retention. *J Cell Biol* **1996,** 132, (4), 511-22.

Legends to figures

Fig. 1. Workflow for comparisons of iTRAQ-label and label-free quantitations. (A), experimental procedures for the iTRAQ-label and label-free methods. A549 cells were infected with HAdV-B3 and HAdV-C5 using an MOI of 200. The cells were harvested at 24 h p.i.. Resulting cell lysates were used for either iTRAQ-label or label-free quantitation. For iTRAQ-label quantitation, tryptic peptides were separated by SCX-HPLC prior to LC-MS/MS by MALDI-TOF/TOF instrument. The PP and Sc+ were used for analyses of protein quantitation. For the label-free quantitation, tryptic peptides were injected directly to LC-MS/MS (LTQ-FT-ICR) without pre-fractionation. The data generated by label-free approach was quantified by using PL and PF2 and PF3. (B), comparative analyses performed for reproducibility of biological replicates, quantification of iTRAQ-label/label-free with different software, and quantitation between iTRAQ-label vs label-free methods.

Fig. 2. Number of quantified proteins in HAdV-B3 and HAdV-C5-infected cells using iTRAQ-label and label-free methods and their pair-wise comparisons. PP and Sc+ softwares were used to analyze iTRAQ data, while PL, PF2 and PF3 software was applied for label-free quantitations.

Fig. 3. Reproducibility of two independent biological replicates using either iTRAQ-label or label-free method and comparison within the iTRAQ-label or non-label with different quantitation software. Different expression of proteins in HAdV-B3-infected cells (red) and HAdV-C5-infected cells (black) is shown based on log2 ratio. Scatter plot for quantified proteins was analyzed by PP (A), Sc+ (B), PL (C), and by PF2 (D), comparison of PP vs Sc+ (E) and PL vs PF2 (F).

Fig. 4. Comparisons of iTRAQ-label-based vs label-free quantitation. All four comparisons are given by log2 ratios with HAdV-B3-infected cells (red) and HAdV-C5-infected cells (black). Scatter plot analysis for quantified proteins was performed by PP vs PL (A), PP vs PF2 (B), Sc+ vs PL (C), and Sc+ vs PF2 (D).

Fig. 5. Western blot analysis of LGALS1 and TFRC and comparison of different quantitation methods. (A), lysates of HAdV-B3-infected A549 cells were immuno-stained for LGALS1 and TFRC. Tubulin (Tub) was used as loading control to normalize LGALS1 and TRFC signals.

Comparison of quantitative assesment by Western blot analysis, label-free method and iTRAQ-quantitation for LGALS1 (B), and TRFC (C).

Legends to supplemental figures and tables

SFig. 1. Comparison of PF2 and PF3 for label-free quantitations with samples obtained from HAdV-B3-infected cells (red), and HAdV-C5 infected cells (black), based on log2 ratios.

STable 1. List of pairwise comparisons for commonly quantified proteins given by log2 ratios. (*) indicates values corresponding to (*) given by the software.

STable 2. List of significantly up- or down-regulated viral and cellular proteins quantified by iTRAQ-label and/or by label-free methods. Proteins with significant (Sig) fold change higher than 0.6 (log2 ratio) are shown in bold. Viral proteins encoded by HAdV-B3 and HAdV-C5 are shown in red and blue, respectively; cellular proteins appear in black

Fig. 1

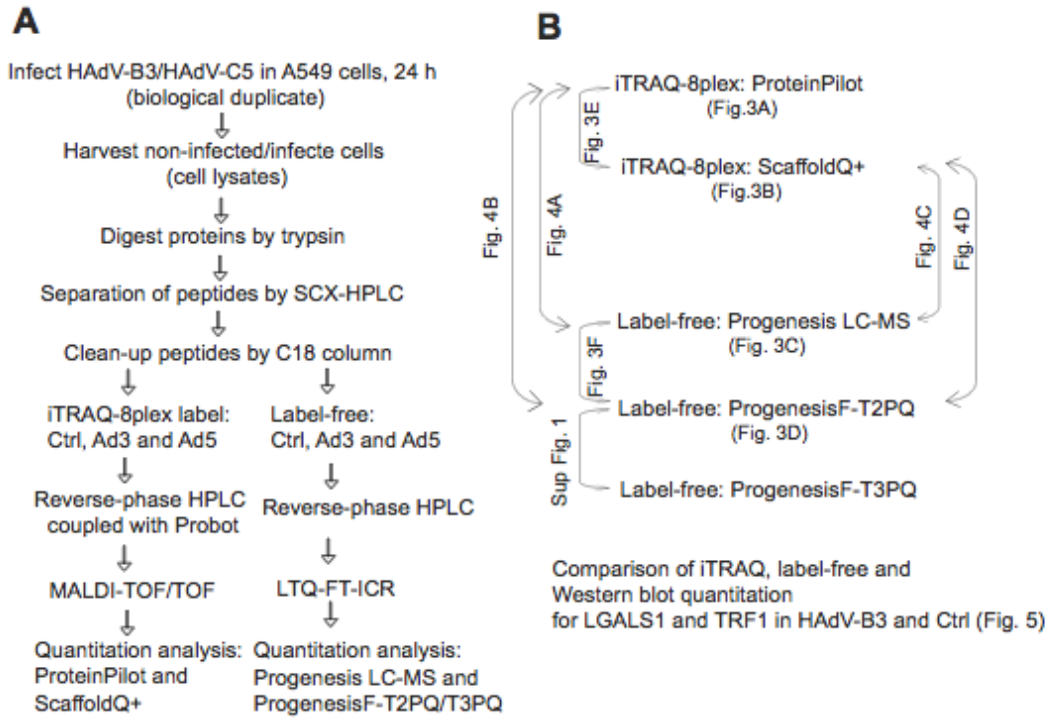
A
Infect HAdV-B3/HAdV-C5 in A549 cells, 24 h
(biological duplicate)
Harvest non-infected/infecte cells
(cell lysates)
Digest proteins by trypsin
Separation of peptides by SCX-HPLC
Clean-up peptides by C18 column
iTRAQ-8plex label:
Ctrl, Ad3 and Ad5
Label-free:
Ctrl, Ad3 and Ad5
Reverse-phase HPLC
coupled with Probot
Reverse-phase HPLC
MALDI-TOF/TOF
LTQ-FT-ICR
Quantitation analysis:
ProteinPilot and
ScaffoldQ+
Quantitation analysis:
Progenesis LC-MS and
ProgenesisF-T2PQ/T3PQ
B
iTRAQ-8plex: ProteinPilot
(Fig.3A)
iTRAQ-8plex: ScaffoldQ+
(Fig.3B)
Label-free: Progenesis LC-MS
(Fig. 3C)
Label-free: ProgenesisF-T2PQ
(Fig. 3D)
Label-free: ProgenesisF-T3PQ
Fig. 3E
Fig. 3F
Fig. 4A
Fig. 4B
Fig. 4C
Fig. 4D
Sup Fig. 1
Comparison of iTRAQ, label-free and
Western blot quantitation
for LGALS1 and TRF1 in HAdV-B3 and Ctrl (Fig. 5)

Fig. 2

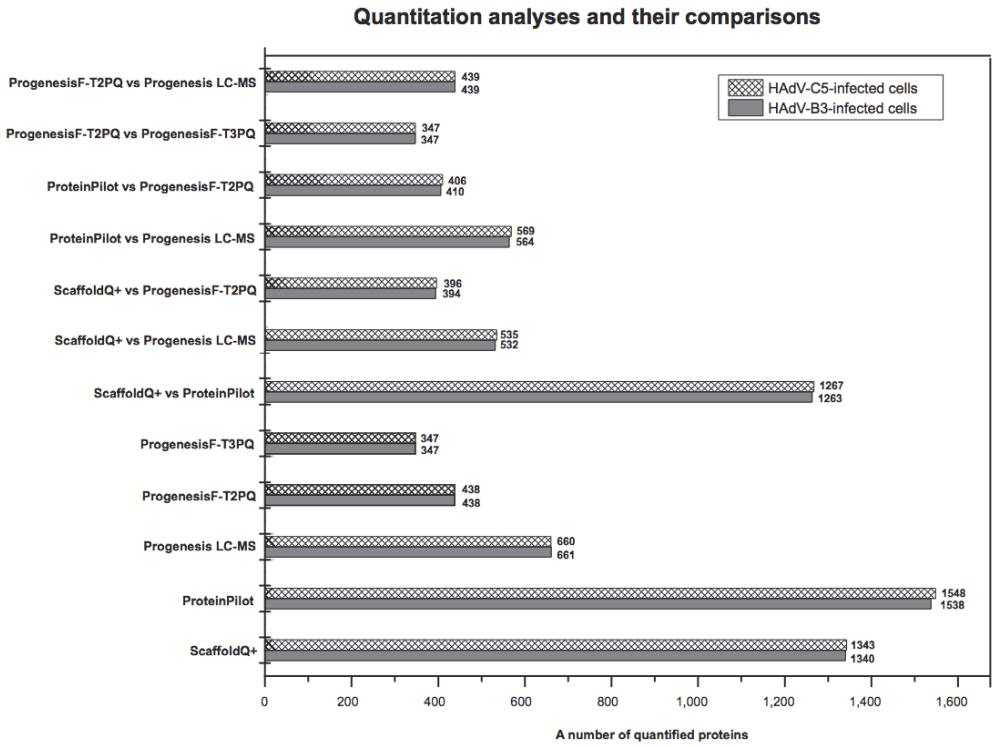
Quantitation analyses and their comparisons
HAdV-C5-infected cells
HAdV-B3-infected cells
ProgenesisF-T2PQ vs Progenesis LC-MS
439
439
ProgenesisF-T2PQ vs ProgenesisF-T3PQ
347
347
ProteinPilot vs ProgenesisF-T2PQ
406
410
ProteinPilot vs Progenesis LC-MS
569
564
ScaffoldQ+ vs ProgenesisF-T2PQ
396
394
ScaffoldQ+ vs Progenesis LC-MS
535
532
ScaffoldQ+ vs ProteinPilot
1267
1263
ProgenesisF-T3PQ
347
347
ProgenesisF-T2PQ
438
438
Progenesis LC-MS
660
661
ProteinPilot
1548
1538
ScaffoldQ+
1343
1340
0
200
400
600
800
1,000
1,200
1,400
1,600
A number of quantified proteins

Fig. 3

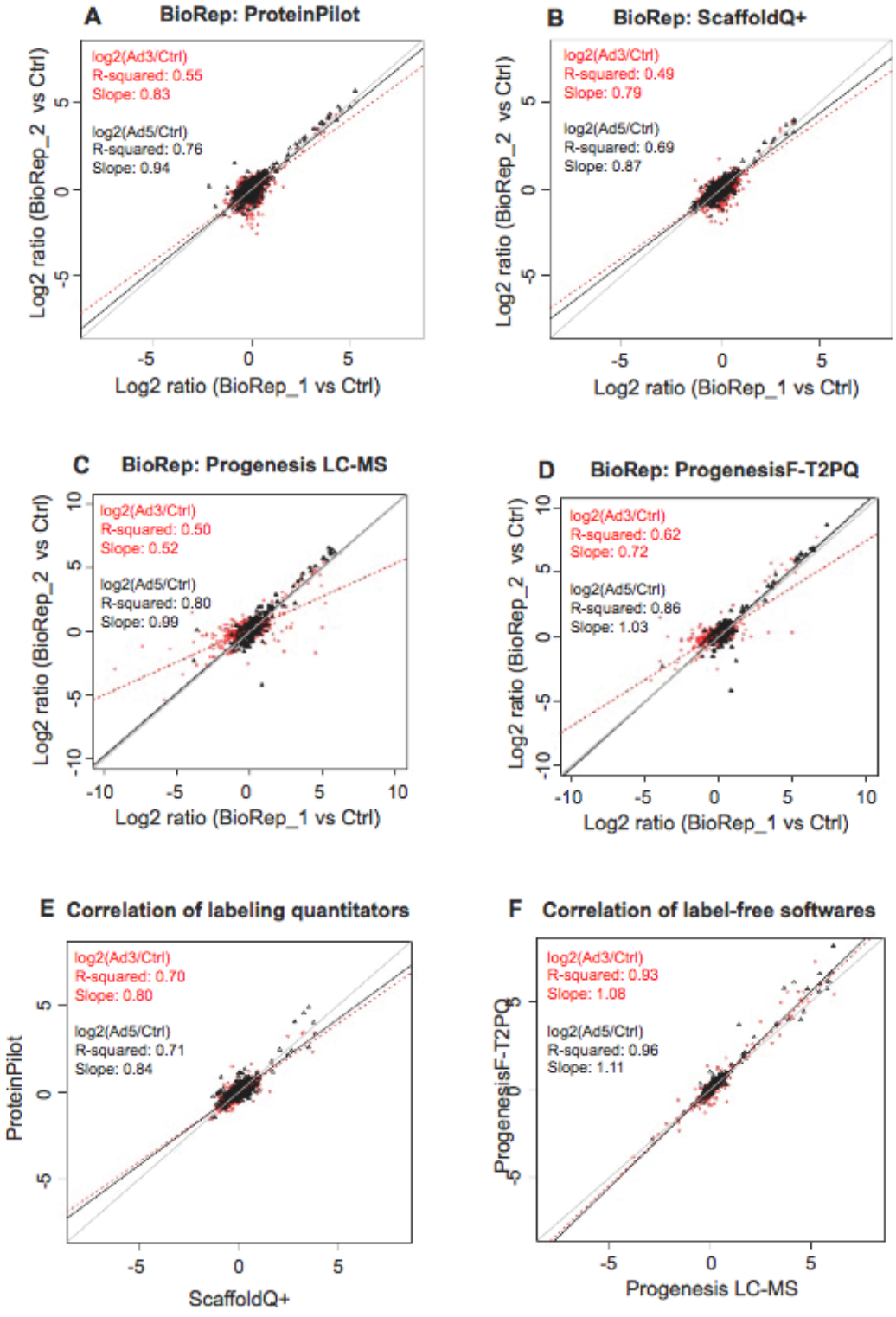
A
BioRep: ProteinPilot
log2(Ad3/Ctrl)
R-squared: 0.55
Slope: 0.83
log2(Ad5/Ctrl)
R-squared: 0.76
Slope: 0.94
Log2 ratio (BioRep_2 vs Ctrl)
Log2 ratio (BioRep_1 vs Ctrl)
B
BioRep: ScaffoldQ+
log2(Ad3/Ctrl)
R-squared: 0.49
Slope: 0.79
log2(Ad5/Ctrl)
R-squared: 0.69
Slope: 0.87
Log2 ratio (BioRep_2 vs Ctrl)
Log2 ratio (BioRep_1 vs Ctrl)
C
BioRep: Progenesis LC-MS
log2(Ad3/Ctrl)
R-squared: 0.50
Slope: 0.52
log2(Ad5/Ctrl)
R-squared: 0.80
Slope: 0.99
Log2 ratio (BioRep_2 vs Ctrl)
Log2 ratio (BioRep_1 vs Ctrl)
D
BioRep: ProgenesisF-T2PQ
log2(Ad3/Ctrl)
R-squared: 0.62
Slope: 0.72
log2(Ad5/Ctrl)
R-squared: 0.86
Slope: 1.03
Log2 ratio (BioRep_2 vs Ctrl)
Log2 ratio (BioRep_1 vs Ctrl)
E
Correlation of labeling quantitators
log2(Ad3/Ctrl)
R-squared: 0.70
Slope: 0.80
log2(Ad5/Ctrl)
R-squared: 0.71
Slope: 0.84
ProteinPilot
ScaffoldQ+
F
Correlation of label-free softwares
log2(Ad3/Ctrl)
R-squared: 0.93
Slope: 1.08
log2(Ad5/Ctrl)
R-squared: 0.96
Slope: 1.11
ProgenesisF-T2PQ
Progenesis LC-MS

Fig. 4

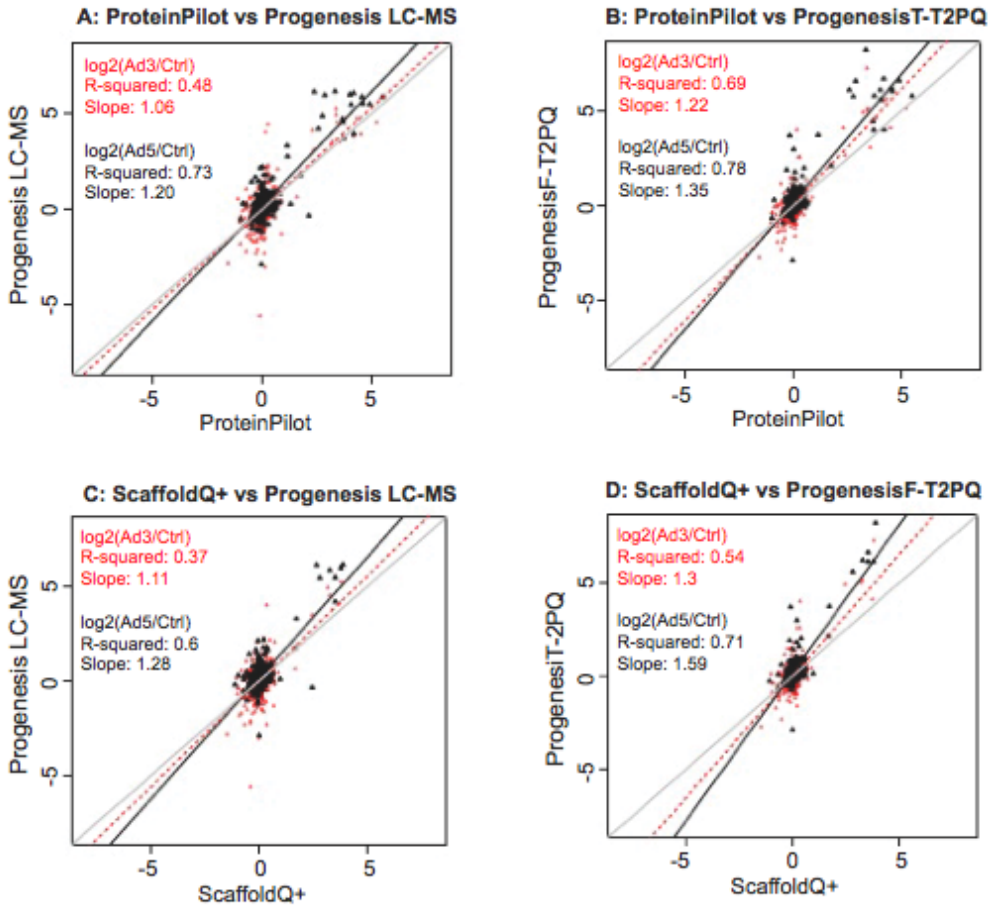
A: ProteinPilot vs Progenesis LC-MS
log2(Ad3/Ctrl)
R-squared: 0.48
Slope: 1.06
log2(Ad5/Ctrl)
R-squared: 0.73
Slope: 1.20
Progenesis LC-MS
ProteinPilot
B: ProteinPilot vs ProgenesisT-T2PQ
log2(Ad3/Ctrl)
R-squared: 0.69
Slope: 1.22
log2(Ad5/Ctrl)
R-squared: 0.78
Slope: 1.35
ProgenesisF-T2PQ
ProteinPilot
C: ScaffoldQ+ vs Progenesis LC-MS
log2(Ad3/Ctrl)
R-squared: 0.37
Slope: 1.11
log2(Ad5/Ctrl)
R-squared: 0.6
Slope: 1.28
Progenesis LC-MS
ScaffoldQ+
D: ScaffoldQ+ vs ProgenesisF-T2PQ
log2(Ad3/Ctrl)
R-squared: 0.54
Slope: 1.3
log2(Ad5/Ctrl)
R-squared: 0.71
Slope: 1.59
ProgenesiT-2PQ
ScaffoldQ+

Fig. 5

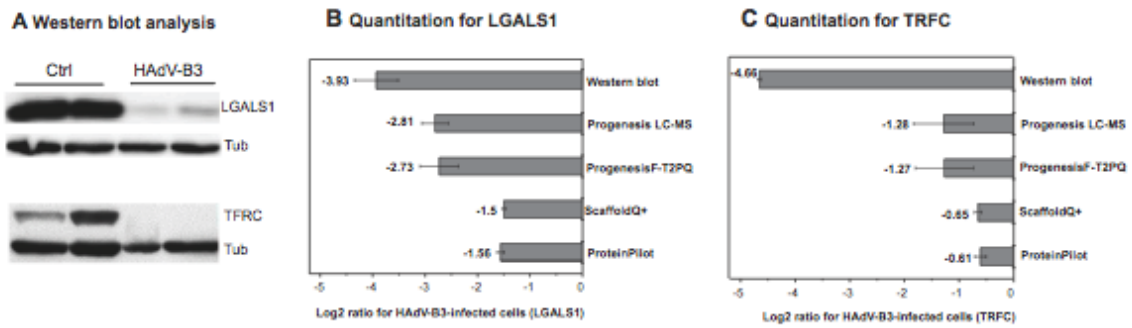
A Western blot analysis
Ctrl
HAdV-B3
LGALS1
Tub
TFRC
Tub
B Quantitation for LGALS1
-3.93
Western blot
-2.81
Progenesis LC-MS
-2.73
ProgenesisF-T2PQ
-1.5
ScaffoldQ+
-1.56
ProteinPilot
-5
-4
-3
-2
-1
0
Log2 ratio for HAdV-B3-infected cells (LGALS1)
C Quantitation for TRFC
-4.66
Western blot
-1.28
Progenesis LC-MS
-1.27
ProgenesisF-T2PQ
-0.65
ScaffoldQ+
-0.61
ProteinPilot
-5
-4
-3
-2
-1
0
Log2 ratio for HAdV-B3-infected cells (TRFC)

SFig. 1

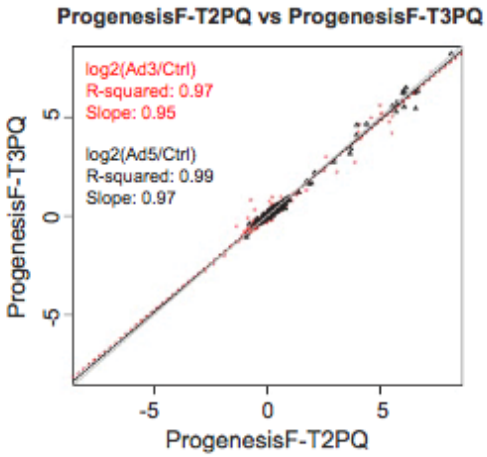
ProgenesisF-T2PQ vs ProgenesisF-T3PQ
log2(Ad3/Ctrl)
R-squared: 0.97
Slope: 0.95
log2(Ad5/Ctrl)
R-squared: 0.99
Slope: 0.97
ProgenesisF-T3PQ
ProgenesisF-T2PQ
5
0
-5
-5
0
5

Identification of virus-derived small RNAs encoded by human adenovirus type 3 using computational and experimental analyses

Hung V. Trinh[1,2], Silvia Gutnik[1], Guillaume Lesage[1], Remy Bruggmann[3], Malik Yousef[4], Weihong Qi[3], Sirisha Aluri[3], Gunter Meister[5], Markus Stoffel[6], Urs Greber[1], Silvio Hemmi[1]*

[1]*Institute of Molecular Life Sciences, University of Zurich, Winterthurerstrasse 190, CH-8057 Zurich, Switzerland*

[2]*Life Science Zurich Graduate School, Molecular Life Science Program*

[3]*Functional Genomics Center Zurich, University of Zurich, Winterthurerstrasse 190, Zurich 8057, Switzerland*

[4]*The Regional R&D. Center The Galilee Society, P.O. Box 437, 20200 Shefa Amr, Israel*

[5]*University of Regensburg, 93053 Regensburg, Germany*

[6]*Institute of Molecular Systems Biology, ETHZ Zurich, Wolfgang-Pauli-Str. 16, 8093 Zurich, Switzerland*

Corresponding author:* Dr. Silvio Hemmi, *Institute of Molecular Life Sciences Zurich, Winterthurerstrasse 190, CH-8057 Zurich, Switzerland; Phone: +41 44 635 3120; Fax: +41 44 635 6811; E-mail: silvio.hemmi@imls.uzh.ch*

Abbreviations: HAdV, human adenovirus; HAdV-B3, human adenovirus species B type 3; CAR, Coxsackie virus B and adenovirus receptor; MOI, multiplicity of infection; p.i. post infection; vp, virus particle

Running title: vsRNAs of HAdV-B3

Abstract: 243 words
Total text: 8,590 words

Abstract

miRNAs function as key posttranscriptional regulators of gene expression not only in a range of eukaryotic species, but are also believed to potentially play a critical role in the life cycle of many viruses, in particular double-stranded DNA viruses. For human adenovirus (HAdV), a single miRNA (mivaRNAI-138) derived from the 3'-end of HAdV-C5 VA-RNAI has recently been described to target the splicing and translation regulator TIA-1, and additional genes that are important for cell growth, transcription, RNA metabolism and DNA repair. To uncover vsRNAs encoded by HAdV B species type 3 (HAdV-B3), we combined bioinformatic tools and experimental validation and evaluated putative novel vsRNAs for this important serotype. From the 75 vsRNA candidates predicted by three different programs, 25 were confirmed by stem-loop RT-PCR and 12 by microarray analysis in HAdV-B3 infected cells. Among these detectable putative vsRNAs, four were commonly detected by both methods. However, none of these were further confirmed when small RNA products were analyzed by deep sequencing, which gave rise to 32 small RNA sequence reads over a threshold of 20 counts. The deep sequencing vsRNAs candidates derived from VA-RNAI and VA-RNAII revealed high correlation with additionally performed microarray analysis of the tilled VA-RNA region. Five of these putative vsRNAs were further corroborated by Northern blot analysis and by stem-loop RT PCR with argonaute 2 immunoprecipitated RNA. To search for the potential cellular targets of the putative vsRNAs, we compiled cellular target prediction data obtained by TargetScan and miRanda analyses with results from a transcriptome analysis of HAdV-B3-infected cells, acquired in a separate study. To search for potential target sequences within the HAdV-B3 genome or the according annotated transcripts, we utilized the miRanda prediction tool. Both tools revealed a large number of potential targets, which need to be further evaluated. In summary, we hope that elucidation of vsRNA pathways in HAdVs eventually will lead to a better design of HAdV vectors for gene therapy, with higher efficacy and lower toxicity than the ones currently used.

Introduction

Viral miRNAs encoded by viruses.

MicroRNAs (miRNAs) are small non-coding RNAs of 18–24 nucleotides in length. The miRNA lin-4 and its target mRNA, lin-14 were discovered by Ambros, Ruvkun and colleagues in *Caenorhabiditis elegans* [1,2]. Subsequently, an increasing number of miRNAs were identified in the major metazoan species such as human [3,4] and viruses [5]. Up to now, 235 experimentally characterized virus-derived small RNAs (vsRNAs) are registered in the miRNA database miRbase 16 (http://microrna.sanger.ac.uk/). The vsRNAs are processed via their host miRNA biogenesis pathway, which is initiated with its transcription by RNA polymerase II or III in the nucleus to form large pri-miRNA transcripts. Next, they are processed by the microprocessor Drosha-DGCR8 (Pasha) into pre-miRNAs of 70-110 nucleotides (nt), which are translocated into the cytoplasm by Exportin 5. Subsequently, the pre-miRNAs are recruited by Dicer to generate single-strand mature miRNAs of 18-24 nt, which are incorporated into the miRNA-associated multiprotein RNA-induced silencing complex (miRISC). miRNAs bind to the 3' untranslated regions (3'UTRs) of the target mRNAs, which results in their sequence-specific cleavage, translational repression or deadenylation, resulting in post-transcriptional gene silencing [6-8]. More recently, it has become evident that miRNAs are involved in many biological processes such as developmental timing, differentiation and cell death [9], cancer [10,11], diabetes [12] cardiovascular diseases [13,14] and virus infections [15,16]. A promising result in miRNA related therapeutics against chronic hepatitis C virus infection was recently provided in primates by targeting miR-122 with locked nucleic acid (LNA) [17].

It is not surprising that viruses also encode their own endogenous vsRNAs, given their omnipresence in multicellular organisms. Pfeffer *et al.* identified the first virus-encoded miRNAs expressed in B cells latently infected with the γ herpes virus family member Epstein Barr virus (EBV) [5]. Since then, twenty-five EBV pre-miRNAs have been reported in B cells and nasopharyngeal carcinomas [18-20]. In influenza A, each 5'-end of the eight viral RNA genomic segments was found to encode a vsRNA [21]. In various influenza A virus subtypes across multiple host species vsRNAs were detectable during replication and were found

associate with the RNA-dependent RNA polymerase. Depletion of these vsRNAs resulted in a dramatic loss of vsRNAs in a segment-specific manner [21], suggesting that vsRNAs regulate the switch from transcription to replication. In herpes simplex virus 1 (HSV), vsRNAs contribute to maintaining the latent infection state [22]. Hsv1-miR-H6 derived from a latency-associated transcript targets the transcription factor ICP4, which is required for expression of most of the HSV-1 genes during productive infection, thereby establishing viral latency [22,23]. In a comprehensive study on vsRNAs in Hepatitis C, Polio, Dengue, Vesicular Stomatitis, and West Nile virus, expression of vimiRNAs was found to vary considerably during infection, from very low abundance to high abundance compared to abundant host miRNAs [24]. In addition to the appearance of vsRNAs during infection, the authors also noticed a number of specific changes in host miRNA profiles. This likely resulted from the limited processing capacity of the mRISC with argonaute proteins as major components, leading to deregulation of host gene expression profiles [24].

***In silico* predictions for virus-derived small RNAs.**

Along with the emergence of miRNAs as key posttranscriptional regulators of gene expression, the scientific community needed to obtain improved tools to recognize those minute sequences hidden in the maze of the genomes. Consequently, bioinformatic programs were developed aiming at the systematic identification of miRNAs [25,26]. The principle of these computational approaches relies on two major features including sequence conservation within different species and formation of stem–loop structure by pre-miRNAs. However, the prediction approaches are more challenging in the case of viruses, as vsRNAs are rarely evolutionarily conserved. Thus, to address this issue, Li *et al.* developed an *in silico* tool specifically applied for predicting vsRNAs [27]. The Vir-Mir db tool developed by Grad *et al.* makes use of the Srnaloop program in order to predict the putative secondary structure from given sequences [28]. Unlike the Vir-Mir db tool, the BayesMiRNAfind program is based on a “machine-learning” approach with a Naïve Bayes classifier, which calculates the probability that a given sequence belongs to a certain Naïve Bayes class, by fulfilling defined criteria from known miRNA in various species [29]. Alternatively, Yousef *et al.* recently developed the Bayes-SVM-MiRNA tool (unpublished), which uses a two-machines learning

approach, the Naïve Bayes and the Support-Vector-Machines (SVM), allowing the identification of both novel and conservative sequences.

Roles of vsRNAs in controlling viral and cellular gene expression.

Current evidence indicates that viruses use their own vsRNAs to manipulate both cellular and viral gene expression [30] or to regulate cellular miRNAs [24,31,32]. An example of how a vsRNA controls its own viral gene expression was elucidated in SV40, where the sv40-miR-S1 was found to down-regulate the early SV40 T antigen at the late stage of infection. This is advantageous for the virus because it limits susceptibility of infected cells to cytotoxic T cells [33]. Another example for a vsRNA targeting viral gene expression is the EBV miR-BART2, which targets viral DNA polymerase (BALF5). miR-BART2 is expressed during latent infection leading to BALF5 mRNA cleaveage [34]. Transition to lytic replication is accompanied by miR-BART2 expression reduction, suggesting that miR-BART2 may regulate the latent-lytic switch. Another EBV-encoded gene LMP1, which is involved in inducing cell growth and transformation, is targeted by three EBV miRNAs, including miR-BART1-5p, miRBART16, and miR-BART17-5p. Overexpression of these vsRNAs during virus latency causes inhibition of viral growth [35].

On the other hand, vsRNAs target cellular genes involved in cell proliferation, survival and antiviral defense pathways [30]. An example was found in the β-herpesvirus family member Human cytomegalovirus (HMCV) which expresses an immunoevasion miRNA that targets the mRNA encoding major histocompatibility complex class I polypeptide-related sequence B (MICB) [36]. MICB is a ligand for a cell-surface receptor of natural killer (NK) cells. The MICB–receptor interaction is a key regulator of NK-cell activity and hence of NK-cell killing of virus-infected cells. Cellular Bcl2-associated factor (BCLAF1), a protein involved in apoptosis, was identified as a target of γ herpes virus family member Kaposi's sarcoma-associated herpesvirus (KSHV) miR-K5 and several other KSHV miRNAs in both B cells and endothelial cells [37]. Antagonism of these small interfering RNAs resulted in decreased virus production, suggesting that BCLAF1 impairs lytic viral replication and that modulation of BCLAF1 by KSHV miRNAs might promote the reversibility of latent infection.

vsRNAs encoded by human adenoviruses.

Human adenoviruses (HAdVs) express highly abundant VA-RNAI and VA-RNAI, which are composed of 160-176 nt that reveal dsRNAs hairpin structures. The major structural features of these regulatory RNAs including the terminal stem, apical stem-loop and central domain are conserved in all HAdVs except the location of the loop [38]. VA-RNAI and VA-RNAII were found to be transported by Exportin 5 to the cytoplasm, where they accumulate in the late phase of virus infection [39]. Removal of both VA-RNAI and VA-RNAII resulted in a dramatic decrease in viral replication capacity [40]. It has been suggested that VA-RNAI may serve two functions during HAdV propagation. Thus, it appears to antagonize the cellular defense pathways against both long and short dsRNA by binding the two key enzymes in the respective pathways, dsRNA-activated protein synthesis inhibitor (DAI) of the IFN pathway and Dicer of the RNA silencing pathway [41]. DAI is a kinase, which is activated by viral replication, leading to phosphorylation of eukaryotic initiation factor 2, which prevents initiation of translation [42].

VA-RNAI was found to be processed into 22 nt RNAs, but seems to be a poor Dicer substrate, as only 1% of VA-RNAI molecules was processed [43]. 80% of the RISC complexes were loaded with VA-RNAII, although VA-RNAI is the more abundantly expressed RNA [44]. More recently, targets of the viral miRNA mivaRNAI-138 derived from 3'-end of HAdV-C5 VA-RNAI were found to include the splicing and translation regulator TIA-1 was down-regulated in infected cells or in transfected cells expressing mivaRNAI-138 [45]. In addition, transfection of a plasmid expressing both VA-RNAs caused down-regulation of another 33 genes, while transfection of VA-RNAI alone resulted in down-regulation of 30 genes, and transfection of mivaRNAI-138 in down-regulation of 26 genes. These finding strongly suggest that endogenous miRNAs play important roles in the infectious life cycle in HAdV.

Human adenovirus and their applications in gene therapy.

HAdVs have served as a model system to study various aspects of molecular and cellular biology, including DNA replication, gene and cell cycle regulation, RNA splicing, and viral entry and transformation [46]. HAdVs have also become the most widely used and most extensively studied viruses for gene delivery/therapy purposes such as targeting genetic diseases, for cancer treatment and vaccination [47,48]. HAdVs are non-enveloped icosahedral particles composed of 20 facets and 12 vertices with a diameter of 70 to 100 nm [49,50]. The particles are composed of an outer protein capsid and an inner, linear dsDNA-associated core. A total of 55 different human HAdV serotypes have been identified, which are classified into species A-G [51,52].

In general, HAdVs cause mild infection of the upper respiratory tract, gastrointestinal tract, and the eye [53,54]. Infections with HAdV-B3 are a major cause of acute febrile and severe respiratory illness, and most symptomatic HAdV infections affect children or military recruits [55]. HAdV-B3 encodes 46 ORFs [56], and binds to complement activation membrane cofactor protein CD46 and desmoglein 2 as an attachment receptor [57-60]. Since the tropism of species B viruses is broader than that of the C species, and includes cancer cells, dendritic cells and hematopoietic stem cells, vectors based on B species gain interest for gene therapy and vaccination approaches [61].

Here we investigated whether HAdV-B3 encodes vmirRNAs and what viral and cellular mRNAs are targeted. We used bioinformatic tools to predict vsRNAs, followed by experimental verification using deep sequencing, stem-loop RT-PCR, miRNA microarray, Northern blot analysis and RISC-immunoprecipitation. *In silico* predicted targets of these vsRNAs were compared to transcriptome analysis of HAdV-B3-infected human A549 lung cells. Elucidation of vsRNAs encoded by HAdV-B3 will provide new insights in virus-host interactions and regulations and possibly lead to improve clinical HAdV vectors.

Materials and Methods

Cell culture, virus infection and RNA sample preparation.

A549 human lung adenocarcinoma epithelial cells were cultured in the Dulbecco's modified Eagle medium (Sigma) supplemented with 8% of fetal bovine serum (Invitrogen). HAdV-B3 was purified by double cesium-chloride gradient as previously described [56]. Infections with HAdV-B3 were performed with a multiplicity of infection (MOI) of 200 in A549 cells. Total RNAs from non-infected cells (Ctrl) and infected cells at 3, 12, 24, 36 and 48 hours (h) post infection (p.i.) were extracted using the mirVana kit (Ambion). Quality of total RNAs was monitored by determining the 260/230-nm absorption ratio (NanoDrop) and integrity of total RNAs was checked by using the Agilent 2100 bioanalyzer system of the Small RNA Chip Kit. For Northern blot analyses, total RNAs extracted with the mirVana kit were further isolated using YM-100 microspin columns (Millipore).

miRNA microarray analysis.

All together, 3,917 probes were spotted on the array, including 75 x 5 probes for the predicted mature sequences of the vsRNAs, 864 x 3 probes for cellular miRNAs listed at human miRbase 12 at the time, and 22 x 3 for VA-RNAI and 20 x 3 probes for VA-RNAII tilling using the Array Designer software (Premier Biosoft) including 24 nt in length and 16 nt overlap between two adjacent probes. In addition, we included positive probes like tRNAs and snoRNAs, negative probes like random sequences and sequences from other species, degradation probes for actin and heat shock protein, and probes serving as internal controls for normalization purposes and for correction of variations from array to array. Each oligonucleotide sequence was randomly spotted on the array, using five and three replicates for predicted vsRNAs and VA-RNAI/VA-RNAII tilling, respectively. Total RNAs isolated from A549 cells infected at a MOI 200 were first transcribed into cDNAs and labeled by using dual colors of Cy3 and Cy5 in which Ctrl was labeled with Cy3, and 24- or 48 h-HAdV-B3-infected samples were labeled with Cy5, and vice versa to avoid possible dye effects. Spotting of

arrays based on custom design, labeling, scanning and quality control was all carried out by LC Sciences services.

For cellular gene expression profiling, the same total RNA samples used for miRNA microarray were analyzed including additional time points of 3 and 12 h. The cDNA microarray used for the Agilent platform (4x44K format) contained the complete human gene probes used by Agilent, plus in addition viral genes of HAdV-B3. Total RNAs were first transcribed into cDNAs and labeled by Cy3/Cy5 (Agilent). Each condition contained at least biological triplicates. Statistical analysis was performed with two-tailed Student's t-test.

Stem-loop RT-PCR analysis.

Stem-loop RT-PCRs were carried as described by Chen *et al.* [62], with slight modifications for the RT-PCR cycle program. All oligonucleotide sequences used in this study including stem-loop, universal reverse and forward primers are shown in STable 2. The cDNA reactions consisted of 50 nM stem-loop primer, 0.25 mM dNTPs each, 10 mM DTT, 4 units/µl RNAout inhibitor (Invitrogen), 1x first-strand buffer, 50 units/µl SuperScript III RT (Invitrogen) and 10-50 ng/µl of total RNAs as a final concentration. In case of RT minus (negative control), the SuperScript III was omitted. The cDNA reaction was allowed to proceed for 30 minutes (min) at 16°C. The following 60 PCR cycles included 30°C for 30 sec, 42°C for 30 seconds (sec) and 50°C for 1 sec. The SuperScript III was inactivated at 85°C for 5 min. The real-time RT-PCR reaction was composed of 1-2 µl cDNA, 1x SYBR (Applied Biosystems), 0.5 µM universal reverse primer and 0.5 µM forward primer with total volume of 10 µl. The thermo cycles included four stages; 50°C for 2 min (stage 1, 1 cycle), 95°C for 5 min (stage 2, 1 cycle), 95°C for 15 sec, and 60°C for 1 min (stage 3, 45 cycles), 95°C for 15 sec and 60°C for 15 sec and 95°C for 15 sec (stage 4, 1 cycle) to dissociate products. The kinetics of the PCR product amplification was measured by incorporation of the intercalating SYBR Green dye [63] using an Applied Biosystems 7900 instrument. Quantitation for stem-loop RT-PCR data was performed according to Vandesompele *et al.* [64] using two internal controls, which included tRNA and snoRNA U8 for normalization.

Northern blot analysis.

Antisense oligonucleotide probes (STable 2) were prepared as follows. 1 µl antisense (22 nt) oligonucleotide (20 µM), 2.5 µl Gamma-^{32}P-ATP (10,000Ci/ul), 2 µl 10X T4 PNK buffer A (Fermentas), 0.4 µl T4 PNK (10 U/µl) and DEPC-water were filled up to 20 µl, followed by incubation at 37°C for 1 h. PNK was inactivated by addition of 20 µl 50 mM ETDA and heating to 95°C for 2 min. The labeling reactions were cleaned up using microspin G25 columns (GE Healthcare). For labeling of the Ambion Decade™ Marker (Ambion), the labeling reaction was followed according to the manufacture's instructions.

Total RNAs or enrichment of miRNAs were separated on 15% Urea-PAGEs in TBE buffer. Quality of RNA separation was visualized by ethidium bromide staining. In addition, intensity of tRNAs in the ethidium bromide stain was used to normalize for a loading control. RNAs from urea-page were transferred in TBE buffer to GeneScreen plus membranes (NEF1017001PK, PerkinElmer), applying 200 mA/gel for 1 h on a SemiDry Transfer device (Bio-Rad). Membranes were dried at room temperature before exposure to UV crosslinking (Stratagene, auto-crosslink, 1200 J, 90 sec). Subsequently, the membranes were baked for 1 h at 80°C. The membranes were prehybridized at 55°C in 6X SSC, 5X Denhardt's, 0.2% SDS for at least 1 h. Hybridization with the labeled probe solution was performed overnight at 42°C for at least 16 h, followed by an increase of hybridization temperature to 45°C for at least 4 h. Membranes were washed 3 times at room temperature with pre-warmed wash buffer (6X SSC and 0.2% SDS) for 5 min each, followed by a wash at 42°C for 10 min. Membranes were exposed to phosphoimager screens and signals were scanned with Phosphoimager FLA-7000 (FUJIFILM Science Lab). Quantitations for Northern blot signals were processed by ImageGauge version 4 (FUJIFILM Science Lab).

Argonaute 2 immunoprecipitation of RNA.

Argonaute 2 immunoprecipitation (Ago2-IP) experiments were performed as described by Rudel *et al.* [65], with slight modifications. Lysates of non-infected (Ctrl) or HAdV-B3-infected A549 cells harvested at 48 h p.i. were immunoprecipitated with a rat anti-human Ago2 monoclonal antibody or a control rat anti-human ICAM antibody using protein G sepharose

beads (GE Healthcare). The beads were washed, followed by RNA extraction using Trizol. Eluted RNAs were further characterized by stem-loop RT-PCR or Northern blot analysis.

Deep sequencing procedures and data analysis.

Total RNAs derived from non-infected control and HAdV-B3-infected A549 cells using an MOI of 200 were isolated 24 h p.i.. Generation of small RNA libraries for SOLiD™ sequencing was performed using the SOLiD™ small RNA expression kit (Applied Biosystems), following the manufacture's instructions. In brief, enriched RNA samples were ligated to either adapter mix A or adapter mix B at 16°C for at least 8 h. Ligation products were reverse transcribed into cDNAs at 42°C for 30 min following RNase H treatment at 37°C for 30 min. The PCR master mix was added to amplify the cDNA libraries, followed by size-fractionation on PAGE. Sequencing of small RNAs was performed using SOliD™ v3 (Applied Biosystems). Sequence reads were analyzed with SOLiD™ System Small RNA Analysis Tool using a SGE unix computer cluster. All reads were first filtered by mapping them against the P2 adaptor sequence and human repeats. The remaining reads were mapped against the precursor sequences of known human miRNAs present in the Sanger miRBase version 12. The further remaining reads were mapped to the human genome (UCSC Genome Database Hg18) and the HAdV-B3 genome database (NCBI).

***In silico* prediction for vsRNAs and for vsRNA targets in cellular and viral genes.**

Three different bioinformatics tools were applied to predict vsRNAs in HAdV-B3. These included BayesMiRNAfind [66], Bayes-SVM-MiRNA [66] and Vir-Mir db [27]. For the cellular miRNA target predictions, we employed either TargetScan 5.1 [67,68] (http://www.targetscan.org/) or miRanda v1.0b [69]. In TargetScan, nucleotides 2-8 at the 5'-end of the seed sequences of vsRNAs are used for searching the 3'UTR human sequences. In miRanda, default setting parameters including -2.0 for open gap penalty, -8.0 for gap extend, 80.0 for score threshold, -14.0 kcal/mol for energy threshold and 2.0 for scaling parameter were applied for the search of 3'UTR human sequences. To search for potential vsRNA binding sites within the HAdV-B3

genome and their transcripts (NCBI accession number: DQ086466), we utilized miRanda v1.0b with the same setting parameter mentioned above.

Results

In silico prediction of vsRNAs encoded by HAdV-B3.

We applied three in *silico* tools including BayesMiRNAfind [66], Bayes-SVM-MiRNA [66] and Vir-Mir db [27] to predict potential vsRNAs encoded by HAdV-B3. All together, 40 precursor vsRNAs were predicted, which gave rise to 75 mature vsRNAs (STable 1). Since precursor vsRNAs predicted by BayesMiRNAfind and Bayes-SVM-MiRNA tools give rise to a single mature vsRNA, and Vir-Mir db-predicted precursor vsRNAs give rise to two mature vsRNAs, this number breaks down to one (Bayes-1) and four (NBayes-2-5) mature vsRNA candidates predicted by BayesMiRNAfind and Bayes-SVM-MiRNA, respectively, and 70 mature vsRNA candidates predicted by Vir-Mir db. All five mature vsRNA candidates predicted by BayesMiRNAfind and Bayes-SVM-MiRNA were encoded on the plus strand, whereas vsRNA candidates predicted by Vir-Mir were distributed along the virus genome with 32 and 38 encoded on the plus and minus strand, respectively. Of note, no vsRNA candidates were predicted from the two VA-RNA regions encompassing nt 10,417-10,840. This is due to a upper size limit of 110 nt used as selection criteria for miRNA precursors by all three *in silico* miRNA prediction tools applied here, thus excluding VA-RNAs as potential miRNA precursors.

Experimental validation of predicted vsRNAs by stem-loop RT-PCR and miRNA microarray analysis.

In order to experimentally evaluate the predicted vsRNAs, we first performed stem-loop RT-PCR. To cover the sequential phases of HAdV-B3 infection, human lung A549 cells were infected with a MOI of 200, and total RNA samples were harvested 24 and 48 h p.i.. Quantitative stem-loop RT-PCR reactions were performed for all 75 predicted vsRNAs candidates, including in addition RT-PCR reactions for the four known human miRNAs miR-103, miR-24-1*, miR-181a* and miR-208 as controls (Fig. 1A). The human miR-103, miR-24-1*, and miR-181a* gave rise to similar expression levels in Ctrl and HAdV-B3-infected cells, at either 24 or 48 h p.i., suggesting that virus infection did not greatly affect expression levels

of these cellular miRNAs. Since hsa-miR-208 is a heart tissue-specific miRNA [70], no expression was detected in lung adenocarcinoma cells (data not shown). From the 75 predicted vsRNAs, 25 revealed significant expression level differences in HAdV-B3-infected cells compared to Ctrl. Seven predicted vsRNAs resulted in high expression levels with over 100-fold differences at both 24 and 48 h p.i compared to Ctrl. These included, VirMir-4871*: 24,967-24,992, VirMir-4824*: 16,091-16,116, VirMir-4822: 15,598-15,623, VirMir-4805*: 13,016-13,041, VirMir-4800*: 12,462-12,487, VirMir-4799*: 10,205-10,230 and VirMir-4792: 9,544-9,569. Among these, VirMir-4792: 9,544-9,569 showed a remarkable high expression with an over 10,000- and 3,600-fold difference at 24 and 48 h, respectively. We noticed that all seven vsRNA candidates revealing high expression differences were derived from the VirMir-db prediction tool, while one of the four candidates predicted by Bayes-SVM-MiRNA (NBayes-2: 1,703-1,723) revealed 133- and 84-fold enhancement at 24 and 48 h p.i., respectively.

As a next, we validated the predicted vsRNAs by miRNA microarray analysis. All together, 3,917 probes were spotted on the array, including probes for the 75 predicted vsRNAs, cellular miRNAs, tilling probes for VA-RNAI (see below), and additional control probes (see Materials and Methods). Data describing changes of cellular miRNAs expression levels will be reported separately (Hung V. Trinh, manuscript in preparation). The vsRNA screen by microarray analysis revealed 11 vsRNA candidates with significantly increased expression levels in samples derived from 24 and at 48 h p.i., when compared to Ctrl (Fig. 1B). When compared to the results obtained from the stem-loop RT-PCR, four predicted vsRNA candidates were commonly detected by both methods and included VirMir-4796: 13,746-13,771, 4799*: 10,205-10,230, VirMir-4792: 9,544-9,569, and VirMir-4824: 16,056-16,081. We noticed that fold-changes in the miRNA microarray analysis were not as high as detected by stem-loop RT-PCR, although the same total RNA samples were used for both assays.

Since Aparicio *et al.* recently reported a HAdV-C5 vsRNA in, which was derived from the 3'-end of VA-RNAI region [45], we also included a careful analysis of both VA-RNA regions contained in HAdV-B3. For this, probes resulting from tilling the VA-RNAI and VA-RNAII regions were included in the miRNA microarray analysis (Fig. 2). At both time points of 24 and 48 h p.i., we observed high signal intensities in HAdV-B3 infected cells, when compared

to non-infected control cells. In general, signals derived from the 5'- and 3'-end of both VA-RNA regions revealed higher intensities than signals derived from the intermediate sequence of the two regions. The signals derived from the VA-RNAI region were about equal at both time points, but were much higher compared to signals derived from the VA-RNAII region. In contrast, signals for the 5'- and 3'-ends of the VA-RNAII region revealed higher expression at 48 than at of 24 h (Fig. 2B). This suggests that under the described conditions here, small RNA products derived from VA-RNAI reached maximum expression levels already at 24 h p.i., whereas processing of VA-RNAII products might be kinetically delayed. For signals derived from the VA-RNAI region, five probes from the 5'- and 3'-end reached fold-induction levels > 500, including probes 10,425-10,488, 10,433-10,456, 10,441-10,464, 10,561-10,584, and 10,577-10,600. Another ten probes gave rise to signals between 100 and 500, whereas the residual seven probes gave rise to signals in the range of 6 to 100. For signals derived from the VA-RNAII region, only the two 5'- and 3'-end probes 10,665-10,688 and 10,817-10,840 revealed fold inductions > 10. Another two probes were around 5-fold induction, and the residual probes revealed signals close to 1. Thus, the finding of a dynamic expression of sequential probes distributed in particular over the VA-RNAI, suggests that multiple small RNA products were generated from the VA-RNAI region, and possibly from the VA-RNAII region.

Identification of HAdV-B3-encoded vsRNA candidates by deep sequencing.

Since deep sequencing is now commonly used to characterize vsRNAs, we used this method to determine HAdV-B3vsRNAs. Total RNAs derived from non-infected control and HAdV-B3-infected A549 cells at 24 h p.i. were isolated and used for analysis. We obtained 26,090,995 sequence reads for the Ctrl sample and 26,257,331 sequence reads for HAdV-B3-infected cells. The deduced sequence reads were aligned to plus and minus strand of the HAdV-B3 genome (Fig. 3A). The top 32 highest RNA intensity sequence reads for small RNAs in the range of 19-24 nt were further broken down (Fig. 3B). Among these, a single read was obtained from the minus strand genome, whereas the residual 31 reads all aligned to the plus strand genome sequence. As expected, we obtained very high count numbers in the VA-RNAI and RNAII regions located at 10,417–10,840, which is in agreement with our

data obtained by miRNA microarray analysis (Fig. 2A, B). Four clusters of sequence reads corresponding to the 5'- and 3' ends each of the VA-RNAI and II regions highly correlated to the probes with the highest fold induction in miRNA microarray analyses. These included at the 5'- end of the VA-RNAI region four overlapping reads from 10,418-10,460, which coincide with the three microarray probes 10,425-10,488, 10,433-10,456, and 10,441-10,464. At the 3'- end of the VA-RNAI region, three overlapping reads from 10,563-10,594 coincide with two microarray probes 10,561-10,584 and 10,577-10,600. Likewise, at the 5'- end of the VA-RNAII region, two overlapping reads from 10,662-10,688 corresponded to microarray probe 10,665-10,688, and at the 3'- end of the VA-RNAII region, a single read from 10,818-10,839 overlapped with microarray probe 10,817-10,840.

In addition to these four clusters of high sequence reads, we found an accumulation of four reads in the range of 77 to 182 counts within the genome sequence from 5,893 to 6,209 of the plus strand, consisting of reads 5,905-5,924; 5,915-5,935; 5,936-5,956; and 6,187-6,209 (Fig. 3B). Sequence read 6,187-6,209 coincided with the sequence of the hypothetical 11.5-kDa gene [56], whereas the rest of the reads correlated to sequences within the non-coding genome. Other reads >100 included a cluster of two reads within the genome sequence from 18,231-18,264 in the pVI gene, and a isolated read sequence 9,664-9,687 in the non-coding region.

Experimental validations of vsRNAs by Northern blot analysis and stem-loop RT-PCR with argonaute 2-precipitated RNA.

Two additional methods were performed to further evaluate the *in silico* predicted or deep sequencing-derived vsRNA candidates of HAdV-B3. These included Northern blot analysis using size-fractionated RNAs and stem loop RT-PCR with argonaute 2 (Ago2)-precipitated RNA [65]. A549 cells were infected with HAdV-B3 and the kinetics of small RNA appearance was analyzed by Northern blotting using RNA samples harvested at the five time points 3, 12, 24, 36 and 48 h (Fig. 4B-E). The five hybridization probes derived from deep sequencing included sequence read 6,187-6,209 (hypothetical 11.5-kDa gene), 10,430-10,452 and 10,474-10,496 (5'-end of VA-RNAI) and 10,563-10,584 and 10,573-10,594 (3'-end of VA-

RNAI). Quantitative evaluation of the Northern blots is shown in Fig. 4F. All five Northern probes gave rise to signals of about 17-27 nt in size for RNAs isolated from HAdV-B3-infected cells, but not for RNAs of non-infected cells. In all blots with VA-RNAI-derived probes, larger size precursors in the range of 150 to 200 nt could be observed, corresponding to the sizes of 170 and 172 nt for HAdV-B3 VA-RNAI and II, respectively [56]. In the Northern blot with the 6,187-6,209 sequence probe, a prominent precursor of about 90 nt was visible. For most probes, no significant expression was detected at the earliest time point of 3 h, but expression became visible at 12 h. Peak expression for all four probes derived from the VA-RNAI sequence were found either at 24 or 36 h p.i., followed by a decrease of expression at 48 h. In contrast, peak expression for the 6,187-6,209 sequence probe was reached at 12 h p.i.. Fold-induction of signals were higher for the small RNA hybridizing probes derived from the 5'- and 3'- ends of the VA-RNAI region and were in the range of 31.88- to 91.2-fold, whereas RNAs hybridizing to probe 6,187-6,209 and the probe derived from the intermediate sequence of the VA-RNAI region revealed signals of 3.69- and 7.79-fold induction over background, respectively. In case of the sequence read 10,563-10,584-probe derived from VA-RNAI, two small RNA bands were apparent, one at ≈ 26 nt and another at ≈ 17 nt (Fig. 4D).

miRNAs and vsRNAs are generated by the same cellular biogenesis pathway. Thus, precipitation of Ago2-associated RISC combined with characterization of comprised vsRNAs adds considerable specificity to vsRNA evaluation. For this, A549 were infected with HAdV-B3 and cell lysates were prepared 48 h p.i., followed by RNA immunoprecipitation. PCR was set-up for all five vsRNA candidates previously evaluated by Northern blot analysis, and two cellular miRNAs including hsa-mir-181 and hsa-mir-24. As a result, we detected expression enhancement in the range of 5.6- to 316.68-fold in HAdV-B3 infected cells compared to non-infected cells (Fig. 5), while no overt changes in the expression levels of hsa-mir-181 and hsa-mir-24 was observed. A comparison to the five vsRNAs used in Northern blot quantitation (Fig. 4) revealed that the deduced fold-inductions were in general higher for RT-PCR/Ago2-IP-method. This difference in sensitivity is likely due to differences in the dynamic range of the two methods. Despite the considerable signal enhancements found for four of the five vsRNAs tested, miRNA signals were not in general increased, since expression of the cellular hsa-mir-181 and hsa-mir-24 were only minimally enhanced. Furthermore, no RT-

PCR signals were obtained when control pull-downs were made including a nonspecific antibody (data not shown). In summary, we confirmed the presence of five vsRNAs by multi-detection methods including deep sequencing, Northern blot and Ago2-IP.

In order to visualize the location of the 16 by deep sequncing-derived putative vsRNAs contained in the VA-RNAI and VA-RNAII regions, we used the mfold software tool to generate secondary structure models for both RNAs [71]. The same mfold software had been used previously to predict VA-RNA structures of various HAdV serotypes, but not for HAdV-B3 [38]. Alignment of the 12 putative vsRNAs of VA-RNAI is shown in Fig. 6A, and alignment of four vsRNAs of VA-RNAII is shown in Fig. 6B.

***In silico* prediction of vsRNAs cellular and viral targets.**

We next addressed the question which cellular or viral genes could be potentially targeted by the discovered vsRNA candidates. By applying TargetScan [67,68], or miRanda [69], we first searched the 3'UTRs of human transcripts for binding sites to the vsRNA seed sequences encompassing 2-8 nt. The five vsRNA candidates included for the analysis were the same also tested for Northern blot analysis. The obtained *in silico* target data from either TargetScan or miRanda were then compiled with our quantitative transcriptome data which we acquired in a separate study, including a detailed expression analysis of HAdV-B3-infected A549 cells at four time points of 3, 12, 24 and 48 h (Hung V. Trinh, unpublished data). The transcriptome-filtered (with log2 ratio ≤ -0.6 and p-value ≤ 0.05) TargetScan and miRanda data sets are shown in STable 3, and STable 5, respectively, whereas STable 4 lists the complete cellular target sites determined by miRanda. Applying stringent exclusion criteria, 16 cellular vsRNA targets were predicted by TargetScan, with four of them showing relative consistent and significant down-regulation for most time points. These included the KLF3, CIT, ETV1, and KCNMA1 genes. The miRanda tool predicted 44 cellular mRNA targets (STable 5), with a single target (ubiquitin-conjugating enzyme E2) and a related target (kelch-like 3 and kelch-like 2) commonly predicted by both tools. One gene (EDN2) with binding sites for all five putative vsRNA revealed significant reduction for all time courses, whereas most other genes revealed significant downregulation for the three time

points 12, 24 and 48 h. Most of these targets contained multiple binding sites for several of the five vsRNA tested.

In order to find out whether the potential HAdV-B3 vsRNA candidates target viral gene expression in an autoregulatory fashion, we applied the miRanda target prediction tool to either the complete viral genome in both plus and minus strands (STable 6), or to the annotated coding sequences (STable 7). As a result, multiple binding sites were found in different regions of the viral genomes or viral transcripts. Particularly, we observed that basically all viral transcripts contained multiple binding sites for the vsRNAs tested. It thus seems mandatory to apply additional filtering parameters like binding energy and perfect alignment of seed sequences to reduce the number of false positive targets.

Discussion

In silico vsRNA prediction and deep sequencing analysis

In silico prediction of cellular miRNAs and vsRNAs relies on inherent structural constraints such as hairpin structure contained in most miRNAs. All three *in silico* prediction tools applied here for determination of HAdV-B3 vsRNAs are based on this premise. However, the number of predicted vsRNAs candidates varied considerably depending on which *in silico* tool was used. Whereas the BayesMiRNAfind program predicted a single mature vsRNA, Bayes-SVM-MiRNA predicted four, and Vir-Mir db even 70 mature vsRNAs, which were distributed all over the viral genome in both plus and minus strand. None of the vsRNA predicted by the three different tools showed complete sequence overlap, but partial overlap of sequences was found for some predicted mature vsRNAs including VirMir-4728*: 1,687-1,712 (VirMir-db) and NBayes-2: 1,703-1,723 (Bayes-SVM-MiRNA) with 10 nt, and NBayes-4: 3,337-3,357 (Bayes-SVM-MiRNA) Bayes-1: 3,649-3,669 (BayesMiRNAfind). Validations for all 75 predicted vsRNAs revealed experimental detection of 25 vsRNAs by stem-loop RT-PCR, and 12 vsRNAs by miRNA microarray analysis. Four of these vsRNAs candidates were commonly detected by both methods. This numerical difference between the two methods may on one side be due to limited sensitivity of the microarray high throughput method, and on the other side it could turn up from erroneous amplifications by the stem-loop RT-PCR method resulting from degraded mRNAs [62].

As previously report, the Bayes miRNAfind tool revealed very high accuracy of 91.3% in EBV (21 predicted out of 23 known vsRNAs), 90.91% accuracy in HCMV (10 predicted out of 11 known vsRNAs), 69.23% accuracy in KSHV (9 predicted out of 11 known vsRNAs) and 100% accuracy in herpes simplex virus (2 predicted out of 2 vsRNAs) [72]. In addition, by utilizing Bayes miRNAfind, Jaber *et al.* could identify the mature svRNA sequence in Bovine Herpesvirus 1 [73]. In contrast to the Bayes miRNAfind tool, the VirMir-db tool which is based on SVM algorithm revealed a higher false positive prediction rate, as for example, an implausible high 579 vsRNA precursors were predicted in mouse CMV using VirMir-db [74]. To improve reliability of the VirMir-db bioinformatic tool, Buck *et al.* introduced an additional

ranking of top SVM score. Experimental validation in this system revealed four confirmed vsRNAs among the top ten predicted precursors [74].

Despite that particularly in DNA viruses *in silico* prediction methods contributed considerably to identify novel vsRNAs, ,the recent development and application of mass parallel (deep) sequencing increasingly displaced *in silico* predictions. Since deep sequencing not only provides more precise sequence information of mature vsRNAs but at the same time also allows to quantify vsRNA abundance, this method has become the standard for vsRNAs determination. For examples, deep sequencing has been used to identify vsRNAs in Hepatitis C, Polio, Dengue, Vesicular Stomatitis, West Nile, Epstein Bar, and Influenza A virus [21,24,75].

In this study, deep sequencing revealed multiple small RNA sequence reads encoded by HAdV-B3. The top 32 highest RNA intensity sequence reads consisted of 16 encoded in the VA-RNAI and II regions, and another 16 encoded in other viral genes or in non-coding sequences. The vsRNAs derived from VA-RNAI appeared in remarkable high quantities, in particular those from the 5'-arm and 3'-arm ends of VA-RNAI. In agreement with HAdV-C5, 3'-end of VA-RNAI also encoded a vsRNA mivaRNAI-138 [45]. The VA-RNAI: 10,573-10,594 in HAdV-B3 and mivaRNAI-138 derived from the same location in VA-RNAI but the seed sequence. Expression of these vsRNAs candidates also correlated well with microarray data obtained from tilling the VA-RNAI and VA-RNAII region. Northern blot analysis with time courses of infections starting from 3 to 48 h p.i. revealed beginning of expression at the 3 h time point, which then remained high up to the late time phase, suggesting these vsRNAs might be required for the late phase of virus infection. None of the 32 top sequence reads determined by deep sequencing overlapped with the *in silico* prediction. This is in part explained by the constitution of viral genome sequence. VA-RNAI and VA-RNAII give rise to transcripts of 170 and 172 nt, respectively. Since the *in silico* miRNA prediction tools set a length limit of 110 nt for miRNA precursors, VA-RNAI and VA-RNAII transcripts were filtered out.

The 16 vsRNAs candidates derived from intronic or non-coding regions represent rather novel types of vsRNAs as the only so far reported HAdV vsRNA is encoded in the VA-RNA

region [45]. Particularly, we found an intronic region coding for three to five potential vsRNAs, which could form a discrete cluster of miRNAs.

HAdV-B3 encoded vsRNA candidates and their potential targets

Cellular target prediction for a first set of five potential HAdV-B3 vsRNAs in combination with an in parallel performed transcriptome analysis of HAdV-B3- infected cells revealed 16 significant hits for the TargetScan search, and 44 hits for the miRanda search (STable 3, 5). Although in general there was not a substantial overlap observed using these prediction tools, we noticed that proteins involveing in the ubiquitination pathway were commonly predicted by both these target tools. This included the E2 ubiquitin-conjugating enzymes UBE2L3 (predicted by TargetScan), and the related UEBE2J2 (predicted by miRanda) and the ubiquitin protein ligase E3 (UBR4) predicted by miRanda only. Of note, miRanda prediction for UBR4 included binding sites for all five vsRNA candidates (STable 4). Ubiquitination of proteins represents an important cellular mechanism for targeting proteins to degradation, and involves at least three classes of enzymes that include ubiquitin-activating enzymes (E1s), ubiquitin-conjugating enzymes (E2s), and ubiquitin-protein ligases (E3s) [76]. The recognized UBR4 is an E3 ubiquitin-protein ligase, which belongs to the E3s family. UBR4 (or p600) interacts with retinoblastoma protein in the nucleus and with calcium-bound calmodulin in the cytoplasm. It recognizes and binds to proteins bearing specific N-terminal residues, which leads to their ubiquitination and subsequent degradation [77]. Together with clathrin, UBR4 is involved in membrane morphogenesis and cytoskeletal organization, which regulates integrin-mediated signaling via activation of focal adhesion kinase in response to cell-matrix interactions [78]. In addition, it binds to protein E7 from human papilloma virus (HPV)-16, HPV-6B and HPV-11 [78,79]. The ubiquitin-conjugating enzyme UBE2J2 belongs to the E2s family, which was significantly downregulated in HAdV-B3 infections upon 12, 24 and 48 h (STable 5). UEB2J2 was predicted by the miRanda tool to contain multiple binding sites for all five vsRNAs. It has been reported that various viruses modulate the ubiquitination system to enable replication, egress and immune evasion [80,81]. For HAdV-C2, Balakirev *et al.* showed that virus infection was accompanied by an increased ubiquitin-cleaving (deubiquitinating) activity in host cells [82]. This activity was excerted by the

viral L3 23K proteinase, which was found to associate with ubiquitin aldehyde. The viral protease is a necessary protein for the processing of viral precursor proteins during virion maturation. Therefore, our finding that vsRNAs target enzymes of the ubiquitination pathway may open new insights of virus-host modulation via this important pathway.

Another possible vsRNA-targeted protein was endothelin 2 (EDN2), which was downregulated at all time points of HAdV-B3 infection (STable 5). EDN2 encodes a member of the endothelin protein family of secretory vasoconstrictive peptides [83], which acts as a ligand for the endothelin receptors to initiate intracellular signaling events involving a wide range of biological processes such as hypertension and ovulation [84]. A further target was microtubule-actin crosslinking factor 1 (MACF1), which belongs to the plakin family of cytoskeletal linker proteins [85,86]. MACF1 functions by forming bridges between different cytoskeletal elements through specialized modular domains including actin and microtuble binding domains. It appears to stabilize actin at sites where microtubules and microfilaments meet, suggesting to function in microtubule dynamics and to facilitate actin-microtubule interactions. Of note, HAdVs also utilize microtubles for their transport [87], and downregulation of microtubles triggered by vsRNAs may reduce the virus transport and spreading, which could help viruses to maintain latent infections.

We also noticed that DNA cross-link repair 1B transcript (DCLRE1B), which is involved in repair of interstrand cross-links [88], was significantly downregulated during virus infections (STable 5). Its 5'-3' exonuclease plays a central role in telomere maintenance and protection during S-phase [89]**.** DCLRE1B participates in the protection of telomeres against non-homologous end-joining (NHEJ)-mediated repair, thereby ensuring that telomeres do not fuse [90-92]. Together with TERF2, DCLRE1B is required to protect telomeres from replicative damage during replication by controlling the amount of DNA topoisomerases during fork passage and to prevent aberrant telomere topology [93].

Experiments for further characterization of vsRNA candidates

We so far obtained good evidence for the presence of at least five vsRNAs encoded by HAdV-B3. Cellular and eventual viral targets for these vsRNAs remain to be characterized.

This will include functional analyses such as loss-of-function and gain-of-function approaches. The strategy for loss-of-function of vsRNAs is based on miRNA inhibitors such as antagomirs [94], or knock down with "Locked Nucleic Acid probes" [95]. Quantitative transcriptomics will be used to analyze gene expression in virus-infected cells pre-treated with such inhibitors. Data obtained from such experiments will be compared with *in silico* target predictions. Gain-of-function approaches for vsRNAs will be done by cloning target sequences downstream of luciferase and evaluate co-expression effects with miRNA-expressing plasmids. Alternatively, targets of vsRNAs candidates can be studied by Ago2-IP in combination with deep sequencing, similar as it has been recently done in human γ-herpesviruses [96].

It has been shown that vsRNAs can also bind to 5'UTRs [97] or encoding sequences of cellular genes [98], possibilities that we have not investigated in this study, but could be taken up in a follow-up investigation.

Final efforts will be dedicated to identify virus-host interaction networks involving vsRNA regulations, with the ultimate goal to uncover novel aspects of the HAdV-B3 infection process. Important question that need to be addressed will include identification of the vsRNAs targets, whether these are involved in entry, endocytosis, trafficking, replication or egress of the virus, and to what extent triggering of signaling pathways are involved. Possible implications of the anticipated results may include discovery of new antiviral mechanisms triggered by vsRNA, subversion of cellular miRNAs by the virus, development of HAdV-B3 vectors with less immunoreactivity for gene therapy, and, more far fetched, mechanistic insights into the regulation of latent HAdV infections in human mucosal T cells.

Acknowledgements

We thank Leta Fuchs (University of Zurich) for technical assistance, Sung-Chou Li, Institute of Biomedical Science, Academia Sinica, Taiwan for providing miRNA prediction tool expertise for Vir-Mir db. This work was supported by Zurich Forschungskredit (credit number: 57113401) and University Research Priority Program (URPP)/Systems Biology, University of Zurich.

References

1. Lee, R.C., Feinbaum, R.L. & Ambros, V. The C. elegans heterochronic gene lin-4 encodes small RNAs with antisense complementarity to lin-14. *Cell* **75**, 843-854 (1993).
2. Wightman, B., Ha, I. & Ruvkun, G. Posttranscriptional regulation of the heterochronic gene lin-14 by lin-4 mediates temporal pattern formation in C. elegans. *Cell* **75**, 855-862 (1993).
3. Bentwich, I.*, et al.* Identification of hundreds of conserved and nonconserved human microRNAs. *Nat Genet* **37**, 766-770 (2005).
4. Calin, G.A.*, et al.* Frequent deletions and down-regulation of micro- RNA genes miR15 and miR16 at 13q14 in chronic lymphocytic leukemia. *Proc Natl Acad Sci U S A* **99**, 15524-15529 (2002).
5. Pfeffer, S.*, et al.* Identification of virus-encoded microRNAs. *Science* **304**, 734-736 (2004).
6. Filipowicz, W., Bhattacharyya, S.N. & Sonenberg, N. Mechanisms of post-transcriptional regulation by microRNAs: are the answers in sight? *Nat Rev Genet* **9**, 102-114 (2008).
7. Kim, Y.K. & Kim, V.N. Processing of intronic microRNAs. *EMBO J* **26**, 775-783 (2007).
8. Winter, J., Jung, S., Keller, S., Gregory, R.I. & Diederichs, S. Many roads to maturity: microRNA biogenesis pathways and their regulation. *Nat Cell Biol* **11**, 228-234 (2009).
9. Reinhart, B.J.*, et al.* The 21-nucleotide let-7 RNA regulates developmental timing in Caenorhabditis elegans. *Nature* **403**, 901-906 (2000).
10. Lu, J.*, et al.* MicroRNA expression profiles classify human cancers. *Nature* **435**, 834-838 (2005).
11. O'Donnell, K.A., Wentzel, E.A., Zeller, K.I., Dang, C.V. & Mendell, J.T. c-Myc-regulated microRNAs modulate E2F1 expression. *Nature* **435**, 839-843 (2005).
12. Poy, M.N.*, et al.* A pancreatic islet-specific microRNA regulates insulin secretion. *Nature* **432**, 226-230 (2004).
13. Chen, J.F.*, et al.* Targeted deletion of Dicer in the heart leads to dilated cardiomyopathy and heart failure. *Proc Natl Acad Sci U S A* **105**, 2111-2116 (2008).
14. Zhao, H., Granberg, F. & Pettersson, U. How adenovirus strives to control cellular gene expression. *Virology* **363**, 357-375 (2007).
15. Jopling, C.L., Yi, M., Lancaster, A.M., Lemon, S.M. & Sarnow, P. Modulation of hepatitis C virus RNA abundance by a liver-specific MicroRNA. *Science* **309**, 1577-1581 (2005).
16. Lecellier, C.H.*, et al.* A cellular microRNA mediates antiviral defense in human cells. *Science* **308**, 557-560 (2005).
17. Lanford, R.E.*, et al.* Therapeutic silencing of microRNA-122 in primates with chronic hepatitis C virus infection. *Science* **327**, 198-201 (2010).
18. Cai, X. & Cullen, B.R. Transcriptional origin of Kaposi's sarcoma-associated herpesvirus microRNAs. *J Virol* **80**, 2234-2242 (2006).
19. Grundhoff, A., Sullivan, C.S. & Ganem, D. A combined computational and microarray-based approach identifies novel microRNAs encoded by human gamma-herpesviruses. *RNA* **12**, 733-750 (2006).
20. Zhu, J.Y.*, et al.* Identification of novel Epstein-Barr virus microRNA genes from nasopharyngeal carcinomas. *J Virol* **83**, 3333-3341 (2009).
21. Perez, J.T.*, et al.* Influenza A virus-generated small RNAs regulate the switch from transcription to replication. *Proc Natl Acad Sci U S A* **107**, 11525-11530 (2010).
22. Umbach, J.L.*, et al.* MicroRNAs expressed by herpes simplex virus 1 during latent infection regulate viral mRNAs. *Nature* **454**, 780-783 (2008).
23. Preston, C.M. Control of herpes simplex virus type 1 mRNA synthesis in cells infected with wild-type virus or the temperature-sensitive mutant tsK. *J Virol* **29**, 275-284 (1979).
24. Parameswaran, P.*, et al.* Six RNA viruses and forty-one hosts: viral small RNAs and modulation of small RNA repertoires in vertebrate and invertebrate systems. *PLoS Pathog* **6**, e1000764 (2010).
25. Berezikov, E., Cuppen, E. & Plasterk, R.H. Approaches to microRNA discovery. *Nat Genet* **38 Suppl**, S2-7 (2006).
26. Berezikov, E.*, et al.* Phylogenetic shadowing and computational identification of human microRNA genes. *Cell* **120**, 21-24 (2005).
27. Li, S.C., Shiau, C.K. & Lin, W.C. Vir-Mir db: prediction of viral microRNA candidate hairpins. *Nucleic Acids Res* **36**, D184-189 (2008).
28. Grad, Y.*, et al.* Computational and experimental identification of C. elegans microRNAs. *Mol Cell* **11**, 1253-1263 (2003).

29. Yousef, M.*, et al.* Combining multi-species genomic data for microRNA identification using a Naive Bayes classifier. *Bioinformatics* **22**, 1325-1334 (2006).
30. Skalsky, R.L. & Cullen, B.R. Viruses, microRNAs, and host interactions. *Annu Rev Microbiol* **64**, 123-141 (2010).
31. Cazalla, D., Yario, T. & Steitz, J.A. Down-regulation of a host microRNA by a Herpesvirus saimiri noncoding RNA. *Science* **328**, 1563-1566 (2010).
32. Nachmani, D., Lankry, D., Wolf, D.G. & Mandelboim, O. The human cytomegalovirus microRNA miR-UL112 acts synergistically with a cellular microRNA to escape immune elimination. *Nat Immunol* **11**, 806-813 (2010).
33. Sullivan, C.S., Grundhoff, A.T., Tevethia, S., Pipas, J.M. & Ganem, D. SV40-encoded microRNAs regulate viral gene expression and reduce susceptibility to cytotoxic T cells. *Nature* **435**, 682-686 (2005).
34. Barth, S.*, et al.* Epstein-Barr virus-encoded microRNA miR-BART2 down-regulates the viral DNA polymerase BALF5. *Nucleic Acids Res* **36**, 666-675 (2008).
35. Lo, A.K.*, et al.* Modulation of LMP1 protein expression by EBV-encoded microRNAs. *Proc Natl Acad Sci U S A* **104**, 16164-16169 (2007).
36. Stern-Ginossar, N.*, et al.* Host immune system gene targeting by a viral miRNA. *Science* **317**, 376-381 (2007).
37. Ziegelbauer, J.M., Sullivan, C.S. & Ganem, D. Tandem array-based expression screens identify host mRNA targets of virus-encoded microRNAs. *Nat Genet* **41**, 130-134 (2009).
38. Ma, Y. & Mathews, M.B. Structure, function, and evolution of adenovirus-associated RNA: a phylogenetic approach. *J Virol* **70**, 5083-5099 (1996).
39. Lu, S. & Cullen, B.R. Adenovirus VA1 noncoding RNA can inhibit small interfering RNA and MicroRNA biogenesis. *J Virol* **78**, 12868-12876 (2004).
40. Bhat, R.A. & Thimmappaya, B. Adenovirus mutants with DNA sequence perturbations in the intragenic promoter of VAI RNA gene allow the enhanced transcription of VAII RNA gene in HeLa cells. *Nucleic Acids Res* **12**, 7377-7388 (1984).
41. Thimmappaya, B., Weinberger, C., Schneider, R.J. & Shenk, T. Adenovirus VAI RNA is required for efficient translation of viral mRNAs at late times after infection. *Cell* **31**, 543-551 (1982).
42. Siekierka, J., Mariano, T.M., Reichel, P.A. & Mathews, M.B. Translational control by adenovirus: lack of virus-associated RNAI during adenovirus infection results in phosphorylation of initiation factor eIF-2 and inhibition of protein synthesis. *Proc Natl Acad Sci U S A* **82**, 1959-1963 (1985).
43. Sano, M., Kato, Y. & Taira, K. Sequence-specific interference by small RNAs derived from adenovirus VAI RNA. *FEBS Lett* **580**, 1553-1564 (2006).
44. Xu, N., Segerman, B., Zhou, X. & Akusjarvi, G. Adenovirus virus-associated RNAII-derived small RNAs are efficiently incorporated into the rna-induced silencing complex and associate with polyribosomes. *J Virol* **81**, 10540-10549 (2007).
45. Aparicio, O.*, et al.* Adenovirus VA RNA-derived miRNAs target cellular genes involved in cell growth, gene expression and DNA repair. *Nucleic Acids Res* **38**, 750-763 (2010).
46. Philipson, L. Adenovirus--an eternal archetype. *Curr Top Microbiol Immunol* **199 (Pt 1)**, 1-24 (1995).
47. McConnell, M.J. & Imperiale, M.J. Biology of adenovirus and its use as a vector for gene therapy. *Hum Gene Ther* **15**, 1022-1033 (2004).
48. Tatsis, N. & Ertl, H.C. Adenoviruses as vaccine vectors. *Mol Ther* **10**, 616-629 (2004).
49. Shenk, T. Adenoviridae: the viruses and their replication. in *Virology* (eds. Fields, B.N., Howley, P.M., Griffin, D.E. & al., e.) 2265-2300 (Lippincott-Raven Publisher, Philadelphia, 2001).
50. Russell, W.C. Adenoviruses: update on structure and function. *J Gen Virol* **90**, 1-20 (2009).
51. Benkö, M., Harrach, B. & Russell, W.C. Family Adenoviridae. in *Virus Taxonomy: classification and nomenclature of viruses. Seventh report of the International Committee on Taxonomy of Viruses* (eds. Van Regenmortel, M.H.V.*, et al.*) 227-238 (Academic Press, San Diego, 2000).
52. Walsh, M.P.*, et al.* Computational Analysis Identifies Human Adenovirus Type 55 as a Re-emergent Acute Respiratory Disease Pathogen. *J Clin Microbiol* (2009).
53. Wadell, G. Adenoviruses. in *Encyclopedia of virology*, Vol. 1 (eds. Webster, R.G. & Granoff, A.) 1-7 (Academic Press Inc., New York, 1994).
54. Horwitz, M. The Adenoviridae and their replication. in *Virology*, Vol. 2 (ed. Fields, B.N.a.K., D. M.) 1679-1721 (Raven Press, New York, 1990).

55. Ryan, M.A.*, et al.* Large epidemic of respiratory illness due to adenovirus types 7 and 3 in healthy young adults. *Clin. Infect. Dis.* **34**, 577-582 (2002).
56. Sirena, D., Ruzsics, Z., Schaffner, W., Greber, U.F. & Hemmi, S. The nucleotide sequence and a first generation gene transfer vector of species B human adenovirus serotype 3. *Virology* **343**, 283-298 (2005).
57. Sirena, D.*, et al.* The Human Membrane Cofactor CD46 Is a Receptor for Species B Adenovirus Serotype 3. *J Virol* **78**, 4454-4462 (2004).
58. Fleischli, C.*, et al.* Species B adenovirus serotypes 3, 7, 11 and 35 share similar binding sites on the membrane cofactor protein CD46 receptor. *J Gen Virol* **88**, 2925-2934 (2007).
59. Trinh, H.V.*, et al.* Avidity binding of human adenovirus serotypes 3 and 7 to the membrane cofactor CD46 triggers infection.
60. Wang, H.*, et al.* Desmoglein 2 is a receptor for adenovirus serotypes 3, 7, 11 and 14. *Nat Med* **17**, 96-104 (2010).
61. Sakurai, F., Akitomo, K., Kawabata, K., Hayakawa, T. & Mizuguchi, H. Downregulation of human CD46 by adenovirus serotype 35 vectors. *Gene Ther* **14**, 912-919 (2007).
62. Chen, C.*, et al.* Real-time quantification of microRNAs by stem-loop RT-PCR. *Nucleic Acids Res* **33**, e179 (2005).
63. Varkonyi-Gasic, E., Wu, R., Wood, M., Walton, E.F. & Hellens, R.P. Protocol: a highly sensitive RT-PCR method for detection and quantification of microRNAs. *Plant Methods* **3**, 12 (2007).
64. Vandesompele, J.*, et al.* Accurate normalization of real-time quantitative RT-PCR data by geometric averaging of multiple internal control genes. *Genome Biol* **3**, RESEARCH0034 (2002).
65. Rudel, S., Flatley, A., Weinmann, L., Kremmer, E. & Meister, G. A multifunctional human Argonaute2-specific monoclonal antibody. *RNA* **14**, 1244-1253 (2008).
66. Yousef, M., Jung, S., Kossenkov, A.V., Showe, L.C. & Showe, M.K. Naive Bayes for microRNA target predictions--machine learning for microRNA targets. *Bioinformatics* **23**, 2987-2992 (2007).
67. Friedman, R.C., Farh, K.K., Burge, C.B. & Bartel, D.P. Most mammalian mRNAs are conserved targets of microRNAs. *Genome Res* **19**, 92-105 (2009).
68. Grimson, A.*, et al.* MicroRNA targeting specificity in mammals: determinants beyond seed pairing. *Mol Cell* **27**, 91-105 (2007).
69. Enright, A.J.*, et al.* MicroRNA targets in Drosophila. *Genome Biol* **5**, R1 (2003).
70. van Rooij, E.*, et al.* Control of stress-dependent cardiac growth and gene expression by a microRNA. *Science* **316**, 575-579 (2007).
71. Zuker, M. Mfold web server for nucleic acid folding and hybridization prediction. *Nucleic Acids Res* **31**, 3406-3415 (2003).
72. Kumar, S., Ansari, F.A. & Scaria, V. Prediction of viral microRNA precursors based on human microRNA precursor sequence and structural features. *Virol J* **6**, 129 (2009).
73. Jaber, T., Workman, A. & Jones, C. Small noncoding RNAs encoded within the bovine herpesvirus 1 latency-related gene can reduce steady-state levels of infected cell protein 0 (bICP0). *J Virol* **84**, 6297-6307.
74. Buck, A.H.*, et al.* Discrete clusters of virus-encoded micrornas are associated with complementary strands of the genome and the 7.2-kilobase stable intron in murine cytomegalovirus. *J Virol* **81**, 13761-13770 (2007).
75. Chen, S.J.*, et al.* Characterization of Epstein-Barr virus miRNAome in nasopharyngeal carcinoma by deep sequencing. *PLoS One* **5**(2010).
76. Schwartz, A.L. & Ciechanover, A. Targeting proteins for destruction by the ubiquitin system: implications for human pathobiology. *Annu Rev Pharmacol Toxicol* **49**, 73-96 (2009).
77. Tasaki, T.*, et al.* A family of mammalian E3 ubiquitin ligases that contain the UBR box motif and recognize N-degrons. *Mol Cell Biol* **25**, 7120-7136 (2005).
78. Nakatani, Y.*, et al.* p600, a unique protein required for membrane morphogenesis and cell survival. *Proc Natl Acad Sci U S A* **102**, 15093-15098 (2005).
79. Huh, K.W.*, et al.* Association of the human papillomavirus type 16 E7 oncoprotein with the 600-kDa retinoblastoma protein-associated factor, p600. *Proc Natl Acad Sci U S A* **102**, 11492-11497 (2005).
80. Blanchette, P. & Branton, P.E. Manipulation of the ubiquitin-proteasome pathway by small DNA tumor viruses. *Virology* **384**, 317-323 (2009).
81. Randow, F. & Lehner, P.J. Viral avoidance and exploitation of the ubiquitin system. *Nat Cell Biol* **11**, 527-534 (2009).

82. Balakirev, M.Y., Jaquinod, M., Haas, A.L. & Chroboczek, J. Deubiquitinating function of adenovirus proteinase. *J Virol* **76**, 6323-6331 (2002).
83. Bloch, K.D., Hong, C.C., Eddy, R.L., Shows, T.B. & Quertermous, T. cDNA cloning and chromosomal assignment of the endothelin 2 gene: vasoactive intestinal contractor peptide is rat endothelin 2. *Genomics* **10**, 236-242 (1991).
84. Al-Alem, L.*, et al.* Endothelin-2 induces oviductal contraction via endothelin receptor subtype A in rats. *J Endocrinol* **193**, 383-391 (2007).
85. Sun, Y.*, et al.* Molecular cloning and characterization of human trabeculin-alpha, a giant protein defining a new family of actin-binding proteins. *J Biol Chem* **274**, 33522-33530 (1999).
86. Sun, D., Leung, C.L. & Liem, R.K. Characterization of the microtubule binding domain of microtubule actin crosslinking factor (MACF): identification of a novel group of microtubule associated proteins. *J Cell Sci* **114**, 161-172 (2001).
87. Gazzola, M.*, et al.* A stochastic model for microtubule motors describes the in vivo cytoplasmic transport of human adenovirus. *PLoS Comp Biol* **in revision**(2009).
88. Demuth, I., Digweed, M. & Concannon, P. Human SNM1B is required for normal cellular response to both DNA interstrand crosslink-inducing agents and ionizing radiation. *Oncogene* **23**, 8611-8618 (2004).
89. Hejna, J., Philip, S., Ott, J., Faulkner, C. & Moses, R. The hSNM1 protein is a DNA 5'-exonuclease. *Nucleic Acids Res* **35**, 6115-6123 (2007).
90. Lenain, C.*, et al.* The Apollo 5' exonuclease functions together with TRF2 to protect telomeres from DNA repair. *Curr Biol* **16**, 1303-1310 (2006).
91. van Overbeek, M. & de Lange, T. Apollo, an Artemis-related nuclease, interacts with TRF2 and protects human telomeres in S phase. *Curr Biol* **16**, 1295-1302 (2006).
92. Lam, Y.C.*, et al.* SNMIB/Apollo protects leading-strand telomeres against NHEJ-mediated repair. *EMBO J* **29**, 2230-2241 (2010).
93. Ye, J.*, et al.* TRF2 and apollo cooperate with topoisomerase 2alpha to protect human telomeres from replicative damage. *Cell* **142**, 230-242 (2010).
94. Krutzfeldt, J.*, et al.* Silencing of microRNAs in vivo with 'antagomirs'. *Nature* **438**, 685-689 (2005).
95. Elmen, J.*, et al.* LNA-mediated microRNA silencing in non-human primates. *Nature* **452**, 896-899 (2008).
96. Dolken, L.*, et al.* Systematic analysis of viral and cellular microRNA targets in cells latently infected with human gamma-herpesviruses by RISC immunoprecipitation assay. *Cell Host Microbe* **7**, 324-334 (2010).
97. Grey, F.*, et al.* A viral microRNA down-regulates multiple cell cycle genes through mRNA 5'UTRs. *PLoS Pathog* **6**, e1000967 (2010).
98. Lin, H.R. & Ganem, D. Viral microRNA target allows insight into the role of translation in governing microRNA target accessibility. *Proc Natl Acad Sci U S A* **108**, 5148-5153 (2011).
99. Wuchty, S., Fontana, W., Hofacker, I.L. & Schuster, P. Complete suboptimal folding of RNA and the stability of secondary structures. *Biopolymers* **49**, 145-165 (1999).

Legends to figures

Fig. 1. Verification of *in silico*-predicted HAdV-B3 vsRNA candidates by stem-loop RT-PCR and miRNA microarray analysis. All 75 predicted vsRNAs and two known cellular miRNAs including hsa-miR-24 and hsa-miR-181a* were quantified using biological and technical replicates. (A) Detection of predicted vsRNAs was performed by stem-loop RT-PCR, which was set with threshold of over 2-fold changes for both HAdV-B3 infected-cells at 24 and 48 h p.i. vs non-infected cells. (*) refers to vsRNA derived from the opposing arm, (+) and (-) indicate location of predicted vsRNAs in plus or minus viral DNA strand. (B) Detection of predicted vsRNAs was performed by miRNA microarray, which was set with threshold over 2-fold changes for both HAdV-B3 infected-cells at 24 and 48 h p.i. vs non-infected cells. Ratios were determined by normalizing the data obtained from infected cells to date from non-infected (Ctrl) samples. (x) indicates that no signal was detected in non-infected cells, but signal was obtained in the microarray analysis of HAdV-B3-infected samples.

Fig. 2. Expression analysis of small RNAs derived from HAdV-B3 VA-RNAI and VA-RNAII regions by miRNA microarray. Total RNAs as in Fig. 1B were used for hybridization to VA-RNAI and VA-RNAII tilling probes encompassing nucleotides 10,422-10,596 and 10,666-10,837, respectively.

Fig. 3. Identification of HAdV-B3 vsRNA candidates by deep sequencing. RNA samples of non-infected and HAdV-B3-infected A549 cells were isolated 24 h p.i. (A) Overview of the possible vsRNA (19-24 nt) sequence reads with > 10 counts plotted to HAdV-B3 genome of 35,343 bp (NCBI accession no. DQ086466). The upper panel represents sequence counts in the HAdV-B3 (-) strand, while the lower panel indicates read counts of the (+) strand. (B), sequence reads of the top 32 sequence reads with assignment to their location in the HAdV-B3 genome.

Fig. 4. Characterization of HAdV-B3 vsRNA candidates by Northern blot analysis. (A-E) Total RNAs from non-infected and HAdV-B3-infected cells were isolated at 3, 12, 24, 36 and 48 h p.i. and size-fractionated on 7M Urea-PAGEs, followed by transfer to membranes. ^{32}P-labelled probes included hyp 11.5-kDa: 6,187-6,208 (A), VA-RNAI: 10,430-10,452 (B), VA-RNAI: 10,475-10,496 (C), VA-RNAI: 10,563-10,584 (D), VA-RNAI: 10,563-10,584 (E). (F)

Quantification of ~17-27 nt bands of Northern blots A-E. In case of VA-RNAI: 10,563-10,584, two different signals were recorded, one larger than 20 nt (++), and one smaller than 20 nt (+).

Fig. 5. Quantification of five HAdV-B3 vsRNA candidates by stem-loop RT-PCR combined with argonaute 2 immunoprecipitation. RNA samples were isolated from non-infected or HAdV-B3-infected A549 cells 48 h p.i.. The five vsRNA candidates examined were the same as tested by Northern blotting in Fig. 4. The two cellular hsa-mir-181 and hsa-mir-24 were additionally included as controls.

Fig. 6. Alignment of 16 vsRNAs candidates obtained from deep sequencing analysis to predicted secondary structure of VA-RNAI and VA-RNAI by mfold (http://mfold.rna.albany.edu/). vsRNA candidates verified by Northern blot analysis and Ago2-IP combined with stem-loop RT-PCR are shown in red. vsRNAs candidates obtained from deep sequencing, but not been confirmed by Northern blot analysis and Ago-IP, are shown in bold black.

Legends to supplemental tables

STable 1. Precursor and mature sequences of predicted vsRNAs encoded by HAdV-B3. vsRNAs *in silico* predictions were performed using three bioinformatics tools including BayesMiRNAfind, Bayes-SVM-MiRNAs and Vir-Mir db. Indicated are size and location of predicted precursors as well as of mature vsRNAs within the HAdV-B3 genome. Each precursor miRNAs predicted by Vir-Mir db gives rise to two mature vsRNAs, while miRNA precursor derived from BayesMiRNAfind and Bayes-SVM-MiRNAs give rise to single mature vsRNAs.

STable 2. List of oligonucleotide primers used for this study. These include forward and universal reverse primers used for stem-loop RT-PCR, and primers used as Northern blot probes.

STable 3. Comparison of predicted cellular targets for five HAdV-B3 vsRNA candidates using TargetScan and transcriptome analysis of infected A549 cells. Transcriptome analysis was filtered by significant changes of gene expression (log2 ratio ≤ -0.6 and p value ≤ 0.05, indicated in bold) for at least one time point of virus infection (3, 12, 24, and 48 h) compared to non-infected cells.

STable 4. Cellular target prediction for five HAdV-B3 vsRNA candidates using miRanda. Indicated are the individual binding sites with their locations in the 3'UTRs. Score represents ranking based on alignment. Energy describes optimal strand-strand interaction between miRNA and UTR and was calculated using the Vienna package [99]. Align miRNA length indicates the sequence of vsRNAs used for the alignment, with start and stop nt. Target sequence represents the location of binding sequences at the 3'UTR.

STable 5. Comparison of predicted cellular targets for five HAdV-B3 vsRNA candidates using miRanda and transcriptome analysis. Significantly downregulated genes (log2 ratio ≤ -0.6) and their p value ≤ 0.05 are indicated in bold.

STable 6. Prediction of targets for five vsRNA candidates within the HAdV-B3 genome by miRanda. Target sequence represents the location of binding sequences on either plus or minus strand of the HAdV-B3 genome.

STable 7. Prediction of targets for five vsRNA candidates in HAdV-B3 annotated coding sequences (NCBI accession no. DQ086466) by miRanda. Target sequence represents the location of binding sequences on HAdV-B3 transcripts.

FIG. 1.

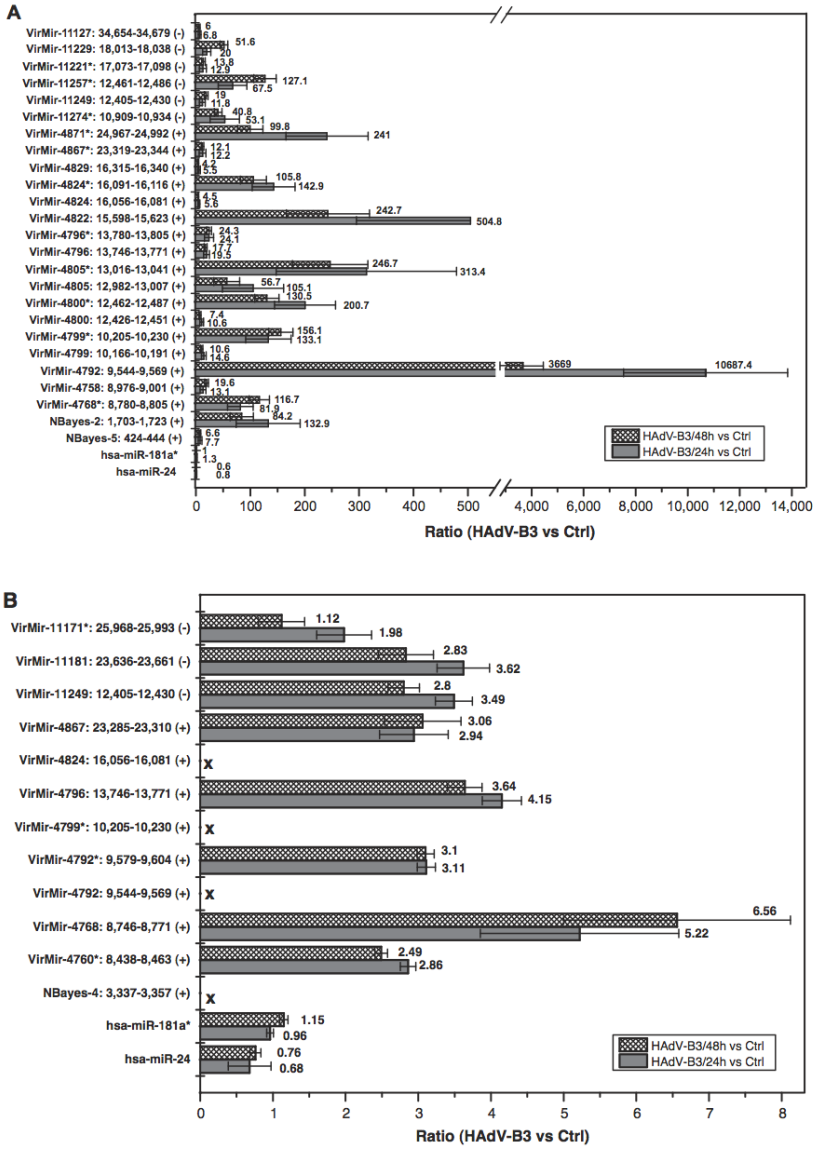
A
VirMir-11127: 34,654-34,679 (-)
VirMir-11229: 18,013-18,038 (-)
VirMir-11221*: 17,073-17,098 (-)
VirMir-11257*: 12,461-12,486 (-)
VirMir-11249: 12,405-12,430 (-)
VirMir-11274*: 10,909-10,934 (-)
VirMir-4871*: 24,967-24,992 (+)
VirMir-4867*: 23,319-23,344 (+)
VirMir-4829: 16,315-16,340 (+)
VirMir-4824*: 16,091-16,116 (+)
VirMir-4824: 16,056-16,081 (+)
VirMir-4822: 15,598-15,623 (+)
VirMir-4796*: 13,780-13,805 (+)
VirMir-4796: 13,746-13,771 (+)
VirMir-4805*: 13,016-13,041 (+)
VirMir-4805: 12,982-13,007 (+)
VirMir-4800*: 12,462-12,487 (+)
VirMir-4800: 12,426-12,451 (+)
VirMir-4799*: 10,205-10,230 (+)
VirMir-4799: 10,166-10,191 (+)
VirMir-4792: 9,544-9,569 (+)
VirMir-4758: 8,976-9,001 (+)
VirMir-4768*: 8,780-8,805 (+)
NBayes-2: 1,703-1,723 (+)
NBayes-5: 424-444 (+)
hsa-miR-181a*
hsa-miR-24
HAdV-B3/48h vs Ctrl
HAdV-B3/24h vs Ctrl
0
100
200
300
400
500
4,000
6,000
8,000
10,000
12,000
14,000
Ratio (HAdV-B3 vs Ctrl)
B
VirMir-11171*: 25,968-25,993 (-)
VirMir-11181: 23,636-23,661 (-)
VirMir-11249: 12,405-12,430 (-)
VirMir-4867: 23,285-23,310 (+)
VirMir-4824: 16,056-16,081 (+)
VirMir-4796: 13,746-13,771 (+)
VirMir-4799*: 10,205-10,230 (+)
VirMir-4792*: 9,579-9,604 (+)
VirMir-4792: 9,544-9,569 (+)
VirMir-4768: 8,746-8,771 (+)
VirMir-4760*: 8,438-8,463 (+)
NBayes-4: 3,337-3,357 (+)
hsa-miR-181a*
hsa-miR-24
HAdV-B3/48h vs Ctrl
HAdV-B3/24h vs Ctrl
0
1
2
3
4
5
6
7
8
Ratio (HAdV-B3 vs Ctrl)

FIG. 2.

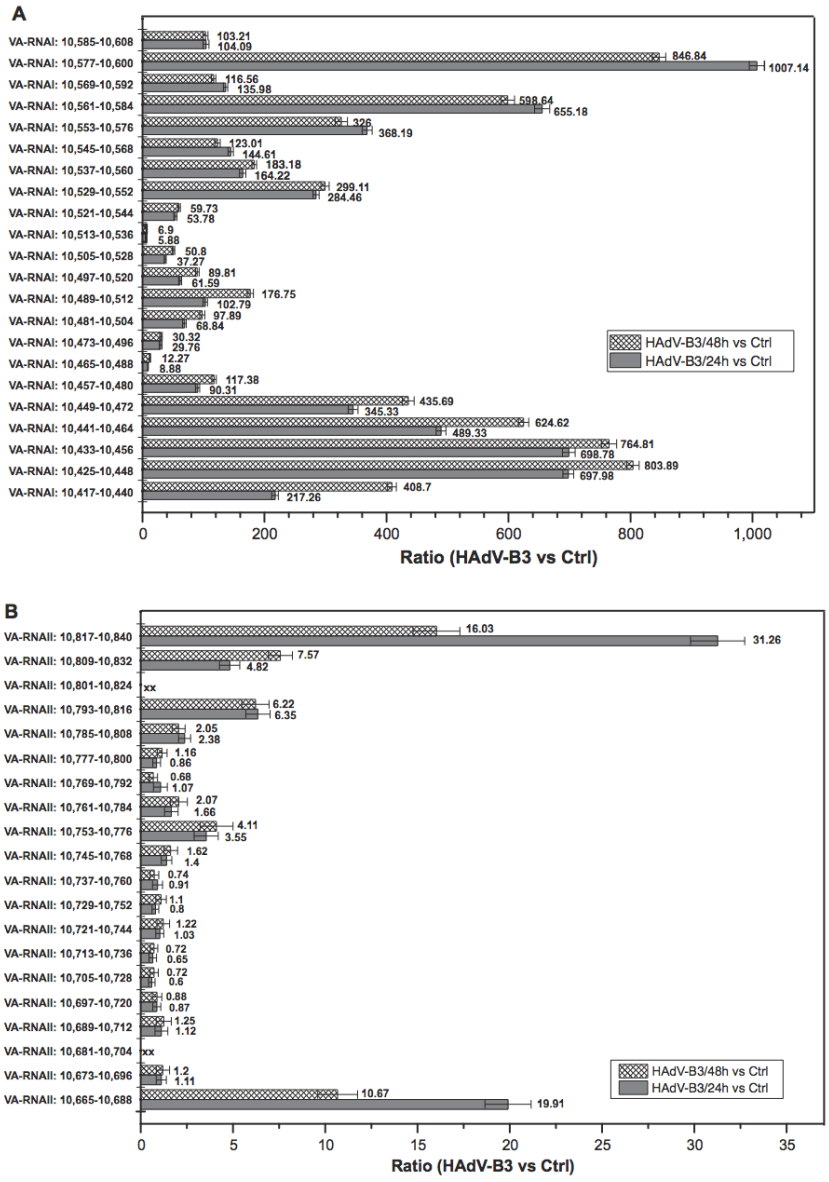
A
VA-RNAI: 10,585-10,608
VA-RNAI: 10,577-10,600
VA-RNAI: 10,569-10,592
VA-RNAI: 10,561-10,584
VA-RNAI: 10,553-10,576
VA-RNAI: 10,545-10,568
VA-RNAI: 10,537-10,560
VA-RNAI: 10,529-10,552
VA-RNAI: 10,521-10,544
VA-RNAI: 10,513-10,536
VA-RNAI: 10,505-10,528
VA-RNAI: 10,497-10,520
VA-RNAI: 10,489-10,512
VA-RNAI: 10,481-10,504
VA-RNAI: 10,473-10,496
VA-RNAI: 10,465-10,488
VA-RNAI: 10,457-10,480
VA-RNAI: 10,449-10,472
VA-RNAI: 10,441-10,464
VA-RNAI: 10,433-10,456
VA-RNAI: 10,425-10,448
VA-RNAI: 10,417-10,440
103.21
104.09
846.84
1007.14
116.56
135.98
598.64
655.18
326
368.19
123.01
144.61
183.18
164.22
299.11
284.46
59.73
53.78
6.9
5.88
50.8
37.27
89.81
61.59
176.75
102.79
97.89
68.84
30.32
29.76
12.27
8.88
117.38
90.31
435.69
345.33
624.62
489.33
764.81
698.78
803.89
697.98
408.7
217.26
HAdV-B3/48h vs Ctrl
HAdV-B3/24h vs Ctrl
0
200
400
600
800
1,000
Ratio (HAdV-B3 vs Ctrl)
B
VA-RNAII: 10,817-10,840
VA-RNAII: 10,809-10,832
VA-RNAII: 10,801-10,824
VA-RNAII: 10,793-10,816
VA-RNAII: 10,785-10,808
VA-RNAII: 10,777-10,800
VA-RNAII: 10,769-10,792
VA-RNAII: 10,761-10,784
VA-RNAII: 10,753-10,776
VA-RNAII: 10,745-10,768
VA-RNAII: 10,737-10,760
VA-RNAII: 10,729-10,752
VA-RNAII: 10,721-10,744
VA-RNAII: 10,713-10,736
VA-RNAII: 10,705-10,728
VA-RNAII: 10,697-10,720
VA-RNAII: 10,689-10,712
VA-RNAII: 10,681-10,704
VA-RNAII: 10,673-10,696
VA-RNAII: 10,665-10,688
16.03
31.26
7.57
4.82
xx
6.22
6.35
2.05
2.38
1.16
0.86
0.68
1.07
2.07
1.66
4.11
3.55
1.62
1.4
0.74
0.91
1.1
0.8
1.22
1.03
0.72
0.65
0.72
0.6
0.88
0.87
1.25
1.12
xx
1.2
1.11
10.67
19.91
HAdV-B3/48h vs Ctrl
HAdV-B3/24h vs Ctrl
0
5
10
15
20
25
30
35
Ratio (HAdV-B3 vs Ctrl)

FIG. 3.

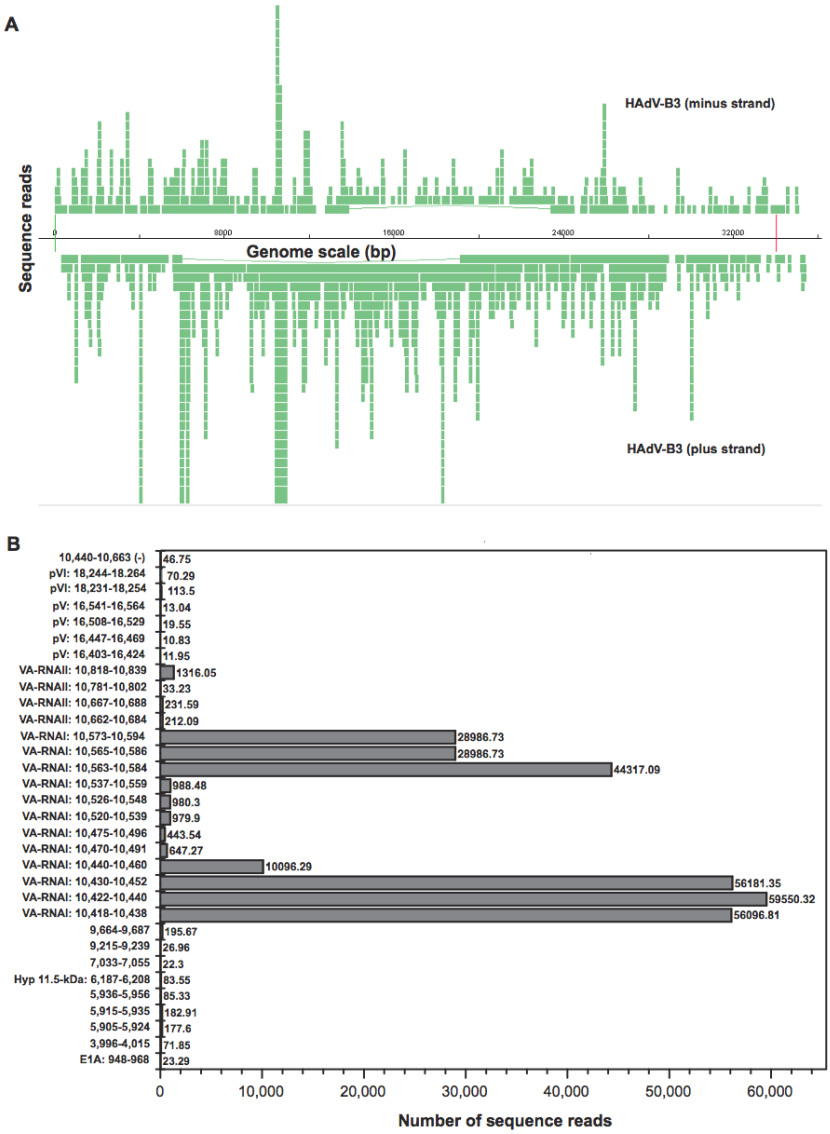
A
HAdV-B3 (minus strand)
Sequence reads
0
8000
16000
24000
32000
Genome scale (bp)
HAdV-B3 (plus strand)
B
10,440-10,663 (-)
pVI: 18,244-18,264
pVI: 18,231-18,254
pV: 16,541-16,564
pV: 16,508-16,529
pV: 16,447-16,469
pV: 16,403-16,424
VA-RNAII: 10,818-10,839
VA-RNAII: 10,781-10,802
VA-RNAII: 10,667-10,688
VA-RNAII: 10,662-10,684
VA-RNAI: 10,573-10,594
VA-RNAI: 10,565-10,586
VA-RNAI: 10,563-10,584
VA-RNAI: 10,537-10,559
VA-RNAI: 10,526-10,548
VA-RNAI: 10,520-10,539
VA-RNAI: 10,475-10,496
VA-RNAI: 10,470-10,491
VA-RNAI: 10,440-10,460
VA-RNAI: 10,430-10,452
VA-RNAI: 10,422-10,440
VA-RNAI: 10,418-10,438
9,664-9,687
9,215-9,239
7,033-7,055
Hyp 11.5-kDa: 6,187-6,208
5,936-5,956
5,915-5,935
5,905-5,924
3,996-4,015
E1A: 948-968
46.75
70.29
113.5
13.04
19.55
10.83
11.95
1316.05
33.23
231.59
212.09
28986.73
28986.73
44317.09
988.48
980.3
979.9
443.54
647.27
10096.29
56181.35
59550.32
56096.81
195.67
26.96
22.3
83.55
85.33
182.91
177.6
71.85
23.29
0
10,000
20,000
30,000
40,000
50,000
60,000
Number of sequence reads

FIG. 4.

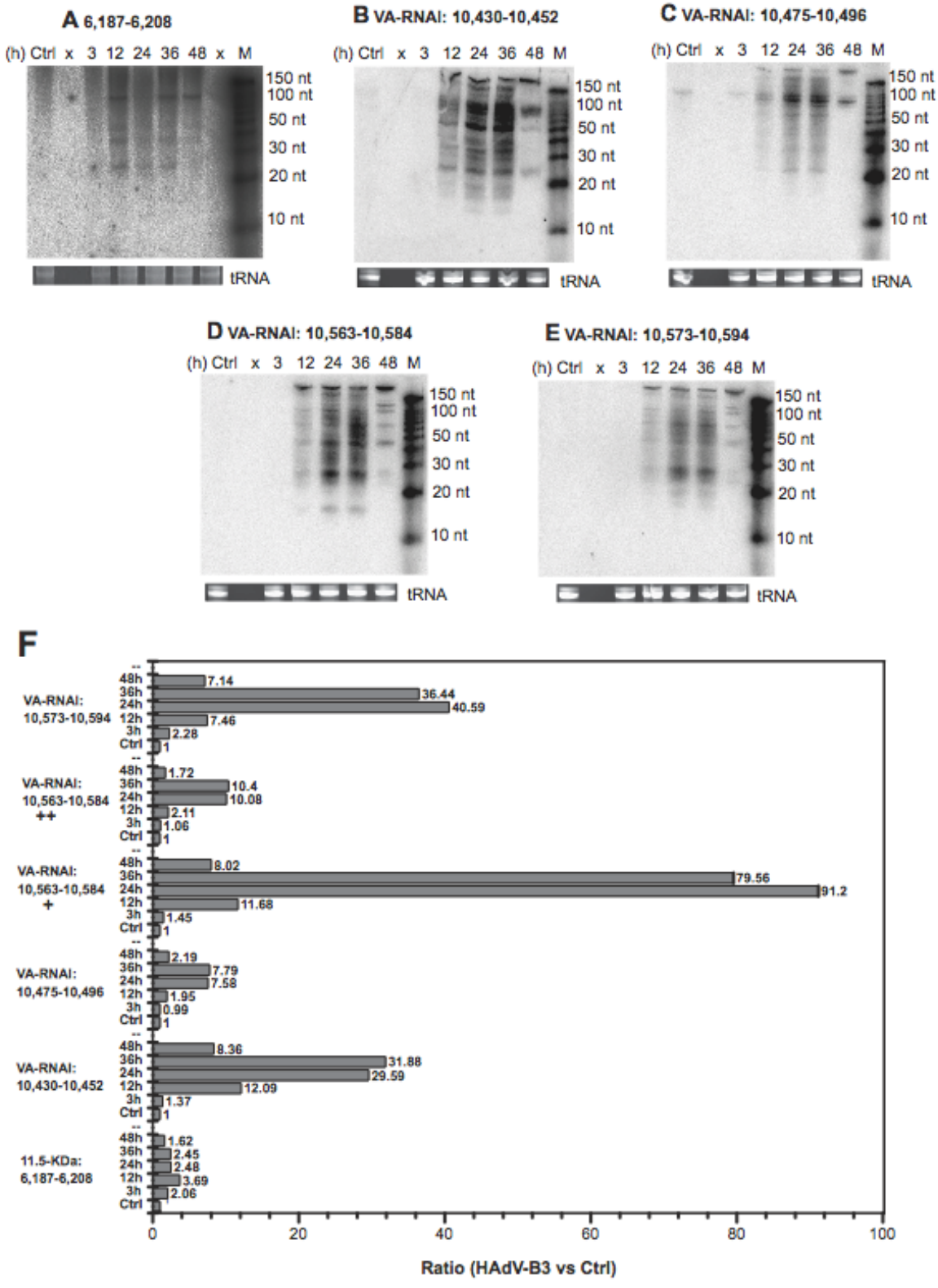
A 6,187-6,208
(h) Ctrl x 3 12 24 36 48 x M
150 nt
100 nt
50 nt
30 nt
20 nt
10 nt
tRNA
B VA-RNAI: 10,430-10,452
(h) Ctrl x 3 12 24 36 48 M
C VA-RNAI: 10,475-10,496
D VA-RNAI: 10,563-10,584
E VA-RNAI: 10,573-10,594
F
VA-RNAI: 10,573-10,594
VA-RNAI: 10,563-10,584 ++
VA-RNAI: 10,563-10,584 +
VA-RNAI: 10,475-10,496
VA-RNAI: 10,430-10,452
11.5-KDa: 6,187-6,208
48h 36h 24h 12h 3h Ctrl
7.14 36.44 40.59 7.46 2.28 1
1.72 10.4 10.08 2.11 1.06 1
8.02 79.56 91.2 11.68 1.45 1
2.19 7.79 7.58 1.95 0.99 1
8.36 31.88 29.59 12.09 1.37 1
1.62 2.45 2.48 3.69 2.06
0 20 40 60 80 100
Ratio (HAdV-B3 vs Ctrl)

FIG. 5.

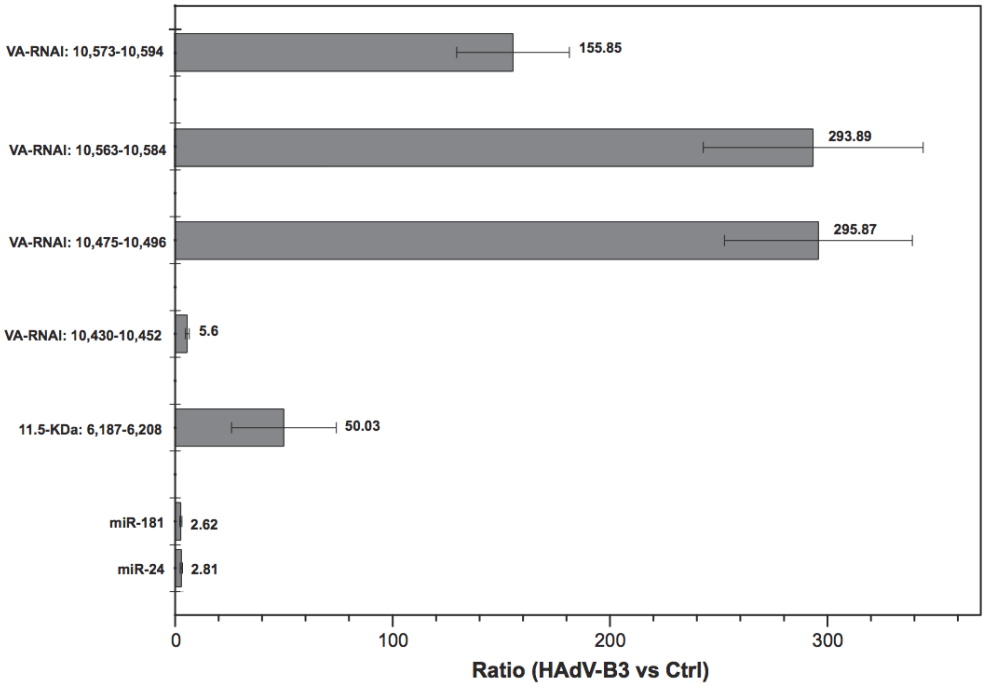
VA-RNAI: 10,573-10,594
155.85
VA-RNAI: 10,563-10,584
293.89
VA-RNAI: 10,475-10,496
295.87
VA-RNAI: 10,430-10,452
5.6
11.5-KDa: 6,187-6,208
50.03
miR-181
2.62
miR-24
2.81
0
100
200
300
Ratio (HAdV-B3 vs Ctrl)

FIG. 6.

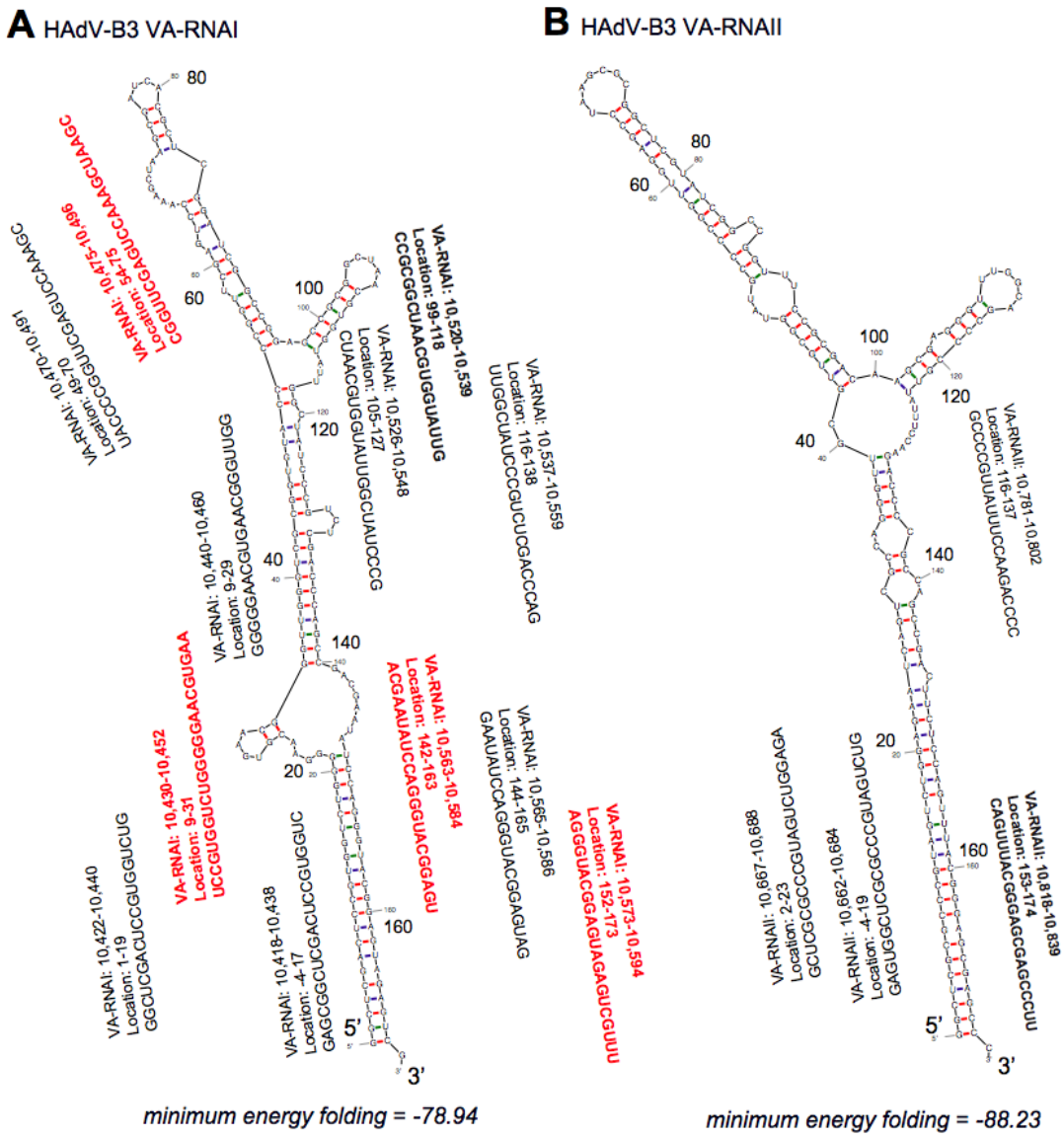
A HAdV-B3 VA-RNAI
B HAdV-B3 VA-RNAII
VA-RNAI: 10,422-10,440
Location: 1-19
GGCUCGACUCCGUGGUCUG
VA-RNAI: 10,430-10,452
Location: 9-31
UCCGUGGUCUGGGGGAACGUGAA
VA-RNAI: 10,440-10,460
Location: 9-29
GGGGGAACGUGAACGGGUUGG
VA-RNAI: 10,418-10,438
Location: 4-17
GAGCGGCUCGACUCCGUGGUC
VA-RNAI: 10,526-10,548
Location: 105-127
CUAACGUGGUAUUGGCUAUCCCG
VA-RNAI: 10,520-10,539
Location: 99-118
CCGCGGCUAACGUGGUAUUG
VA-RNAI: 10,563-10,584
Location: 142-163
ACGAAUAUCCAGGGUACGGAGU
VA-RNAI: 10,537-10,559
Location: 116-138
UUGGCUAUCCCGUCUCGACCCAG
VA-RNAI: 10,565-10,586
Location: 144-165
GAAUAUCCAGGGUACGGAGUAG
VA-RNAI: 10,573-10,594
Location: 152-173
AGGGUACGGAGUAGAGUCGUUU
VA-RNAI: 10,475-10,496
Location: 54-75
CGGGUUCGGAGUCCAAGCUAAGC
VA-RNAI: 10,470-10,491
Location: 49-70
UACCCCGCGGUUCGAGUCCGCAAGC
VA-RNAII: 10,667-10,688
Location: 2-23
GCUCGCGCCCGUAGUCUGGAGA
VA-RNAII: 10,662-10,684
Location: -4-19
GAGUGGCUCGCGCCCGUAGUCUG
VA-RNAII: 10,781-10,802
Location: 116-137
GCCCCGUUAUUUCCAAGACCCC
VA-RNAII: 10,818-10,839
Location: 153-174
CAGUUUACGGGAGCGAGCCCUU
5'
3'
minimum energy folding = -78.94
minimum energy folding = -88.23

ABBREVIATIONS

Name	Description
A549	human lung adenocarcinoma epithelial cells
Ago2	argonaute 2
APEX	absolute proteomics expression
ATF	cyclic AMP-dependent transcription factor
BALF5	Epstein-Barr virus DNA polymerase catalytic subunit
C18	reverse phase C18 matrix
CAR	coxsackie virus B and adenovirus receptor
CD46	cluster of differentiation 46, complement regulatory protein
CID	collision-induced dissociation
c-MYB	proto-oncogene protein
COPI	α-subunit of the coat protein I
CRD	carbohydrate-recognition domains
DBP	DNA binding protein
DC	dendritic cell
DGCR8	DiGeorge syndrome critical region 8/Microprocessor complex subunit DGCR8
DIGE	difference gel electrophoresi
DNA	Deoxyribonucleic acid
dNTP	deoxynucleotide triphosphate
DOC	Deoxycholate
Drosha	Ribonuclease 3
ds	double-strand
DSG2	desmoglein 2
EBER	Epstein-Barr virus non-coding ribonucleic acid
EBV	Epstein-Barr virus
EGFR	epidermal growth factor receptor
ESI	electrospray ionization
ETD	electron-transfer dissociation
FACS	fluorescence activated cell sorting
FBS	fetal bovine serum
FCS	fetal calf serum
FDA	Food and Drug Administration
FDR	false discovery rate
FITC	fluorescein isothiocyanate
FK	fiber knob
FRAP	fluorescence recovery after photobleaching
gal-1	galectin-1
gal-3	galectin-3
GFP	green fluorescent protein
GON	group-of-nine
GOS	group-of-six
h	hour
H2B	histone 2B
HAdV	human adenovirus
HAdV-B11	human adenovirus species B serotype 11
HAdV-B14	human adenovirus species B serotype 14
HAdV-B16	human adenovirus species B serotype 16
HAdV-B21	human adenovirus species B serotype 21
HAdV-B3	human adenovirus species B serotype 3
HAdV-B34	human adenovirus species B serotype 34
HAdV-B35	human adenovirus species B serotype 35
HAdV-B50	human adenovirus species B serotype 50

HAdV-B7	human adenovirus species B serotype 7
HAdV-C2	human adenovirus species C serotype 2
HAdV-C5	human adenovirus species C serotype 5
HAdV-D37	human adenovirus species D serotype 37
HAdV-D49	human adenovirus species D serotype 49
HCMV	human cytomegalovirus
HCV	hepatitis C virus
HIV	human immunodeficiency virus
HSV	herpes simplex virus
IAA	iodoacetamide
ICAT	isotope coded affinity tags
IFN	Interferon
IP	immunoprecipitation
iTRAQ-8plex	isobaric tag for relative and absolute quantitation - multiplex 8 plex
KSHV	Kaposi's sarcoma-associated herpesvirus
LC-MS/MS	liquid chromatography tandem mass spectrometry
LMP-1	Epstein-Barr virus latent membrane protein 1
LTQ-FT-ICR MS	linear ion trap-Fourier-transform ion cyclotron resonance mass spectrometry
M	Mascot
MALDI-TOF/TOF	Matrix-assisted laser desorption/ionization-time of light/time of light
MCMV	murine cytomegalovirus
MDA-5	melanoma differentiation-associated protein 5
MFI	mean fluorescence intensity
MHC	major histocompatibility complex
MICB	major histocompatibility complex class I polypeptide-related sequence B
miRNAs	small miRNAs
MLP	major late promoter
MMTS	methyl methanethiosulfonate
MOI	multiplicity of infection
MV	measles virus
NK	natural killer
NP-40	Nonidet P40
N-WASP	neuronal Wiskott-Aldrich Syndrome protein
ORF	open reading frame
PL	Progenesis LC-MS
p.i.	post infection
PF2	ProgenesisF-T2PQ (combined of export feature of Progenesis LC-MC and top 2 peptide quantitation)
PF3	ProgenesisF-T3PQ (combined of export feature of Progenesis LC-MC and top 3 peptide quantitation)
PAMP	pathogen-associated molecular pattern
PBS	phosphate-buffered saline
pfu	plaque forming unit
PI4KA	phosphatidylinositol 4-kinase
PKA	protein kinase RNA-activated
PKR	double-stranded RNA-activated protein kinase
Pol	DNA polymerase
PP	ProteinPilot
PTM	post translational modification
PVDF	polyvinylidene fluoride
Q-TOF	hybrid quadrupole time of flight mass spectrometer
RID	receptor internalization and degradation
RIG-1	retinoid-inducible gene 1
RISC	RNA-induced silencing complex

RNA	Ribonucleic acid
ROI	region of interest
RRV	rhesus monkey rhadinovirus
RT-PCR	real time - polymerase chain reaction
RU	resonance units
S	ScaffoldQ+
SCR	short consensus repeats
SCX-HPLC	strong cationic exchange - high performance liquid chromatography
SDS	Sodium Dodecyl Sulfate
SDS-PAGE	sodium dodecyl sulfate polyacrylamide gel electrophoresis
SILAC	cell-culture enriched stable isotope labeled amino acids
siRNA	interference ribonucleic acid
SPR	surface plasmon resonance
SPT	using single-particle tracking
SRM	selected reaction monitoring
ss	single-strand
TCA	trichloroacetic acid
TCEP	Tris[2-carboxyethyl] phosphine
TFA	trifloroacetic acid
TIA1	T-cell-restricted intracellular antigen-1
TLR	toll-like receptor
TNF	tumor necrosis factor
TNPQ	top N peptide quantitation
TP	binding protein
TRF	transferrin receptor/CD71
Tub	tubulin
UTR	untranslated region
vmiRNAs	viral small miRNAs
vp	virus particle
WNV	West Nile virus

CURRICULUM VITAE

Name: TRINH

First name: Hung

Middle name: Viet

Born: 03.07.1980

Native place: Hanam, Vietnam

Education:

1995-1998: Baccalaureate

1998-2002: Bachelor, Faculty of Biology, Vietnam National University, Hanoi, VIETNAM

2003-2005: Master in Biochemistry, Sun Moon University, S. KOREA

Title of the master thesis: "*Application of genetic engineering to enhance clavulanic acid production from Streptomyces clavuligerus NRRL3585.*"

Supervised by Prof. Sohng Jae Kyung

2007-2011: Ph.D. student at the Institute of Molecular Life Sciences, University of Zurich, Faculty of Mathematical and Natural Sciences

Title of the Ph.D. thesis: *"Functional genomic approaches to study human adenoviruses and frontier research on miRNAs "*

Supervised by **PD. Dr. S. Hemmi**

MEMBERSHIPS

American Society for Mass Spectrometry, Scientific American, Swiss Chemical Society

SCHOLARSHIPS, PRIZES AND AWARDS

- Sun Moon Fellowships (Mar 03–Sep 05): master study

- Swedish Institute Scholarships (Sep 04-Dec 04): short time visit

- Forschungskredit Grant (Aug 08–Jan 10): Adenovirus-encoded miRNA project

- University Research Priority Program Grant (2008): systems biology project

- Swedish Research Links Grant (2008): Colorectal cancer between Sweden and Vietnam

- University Research Priority Program Travel (2008, 2009): lab visits in Israel and US

- Swiss Chemical Society Fellowship (2008, 2009): conferences in US

- 21st IUBMB and 12th FAOBMB Fellowship (2009): conference in China

- American Society for Mass Spectrometry Fellowship (2009): workshop in US

- Forschungskredit Grant (Oct 10 –Mar 11): miRNA project (extension)

Scientific communications and manuscripts:

Poster and oral presentations

Trinh, H.V., Eisenhut, M., Greber, U.F. and Hemmi, S. (2008). Functional genomic approaches to study adenovirus species B receptors. 56th ASMS Conference on Mass Spectrometry. Abstract, June 01-05, Denver, Colorado, USA.

Trinh, H.V., Chennamparampil, V., Schauer, S., Greber, U.F. Hemmi, S. (2008). Towards determination of affinities between Adenovirus fiber knobs of different serotypes and soluble CD46. Swiss Chemical Society, Abstract, September 11, Zurich, Switzerland.

Trinh, H.V., (2008). Frontier research in human and adenovirus miRNAs. The Galilee Society Institute of Applied Research, Israel. December 03. Invited talk.

Trinh, H.V., Chennamparampil, V., Schauer, S., Greber, U.F. and Hemmi, S. (2009). Functional genomic approaches to study human adenoviruses. Swiss Snow Symposium. Abstract, February 06-08, Lenk, Switzerland. Oral presentation.

Trinh, H.V., Gehrig, P., Grossmann, J., Roschitzki, B., Rehrauer, H., Rutishauser, D., Greber, U.F., Hengartner, M. and Hemmi, S. (2010). Functional genomics approaches to study molecular system dynamics of human adenovirus infection. Swiss Proteomics Society, Abstract, December 02-04, Zurich, Switzerland. Oral presentation.

Trinh, H.V., Lesage, G., Zoller, S., Roschitzki, B., Rehrauer, H., Patrignani, A., Gehrig, P., Greber, U.F. and Hemmi, S. (2009). Functional genomics approaches to study molecular system dynamics of human adenovirus infection. 21st IUBMB International Congress of Biochemistry and Molecular Biology and 12th FAOBMB Congress, Abstract, July 30-August 07, Shanghai, China.

Trinh, H.V., Gehrig, P., Baetschmann, H., Grossmann, J., Schlapbach, R., Greber, U.F. and Hemmi S. (2010). Quantitative proteomics analysis of human adenovirus infections by iTRAQ-8plex. 58th ASMS Conference on Mass Spectrometry. Abstract, May 23-27, Salt Lake City, Utah, USA.

Trinh, H.V, Gehrig, P., Baetschmann, H., Grossmann, J., Schlapbach, R., Greber, U.F. and Hemmi, S. (2010). Quantitative proteomics analysis of human adenovirus infections by iTRAQ-8plex. SPS PhD Students' Symposium, Abstract, December 01-02, 2010, Basel, Switzerland. Oral presentation.

Manuscripts

Trinh, H.V*., Lesage, G*., Chennamparampil, V., Burckhardt, C., Schauer, S., Havenga, M., Greber, U.F. and Hemmi, S. (2011). Avidity binding of human adenovirus serotypes 3 and 7 to the membrane cofactor CD46 triggers infection (submitted to J. Virol), notice (*): equal contribution.

Trinh, H.V., Grossmann, J., Gehrig, P., Roschitzki, B., Greber, U.F. and Hemmi, S. Comparative analyses of quantitative iTRAQ-8plex-based and label-free proteomics for human adenovirus infections (proposed to submit in J. Proteome Res in the first week of June).

Trinh, H.V., Roschitzki, B., Gehrig., Greber, U.F. and Hemmi, S. Identification of viral, cellular proteins and phosphorylation sites in human adenovirus type 3 (manuscript in preparation).

Trinh, H.V., Gehrig, P, Baetschmann, H., Rehrauer, H., Patrignani, A., Grossmann, J., Michael O Hengartner, M.O., Greber, U.F. and Hemmi, S. Functional genomics approaches to study molecular system dynamics of human adenovirus type 3 infection (manuscript in preparation).

Trinh, H.V., Bruggmann, R., Yousef, M., Qi, W., Aluri, S., Meister, G., Stoffel, M., Greber, U.F. and Hemmi. S. Computational and experimental analysis of potential miRNAs encoded by human adenoviruses type 3 (manuscript in preparation).

Trinh, H.V., Gehrig, P., Baetschmann, H., Roschitzki, B., Grosmann, J., Nickel, W., Greber, U.F. and Hemmi, S. Infection of human adenovirus type 3 induces secretion of galectin-1 (manuscript in preparation).

ACKNOWLEDGEMENTS

PhD committee

PD. Dr. Silvio Hemmi (supervisor, IMLS, University of Zürich)

Prof. Dr. Urs F. Greber (chairman, IMLS, University of Zürich)

Prof. Dr. Michael O. Hengartner (IMLS, University of Zürich)

Prof. Dr. Gunter Meister (University of Regensburg, Germany)

Prof. Dr. Markus Stoffel (Institute of Molecular Systems Biology, ETH Zürich)

It was a great pleasure for me to receive the support and advice form all committee members.

I gratefully thank Dr. Silvio Hemmi for his support and his carefully correcting of the doctoral thesis and his kindness.

I deeply thank Prof. Urs F. Greber for his research vision advice and his kindness.

Hemmi group and all his laboratory members

Guillaume Lesage (took part in writing proposals for URPP/Systems Biology, Forschungskredit and SNF; took part in FRAP experiments; performed inhibition assays for avidity effect; performed projects for vsRNAs encoded by HAdV-C5)

Leta Fuchs (organizing research materials and assistance)

Venus Chennamparampil (Master student, contributed to production of recombinant HAdV-FKs and inhibition assays)

Silvia Gutnik (Master student, involved in characterization of vmiRNAs encoded by HAdVs and cellular miRNAs following HAdV infection, University of Zürich)

Jennifer Tscherrig (Master student, involved in defining roles of galectin-1/3 upon viral infections, University of Zürich)

Willy Decurtins (Master student, involved in production of recombinant MAdV-1/MAdV-2-FK)

Rene Platzer (3-month internship student, involved in investigation of Gal-1/3 secretion and down-regulation of EphA2 upon HAdV infections, University of Vienna, Vienna)

Anita Murer (2-month BUSS student, involved in production of recombinant GST-Gal-1 and GST-Gal-3 proteins and anti-Gal-1/Gal-3 immunoprecipitation experiments, University of Zürich)

Anna M Sergeeva (2-month BUSS student, involved in down-regulation studies of Gal-1/Gal-3 following HAdV infections, Lomonosov Moscow State University, Moscow)

Paul Mac Eoin (2-month BUSS student, involved in production of recombinant HAdV-FKs and CD46 proteins using Baculovirus system, National University of Ireland, Galway)

Greber group and all his laboratory members (University of Zürich)

Dr. Markus Eisenhut (HAdV-C5 proteome analysis)

Dr. Christoph Burckhardt (analysis for FRAP data)

Dr. Wolfrum Nina (assistance of light microscopy and siRNA set-up)

Dr. Suomalainen Maarit (providing of antibodies and scientific discussions)

Corinne Wilhelm (Western blot analysis for HAdVs with H2B and tubulin)

Engelke Martin (assistance for light microscopy)

Boucke Karin (analysis with electron microscopy)

FGCZ (ETH Zürich)

Dr. Stefan Schauer (Biacore, training and assistance for protein kinetics/affinity)

Dr. Peter Gehrig (proteomics, training and assistance for LC-probot, MALDI-TOF/TOF, experimental design)

Dr. Bernd Roschitzki (proteomics, training and assistance for LTQ-FT-ICR, Orbitrap, experimental design)

Dr. Jonas Grossmann (proteomics, generating database, label-free data analysis)

Claudia Fortes (proteomics, assistance in SCX-HPLC)

Dr. Endre Laczko (proteomics, training and assistance for TSQ Quantum and TSQ Vantage)

Dr. Dorothea Rutishauser (proteomics, testing the quantitation of iTRAQ-8plex with Orbitrap-XL)

Hansruedi Baetschmann (bioinformatics, analysis of transcriptiomics and proteomics data)

Dr. Hubert Rehrauer (bioinformatics, analysis of transcriptiomics data)

Andrea Patrignani (transriptomics, web-lab)

Dr. Stefan Neuenschwander (miRNA microarray web-lab)

Stefan Zoller (bioinformatics, tilling array and miRNA data analysis)

Dr. Remy Bruggmann (analysis for deep sequencing data)

Dr. Sirisha Aluri (deep sequencing, web-lab)

Dr. Weihong Qi (analysis for deep sequencing data)

Dr. Marzanna Künzli-Gontarczyk (initial project of deep sequencing work)

Dr. Jens Sobek (support and assistance for Safire2 scanner)

Prof. Ralph Schlapbach (management and support)

Center for Microscopy and Image Analysis

Caroline Aemissegger (training and assistance in confocal microscopy SP2 and SP5)

Dr. Urs Ziegler (supporting and management of the core facility)

Collaborators

Prof. Dr. Gunter Meister (providing the Ago2 antibody, scientific advices, Germany)

Prof. Walter Nickel (providing expression plasmids including pGEX-Gal-1 and pGEX-Gal-3 and rabbit polyclonal antibodies including anti-Gal-1 and anti-Gal-3, Germany)

Dr. Malik Yousef (providing the *in silico* miRNA prediction tools for HAdVs, The Institute of Applied Research-The Galilee Society, Shefa-Amr, Israel)

Dr. Sung-Chou Li (providing the *in silico* miRNA prediction tool (VirMir-db) for HAdVs, Institute of Biomedical Science, Academia Sinica, Taiwan)

Prof. Totomu Shimaoka (collaboration in miRNA projects, Harvard Medical School, Boston, USA)

Prof. Jennifer Lippincott-Schwartz (provided plasmids with TRFC mCheery and GFP, National Institutes of Health, Bethesda, USA)

Funding support

Dr. Cornelia Schauz (URPP/Systems Biology)

Dr. Beatrice Scherrer (Forschungskredit Universität Zürich)

Swiss National Foundation (SNF)

Family and friends

I would like to acknowledge **Dr. Gerd Stuckmann** and **Prof. Jan Dimberg** for encouragement and enjoyment of life beyond scientific work.

Finally, I am forever indebted to my parents for their understanding, endless patience and encouragement. I specially thank my beloved wife **Loan Mai Nguyen** for her understanding, encouragement and love. The birth of our child **Trang Huyen Trinh** during my PhD study has brought much motivation and productivity.